BIOLOGICAL AND CLINICAL EVALUATION OF INTENSITY MODULATED RADIOTHERAPY FOR BRAIN TUMOURS

Suganya Sivabalasingham

UCL Cancer Institute, University College London

A thesis submitted to University College London

for the degree of MD (Res)

To Henry, Thomas, Sarasa, and my parents,

for their support, patience and encouragement.

Declaration

I, Suganya Sivabalasingham, confirm that the work presented in this thesis is my own. Where information has been derived from other sources, I confirm that this has been indicated in the thesis.

Abstract

Intensity modulated radiotherapy has gained attention in recent years as a high precision radiation technique, allowing tumour dose escalation and reductions in high dose to adjacent normal organs. IMRT optimises the therapeutic ratio even further than conventional conformal radiation techniques, providing effective dose for tumour control, whilst minimising side effects.

Despite these potential benefits, there is concern regarding long term effects from the associated low dose bath, exposing more normal tissue to lower radiation dose as compared to more conventional radiation techniques. However, the effects of this low dose radiation have yet to be established.

In this thesis, γ-H2AX was used to assess radiation-induced DNA damage within peripheral blood lymphocytes of patients undergoing fixed gantry or static field IMRT (SF-IMRT). The reproducibility and sensitivity of γ-H2AX as a comparison of DNA damage following differing radiation techniques has been documented, with significant differences in γ-H2AX foci seen following SF-IMRT in comparison to volumetric arc-IMRT and 3D conformal radiation. Efforts have been made to demonstrate a difference in whole body exposure from these techniques and variations in γ-H2AX foci distributions seen following techniques may reflect greater whole body exposure following SF-IMRT, which may have impact on long term toxicity.

The benefits of IMRT to treat complex shaped meningiomas, often located close to critical dose limiting structures, have been investigated in a clinical phase I/II study. The feasibility of using IMRT to deliver conformal radiation to meningiomas, whilst respecting normal tissue tolerance has been demonstrated here. The preliminary report from this ongoing clinical study documents effective, safe treatment with acceptable toxicity levels and comparable local control, particularly within grade I meningiomas. Prospective data collection has revealed improvements in neurological symptoms and no significant quality of life deterioration.

The findings in this thesis provide further information to guide future work, examining the biological and clinical long term effects of new radiation techniques.

Acknowledgments

Professor Susan Short, who provided me with the opportunity to undertake this research and who, as my supervisor, has supported and guided me in my efforts.

Without the contributions of the following people, the work described in this thesis would not be possible.

Radiation Biology Group, UCL Cancer Institute

Professor Susan Short, Dr Mulugeta Worku, Dr Natasha Iles, Dr Marissa Alcaide, Dr Charlotte Westbury

Neuro-oncology Unit, University College London Hospital NHS Trust

Professor Susan Short, Dr Naomi Fersht and the clinical team of the neuro-oncology unit

Radiotherapy Physics Department, University College London Hospitals NHS Trust

Derek D'Souza, Phil Davies, Chris Stacey, Narinder Lalli

Radiotherapy Department, University College London Hospitals NHS Trust

Radiographers, radiotherapy nurses and reception staff.

UCLH Clinical Trials Unit

Ms Adrienne Abioye

Head and Neck Oncology Group, Department of Oral pathology, King's College London

Teresa Guerrero Urbano, Yae-Eun Suh, Jessica Bullenkamp, Mahvash Tavassoli, who kindly facilitated the ex-vivo γ-H2AX work described in chapter 2.

Comprehensive Biomedical Research Centre, UCL, who funded this work

Data evaluation and statistical analysis was performed by me using PASW® 18.0 statistical package (SPSS Inc., Chicago). Some support was obtained from the UCL Research Support Centre to ensure that appropriate statistical analysis was being performed.

Study patients undergoing treatment at University College London Hospitals NHS Trust, without whom this research could not have taken place.

Table of Contents

List of Tables

List of Figures

CHAPTER 1

Introduction

IMRT is a high precision technique that aims to individualise radiation therapy to maximize tumour dose while simultaneously protecting the surrounding normal tissue from high dose radiation. Its use has been increasing and has extended to a wide range of tumour groups. However, the long term effects of this delivery technique are still being examined.

1.1 Intensity modulated radiotherapy

1.1.1 Background

The need to improve local tumour control, whilst minimizing treatment related toxicity by improving the differential dose distribution of external beam irradiation between tumour and normal tissues, remains a major goal in modern radiotherapy [1,2]. Conventional conformal radiotherapy using small numbers of simply shaped beams can achieve the goal of homogeneous dose delivery to the target tumour, but in many cases may also lead to unnecessarily large volumes of normal tissue being irradiated to high doses. The dose tolerance of these adjacent normal tissues precludes high doses of radiation being delivered to the tumour and therefore may have an effect on local control and perhaps even metastatic potential of tumours [1]. Conformal radiotherapy has evolved since the mid-20th century with the use of

rotational and non co-planar fields, blocks, wedges, compensators and through the development of radiation dosimetry; all performed with the aim of concentrating radiation dose in the tumour whilst attempting to spare normal tissue [3].

Progression to three dimensional conformal radiotherapy (3D-CRT) was made possible with the use of improved three dimensional imaging, adequate immobilization and computer controlled delivery systems [1,2], providing the capability to conform the shape of the beams to the shape of the target from each beam's eye view, as well as being able to calculate three dimensional (3D) dose distributions [4,5]. The ability to conform the prescribed dose to the 3D target volume is typically achieved with a set of fixed field radiation beams of uniform intensity, whilst the intensity of these beams can be modified with wedges or compensators to accommodate missing tissue and shape dose distributions, allowing for a reduction of normal tissue within the high dose volume (and therefore a potential reduction in late toxicity) compared to more conventional techniques [1,6-13]. However, the ability to dose escalate within the tumour, whilst respecting normal tissue tolerance, is still challenging with 3D-CRT alone.

By the late 1900's, intensity modulated radiotherapy (IMRT) was being developed as a further enhancement on conformal radiotherapy, allowing the delivery of tumour doses to the target volume whilst making low doses to the critical organs more achievable [14] and it remains one of the major technical advances in modern radiotherapy. IMRT allows the delivery of concave isodose dose distributions and uses computer controlled linear accelerators to produce non-uniform beam intensity patterns in an effort to achieve superior dose distributions. By comparison, 3D-CRT allows the outlined shape of each beam to be controlled, but the intensity (or

fluence) generally remains uniform across the beam. Although use of wedges and tissue compensators can modulate the beam intensity, this is usually only in one dimension per beam.

IMRT enhances 3D-CRT through its capabilities in manipulating intensities of individual rays within each beam (by means of a combination of geometrical and fluence shaping) to allow greater control of the dose distribution [15], create more conformality and with the added benefit of generating a concave dose distribution [16]. This modulation of radiation fluence can be achieved by either interrupting the X-ray fluence through collimation and/or compensation or by temporally modulating the fluence and varying the temporal modulation in space [17]. In this way, and when combined with image guided techniques to accurately delineate target volumes and deliver the planned treatments, radiation can be delivered more precisely to the tumour with greater sparing of the surrounding normal tissues, thus aiming to improve tumour control and reduce normal tissue toxicity [18].

The first papers on IMRT described a process, beginning with a desired dose distribution and producing a specification on how to create the required fluence modulation [19]; a process we know today as 'inverse planning'. In fact, most modern IMRT plans are often generated by means of inverse planning or automated optimization 3D-RTP (radiotherapy planning) systems; using computer optimization techniques to determine the distribution of intensities across the target volume and improve the shape of these dose distributions with the capability of producing concavities within these distributions [3]. This, in turn, can deliver steep dose gradients to create specific sparing of sensitive normal structures within complex treatment geometries [6,20-24]. Therefore, defining the optimal beam

fluence becomes an integral component of IMRT. This involves determining the physically deliverable modulated beam fluence profile, which results in a dose distribution that most closely matches the desired one. IMRT allows the delivery of dose distributions with complex isodose profiles so that radiosensitive normal tissue can be spared from radiation injury [6]. The advantages of this have been demonstrated in several studies, particularly in the fields of prostate and head and neck cancer [25-27].

1.1.2 IMRT delivery techniques

Several IMRT delivery techniques have been described in the literature, from the very simple method of metal compensators to much more sophisticated techniques described below.

Metal compensators of variable thickness can simply be placed in front of the beam to yield a modulated beam. However, this is often an awkward, expensive, time consuming arrangement and frequently difficult to position with accuracy and therefore limits the quality of beam modulation [6,28].

Many different IMRT delivery techniques now exist and the more modern techniques can be broadly categorized as follows:

Fixed gantry

- Step and shoot
- Dynamic delivery

Rotational techniques

- Tomotherapy helical delivery
- Linac-based arc therapy

1.1.2.1 Fixed gantry IMRT (SF-IMRT)

1.1.2.1.1 Scanned photon and electron beam IMRT

The use of computer-controlled beam steering magnets to direct the high energy electron beam onto the X-ray target was one of the first modern IMRT delivery techniques described [16]. Control of the angle and intensity at which the electron beam hits the X-ray target creates bremsstrahlung X-ray beams which can be placed anywhere within the radiation field using a 'scan pattern', giving beam location and intensities without the need to increase treatment times [29]. However, the resolution of these techniques can be limited due to the full-width half maximum; even with beams of 50MV photons, this can be several centimetres. An increase in energy from 50 to 60MV can result in a reduction of the half width of photon beams down to 15mm and in the electron beams to 5 mm [29], which can be useful for conformal delivery of dose.

Electron energies, typically those of high energy, such as 25-50MeV, can also be used for IMRT with this technique [29-32] and more recently there have been improvements on scanning photon beams with sizes down to 1.2cm using 50MeV [33].

Scanned narrow Bremsstrahlung beams in the presence of multileaf collimators (MLC) can produce enhanced dose delivery, which can be improved further by reducing the source to isocentre distance and size of the elementary photon beam. Decreasing the initial electron energy can reduce the width of the photon pencil beam further [29,33].

More recently, there has been increasing focus on implementing this concept [34] with the use of fast narrow high energy (50MV) scanned photon beams to deliver biologically optimized radiation therapy [35].

1.1.2.1.2 Conventional MLC IMRT

Conventional MLCs can be used to deliver IMRT using a linear accelerator under computer control. The most efficient way to deliver fixed-field (static field) IMRT is by using standard MLCs in dynamic mode. Other methods may use compensators, but these are very time consuming procedures. Several MLC applications for IMRT are well known now (including 'step and shoot' IMRT or dynamic 'sliding window' IMRT). Standard MLCs can be used to deliver the optimized fluence distribution in either dynamic mode (leaves move whilst radiation is on) or static mode, often termed 'step and shoot' IMRT or SMLC IMRT (segmental MLC IMRT).

1.1.2.1.2.1 Step-and-shoot (SMLC) IMRT

Step and shoot IMRT describes a technique where each treatment field is further subdivided and then delivered in succession. A series of multiple segment fields, in which each field is composed of several small segments (or subfields) that can be

delivered sequentially in a ‘step and shoot’ method, provide an intensity modulated beam. Each segment is made with a series of MLC shapes (segments) and can be used to deliver IMRT from the same gantry angle. Each field may consist of 3-20 segments delivered sequentially. Multiple segment fields are set up at selected orientations of the gantry under computer control. In contrast to dynamic MLC, the MLC leaves travel to discrete positions whilst the radiation beam is off. The beam is turned on during the ‘step’ phase of treatment so that MLC movement and radiation delivery does not take place simultaneously, resulting in discrete intensity levels.

1.1.2.1.2.2 Sliding window or Dynamic MLC (DMLC) IMRT

The dynamic MLC technique relies on pairs of moving MLC leaves. With a fixed gantry position, the opening, formed by a pair of opposing MLC leaves under computer control, is swept across the target volume whilst the radiation beam is on to produce the desired fluence profiles. The width of the window and speed of leaves are continuously adjusted whilst radiation is being delivered to produce the required intensity patterns. This type of IMRT was first implemented in Memorial Sloane-Kettering [36,37] and has the advantage of delivering any number of intensity levels without a significant increase in treatment time, although more accurate synchronization of leaf positions with ‘beam on time’ is required.

Beam modulation is proportional to the delivery complexity, so that the more modulated a beam, the more complex its delivery. In particular, the number of monitor units required with dynamic MLC techniques is directly proportional to the sum of rising fluence changes as the leaves move across the aperture [17] and it is therefore advantageous to limit beam modulation to the minimum required for conformality, with as little ‘noise’ as possible. There have been reports that DMLC

requires 15-20% more monitor units compared to SMLC techniques, although can be associated with faster treatment times [38,39].

The delivered dose is directly proportional to the MLC gap between opposed leaves as they move across a treatment field. It is therefore imperative that any error in gap width is avoided as even small errors can lead to large dose errors. The tolerances accepted for 3D-CRT are generally insufficient for IMRT delivery. For example, if there is a 2mm error in a leaf gap of 2cm, this can produce an absorbed dose error of approximately 15%. Therefore accuracy generally needs to be within 1mm.

Transmission and leakage radiation through the ends of MLC leaf pairs and between adjacent MLC leaves does occur and can vary between 3-6% of the total target dose [40]. However, the interleaf leakage can be minimised to some extent by the manufacture of MLC leaf edges with a tongue and groove design. Nevertheless, there is still some radiation leakage and this must also be taken into account during the dose calculation process. In the past, rates of leakage radiation have varied from 1.5 to 3%. However, the tongue and groove design may actually block or scatter radiation causing significant underdosage in the treatment field during beam delivery. This has been estimated at 10-25% [41] due to the tongue and grove phenomenon, but can be reduced to as little as 3% by a process of leaf synchronization [42,43].

1.1.2.2 Rotational IMRT

1.1.2.2.1 Tomotherapy

Tomotherapy or ‘slice therapy’ describes an approach to deliver IMRT using a narrow rotating slit beam [44-46], similar to techniques used for computed tomography (CT) imaging scans. The linear accelerator rotates during delivery and the beam is modulated during rotation. A temporally modulated slit MLC is used to rapidly move the leaves in or out of the slit and, in the same method used in a CT unit, the radiation source and the collimator continuously revolve around the patient. Either the patient is moved between successive rotations (serial tomotherapy) or during rotation (helical tomotherapy).

1.1.2.2.1.1 Serial Tomotherapy

A temporally modulated binary mini MLC was developed commercially by Peacock MIMiC, Nomos Corporation and became available in 1996. Serial tomotherapy uses this Peacock system MIMiC, mounted to a medical linear accelerator, and can deliver treatment to a narrow slice of the patient using arc rotation. The beam is collimated to a narrow slit (usually 2cm x 20cm) and beamlets of varying intensity are created by driving the MIMiC’s leaves in and out of the radiation beam’s path as the gantry rotates around the patient. The modulation of the beam is created by computer controlled opening and closing of the leaves and the leaf opening pattern is predetermined by the treatment planning system. The relative intensities of each beam are determined by the fraction of arc travel that each leaf is open.

As a result of the narrow spacing between the independently modulated segments, there is greater flexibility in modulating the fluence, allowing for highly conformal dose distributions [47,48]. A full treatment is accomplished by serial delivery to adjoining axial slices. As such, accuracy in the couch motion is imperative (especially with irradiation of large areas), as the treatments are delivered in a series of adjacent arc strips. Even errors of 1mm can result in dose errors of 10-20% in these adjacent (or abutment) areas [49-51], depending on the isocentre and arc length used. Reports have suggested that shorter arc lengths are associated with higher dose errors [51], whereas arcs of 300 degrees are able to maintain an abutment homogeneity of approximately 10% [52].

The first clinical use of IMRT was undertaken in Houston, Texas using the Peacock NOMOS MIMiC delivery technique in 1994, where a variety of patients were treated with tumours of the CNS, head and neck and prostate and also in those who had been previously irradiated [53]. They demonstrated the feasibility of dose escalation as a way of attempting to improve tumour control, in addition to introducing the concept of SMART (simultaneous modulated accelerated radiation therapy) boost to shorten the overall treatment time.

1.1.2.2.1.2 Helical Tomotherapy

Helical tomotherapy was first defined by Mackie et al in 1993 [44], whereby radiation could be delivered in a continuous spiral. They described a system of delivering IMRT while the patient on the treatment couch is moved through a moving ring gantry, in a similar way to a helical CT scanner.

Helical tomotherapy may address the abutment heterogeneity problem posed by serial tomotherapy since it delivers IMRT in a continuous manner as the patient is moved through a ring-gantry during treatment, rather than delivering a series of adjoining strips of radiation. The intensity of the beam is modulated throughout delivery by dynamic MLC movement, whilst the dose rate and gantry speed are kept constant. The beamlets are created using temporally modulated binary mini-MLC similar to the Peacock's system and also uses a low energy linear accelerator mounted in a modified CT scanner gantry.

Helical tomotherapy can generally achieve similar dose distributions to static field MLC based IMRT with variable results on treatment times.

1.1.2.2.2 Intensity modulated arc therapy

The basic theory behind arc therapy is to deliver radiation treatment from a continuous rotation of the gantry. Intensity-modulated arc therapy (IMAT), first proposed by Yu et al in 1995 [54,55] as an alternative to tomotherapy, delivers radiation using superimposing arcs and can be implemented on existing linear accelerators equipped with MLCs to combine the spatial and temporal intensity modulation with movement of the gantry. MLC-shaped fields, with the ability to change during gantry rotation, are used to deliver dose to the target. However, in order that the gantry can move continuously throughout treatment delivery, the changes in MLC leaf positions between the consecutive gantry positions often need to be limited. Initial studies have tried to overcome this issue with the use of multiple superimposed treatment arcs, although this has frequently resulted in an increase in radiotherapy treatment times [54,56,57].

The optimization of this dynamic gantry motion is usually carried out by taking a 'sample' or snapshot of the gantry and MLC positions at a particular time point during the delivery. The continuous gantry and MLC motion is then approximated by individual beams that are optimized at 5-10 degree gantry angle intervals and causes changes in MLC leaf positions of 2- 4cm between the gantry angle samples [56-58]. However, poor sampling may lead to a reduction in quality and the potential for dosimetric error [57], whereas increasing the sampling at smaller gantry intervals may restrict the ability of optimization and leaf sequencing algorithms to provide an efficient and acceptable plan.

RapidArc® (Varian Medical Systems, Palo Alto, CA) or volumetric modulated arc therapy (a solution to IMAT) was first approved for clinical use in 2008 by Otto [59]. He described a system where treatment could be delivered efficiently and accurately using a single dynamically modulated arc. This has the capability of delivering IMRT with different monitor units at varying dose rates while MLCs are continuously moving as the gantry is simultaneously rotating with variable speed and, therefore, has the potential to deliver intensity modulated radiation more efficiently than static field IMRT.

An aperture-based algorithm has been utilized for treatment plan optimization, where dose can be delivered during a single gantry arc of 260 degrees. Although this is a similar technique to tomotherapy, it is different in that the entire dose volume is delivered in a single source rotation, rather than with several slices. IMAT uses multiple irregular fields shaped with a conventional MLC during gantry rotation and is planned as a series of static fields, every 5-10 degrees apart, but delivered with multiple superimposing arcs; the MLC shape continuously changing as a

function of gantry angle on the basis of the results of optimization, such that the cumulative intensity distribution leads to the desired dose distribution. In this technique, dose is delivered using single or multiple radiation beams which sweep in an uninterrupted arc or arcs around the patient. The intensity of the radiation beam is modulated throughout delivery by varying the dose rate and speed of the gantry rotation as well as dynamic MLC movement.

Other IMRT techniques, such as static field IMRT, can increase treatment times by requiring a larger number of beam directions, monitor units and, in the case of tomotherapy, with slice by slice delivery. With these techniques and through the development of image guided positioning and plan adaptation, treatment times may be increased. In contrast to static field IMRT, the MLC leaf motion and number of monitor units per degree of gantry rotation with arc therapy is restricted during optimization so that the speed of gantry movement, speed of leaf translation and the dose rate maxima do not limit the delivery efficiency. Otto presented work that demonstrated efficient treatment with a single arc producing high dose conformality and high-resolution sampling of beam directions during planning (starting with a smaller number of samples and gradually introducing new samples). He also documented that delivery times using VMAT can be reduced to approximately 1.5-3 minutes for a 2Gy fraction [59]. In fact, others have proceeded to examine the potential advantage that VMAT offers over static field IMRT when treating various sites of disease [25,60-63]. A direct comparison of static field IMRT and RapidArc (RA) using either 1 or 2 arcs for treating prostate cancer found that treatment times were reduced by 2-7 minutes using RA compared to static field IMRT with a monitor unit reduction of between 37-66% [60]. A further study demonstrated a reduction of 63% in average treatment times (165 seconds with RapidArc and 447 seconds with static field IMRT) and a 60% reduction in monitor units with RapidArc (550 MU

compared to 1379MU with static field IMRT) when treating nasopharyngeal cases [25]. A review in 2013 documented that VMAT treatment typically took 2.08minutes (with SRS/SBRT taking 4.06 minutes) and required an average of 285 monitor units (compared to 317MU for the radiosurgical group), providing a monitor unit reduction of 45% in prostate cancer patients, 58% in head and neck cancer patients and 39% in lung cancer patients, although this was seen in a retrospective review involving small patient numbers [61].

In this way, VMAT works by simultaneously varying the gantry rotation speed, treatment aperture shape with MLCs and delivery dose rate [64]. Arc based therapies have the ability to achieve highly conformal dose distributions. The added advantages of RapidArc over static field IMRT appear to be a reduction in treatment times and monitor units required, which may in turn have benefits of a reduction in leakage radiation and therefore a reduction of integral radiation dose to the rest of the body [58,65,66], with less interfraction movement, more accurate treatment delivery and a potential reduction in second cancer risk. This, theoretically, can produce further benefits, including greater patient tolerability, cost effectiveness with quicker and efficient use of machine time.

1.1.2.2.3 Robotic linear accelerator IMRT

The use of a small linear accelerator mounted on an industrial robot is now being used in the clinical setting. The initial idea of highly focused radiation using many beams centred on one point was developed for radiosurgery using the Gammaknife system [67,68]. This consists of cobalt-60 sources distributed through a dome shaped shell so that beams can be focused on a common point. To ensure highly focused treatment, a stereotactic frame is anchored to the patient's skull. However,

this technique is limited to use for central nervous system tumours, although the idea has subsequently been proposed for other clinical settings [69-71].

Stereotactic body radiation therapy (SBRT), delivered using systems such as CyberKnife (Accuray, Inc., Sunnyvale,CA) utilises a 3D co-ordinate system with advanced imaging technology to allow precise tumour localisation. In this way, a stereotactic frame is not required and treatments can be delivered to anywhere in the body, with the added advantage of delivering fractionated treatments if required. This technique uses high levels of accuracy in patient immobilisation and target localization with methods to limit or compensate for tumour movement. Through minimal margins for set up uncertainties and increased normal tissue sparing, delivery of hypofractionated regimes becomes possible. The CyberKnife system, uses a compact linear accelerator mounted on a robotic arm, which can then be moved along predetermined, non-concentric paths around the patient to allow for very conformal therapy [65,71]. This technology can deliver concentrated beams of radiation to the target from multiple positions and angles. Using image guidance, CyberKnife can track the target co-ordinates in real time, allowing the head of the linear accelerator to re-align itself and accommodate any changes in the target position. As a result, high doses can be administered in 1-5 fractions to smaller, harder to treat areas, while also reducing organs at risk. This technique can be useful in patients who have small curable tumours who are not suitable for surgery or in those that have received previous radiation.

In order to deliver dose to a target, stereotactic radiotherapy does require a larger number of monitor units compared to conventional treatments and there have been reports of radiation leakage in older systems, with more recent systems needing additional shielding to reduce this issue.

Unless otherwise specified, MLC based IMRT will be discussed for the rest of this thesis.

1.1.3 Features of IMRT

Several features of IMRT make its use an advantage to the clinical setting.

1.1.3.1 Concave dose distributions

Traditional conformal radiotherapy can produce convex dose distributions. As each of the beams with uniform fluence (as in 3D-CRT) is brought together around an isocentre, a convex volume will be created. This can be suitable for some tumour volumes, however at least 30% of tumours show a concavity in the planning tumour volume [6] and for others, which are close to critical structures, such as in the case of tumours of the central nervous system or where concaved shaped tumours wrap around the spinal canal (as with tumours of the head and neck area), 3D-CRT often fails to produce an acceptable plan [5].

Conversely, with IMRT techniques, the volume at the intersection of fluence modulated beams will have invaginations and therefore will be concave in nature. Treatments can be constructed so that the high dose volume conforms tightly to the shapes and boundaries of the planning target volume, whilst the organs at risk lie in the concavities of the dose distribution. The advantages of this technique are improved target volume conformality, particularly with complex concave shaped volumes. This, in turn, can provide sparing of normal tissues and organs at risk with reduced acute and late toxicities and morbidities [21,22,72].

1.1.3.2 Normal organ sparing

The ability to create shaped dose distributions with IMRT can be exploited to create sharp dose fall offs near the boundaries of the target and critical structures, thus producing a significant reduction in radiosensitive normal tissue areas receiving high dose radiation. If areas close to the PTV are defined (usually as shaped concavities), IMRT can produce dose distributions that imitate these concavities and therefore allow for sparing of normal tissue within these areas. This may, in turn, allow dose escalation in addition to a reduction of normal tissue dose [73,74].

1.1.3.3 Dose homogeneity

Intensity modulated beams from varying directions can be designed to produce dose homogeneity within the target site in comparison to more conventional techniques, allowing sparing of normal structures and superior dose conformity [3]. However, in addition, IMRT can produce intentional dose inhomogeneity or non-uniform absorbed-dose distributions of a certain volume within another defined volume (also known as simultaneous integrated boost techniques) [44].

1.1.3.4 Multiple simultaneous treatments

The features of IMRT allow multiple targets and boost fields to be integrated into a single treatment plan during the whole course of a treatment. This can be more efficient and also optimises the overall doses by considering the interactions of different dose prescriptions. Previous studies, in particular for head and neck cancers, have demonstrated improved tumour control and survival rates with accelerated treatment schedules, some of which have used altered fractionation

and modest dose escalation [75-77]. However, the associated increased toxicity seen with 3D-CRT techniques can limit its use.

IMRT can produce inhomogeneous dose distributions which can be exploited to allow the simultaneous delivery of different doses per fraction to separate areas within a target volume. In particular, during the treatment of head and neck cancer, it is possible to treat more than one volume simultaneously without the need for matching fields, which in turn comes with risk of reduced dose coverage in the area of matching beams. Therefore multiple targets and boost fields can be integrated into a single treatment plan during the entire course of a treatment without actually increasing the overall treatment time. A simultaneous modulated accelerated radiation therapy (SMART) boost technique was developed in 1994 to increase tumour control and allows a larger dose per fraction to the primary tumour, while simultaneously delivering conventional fraction sizes to areas of microscopic disease and whilst delivering this in 5 fractions per week [53,78].

The approach of 'simultaneous integrated boost', a term coined by Wu et al in 2003 [79-81], through its accelerated fractionation, can also manipulate the radiobiological benefits by reducing the effects of accelerated repopulation in tumourogenesis [82-85]. The high dose conformality with IMRT provides the opportunity to do this with the added benefits of reducing normal tissue toxicity by avoiding normal tissue and organs at risk. A phase I study looked at using this regime when treating patients with head and neck cancers [79]. They were able to escalate doses to the gross tumour volume using accelerated fractionation simultaneous integrated boost IMRT with doses up to 73.8Gy, whilst delivering lower doses to the margins around the GTV and uninvolved nodal areas as well as

sparing at least one parotid gland. More recently, similar techniques have been employed to use varying dose per fraction to different target volumes [27].

In a similar way, simple IMRT methods have been used to increase the dose to specific areas of a tumour. A group in the 1990s used MR spectroscopy to identify the dominant intraprostatic lesion corresponding to the area of gross tumour and utilized 18-20 fields and subfields to minimize dose to the rectum, treat the whole prostate to 73.8Gy, whilst simultaneously boosting the area of gross tumour to a higher dose (>90Gy) [86].

The use of larger dose per fraction theoretically may be associated with an increase in late normal tissue radiation effects in structures with a low alpha:beta ratio, such as nerves within the high dose PTV. However, long term follow-up is essential to determine whether this will be clinically significant.

1.1.4 IMRT planning process

1.1.4.1 Immobilization and reproducibility

One of the benefits of IMRT is the ability to produce high dose gradients adjacent to critical normal tissue structures. As a result, reducing patient movement and internal organ motion has become critical for IMRT as dose distributions mould closer to the tumour volume or organ at risk with rapid fall off outside the volume. Thus even a small movement may result in a dramatic difference in dose delivered to a specific volume. With the reduction of areas irradiated to high dose levels with IMRT comes the possibility of geographical miss, as well as longer treatment times

[87]. This may, to some extent, be overcome with four dimensional adaptive image guided radiotherapy.

Adequate immobilization techniques are required to ensure that treatment can take place with accurate and reproducible positioning of the patient. Typically, for tumours of the head and neck or brain, customized thermoplastic shells are used to immobilize the patient during treatment and have been shown to allow a movement error of less than 3mm [88].

In the past stereotactic frames have been used for cranial irradiation and, in particular, skull base tumours [89,90], although less invasive devices such as ankle stocks can also be used for IMRT treatments, for example, when treating tumours of the prostate [91]. However, in general, the necessary degree of accuracy depends on the proximity of the high dose region to organs at risk and the fall off dose around the tumour volume.

Another important consideration is the issue with intra-fraction movement and in particular the uncertainties with internal organ motion. The effects of internal organ motion can be reduced by tumour immobilization or tumour tracking.

The motion of the prostate has been shown to reduce by maintaining a constant bladder and rectal volume [92,93]. Whereas, the motion of the lung by respiration means that accuracy of patient set up has become more challenging. Intra-fraction motion, if not recognized adequately, may lead to a reduction in coverage of the

tumour volume, geographical miss and even an increased dose to organs at risk. Four dimensional 4D CT scanning can allow visualization of the tumour position within the respiratory cycle, so that this can be incorporated into radiotherapy delivery [94] using various techniques, such as the inclusion of tumour movement within the PTV, reducing tumour motion by employing breath hold techniques [95-98], gating of radiation or even marker tracking [99], though these methods do require patient and operator training to ensure adequacy of reproducibility.

There has been intensive investigation into tumour tracking using image guided radiotherapy, offering the possibility of 'real time' tumour tracking. Some methods have used implantable markers, such as fiducial markers for prostate cancer [100] and, more recently, wire clips for breast cancer [101,102]. This involves the incorporation of imaging before and/or during treatment to enable precise verification of treatment delivery and allow for adaptive strategies to improve accuracy of treatment [103,104]. With this comes a requirement for more time on the treatment couch and possibly an increase in the total amount of radiation to patients, especially in those with daily IGRT schedules.

1.1.4.2 Delineation of target volume and critical structures

The success of modern radiotherapy techniques is dependent on the delivery of adequate doses to the tumour, while minimizing dose to organs at risk (OAR). The International Commission on Radiotherapy Units and Measurements (ICRU) has issued several reports to standardise the prescribing, recording and reporting of radiation treatments [105-110]. ICRU 50 introduced the concept of the gross tumour volume (GTV), clinical target volume (CTV) and planning target volume (PTV) [106]. These were refined in the supplement ICRU 62, which allows the

definition of more than one CTV and also introduced the concept of the planning organ at risk volume (PRV) [107]. ICRU 83 further extended these concepts to the prescribing, recording and reporting of IMRT [110].

IMRT planning involves delineation of the target volumes and OARs. The benefits of IMRT depend heavily on the accuracy of the outlined target and critical organs, which should be identified and outlined precisely using one or more imaging techniques. The existence of intra- and inter-observer variation in GTV delineation is well-documented and varies with the tumour site and imaging modality [111,112]. However, variation due to operator inexperience is also recognized and can be improved with training [113]. Multimodality imaging can enhance our knowledge on the extent of disease to be treated and plays an important role in the IMRT process. Such imaging includes CT scans, magnetic resonance imaging (MRI) and, more recently, Positron Emission Tomography (PET) imaging and it is now quite common to fuse these imaging modalities with the CT planning scan to improve target definition [114].

The degree of conformality is a direct function of the resolution power of the diagnostic tools used to define the true anatomical dimensions of the tumour and its relationship to surrounding organs. The improvements in conformality have been enhanced by computerized imaging techniques with the ability to visualise the tumour in three and, now even, four dimensions.

As with conventional planning, the PTV margin is composed of the internal margin (accounting for organ motion) and set-up margin (allowing for set up inaccuracies)

[107]. A further report discussed the systematic error margin and random error margin during planning and treatment delivery, which can contribute to set-up errors and therefore guide the PTV [115]. Systematic errors are those related to treatment preparation, including errors related to delineation, phantom transfer errors and systematic set-up errors, whilst the random error margin represent those related to treatment execution and include set-up errors and target motion.

Precise delineation or contouring the OAR is an important step in RT planning to guide the algorithm on how to form the desired 3D dose distributions. However, with the use of IMRT, it is imperative to contour *the entire* sensitive organ within the irradiated volume, rather than only that seen within the PTV. If this is not done, the planning optimizer may 'dump' inappropriate dose in areas that have not been contoured. Therefore, it is important to identify and define organs or tissues to avoid unwanted dose dumping in these areas.

In fact, due to the number of beams used in IMRT delivery, one needs to be wary of all potential organs at risk. A recent parotid sparing technique, whilst identifying benefits of IMRT in the preservation of salivary function, also incidentally detected a proportion of patients with acute fatigue, in comparison to those treated with 3D-CRT. Further exploration of this has detected significantly higher mean doses to the posterior fossa, brainstem and cerebellum, possibly due to the differing beam portals used [116].

Sensitive normal structures can be considered to be functionally 'serial', 'parallel' or 'serial-parallel'. OAR, such as spinal cord, brain stem, optic nerves and chiasm,

have a high relative seriality so that doses above tolerance limits to even a small volume or subunit of these organs may have severe clinical consequences. However, in organs with a lower relative seriality, the relative risk of damage is often related to the size of volume that is irradiated above a tolerance level. Nevertheless, a PRV margin, analogous to the PTV, is added to further protect the OAR from over-dosage as a result of uncertainties in radiotherapy planning and delivery and may be helpful to allow dose escalation in the vicinity of critical structures.

3D-CRT can offer a partial reduction in the volume of serial organs that are irradiated but, due to their organisational nature, this may not always result in a reduction of toxicity. In these situations, it is common to compromise dose to PTV. IMRT offers a more conformal dose distribution, aiming to avoid these critical structures with the use of concave dose distributions and therefore improving dose to PTV.

1.1.4.3 Treatment planning, objectives, optimization and evaluation

1.1.4.3.1 Treatment planning and optimization

Treatment planning and computer optimization make up the core of IMRT. These processes translate clinical requirements into machine deliverable commands. IMRT plans can be created by using either the ‘forward planning’ or ‘inverse planning’ method [3].

1.1.4.3.1.1 Forward planning

Many aspects of radiotherapy planning require a manual iterative process, often starting with pre-defined beams resulting in desired dose distributions. However, simple IMRT methods have been used for quite some time [5,117,118], utilizing existing 3D treatment planning systems and iterative optimization, with a trial of beam configurations, wedges and weighting. Forward planning IMRT uses similar methods to those used in conventional 3D-CRT, where planners initially define beam directions, shapes and intensities on the basis of planning experience and intuition. Optimising beam orientation with fewer optimally placed beams could be better than using a larger number of sub-optimally or uniformly placed beams and, therefore, leads to more efficient IMRT treatments.

This is followed by a calculation of the 3D dose distribution and subsequent qualitative review of this dose distribution, with plan improvements made by further modification of the beam geometry (beam orientation, shape, modifier, weighting) to improve target coverage or reduce organ at risk dose if necessary. It can often be described as a trial and error process, in which treatment fields and beam weights are modified manually to achieve clinical solutions. It works well for simple shapes that are not surrounded by numerous critical structures. For more complex tumour geometries (such as concave tumours and those surrounded by sensitive structures), forward planning may be limited by the restricted variation in beam intensity within the beam.

A step beyond forward planning, known as ‘aperture-based optimization’, involves the design of several beam shapes for each beam angle and computer optimization to determine intensities or weightings of these beam shapes in all angles [119].

This has the advantage that the planner can control the complexity of a treatment, and is less dependent on the expertise of the planner. Another variation on forward planning, is to select a number of segments or subfields allowed for each beam and for computer optimization to determine the shape of each segment and its associated weighting [120]. These plans often consist of multiple subfields with MLC shaping and are designed to reduce dose to normal structures; commonly termed 'field in field' planning. This progressive form of forward planning may produce comparable plans, in term of quality, to those produced using inverse planning, although with much simpler treatment delivery. Forward planning is possible for some forms of IMRT using segmented field optimisation and initial attempts were made to spare salivary function using this technique when treating head and neck tumours [121]. However, these isodose plans often have large areas of dose inhomogeneity. This method may well be ideal in tumour sites that are surrounded by less sensitive structures, such as breast tumours [122]. However, manual forward planning can be too time consuming for more complex planning problems.

1.1.4.3.1.2 Inverse Planning

IMRT is now capable of generating complex 3D dose distributions to conform closely to the target volume and uses the concept of 'inverse planning' with significant reductions in dose to normal tissue [5]. In contrast to forward planned IMRT, inverse planning begins with a desired dose distribution and planning constraints decided at the outset. With inverse treatment planning, the focus is on the desired outcome, rather than how it will be achieved.

A computer optimisation system is used to adjust beam parameters (usually beam intensities), in an attempt to create fluence distributions that approximate the

desired dose distributions, with the quality of the resultant plan evaluated by a score. The process of inverse planning includes three components, including formulation of the score function (also known as objective function or planning objective), input of dose constraints to tumour targets and normal tissues and methods of computer optimisation that search for optimal plans. An optimisation algorithm is utilised to optimise the dose intensity delivered from each beam to create optimal target volume coverage, whilst avoiding the organs at risk. The iterative inverse planning methods allow many treatment plans to be generated and evaluated prior to arriving at the best solution. This method is capable of generating significant dose gradients between target volumes and adjacent normal structures to provide the required dose-volume prescription [48]. In order for this to be achieved, dose-volume constraints or limits need to be set. These specifications act to drive the computer aided optimisation, so that the constraints are met and the best plan achieved.

The ideal plan should comprise high uniform dose to the tumour and minimal dose to the organs at risk. This is often performed through an optimisation process that translates mathematical formalism of clinical requirements into deliverable intensity patterns. In reality, however, the best plan is a compromise on what is clinically required and what is achievable. This often comes with experience to select appropriate planning parameters and, as experience is gained, ‘class solutions’ are created in order to minimize planning time. Planning studies offer opportunities to assess the advantages of new techniques within each tumour site. Rival techniques can be compared and the best technique used as a basis of a ‘class solution’: a technique that will produce the best results when applied to a group of patients with a particular tumour type [6].

Plan objectives are the mathematical translation of clinical objectives which aim to quantify the underlying clinical goal. Objectives are set for the tumour as well as the organs at risk. The response of tumour and normal tissues is a function of radiation doses, and also of the volumes subjected to each dose level (depending on the type of tissue). Dose-based prescriptions define the dose that the tumour or organ should receive, for example, 60Gy to the PTV. Dose-volume-based objective functions are expressed in terms of limits on the volumes of each structure that may be allowed to receive a certain dose or higher; for example, no more than 5% of the PTV should get less than 60Gy. There is also consideration to be made in areas where the PTV and organ at risk overlap. These overlap areas are considered separately to the rest of the PTV and may be designated a slightly lower dose.

Objectives and constraints are often used interchangeably. However, there is an important distinction between the two terms: objectives are doses that are desired to be met, whereas a constraint is something that must be met. Specifications of these objectives and dose constraints are the only direct input required to steer the inverse planning system towards the desired plan. Unrealistic constraints can lead the computer optimized system to produce an inferior plan. Planning objectives can also be considered as planning tools to achieve the real clinical goals. The key is to prioritise each planning objective and constraint so that the optimiser produces the most desirable plan in terms of tumour dose coverage and normal tissue sparing. These planning objectives and constraints often require modification and weighting to drive the plan to a better clinical solution; often a process of trial and error and frequently the most time consuming part of the planning process. This may involve a certain amount of compromise to the tumour volume to allow adequate sparing of the organs at risk. The inverse planning problem can be specified as a best cost

score; maximizing the tumour control probability (TCP) and allowing for a maximum normal tissue complication probability (NTCP).

1.1.4.3.1.3 Treatment generation (Leaf sequencing)

An IMRT optimised dose distribution needs to be transferred into machine deliverable parameters. Linac-based IMRT requires the formation of leaf position sequences as a function of monitor units (MUs) and beam on time. Conventional MLCs under computer control can be used to deliver IMRT in 3 distinct ways:

1. Sliding window or Dynamic MLC (DMLC).

In fixed gantry positions, this method allows the opening formed by each pair of opposing MLC leaves to be swept across the target volume under computer control whilst the radiation beam is on to produce desired fluence, during which time the gap opening and speed can be optimally adjusted. As the gap slides across a point, the radiation received by the point is proportional to the number of monitor units (MUs) delivered during the time the tip of the leading leaf goes past the point and exposes it, until the tip of the trailing leaf moves in to block it again [123].

2. Step-and-shoot or segmental MLC (SMLC).

This method uses a series of multiple segment fields, where each field is composed of multiple MLC shapes (segments or subfields) delivered from the same gantry angle. The multiple segment fields are set up at selected orientations of the gantry under computer control. However, radiation is only turned on when the MLC leaves are stopped at each prescribed segment position, so that the MLC leaves only move to discrete positions when the beam is off.

3. Intensity modulated arc therapy (IMAT).

This MLC method is similar to that seen in dynamic MLC, although the radiation remains on, not only with movement of the MLCs, but also during rotation of the gantry.

1.1.4.3.2 Plan evaluation

Plan evaluation plays a critical role in defining the original objectives and evaluating the final optimisation results. It involves the assessment of dose, dose–volume and dose-response models to adequately and quantitatively assess the merits of different IMRT plans. This necessitates slice by slice review of the individual isodose distributions, with particular attention to hot and cold spots, which can cause damage to target or normal tissues. If the criteria are not met, it is essential to assess the key limiting factors and whether there are dose constraints that may be impossible to achieve, perhaps due to proximity of the tumour volume to the organ at risk. It is also important to consider areas that are not truly organs at risk, but where planning systems will 'dump' dose in order to allow for better compliance with specified objectives. In such cases, 'dummy volumes' are created to reduce dose to otherwise unassigned normal tissue.

Acceptable dose to the PTV is usually set at +7% and -5% of the prescribed dose. However, for each organ at risk, there is a maximum acceptable dose and goal dose that needs to be adhered to. In these situations, it is important to have an indication of whether the tissue is in-parallel or in-series. There are now dose-volume complication correlations derived from large groups of patients [124,125].

1.1.4.4 IMRT reporting and prescribing

ICRU 83 recommends that the median absorbed dose specified as $D_{50\%}$ should be reported [110]. The $D_{50\%}$ is likely to be a good measure of a typical absorbed dose in a relatively homogeneously irradiated tumour. Therefore it is appropriate to use the median dose for both reporting and prescribing. The near-minimum ($D_{98\%}$) and near-maximum ($D_{2\%}$) values are preferred, as the actual minimum and maximum doses may occur only in a few voxels due to noise or rounding errors in the calculation and may not be representative of dose in the PTV.

Typically plans are also assessed on ability to produce homogeneous and conformal plans. The homogeneity index (HI),

$$HI = \frac{(D_{2\%} - D_{98\%})}{D_{50\%}},$$

can be useful to give an indication on the homogeneity of a plan, with HI levels nearer to 0 suggesting a higher level of homogeneity.

The Conformity index (CI),

$CI = \frac{TV_{95\%}}{PTV}$, where $TV_{95\%}$ = treated volume covered by 95% isodose,

originates from ICRU 62 documentation. However, ICRU has made no formal recommendations on how best to calculate the CI for use in cases of IMRT and its applicability may be limited. However, alternative measures of CI also exist [126],

$$CI = \left(\frac{TV\ PI^2}{TV\ x\ PIV}\right)\ x\ 100\%,$$

where TVPI = volume of target covered by the prescription isodose and PIV=volume of prescription isodose.

The conformity gives a reasonable indication of how conformal a plan is, with CI of 0 indicating a complete miss, and CI values of 100 suggesting perfect conformity.

1.1.4.5 Quality Assurance (QA)

In view of the use of mathematical optimization and beam intensity modulation, IMRT treatment planning and delivery are more complex and less intuitive than conventional 3DCRT techniques. Quality Assurance (QA) becomes a vital step in the IMRT process, to guarantee that "what you plan is what you get". It is feasible that the potential for dose error can be greater for IMRT treatments, because a much steeper dose gradient is, invariably, used near to tumour and critical structure boundaries. Reports have suggested that a 7-10% difference in dose delivery could produce significant change in tumour control probability [18].

Verification is undertaken both before and regularly during treatment to ensure that any underdosage to the tumour and overdosage to the organs at risk is prevented by minimising the systematic and random errors. Accurate verification of treatment delivery entails both quality assurance of the planning and delivery techniques, as well as verification of the treatment for the individual patient. Therefore, quality assurance comprises 2 broad areas: patient QA and equipment QA, although these are not entirely specific for IMRT.

Patient QA encompasses patient set up, absolute dosimetry, relative dosimetry and fluence verification. Patient set-up is key to ensuring accurate treatment. A variety of image guided localization techniques have been used with IMRT treatments, from simple orthogonal films to beams-eye view portal films with IMRT intensity pattern overlay, daily electronic portal imaging (EPI) of implanted fiducial markers, daily ultrasound guided localization and integrated tomotherapy solutions.

Orthogonal images have been used in abundance for verification of the isocentre position. Reference images can be simulator images or digitally reconstructed radiographs. Field sizes were chosen to include the necessary anatomy in order to perform accurate field matching. However, the use of modern devices can also enable 3D volume verification using kilovoltage (kV) cone beam CT and in vivo dosimetry has proved popular with improvements in IMRT techniques and IGRT.

The gamma index is the preferred IMRT quality assurance tool for assessing agreement between phantom measurements and the treatment plan. The gamma index scrutinizes how well the distributions agree within specified acceptance criteria in terms of dose difference and distance-to-agreement distributions and are measured in a phantom [127]. A good QA phantom should have the following features: tissue equivalent density, multiple measurement points/planes, the ability to enable measurement from different gantry angles, easy and quick set-up as machine time is being used. The ionization chamber should measure point doses (i.e. have a small measurement volume, rather than measuring the average dose over a large volume), give accurate and reproducible measurements and measure accurately at low doses for organs at risk (i.e. have a low leakage rate). A daily output correction factor is needed to normalise the measured reading to remove any

daily variation in the linear accelerator's output dose (which has a daily tolerance of +/- 1.5%). The phantom is subsequently set up to deliver the IMRT plan with the chamber positioned at the chosen dose point. Readings are taken for each beam angle individually and can be summed for a total reading, following which a dose can be calculated.

To verify treatment set up accurately and efficiently, EPI is essential. It can be used to verify the individual intensity maps and dose delivered.

Films can also be used for QA. They give a measurement of optical density, performed by creating a calibration curve (plotting optical density against dose in the film). The calibration film is often exposed at the same time as the QA measurements. Small areas of the film are exposed to known doses and the resulting optical density is then plotted against the dose given. The ideal film is one with a linear response between optical density and dose across the dose range of interest. The film is scanned into an appropriate software application; the optical density is converted into dose and then compared to the dose plan predicted by the treatment planning system.

Arrays of detectors can be used to combat the time consuming problem of checking absolute dose at a range of positions. However, arrays must be large enough to cover the region of interest and to provide discrete measurement points. They must be easily manoeuvrable, provide instantaneous read-out and have the facility for quantitative analysis of distribution. The dose at each detector can be compared and the dose mapped onto the dose distribution. The quantitative measure used to

assess the dose distribution is the gamma analysis. Arrays are often preferable to film as they provide instantaneous results without the need for film processing.

Most linear accelerators have a portal imager which can be deployed during treatment. They allow fluence maps to be checked during a patient's treatment as well as in patient-specific QA. Check programmes, used to independently check the monitor units before any radiotherapy is given, are more complex than with non-IMRT plans due to the large number of fields, size and angle of beam delivery. There is also additional dose from transmission through, or leakage between, the MLC leaves.

Equipment QA involves assessment of the MLC leaf positioning and gap testing. This should include testing of the motion, movement and repositioning of the leaves. MLC position errors may present potentially significant dose delivery errors, for example, an error as small as 1mm in leaf opening can produce a 10% error in fluence delivery [40,128].

1.2 Clinical Use of IMRT

Since its conception, IMRT techniques have been described in many clinical retrospective case series. There have also been many comparative studies with conventional radiotherapy, although very few data from randomised controlled trials [23,72] to substantiate that IMRT has an advantage over conventional radiotherapy.

However, IMRT is now becoming part of the standard treatment of patients in many tumour groups.

1.2.1 Indications for IMRT

IMRT may be considered in cases with irregularly shaped targets and tumours close to critical structures. It can cover a volume with narrow margins to protect adjacent structures and can also be considered in a nearby previously irradiated area.

Ideal tumour sites for IMRT should have a positive response to radiation dose with the potential to dose escalate and, therefore, improve local control. Most benefit is seen in tumours that are in close proximity to critical structures or close to a previously treated area (to take advantage of the sharp gradient) and in those where treatment margins and set up inaccuracies are minimal.

Previous radiotherapy studies have looked at various aspects of IMRT. Some have investigated the benefits of IMRT planning in comparison to other methods. Verhey et al. compared conformal and different IMRT plans on 3 patients (with prostate, nasopharynx and paraspinal tumours), demonstrating that the IMRT plans can produce significantly better dose results at the expense of planning time and resources [5]. Others have demonstrated the use and tolerability of IMRT to treat prostatic lesions, up to a dose of 90Gy without exceeding normal tissue tolerances [86,129]. Cardinale et al. found improved conformity and reduction in normal tissue dose with IMRT compared to radiosurgery or standard conformal treatments for brain tumours [130]. Other groups have examined the dosimetric aspects of clinical IMRT treatment techniques and some have reported the outcomes of patients

treated with such techniques. Several groups have demonstrated that IMRT provides an answer for complex planning problems, with surrounding normal tissues limiting prescription dose, for example, in the delivery of high doses to the prostate, whilst limiting rectal toxicity, or similarly for the treatment of head and neck cancers [36,131-133].

IMRT is now being utilised in a variety of tumour sites, most notable in the fields of prostate cancer and head and neck malignancies. Prostate cancer has been one of the initial targets for IMRT worldwide, with the aim of allowing dose escalation to the prostate and pelvic nodes to improve clinical outcomes, whilst simultaneously trying to limit dose to adjacent organs at risk and thereby improving long term toxicity [134-138]. IMRT has also been used to deliver hypofractionated schedules (using 70Gy in 2.5Gy), with rectal late toxicity rates of 5%, in comparison to 12% with 3DCRT [139].

Head and neck cancer radiotherapy can be challenging due to the complex anatomy with bony structures, soft tissues and air cavities in close proximity. Due to the aggressive nature of these tumours, dose escalation is often preferred to gain local control, but can be difficult to achieve due to the proximity of critical structures. In fact, it is difficult to deliver high doses using conventional 3D conformal radiotherapy to some head and neck tumours without significant toxicity to organs, such as parotid glands. IMRT, on the other hand, has been shown to reduce late toxicity such as xerostomia from 74% to 40% in the first year after radiotherapy, through sparing of parotid glands, and without affecting treatment outcomes [24,27,121,140]. There is now increasing interest in trying to prevent other

debilitating long term toxicities, such as dysphagia and sensorineural hearing loss from irradiation of the cochlea [24,141].

One can also exploit the ability to create various dose distributions with IMRT to deliver different doses and potentially dose escalation to head and neck volumes without the need to extend overall treatment times. This can be achieved with the simultaneous integrated boost or simultaneous modulated accelerated radiotherapy techniques highlighted earlier [79], to allow a form of dose painting within a target volume.

Similarly to head and neck tumours, radiotherapy can be challenging for the treatment of central nervous system tumours and especially intracranial tumours due to the proximity to dose limiting critical structures. IMRT has been used to achieve superior dosimetry for glioma treatments compared to conventional 3D-CRT [142], with improvements in progression free survival [143]. Similarly, IMRT has been used to spare the spinal cord during treatment of primary and metastatic disease of the spine, including cases of re-irradiation without spinal cord complications [144,145], whilst also enabling moderate dose escalation [146].

The use of IMRT in the paediatric setting remains controversial due to the potential long term risks of second malignancy highlighted in the literature [147,148]. However, there have been a number of studies demonstrating improvements in normal tissue toxicity, such as reductions in ototoxicity from 64% to 13% with IMRT for paediatric tumours [149].

There is now also interest in the use of IMRT for the treatment of other cranial tumours, including meningioma.

1.2.2 Meningioma

Meningiomas describe a group of tumours originating from the meningeal coverings of the brain and spinal cord, and are by far the most common intracranial tumour [150-152]. In fact, it is estimated that 2-3% of the general population have an asymptomatic meningioma. Most have an unknown aetiology, but there are recognised associated risk factors, including genetic disorders (such as neurofibromatosis), effects from hormones and also as a long term effect of cranial irradiation, with the risk of developing meningioma linked to increasing time from exposure and dose [153,154].

Approximately 80% of meningiomas are considered to be benign, whilst the remainder are classified as more aggressive high grade tumours and associated with increased morbidity and mortality [155]. The WHO histopathological classification has formally separated the meningiomas into grade I (benign); grade II (atypical), making up approximately 15% of cases; grade III (malignant or anaplastic), which account for up to 5% of cases [156,157]. However, there have been new developments in the classification system which have caused some previously designated grade I tumours to be upgraded to grade II tumours [156], making direct study comparisons difficult.

Despite the benign label, grade I meningiomas can spread through the dura and may recur, regardless of surgical resection. Grade II tumours are often associated

with an 8 fold increase in recurrence (up to 52%) and malignant meningiomas, although rare, are associated with much higher rates of recurrence (up to 94%) [152,158-162]. However, grade II meningiomas appear to have a poorer outcome if associated with bony involvement [163] and malignant or anaplastic meningiomas have been shown to have a worse prognosis with a median survival of under 2 years [156]. Attempts have been made to determine those that have a propensity to higher rates of recurrence and the expression of proliferation markers (such as MIB-1 and Ki67) have been shown to correlate with meningioma grade and subsequent recurrence rate [155,164,165].

The management of meningioma largely depends on the grade, age of patient and symptoms produced. Due to the increasing use of CT and MRI, meningiomas are being discovered as an incidental finding and, as such, are often asymptomatic. These patients may be followed with active surveillance using magnetic resonance imaging (MRI), rather than initial surgical resection [166,167]. However, depending on their location and histological grade, meningiomas can become symptomatic with the development of seizure disorders, focal neurological deficits or even neuropsychological and cognitive decline.

The mainstay of treatment is surgical resection, aiming for safe tumour resection, relieving mass effect and associated symptoms, but with the added ability to obtain a diagnosis and histological grade. Nevertheless, due to the high recurrence rates with grade II and III tumours, surgery alone is often inadequate. Simpson described recurrence rates following surgery according to the extent of surgical resection (table 1.1), ranging from a 9% recurrence rate with grade 1 excision, to 29% with a grade 3 resection at 10 years [168], though these rates have been noted to increase

with longer follow up [169]. Often the anatomical locations of the meningiomas mean that significant debulking surgery is difficult and may be associated with considerable morbidity [170].

1.2.2.1 Radiotherapy for Meningiomas

Radiotherapy use in the management of meningiomas is now well established and can be used in the primary setting or as an adjunct to surgery [171-177], with post-operative radiotherapy generating rates of progression free survival over 90% in 10 years follow-up [177]. However, clinical practice has often favoured surgery due to the apparent associated radiation induced long term toxicities and morbidity in a disease which is perceived to be slow growing.

Definitive radiotherapy can achieve high rates of long term tumour control, but is often reserved for situations where surgery is not possible due to tumour location (most notably optic nerve sheath and base of skull lesions [170]), or patient contraindications to a surgical procedure. Large retrospective studies have demonstrated comparable progression free survival outcomes using stereotactic radiosurgery as an alternative to a surgical procedure achieving a Simpson's grade 1 resection, and, in fact, can achieve superior outcomes to surgical resection with Simpson's grade 2 and over [178]. These findings have been replicated in other large series and confirm its use as an alternative to surgery [179-184]. More fractionated regimes with external beam radiotherapy and stereotactic fractionated radiotherapy (SFRT) have also been utilised in this setting, in particular, with meningiomas that are not resectable due their location [174,184-189]. Mendenhall and colleagues found no overall difference in cause specific survival in patients who were treated with radiotherapy alone and in those treated with a combination of

surgery and radiotherapy [174]. SFRT has the additional ability to spare critical adjacent normal structures that are sensitive to the hypofractionated regimes of radiosurgery, in particular in cases of optic nerve sheath meningiomas [190,191].

Due to the progressive nature of grade II and III tumours, radiotherapy may often be employed in addition to surgery or at the time of recurrence and has been shown to reduce recurrence rates and improve overall survival [192,193]. Much of the data comes from observational and retrospective studies [152,194], with very little data from prospective randomised controlled trials. However, there does appear to be a trend towards improved outcomes with adjuvant radiotherapy and one study has concluded a benefit with immediate adjuvant radiotherapy compared to salvage [193]. A single centre series examined outcomes over an 11 year period of 108 patients with atypical meningioma, who had undergone gross total resection (Simpson's grade 1). Of these, only 8 had immediate radiotherapy (stereotactic fractionated) to 1cm around resection cavity. None of these patients recurred, whereas 30 patients recurred in the group receiving surgery alone, although this did not reach statistical significance [195]. They found that actuarial recurrence rates were 7%, 41% and 48% at 1, 5 and 10 years in the entire cohort. In patients who developed a recurrence, disease specific survival was 86% and 69% at 5 and 10 years after the first recurrence.

Despite their dismal prognosis, patients with grade III tumours are not routinely treated with adjuvant radiotherapy [194]. A case series of 13 patients with surgical resection for a grade III meningioma observed that only 3 patients had adjuvant radiotherapy. They reported a recurrence rate of 92% over a period of 0.4-2.8 years, with an associated 47% and 12% actuarial 5 and 8 year survival rates [196],

although other reports have suggested slightly higher 5 and 10 year survival rates of 64.3% and 34.5-40% [197-199]. Several studies have reported on the outcomes of grade III meningiomas (although often combined in the same group as grade II tumours) and have shown benefits in post-surgical radiotherapy with doses over 50Gy [193,200] and some have even recommended higher doses [192,201]. In fact, this is the subject of two current ongoing studies (RTOG 0539 and European Organisation for Research and Treatment of Cancer EORTC 22042-26042), evaluating the role of radiotherapy and dose escalation in non-benign meningiomas. Others have suggested a greater benefit from immediate adjuvant radiotherapy with an increase in disease free survival rates from 15% to 80%, whereas a smaller increase in 2 year disease free survival (50% to 89%) and no significant difference in 5 year disease free survival was seen when radiotherapy was administered at the time of relapse [200].

Despite this, there is dispute over recommendations for radiotherapy further to surgery [202]. Radiotherapy seems to be effective in difficult to resect tumours or in the presence of residual tumour and at skull base locations. Therefore, some would argue that, incompletely resected tumours should be irradiated at some point during the course of the disease, and when the risks of surgery outweigh complications from radiotherapy [152]. However, without any randomised trials, there is much controversy over the clinical value and optimal timing of radiotherapy, either after surgery or as salvage at time of recurrence.

Adjuvant radiotherapy for grade I (benign) tumours is much more controversial, as there is little data to demonstrate long term survival outcome and this needs to be weighed against the potential long term radiation toxicity in, what is essentially, a

slow growing, benign disease. Meningiomas in this group have been observed following surgery, rather than treated with radiotherapy [169,203]. Yet, despite the lack of enhanced overall survival, there is evidence to suggest that the addition of radiotherapy (with doses above 50Gy [204]) provides an improvement in local control following subtotal resections [203-207], with the risk of progression after subtotal resection alone amounting to 35% and 50% at 5 years and 10-15 years respectively, but improving to over 90% 10 year progression free survival with the addition of radiotherapy [177]. In this case, the timing of radiotherapy is critical – should it be offered just after surgery or for salvage? A previous phase III EORTC 26021-22021 study sought to answer this question, but closed early due to poor recruitment. However, there is currently an ongoing RTOG 0539 study, aiming to assess the role radiotherapy (using 3D-CRT or IMRT) and dose escalation for non-benign meningiomas, although it also encompasses an observation only arm for grade I tumours, following either gross total resection or subtotal resection and will attempt to answer the question of radiotherapy timing.

1.2.2.2 IMRT for Meningiomas

Whilst SFRT can achieve good results for meningiomas close to critical structures [181,189], it is often restricted in its use for larger lesions, where non stereotactic treatments may be more appropriate. 3D-CRT has been used in the past with improvements in local control and long term organ preservation [188,192,208-211], with overall actuarial 5 year local control rates of over 90% in patients with grade I tumours [174,210,212], although this technique can also be limited in areas close to critical organs, where dose to these structures can be unavoidably high [210]. IMRT can be useful to ensure improved target volume conformation to the complex-shaped tumours, especially in the skull-base, whilst adjacent organs at risk can be spared and therefore allowing safer delivery of standard meningioma doses of 50-

60Gy, whilst also providing the potential of dose escalation [201,213-216]. With the use of IGRT, IMRT can offer high treatment accuracy, especially when high dose gradients are close to critical structures.

There have only been a few (largely retrospective) reports of using IMRT in patients with meningiomas, many of which have involved tumours of the skull base [201,215,217-221]. Initial studies involved case reports or planning studies, charting the feasibility of IMRT in brain tumours. In the late 1990s, a group compared different shaped targets planned with 5 arc linac stereotactic radiotherapy, 6-fixed non-coplanar 3D custom blocked fields and IMRT using 6 non-coplanar beams and MLCs. They found that arc therapy spared more normal brain tissue for ellipsoid lesions, although IMRT appeared favourable for hemisphere and more irregularly shaped lesions, in terms of dose conformity and low dose normal brain tissue volumes [130]. Another group compared stereotactic radiotherapy with IMRT, using 5 tomotherapy arcs for various small intracranial tumours. They found similar outcomes with the two techniques when treating a petroclival meningioma, but better dose homogeneity with IMRT, although resulting in higher dose to the brain stem. Nevertheless, they concluded that IMRT was valuable for large irregular shaped tumours in close proximity to critical structures [222]. In the same year, Grant et al., reported on one optic sheath meningioma treated to 50Gy in 25 fractions and a craniopharyngioma treated to 50.4Gy in 28 fractions, whilst successfully limiting dose to the optic chiasm to 45Gy using the IMRT Peacocok MIMiC system [219]. An early planning study from the Royal Marsden Hospital, demonstrated a small improvement in PTV coverage of 5 convex-shaped tumours (including a sphenoidal sinus meningioma) using IMRT-tomotherapy method and a transaxial method of arc delivery. However, there were higher doses to optic nerves and optic lenses in comparison to the stereotactic conformal radiotherapy

method, although these doses were still within tolerance [47]. Similar findings came from a group in India, with superior dose distributions and better sparing of critical structures observed with IMRT in comparison to stereotactic radiosurgery [223].

In the early 2000s, Pirzkall and colleagues compared different IMRT techniques to 3D-CRT for complex skull base tumours, including meningiomas and demonstrated improvements in target conformality and coverage, with a 7 coplanar beam method producing the most conformal dose distribution, at the same time as maintaining organ at risk dose constraints [224]. The same group proceeded to look at 20 patients with meningiomas of the skull base and demonstrated better target conformity and homogeneous coverage with IMRT, compared to conformal plans by 10% and 36% respectively, using 5-7 equally spaced coplanar beams. They reported mild and tolerable acute side effects, with 6 patients recording no side effects at all. With a median follow up of 36 months, 60% of patients noted functional improvement of pre-existing neurological symptoms with 2 patients developing late toxicity (pituitary dysfunction and visual impairment), although the authors were uncertain as to whether this was a direct result of IMRT as opposed to natural progression of the meningioma, given its location [201]. They concluded that IMRT could achieve good rates of control, while minimising dose to normal structures and was useful in unresected or subtotally resected tumours.

In 2002, Uy and colleagues published a report of 40 patients (32 with skull base lesions) treated by IMRT using the NOMOS system, delivering a median dose of 50.4Gy to the target volume. They were able to demonstrate good target dose conformity, as well as acceptable levels of toxicity. The dose limiting organs such as optic nerve and chiasm received a mean dose of 47Gy with maximum doses up

to 55Gy. Their cumulative 5 year local control rate was 93% with just 2 patients developing progressive disease (one local and one distal recurrence). Over a median of 30 months follow up, most patients appeared to tolerate their treatment well and only 2 patients experienced late grade 3 CNS toxicity [220].

Following on from this, Milker-Zabel examined the long term experience with IMRT using a median 7 coplanar beams treating to a dose of 50.4Gy in a group of 94 patients with meningiomas of the skull base. Their local control rate was 93.6% over a median follow up of 4.4 years, with 19 patients displaying a radiological reduction in the size of their tumour. They documented a recurrence free survival of 97.5% and 96.3% (grade I tumours) and 89% and 77.8% (grade II) at 3 and 5 years respectively. Almost 40% had improvements in symptoms, 4 patients experienced worsening symptoms and 2 developed new symptoms due to tumour recurrence [215]. They concluded that IMRT was able to improve tumour dose coverage, although recognised a wider spread of low dose into other areas, such as normal brain (which others have also made note of [201,215,223]). This was comparable to previous reports using IMRT, with local control reported as 97% at 3 years, relapses in only 3 patients and no long term complications noted [225].

There have been further attempts to use different IMRT solutions for meningioma, with initial reports suggesting some benefit for tomotherapy over arc and static field IMRT for tumour coverage [221]. However, Fogliata et al. in 2009 reported on the use of RapidArc and static field IMRT for a group of 12 patients with benign intracranial tumours including 5 meningiomas. They found similar levels of dose conformity and organ sparing [213] and this has been replicated in other studies examining different IMRT techniques to allow safe dose escalation in skull base

lesions [226], although there have been reports of an increase in monitor units with static field IMRT compared to arc based solutions [227].

One of the few prospective studies using IMRT (or SFRT) has demonstrated local control rates of 95% and 88% at 5 and 10years following treatment in a group of 507 patients with a median follow up of 10 years. Control rates of 91% at 10 years have been observed in benign tumours and rates 81% and 53% at 5 and 10 years for higher grade tumours [217].

Long term toxicity, including neurocognitive outcomes and quality of life measures have been a concern and important consideration when using radiotherapy for slowly progressing disease. It is unclear to what extent deficits are caused following radiotherapy. The risk, to some extent, may depend on the dose and volume of irradiated normal tissue and may increase over time. However, Combs' group found treatment to be well tolerated, with quality of life in most patients unchanged, or even, improved [217]. It is, therefore, imperative that studies are conducted to examine prospective data, with quality of life and long term follow up, to accurately describe treatment related outcomes and toxicities.

Many groups have considered the use of proton therapy or carbon ions in the management of meningiomas, in an attempt to limit normal tissue toxicity in a group of patients who have prolonged life expectancies, whilst also maintaining or improving local control rates [192,218,228-230]. Some have even shown superior outcomes with reductions in irradiation to normal healthy tissues [229]. Kosaki and colleagues in 2012 reported marginal improvements with protons and carbon ions in

comparison to photon therapy, although acknowledged that this difference may be greater when higher doses are required. However, there was a clear indication that photon therapy produced a larger normal tissue low dose area in comparison to particle therapy plans [218]. Groups have also looked at the combinations of photon and proton therapy and demonstrated impressive long term control rates (especially with doses over 60Gy) for atypical and malignant meningiomas within the post-operative setting [192,231]. Recently Slater and colleagues reported on a series of 72 patients treated with fractionated proton therapy as primary or adjuvant treatment for benign cavernous sinus meningioma, resulting in an overall 5 year actuarial control rate of 96% (with rates of 99% in those with grade 1 histology) [230].

Whilst there are no randomised control trials, proton therapy does offer a potential advantage of further reducing dose to normal tissues and possible dose escalation over the use of current photon therapy. However, the long term toxicity is yet to be fully assessed. With the limited access to proton therapy, it is imperative that highly conformal photon therapies, such as IMRT are exploited.

For maximum value, radiotherapy trials need primary endpoints to define the rates of tumour control, late toxicity and therapeutic ratio [232]. For trials using radiotherapy in potentially curable tumours, it is usual to need 10 years of follow-up to ensure accurate estimates of tumour control and late toxicity. Benign tumours carry long life expectancy and, therefore, any long term effects from radiation become of paramount importance.

1.3 Limitations of IMRT

Despite the obvious benefits of IMRT, there are some possible disadvantages; some of which may improve with experience and others which require more investigation to determine their long term impact to the patient.

1.3.1 Treatment planning and delivery

With the reduction of areas irradiated to high dose levels using IMRT, comes the possibility of geographical miss. As a result there is a requirement for clear and quantitative definition of both target volume and critical organs. This is an important aspect of treatment planning, as IMRT is less forgiving of uncertainties in defining the CTV and critical structures.

Various uncertainties exist in the definition of the planning target volume (PTV) which may limit the efficacy of IMRT, such as those related to the inter-fraction positioning, displacement and distortions of internal anatomy and intra-fraction motion. In fact, the high degree of conformity associated with IMRT may lead to underdosage to a portion of the target (or even high doses to nearby critical structures) and could, therefore, be a cause of subsequent recurrence, especially for disease sites where positioning and motion uncertainties play a large role.

To take full advantage of the sharp gradients and tight dose conformations, IMRT treatments should be accompanied by better immobilization and target localization techniques.

Careful assessment of the balance between the plan quality and the efficiency and accuracy of treatment delivery is required. Certain dose distributions designed by the IMRT planning system may not be physically achievable or may not be delivered with accuracy. In addition, mathematical formulas can create unexpected dose distributions, such as the 'dose dumping' effect in unspecified tissues. Complex plans that use many beams and highest levels of intensity modulations increase 'indirect radiation' to the patient because of scatter and leakage doses and it is important to note that these indirect radiation doses may not be predicted accurately [233].

Standard IMRT plans often require multiple fixed angle radiation beams which can increase treatment times. This can impact on patient comfort, reproducibility of treatment positions and intra-fraction motion, as well as the impact of patient throughput within a radiotherapy department.

Planning and quality assurance (QA) for IMRT are often more complex and time consuming compared with conventional conformal radiotherapy. However, as experience is gained in centres, this can become a less time restraining process, although there still may be a significant bearing on departmental resources [113,234]. QA can often have an impact on linear accelerator time, although many departments are now beginning to perform QA checks in batches in order to streamline the process somewhat.

1.3.2 Uncertainties in dose response data

In contrast to typical IMRT treatments, large and uniform treatment fields are commonly used in 3D-CRT. Previous experience with dose tolerance is based largely on uniformly irradiated organs [124]. However, attempts have been made to determine dose tolerances in the new era of radiotherapy [125]. IMRT dose distributions can have sharp dose gradients, a factor that challenges our clinical knowledge about the dose-volume relationship, especially for critical organs in which the dose gradients usually occur. The risk of a small volume receiving a high dose versus a large volume receiving a low dose is still unknown in many cases. In addition, the effects of fraction sizes used in simultaneous integral boost IMRT for tissues embedded within the CTV is relatively undefined and may present an increased risk of injury or reduction in local control if used inappropriately. Adequate understanding of the radiobiological characteristics, dose, dose-volume and functional characteristics of normal tissue is critical in prescribing IMRT treatments.

1.3.3 Low dose bath

The advantages of high dose conformality with IMRT need to be weighed against the higher volumes of low dose radiation received by non-target areas compared to conventional radiotherapy techniques. Goitein posed the question of 'bath or shower effect': "is it better to dispose of the integral dose by delivering a relatively lower dose over a larger volume or a relatively higher dose over a smaller volume?" [235].

This low dose observation has been noted early in the implementation of IMRT. Verhey et al., in the late 1990s, compared IMRT plans with that of CRT for treatment of a prostate tumour and observed that IMRT plans showed slightly increased low dose distributions to the rectum than CRT plans [5]. In fact, recent studies have also highlighted that, while IMRT can be useful in sparing some organs at risk, inadvertently, due to the increased number of beam portals, it can produce other unexpected adverse effects, such as fatigue, thought to be related to increased outside target dose to the CNS with IMRT techniques for head and neck tumours [116].

Dose outside the treatment volume (also referred to in the literature as peripheral dose or whole body dose) can be a result of many factors (including collimator scatter and transmission, head leakage and internal scatter), which depend on the collimator design and beam delivery technique [236]. The inefficient leakage of photons from the treatment head and collimators is a significant source of this extra dose, although there have been recommendations limiting the maximum dose due to leakage radiation to less than 0.1% of the dose at the isocentre [237].

Scattered radiation originates from two components. The first is generated inside the patient due to the scattered photons of the Compton interaction and is dependent on the dose delivered to the target volume. The second source of scattered radiation comes from the target, collimators and any physical inserts used, and is largely dependent on the number of monitor units. Neutrons, originating in the treatment head and leaking through the head shielding, are also a consideration, although neutron production is likely to be negligible below energy levels of 10MeV [238]. In addition to the factors mentioned above, the increasing

use of IGRT may cause supplementary dose to patients undergoing RT and needs to be considered when treatment is planned.

The inefficient use of a photon beam that is produced by a linear accelerator means that techniques, such as intensity modulation, require a considerable increase in beam-on-time and number of monitor units in comparison to more conventional radiotherapy methods [236,239]. As a consequence of more treatment fields used with IMRT, there is a larger volume of normal tissue exposed to lower doses. Unavoidably, the ratio between integral dose to the tumour and that to the whole body decreases [239].

The increase in monitor unit requirements is a function of many factors, including the complexity of the modulated field [240] and features of the modulating device, such as wedges or multileaf collimators (MLCs). Monitor unit requirements are largely dependent on technique and energy used. The number of monitor units required to deliver a 6MV photon unwedged beam has been found to be 20% more than that required for a comparable 18MV beam and, similarly, requirements are 60% more for a 6MV wedged beam compared to that for an 18MV wedged beam. Comparable findings are seen with a 6MV and 18MV MLC modulated field and tomotherapy field [241]. Nevertheless, there is a definite increase in monitor units required to deliver an MLC modulated field or tomotherapy field compared to conventional techniques and a greater use of monitor units raises the chances of higher whole body dose to the patient by leakage and scattering of X-rays [242]. The exact effects of this are unknown, but may have consequences on the long term effects of radiotherapy, which is a significant issue, especially as newer treatments may lead to improvements in outcome.

The increase in monitor units (MU) to cover the PTV using IMRT is an important factor in treatment consideration. Followill et al. found the number of MU required for SMLC IMRT to be up to 1.4 and 2.8 times that required with conventional radiotherapy (with and without the use of wedges respectively) using 6MV, 18MV and 25MV X-rays [241], with an even greater number of monitor units needed for the use of tomotherapy techniques [241]. Similarly, others have estimated a 2-3 fold increase in monitor unit requirement for IMRT techniques [147,242], whilst some groups have reported an almost 10 fold increase in the mean number of monitor units required for IMRT tomotherapy in comparison to 3D-CRT and an almost doubling of estimates for the effective absorbed dose at various positions outside the target [239].

The link between whole body dose and number of monitor units has been demonstrated by Verellen and Venhavere in 1999. They estimated an 8 times increase in the whole body equivalent dose per MU for IMRT techniques, directly related to the increase in MU with this technique [239]. Similar results have been seen from other studies [241,243,244], although Mutic and colleagues demonstrated somewhat lower whole body dose risk estimates than the predictions of Verellen's group [244].

The increase in MU with IMRT results in an increased amount of leakage radiation in the treatment field, as well as scattered radiation [241] and contributes to an increase in the whole body dose outside the treated area [236]. There have been several predictions in the literature suggesting measured whole body dose to be 300mSv [244] or 543mSv [241] at a distance of 40cm from field edge using a field size of 10x10cm or 20x20cm (respectively) with 6MV serial tomotherapy, whilst

others report 520mSv with 10MV photons [245]. However, the exact values do seem to be less with MLC modulation rather than with tomotherapy techniques: 190mSv for MLC modulation and 543mSv for tomotherapy, when compared to 67mSv and 134mSv with conventional unwedged and wedged plans [241,243]. Out of field dose from tomotherapy has been shown to be much higher than from conventional radiotherapy, with leakage radiation contributing to both out of field dose close to and at distant locations from the treatment field [244,246]. However, Ramsey and colleagues, in 2006, contradicted these results and demonstrated that helical tomotherapy results in an equal or lower leakage dose to non-target volumes compared to MLC IMRT [247]. They postulated that, whilst helical tomotherapy treatment delivery requires 5-15 times longer beam on times, treatment machines were being designed with appropriate shielding to minimise radiation leakage. This was reinforced by Bennett and colleagues, who reported that at 20cm from target edge, a dose of 1% was recorded with MLC based IMRT and 0.4% with helical tomotherapy [248]. However, a recent study has attempted to measure peripheral dose and demonstrated that 0.1% of the dose is recorded at distances over 30cm from the target area, with 0.28% of the dose measured at 17.5 cm from the target volume.[249]

Nevertheless, MLC based IMRT plans use a larger number of monitor units compared with conventional conformal radiotherapy plans. This may cause an increased amount of low dose radiation to the rest of the body. There have been suggestions that, in part, the number of monitor units required depend on the form of static field IMRT technique used; with reports of more monitor units when using the dynamic leaf MLC technique [250-252].

Following on from this, Sharma and colleagues found that peripheral dose was higher with dynamic fields in comparison to open static fields, and larger dose was associated with smaller strip field width (MLC gap) sizes by a factor of 8 and 2 for width sizes of 0.5cm and 2cm respectively [252]. Highly modulated beams often use narrow MLC openings and result in sharp increases in monitor units and thus peripheral dose. However, a slight reduction in peripheral dose can be seen near the edge of a DMLC field, where there is often a wider gap, possibly as a function of a reduction in collimator scatter and transmission of the DMLC fields at these areas. The increase in monitor units for smaller gap widths for the same field and dose, further elevates both scatter and leakage dose, leading to an increase in peripheral dose by a factor of 2-15 with DMLC IMRT (which is similar to the increase in monitor units when compared to open static fields). They also noted that, within 30cm of field edge, peripheral dose estimations appear to vary and seem to be a complex interaction of leaf scatter, leaf end design, MLC placement in the treatment head, MLC motion and beam on time [252], whilst some groups have demonstrated that scattered radiation appears to be the dominant source of radiation up to 14 cm from the beam edge [253] and becomes negligible relative to leakage radiation beyond 20cm [244]. Nevertheless, peripheral dose beyond 30cm from field edge appears to fall exponentially [252]. Some groups have observed higher peripheral doses for low energy and large field sizes (and therefore internal scatter) within 10 cm, whilst head leakage is more dominant at more distant sites [254]. However, other reports have demonstrated a large variation in dose at different anatomical sites, dependent mainly on the distance from the field edge [255,256].

In fact, comparisons of data from treatments using SMLC and DMLCs demonstrate that DMLC produces more out of field dose per monitor unit, although the amount of monitor units rely heavily on the treatment site. Groups have demonstrated that the

use of non-coplanar beams in IMRT can increase the peripheral dose in organs by a factor of 1.8-2.5, due to the associated increase in internal scatter [257]. As expected, tomotherapy seems to produce higher out of field dose compared to most MLC IMRT techniques [258].

As cancer mortality decreases, any increase in low dose radiation to healthy tissues is particularly important. Many patients are surviving for many years after diagnosis and treatment; therefore any treatment related effects need to be minimized.

1.3.4 Second malignancies

A major concern with any radiotherapy technique is the potential risk of radiation-induced second malignancies [258] and in the past estimates have produced a relative risk of up to 4.5 for second malignancy following irradiation of carcinoma of cervix [259] and as much as 6% in those treated for prostate cancer [260], with areas affected either adjacent to or at some distance from the irradiated area and can be present even 40 years after treatment [261]. This potential risk has been debated widely, but accurately assessing these risks is often difficult; due, in part, to confounding lifestyle and genetic factors. Nonetheless, the risks of second malignancy are especially pertinent in young patients and in those with good prognosis tumours, but are also relevant in other groups as treatment regimens improve and the number of long term cancer survivors increase.

Much of our knowledge regarding the potential carcinogenic effects of radiation comes from atomic bomb survivors exposed to low doses, as well as from medical exposures to radiation [262,263]. As such, increasing attention has turned to the low dose effects from IMRT techniques as a cause for long term toxicity [147,239,264]. A more recent study demonstrated an increase in second primary cancer following radiotherapy treatment for prostate cancer, as compared to those receiving surgical treatment alone [265], though they could not detect a difference in second malignancies according to radiotherapy technique when a subset of patients treated with 3D-CRT or IMRT were analysed. The authors acknowledge that this may have been due to the small group of patients treated using these techniques and the relatively short follow up of this cohort.

However, estimates have been made for the risk of radiation induced malignancies following IMRT techniques in comparison to conventional treatments, with as much as a doubling of the risk [147,148] and higher risk estimated with 6MV as opposed to 10MV plans, although highest risks were with energies where neutron contribution was significant [148]. As such, steps to reduce a source of leakage radiation can be made, including increasing shielding from treatment head, secondary beam blocking to reduce leakage radiation through MLCs and reduction of scattered radiation by removal of the unused flattening filter with IMRT treatments [266].

Modelling studies on carcinogenesis have supported a non-linear dose response, meaning that tissue receiving low doses of radiation (for example 3-5Gy) may be at increased risk of second malignancies [267-269]. Some hypothesize that higher radiation doses may actually lead to cell death in potentially oncogenic cells within

the bone marrow and therefore lower the leukaemic potential [260]. Others also seem to suggest that second cancers appear to develop in volumes exposed to low-intermediate doses, rather than within high dose volumes [235,270] and consideration has also been given to the bystander effect, where relatively small doses can have significant radiosensitising effects on nearby tissues [271-273]. There is some evidence to suggest that doses of 10-50mGy are associated with increased cancer risk [274], with some risk estimates below these levels extrapolated from high dose data [250,275-277].

Hall postulated that the smaller volume receiving high dose may lead to a reduction in the number of induced sarcomas and carcinomas within the high dose region in comparison to more conventional techniques. However, due to the increase in low dose volume (and higher whole body dose), they also proposed an increase in radiation induced second malignancies from 1% to 1.75% for patients who survive 10 years or more [147], estimating that an additional 0.5% of patients will develop a second cancer as a result of the low dose bath effect, and an additional 0.25% will develop second cancers due to the effects of increased monitor units. These conclusions are similar to those of Followill et al., who made estimates, based on extrapolation of scatter dose. They estimated at least a doubling of second cancer increased risk from 0.4% to 1% with 6MV, and higher values with 18MV and tomotherapy [241,243].

In a review of 31000 patients treated with radiotherapy, Dorr et al. suggested that most second cancers occurred at a margin around the PTV (within 2.5cm inside to 5cm outside the boundary margin on the PTV), with the majority of tumours observed in the volume of tissue receiving less than 6Gy [269].

Verellen and colleagues aimed to assess the increase risk of second cancers using thermoluminescent badges and neutron bubbles detectors to quantify in vivo measurements of whole-body equivalent dose of conventional and arc IMRT techniques for head and neck tumours. They demonstrated $1.2x10^{(-2)}$mSv/MU for conventional and $1.6x10^{(-2)}$mSv/MU with IMRT respectively, which, when using 70Gy to a target dose, provides an estimated whole-body equivalent dose of 242mSv and 1969mSv respectively. Using the nominal probability coefficient for a lifetime risk of second cancers recommended by the ICRP 60, they suggest that this results in an 8 fold risk for second malignancies [239]. More recently, Ruben and colleagues demonstrated a small increase in relative risk in second cancers with IMRT in comparison to 3D-CRT due to the increased low dose effect and in particular monitor units used [268].

In principle, the lower integral dose (absorbed dose to normal tissues in irradiated area outside the PTV) and smaller radiation volume, the better. More recent IMRT techniques, such as RapidArc, have been shown to have improved integral dose compared to static field IMRT [25]. However, long term follow up of patients currently treated with IMRT is imperative to accurately and fully evaluate the risk of second cancers.

1.4 Biodosimetry

The effect of low dose radiation exposure associated with IMRT is often difficult to quantify. Total body dose, postulated to rise as a result of increased beam-on-time and scatter, is difficult to measure using conventional techniques and often results

in varying observations as detailed in the last section. Some authors have suggested this is increased by as much as a factor of 1.8 when IMRT is compared to conventional techniques [278]. Up to now, these estimates have been based on indirect measures of total body dose, making realistic assessment of risk difficult, but new biological markers of radiation induced damage may provide completely new approaches to this problem.

Data published has shown that phosphorylation of histone H2AX, which occurs at sites of radiation induced DNA double strand breaks, could be used as a marker of damage even at very low dose levels [279].

1.4.1 DNA damage and its measurement

Ionising radiation produces a wide variety of DNA lesions including double strand breaks (DSB), which, if unrepaired, result in cell cycle arrest, apoptosis and cell death [280,281]. However, if repaired incorrectly, carcinogenesis can result [280,282-284]. These DSBs can be produced by ionising radiation, UV light, hypoxia and some chemicals, but can also arise endogenously [285].

Once a DSB occurs, a complex local cellular damage response ensues to allow for subsequent repair [282,286,287]. The MRN (Mre11/RAD50/NSB1) complex binds to DSBs and activates ATM (ataxia telangiectasia Mutated), a P13K related kinase in the DNA damage response. ATM autophosphorylates at the site of DSB, allowing the consequent phosphorylation of substrates including phosphorylation on residue serine 139 of the histone H2AX, an early marker of DSBs [288-290]. The phosphorylated form of this histone, known as γ-H2AX, leads to the accumulation of

DNA damage response proteins at break sites and the subsequent formation of ionizing radiation induced foci (IRIF), whilst also retaining the broken chromosomal ends in close proximity [291,292]. These nuclear foci can be visible after staining under a microscope and are likely to represent a single DSB [279,293,294]. Recruitment of further DNA damage response proteins occurs, including MDC1 (mediator of DNA damage checkpoint protein 1), MRN (MRE11/RAD50/NBS1) complex, 53BP1 (tumour suppressor p53 binding protein 1), NSB1 (Nijmegen breakage syndrome protein), RAP80, KAP-1 and BRCA1 (breast cancer 1 protein) [292,295]. This in turn causes downstream phosphorylation of CHK2, p53 and CDC25, leading ultimately to cell cycle arrest and therefore allows time for DNA repair. In fact, many components of the DNA damage response such as ATM, RAD51, RAD50, 53BP1 and BRCA1, co-localise with the γ-H2AX foci [292,296-298].

Repair takes place in the form of two separate pathways, known as non-homologous end joining repair (NHEJ) and homologous recombination (HR) [299,300]. NHEJ repair can occur at any point in the cell cycle and has no requirement for sequence homology. The two ends of DNA are processed and ligated by the repair complex Mre11/RAD50/NSB1 and Ku70/80/DNS-PK ligase IV and involves the DNA dependent protein kinase catalytic subunits (DNA-PKCs) repair protein [282,283,296]. By contrast, HR has a role in the late S and G2 phases of the cell cycle where sister chromatids are used to allow recombination, utilizing homology to restore any sequence break error-free [283,296]. Once DNA repair has occurred, dephosphorylation of γ-H2AX takes place.

The formation of DNA DSBs following irradiation can be quantified by various methods [287], including those that utilise the physical estimation of DNA size or those that measure chromosomal breaks, such as immunostaining, flow cytometry, immunoblotting and enzyme linked immunoabsorbent assay (ELISA). Total DSBs can also be measured in cell lysates using techniques, such as immunoblotting or pulsed field gel electrophoresis (PFGE), or alternatively directly within the cell using procedures involving microscopy or fluorescence activated cell sorting (FACS). Conventional methods to measure DSBs in cell culture include the Comet assay or PFGE, although these methods tend to be more sensitive following doses of radiation over 5Gy [301,302].

Physical techniques, such as pulsed field gel electrophoresis (PFGE) have been employed extensively [303,304]. This can directly quantify DSB repair by assessing the molecular weights of DNA molecules, although detection is limited to ionising radiation from doses in the region of 10-80Gy[305], rather than with much lower doses.

DSBs can also be measured by cell imaging through the comet assay by suspending cells in an agarose gel using a weak electric field. This forces cellular DNA containing strand breaks to migrate from the nucleus, thus generating a comet tail which is proportional to the level of strand breaks in the cell and can allow the detection of DSBs by fluorescence following doses as low as 0.5Gy [306,307]. Comet assays allow DNA damage detection in single cells, although is less sensitive at determining low damage levels [307,308] and can be subject to poor specificity.

Although these techniques are useful in some contexts, most result in a relatively low rate of DSB detection (with the lower limit of DSB detection approximately 100 DSBs per nucleus) and are unable to determine the localisation of the DSBs within the nucleus [285].

Direct measurement in the cell is often the preferred method due to the formation of bright foci produced by large numbers of γ-H2AX at individual DSB, therefore allowing the quantification of foci as a sensitive assay to detect DNA damage.

1.4.2 Detection of γ-H2AX as a marker of radiation induced DNA damage (and repair)

The knowledge of the cellular response to DNA damage can be used in the detection of DSB and γ-H2AX has been shown to be a rapid, sensitive cellular response to the presence of DNA DSB and, therefore, a surrogate marker for the identification of DSBs [288,289]. Other repair proteins, such as 53BP1, RAD50, MRE11, NSB1, have also been studied as a marker for DNA damage. However, the advantages of using γ-H2AX include its property as a molecule that is directly induced by DNA damage alone, unlike others, such as 53BP1 which use translocation to form foci. In addition, its formation takes place throughout the cell cycle, whilst others can be dissociated from DNA damage during the mitotic stage.[309-311]

Obtaining cells from patients for analysis of DSB can be achieved by using minimally invasive techniques, such as through blood samples and skin punch

biopsies. Peripheral blood lymphocytes (PBLs) are the most common and easiest cells to obtain in order to analyse γ-H2AX formation in vivo. Approximately 2% of lymphocytes reside in the peripheral blood with the remainder in organs such as lymph glands, thymus and other lymphoid tissue. The majority of lymphocytes migrate between the peripheral blood and these organs with a recirculation time of 12 hours [312].

Easily accessible and proliferating skin cells are also useful for the identification of γ-H2AX foci. Several groups have utilised skin cells to assess γ-H2AX foci formation and repair, showing increased residual γ-H2AX foci in DNA repair deficient cells [298,313-315]. Others have looked to animal studies in order to examine γ-H2AX formation and repair in other organs such as heart, small intestine, brain, kidney and spermatozoa with γ-H2AX foci seen in most normal tissue organs [316-319].

Buccal cells have also been used to examine γ-H2AX in a simple and non-invasive manner following low dose irradiation [320]. These cells can be collected by scraping the inner cheek, but this can often lead to a mixture of a limited numbers of cells, including dead and dying squamous cells [311]. Although these cells often have high levels of background DNA damage [312,321,322], they can still be used to measure low dose radiation exposure [320]. In a similar manner, hairs plucked from the scalp or eyebrow have also been used to assess γ-H2AX in follicle cells [311,323].

1.4.2.1 Immunofluorescent staining

In order to study tissue response following radiation, techniques are available that allow quantitative measurements of DNA repair foci in situ. Immunostaining is one of the most accurate measures of recruitment proteins to areas of DSB, such as γ-H2AX, and subsequent analysis using microscopy has been used in the past to detect DNA damage in cell nuclei [279,324-328]. Although high throughput flow cytometry methods have also been utilised, this is associated with less sensitivity [329].

Recent immunofluorescent assays have been developed that are sensitive and specific to identifying γ-H2AX and therefore DNA DSBs [296,313], with the added advantage that one DSB is generally presumed to correlate to one γ-H2AX focus, and likewise, one γ-H2AX focus corresponds to one DSB [279,288], although some have questioned this [287,330].

Using immunohistochemistry, antibodies can be raised against γ-H2AX and when labelled with secondary fluorescence antibodies, allows the sensitive and specific visualisation of γ-H2AX foci [288]. However, antibodies need to be titrated so as to maximise detection of the area of interest, whilst minimising background signal thus avoiding identification of non-specific targets. The secondary antibody is also an important consideration to reduce the impact of autofluorescence. This is seen better with fluorescent dyes that tend to emit in the far red range, such as Alexa 647, compared to those that emit in the orange to red range [331]. The radiation induced foci can then be visualised within cells using high resolution fluorescence optical microscopy [331].

Widefield microscopy utilises an illumination source, such as a lamp or laser, to excite the field of view. Whilst widely available, foci that are out of focus produce a haze or blur, making quantification very difficult. However, microscopes are often enabled with moving platforms that can acquire images at various levels through the cell providing z stack images.

In a similar manner, confocal laser scanning microscopy uses a laser beam to scan across a sample. Foci are not restricted to single plane of view, but are located throughout the nuclear volume and, as such, imaging needs to take account of this. Fluorescence is produced throughout the whole depth of the sample, but a pin hole aperture excludes any fluorescence produced outside the focal point of the lens, allowing improved resolution.

Once appropriate images are obtained through microscopy, the most common method to quantify foci is to manually count γ-H2AX foci by eye. This can be done directly by visualising the number of foci through a microscope or on a captured image. Since the number of foci can appear as different sizes or intensities and, because of the time consuming methods of manual quantification, high throughput foci counting systems are also being developed [311].

1.4.2.2 Other techniques

Flow cytometry allows rapid measurement of γ-H2AX levels in a large number of cells and within different phases of the cell cycle. The fluorescent signal produced allows for the size and number of γ-H2AX in the nuclei [332] and several studies have demonstrated that γ-H2AX levels detected using flow cytometry correlate well

with DSB numbers [329,333,334], while other groups have demonstrated that this approach can be used to detect DSBs in cells exposed to 1-2Gy of radiation [335]. Flow cytometry enables detection of fluorescence intensity within each cell, as opposed to the scoring of each individual focus using microscopy. It is a much quicker method of assessing γ-H2AX when compared to the laborious method of foci counting. However, foci counting has been found to identify γ-H2AX foci following up to 10 times lower doses of radiation [279].

Enzyme Linked Immunosorbent Assay (ELISA) is based on electrochemiluminescent detection to measure γ-H2AX following irradiation and allows objective quantification of γ-H2AX [336]. However, poor sensitivity means that this method is not suitable for clinical samples [311]. Similarly, western blotting is difficult to use in the clinical setting and requires isolation of a large number of cells to obtain a sufficient amount of nuclear protein.

1.4.3 γ-H2AX kinetics

Kinetic studies, using immunofluorescent foci detection, demonstrate that half maximal foci numbers are achieved by 1-3 minutes following radiation exposure (although detection at this point is often difficult due to small foci size [305]), with maximal numbers reached by 10 minutes [289]. At its maximum, approximately 1% of all H2AX becomes phosphorylated per Gy of radiation, corresponding to approximately $2x10^6$bp of DNA DSB [289].

Following this, there is reduction of γ-H2AX foci after 30 minutes over a period of hours [288], although a significant level remains even several hours after irradiation [337]. By 24 hours, the γ-H2AX signal returns to background levels and this is thought to reflect repair of DNA DSB rather than the complete elimination of damaged cells [279,329,338]. However, it has been noticed that some repair does occur within the 30 minute period and, as such, foci numbers may actually underestimate the amount of DSBs (as opposed to PFGE which may conversely overestimate the number) [305,326]. Initial reports have demonstrated a close correlation between the numbers of radiation induced DSBs and numbers of γ-H2AX foci, suggesting that each focus represents a DSB and vice versa [279,288,293].

Radiation doses as low as 1mGy have been shown to lead to the formation of foci and appear to have a linear relationship with dose in the dose range 1mGy to 2Gy [279,313,326,333,334,339-341]. These features mean that γ-H2AX foci can be used as a useful biological assay to measure induction and repair of radiotherapy induced DSBs at varying doses [279,283,285,289,292,342].

1.4.4 γ-H2AX and DNA damage from diagnostic and therapeutic radiation

γ-H2AX is a well-established marker of DNA DSBs and a sensitive measure of radiation damage. It has, therefore, been validated as a measure of whole body exposure in patients exposed to diagnostic and therapeutic ionising radiation [327,340,343,344]. The γ-H2AX assay has been shown to be very sensitive to radiation exposure and has been used to estimate radiation dose ex vivo

[325,345,346], while estimates can also be made on total and partial body irradiation [325], in vivo irradiation in non-human primates [323] and in diagnostic [327], as well as therapeutic radiotherapy [340].

The production and loss of γ-H2AX has been evaluated following doses of radiation as low as 1mGy [279] and evidence supports a linear increase in γ-H2AX foci number per cell with radiation dose [279,313,325,329,338,340,347] in the range 0 to 10Gy within various cell lines [279,288,289,297,312,323,333,348]. In addition, it has also been found to be a useful maker for radiation exposure following radionuclide therapy for doses as low as 20mGy [284].

Correlation of γ-H2AX with DNA damage in PBLs, skin and other human tissue has been observed [337]. Easily accessible PBLs are convenient for determination of γ-H2AX foci by venous blood sampling from patients and, as such, have been widely used in the past [325,327,335,349]. PBLs need to be isolated from blood collection and then purified by density gradient. Although there are many subsets of lymphocytes, any difference in the level of γ-H2AX expression appears to be minimal [329,335]. They have low background levels of γ-H2AX foci [338,350,351] and this makes them ideal for assessing changes in foci following treatment.

Using samples irradiated in vivo and ex-vivo [327,335,338,340,350], various studies have examined γ-H2AX induction 5-30 minutes following radiation exposure by quantifying foci in peripheral blood mononuclear cells (PBMCs) in patients who have undergone diagnostic CT scans and have demonstrated a very good correlation with Monte Carlo estimates of whole body exposure [327,338]. The γ-

H2AX assay has been shown to detect very low radiation doses with an average 0.2-0.4 γ-H2AX foci induced per 10mGy per cell [279,327,338]. Increase in levels by a factor of 10 was seen at 5 minutes and a reduction in foci levels seen 5-30 minutes after irradiation, indicating repair. It has also been noted that foci levels appear to be lower in patients undergoing CT scans of the chest in comparison to patients undergoing whole body CT scans [327]. Similarly, Lobrich and colleagues found that the number of DSB induced by CT scans was dependent on the dose delivered and length of body exposed to radiation [338]. In both studies, γ-H2AX foci levels appear to fall after 30 minutes, with background levels of foci reached in the majority of cases by 24 hours, although it was noted that this was subject to interindividual variability. Others have utilised the γ-H2AX assay to assess DNA damage in patients undergoing cardiac CT and conventional coronary angiography [350,352-354], with suggestions of increased DNA DSBs as a result of conventional coronary angiography as compared to CT angiography [354].

Some groups have demonstrated the feasibility of assessing γ-H2AX foci in lymphocytes following a fraction of therapeutic radiotherapy at various time points after irradiation [349], with maximal levels at 30 minutes and a gradual reduction in levels over 2.5, 5 and 24 hours [349]. Further studies have shown that the assay can also be used to measure radiotherapy related doses and allow an estimation of the applied integral body dose following partial body irradiation due to the redistribution of lymphocytes in blood flow [340,355], but also taking account of the site of irradiation and time taken. This approach has the advantage that DNA damage is visualised directly using easily accessible peripheral blood samples and is very sensitive to very low damage levels.

Studies have examined the use of γ-H2AX following ex vivo irradiation and have shown that this can result in the induction of 10-15 foci per Gy within sampled lymphocytes [279,325,336,337,345]. However, various groups have also attempted to evaluate γ-H2AX following in-vivo irradiation [313,315,327,340,347,356] and have shown that the γ-H2AX levels following in vivo irradiation are often lower and appear to depend on the dose, area of the body exposed to radiation, as well as the duration and fractionation of radiation. Nonetheless, in vivo measurements of foci numbers in PBLs have produced a linear correlation with integrated total body radiation dose [327,338,340,350] and allows accurate assessment of radiation induced DSBs in normal tissues at clinically relevant doses [318,357].

Skin cells have also been used to confirm the ability to determine γ-H2AX following EBRT for prostate cancer [313] 30 minutes following radiation and have demonstrated a linear dose response beyond 0.05Gy [313,315] and additionally shown that repair appears to be complete between radiotherapy fractions [315]. Others have demonstrated a negative correlation following radiotherapy between γ-H2AX foci and TCD50 (dose at which 50% of tumours are controlled) in head and neck squamous cell carcinoma xenograft models, such that the number of residual foci following radiotherapy appears to be a good indicator of radiosensitivity, and is a potential biomarker for local tumour control [358].

The γ-H2AX assay is sensitive enough to detect inter-individual differences in DNA response following irradiation [335,338] and the extent of DNA damage and repair has been considered to be a significant indicator of radiation induced normal tissue toxicity [326]. The ability to use DNA damage markers, as a way of predicting those at higher risk of radiation induced toxicities, has been investigated by a number of

studies. Quantification of γ-H2AX foci and also persistence of γ-H2AX foci (and therefore rate of DNA DSB repair), seen at time points after ex-vivo irradiation, has been shown to identify those at high risk of acute and late toxicity [324,347,359-361], with accumulation of DNA DSBs similarly seen in both acute and late responding tissues during fractionated radiotherapy [362]. Yet, other groups have failed to demonstrate any correlation between γ-H2AX foci levels and intensities with radiation induced toxicities [349,363-365].

Whilst DNA damage following radiation is now established, there have been very few studies examining the differences in DNA damage following various radiotherapy techniques. Zwicker and colleagues, in 2011, investigated DNA damage through γ-H2AX foci levels following 3D-CRT and step and shoot IMRT in patients undergoing prostate radiotherapy [356]. However, their results did not demonstrate any statistically significant difference between the two techniques. A more recent study has demonstrated increased γ-H2AX foci in blood cells taken 30 minutes following prostate IMRT, with some persistence of DNA damage 18-24 hours after irradiation [366]. The authors also found that cell cycle arrest was not activated (and shown not to be activated under a threshold of 200mGy) and they have, therefore, postulated that this, taken together with the persistence of γ-H2AX foci, may lead to continuing unrepaired or mismatched repair breaks, which may, in turn, proceed to cancer induction as a result of low dose irradiation, particularly with IMRT [366].

1.5 Aims of study

This work aims to examine specific biological and clinical implications of IMRT:

1. Investigation of γ-H2AX in peripheral blood lymphocytes (PBL) as a potential surrogate marker for whole body dose after IMRT
2. Investigation of utility of γ-H2AX to compare whole body dose when different radiation delivery techniques are used.
3. Examination of the feasibility of using IMRT for patients with meningioma.

Grade	Description	Rate of symptomatic recurrence at 10years (%)
I	Macroscopically complete removal of tumour, with excision of dural attachment, and any abnormal bone. Includes resection of venous sinus if involved	9
II	Macroscopically complete removal of tumour and its visible extensions with coagulation of its dural attachment	19
III	Macroscopically complete removal of the intradural tumour, without resection or coagulation of its dural attachment or its extradural extensions	29
IV	Partial removal, leaving intradural tumour in situ	44
V	Simple decompression, with or without biopsy	100

Table 1.1: Simpson's grading for meningioma resection and the associated rate of symptomatic recurrences observed at 10 years.

Chapter 2

The feasibility of using γ-H2AX assay during static field IMRT (SF-IMRT)

2.1 Aims

- To determine the feasibility of using the γ-H2AX assay in peripheral blood lymphocytes of patients undergoing radiotherapy as a surrogate for DNA damage caused by ionizing radiation.
- To quantify γ-H2AX foci induction at various time points following SF-IMRT.
- To ascertain whether γ-H2AX foci in lymphocytes can be used as a sensitive and reproducible measure of radiation exposure in patients undergoing SF-IMRT.
- To confirm a linear dose response in γ-H2AX foci formation in lymphocytes following radiation exposure.

2.2 Introduction

IMRT has become the standard approach for the treatment of a wide variety of tumours, aiming to increase tumour control, whilst minimising normal tissue toxicity. Despite a smaller volume of normal tissue receiving a high radiation dose with static field intensity modulated radiotherapy (SF-IMRT) compared to conventional

techniques, there is inevitably a larger volume of normal tissue (outside the target area) which receives a low radiation dose.

In an attempt to document the low radiation dose, this chapter describes the use of the γ-H2AX assay in patients undergoing radiotherapy for brain tumours using SF-IMRT. γ-H2AX has been shown to detect very low radiation doses with reports suggesting 0.2-0.4 γ-H2AX foci per cell for 10mGy [279,327,338]. This assay has been previously used to demonstrate γ-H2AX foci levels following diagnostic CT scans, with levels found to increase linearly with the dose delivered and length of body exposed [327,338]. Others have observed that the assay can also be used to measure radiotherapy-related doses, thereby allowing an estimation of the integral body dose [340,355] and γ-H2AX foci numbers measured, within peripheral blood lymphocytes following in vivo radiation, have been found to show a linear correlation with integral dose [327,338,340,350].

This study was carried out to ascertain whether γ-H2AX foci induction in peripheral blood lymphocytes can be used as a sensitive and reproducible measure of radiation exposure in vivo for patients undergoing SF-IMRT to the brain. Patients with tumour volumes in the brain were chosen as the direct irradiation of circulating blood is minimal, making up approximately 15% of total blood volume [367].

2.3 Methods and Materials

2.3.1 In-vivo lymphocyte irradiation

2.3.1.1 Patient selection

Patients at University College London Hospital (UCLH), due to undergo radical radiotherapy for a tumour of the brain using SF-IMRT, were recruited prospectively. All enrolled patients were recruited as part of the study entitled, “Evaluation of DNA damage and radiation exposure in patients receiving intensity modulated radiotherapy”. Inclusion criteria encompassed all patients with a histological diagnosis of a tumour undergoing radiotherapy treatment with SF-IMRT and also those patients who were suitable to attend regular follow up. Exclusion criteria comprised patients undergoing neoadjuvant, adjuvant or concurrent chemotherapy and those who had a previous or concurrent illness which may have interfered with either completion of therapy or follow up. The study design described in this chapter was conceived and set up was set up by Professor Short and Dr Guerrero Urbano and the protocol was approved by the local ethics committee (ref: 06/Q0512/98). I was involved from the time of patient recruitment and written informed consent was obtained from all patients. All patients were treated with radiotherapy according to the indications set out by the treating clinician.

2.3.1.2 Sample Collection and Beam Parameters

4ml peripheral blood samples were collected for analysis from the anterior cubital vein in each patient at the following time points:

i. Baseline (prior to any ionising radiation exposure, including the radiotherapy planning CT scan, to measure background damage),

ii. Prior to and 30 minutes after the first fraction and then before and after each daily fraction of radiotherapy for the first week (for the first 4 patients only),

iii. Before and after every further 5 fractions (9Gy) of radiotherapy (i.e. weekly measurements)

iv. 2 and 6 weeks following completion of treatment.

Detailed beam and dosimetric data were collected for each patient, including target volume size irradiated, prescribed dose and fractionation, total dose, number of incident fields, beam-on time, number of monitor units and dose rate used (see appendix A). Beam parameters have been identified as contributing to scattered radiation [236], with internal scatter felt to be a reflection of the dose delivered and target size. Additionally, factors such as beam delivery technique, multileaf collimators and the number and orientation of beams also contribute to scatter dose and is thought to be largely dependent on the number of monitor units used and beam-on-time.

2.3.1.3 Sample Processing

Following collection, blood samples were transferred to BD vacutainer® CPT™ (cell preparation tube with sodium citrate) to allow separation of lymphocytes from whole blood by centrifugation (20 min, 1600g). Lymphocytes were washed with 4ml of phosphate buffer solution (PBS) followed by further centrifugation (10 min, 250g). The supernatant was decanted and the remaining cell pellet was resuspended in

100µl PBS. 20µl of this was placed onto a slide, allowed to dry, and then fixed with 100µl of 3.7% paraformaldehyde. Slides were suspended in methanol solution for 10 minutes at -20^{o}C, then in acetone for 1 minute at room temperature to allow better preservation of nucleic acid. The slides were washed with 2% PBS/BSA (bovine serum albumin) to prevent the non-specific binding of the primary antibody. 40µl of mouse anti-γ-H2AX monoclonal antibody (Millipore, CA) with antibody diluent (Dako) at a concentration of 1:300 was added and left at 4^{o}C overnight. Slides were washed in 2% PBS/BSA for 2mins and 80µl (1:500 dilution) of AlexaFluor green 488 Goat anti-mouse secondary antibody (Invitrogen, USA) was added and left for one hour in the dark. Slides were washed again in 2% PBS/BSA and mounted using DAPI/DABCO mounting medium (Vector lab inc., Burlingamo, CA).

2.3.1.4 γ-H2AX Foci Analysis

Foci were visualized with an inverted confocal microscope (SPE inverted microscope, Leica Microsystems CMS), equipped with acquisition software using x63 oil objective and pin hole size of 1 AU (Airy unit). Foci were identified as well-defined green spots within the blue nuclei of lymphocytic cells. Optical sections through the nucleus were obtained at 0.5µm intervals to compose z stack images and combined in a maximum projection so that all the visible foci were recorded. Two sample slides were produced for each time point and at least 150 cells were examined per slide. Images were saved as a TIF (tagged image format) file and transferred to ImageJ64 (National Institute of Health, USA) software. The numbers of foci within each visualized nucleus were counted manually by the same person to reduce inter-observer variability. However, to exclude a significant observer bias, two independent investigators also counted a subset of the samples.

2.3.1.5 Statistical Analysis

Data evaluation and statistical analysis was performed by me using PASW® 18.0 statistical package (SPSS Inc., Chicago). Some support was obtained from the UCL Research Support Centre to ensure that appropriate statistical analysis was being performed. Paired t-tests were used to test for statistical difference between pre and post-radiotherapy samples and repeated measures anova (Greenhouse-Geisser) was used to test for statistical difference between the samples taken at different times of treatment. Statistical significance was set at 5%.

2.3.2 Ex-vivo lymphocyte irradiation

To illustrate and confirm the γ-H2AX foci dose response within lymphocytes, 4ml of peripheral blood was collected from the anterior cubital fossa of 2 healthy volunteers and irradiated ex-vivo using ^{137}Cs source (15.06TBq) at doses of 0.05Gy, 0.1Gy, 0.3Gy, 0.5Gy, 1Gy and 2Gy at a dose rate of 250 +/- 0.59% Gy/hr. Cells were fixed after 30 minutes and analysed for foci formation. Samples were processed and foci analysis was performed in a similar manner to the in vivo samples using inverted confocal microscopy. 10 random images were taken per sample and the mean number of foci calculated. Three experimental repeats were performed. This ex-vivo work was facilitated by the Head and Neck Oncology Group, Department of Oral pathology, King's College London.

2.4 Results

2.4.1 Patient Characteristics

15 patients consented to study entry and all received radiotherapy using SF-IMRT technique. 14 patients received SF-IMRT for a cranial meningioma and 1 patient received radiotherapy for a pituitary adenoma. The median tumour volume (planning target volume [PTV]) irradiated for these patients was 88 cm^3 (range 23.1 to 254.9 cm^3). All radiotherapy was delivered using a linear accelerator with 6MV photons at a median dose of 50.4Gy in 28 fractions over 5 and a half weeks and using a median of 5 intensity modulated fields (range 4 to 7 fields). A median of 518 monitor units (MU) (range 393 to 1014 MU) was needed to deliver this treatment with a median 'beam on time' of 124 seconds (range 98 to 254 seconds). Detailed patient characteristics and beam parameters are summarized in tables 2.1a and 2.1b.

One patient had a large PTV measuring 245.9cm^3 and required 7 modulated fields for adequate treatment. This necessitated a total number of 1014 MU and the longest treatment delivery with beam on time of 245 seconds. In contrast, the patient treated for a pituitary adenoma had a PTV of 23.1 cm^3 and required 5 modulated fields, which needed treatment with 431 MU and a beam on time 0f 109 seconds. However, the patient who had the lowest number of monitor units (393 MU) and shortest treatment time (98 seconds), had a PTV volume of 48.8cm^3 , but required only 4 modulated beams, indicating that monitor units and beam-on-time are directly related, which in turn are likely to be dependent on the number and complexity of modulated beams.

2.4.2 Quantification of γ-H2AX foci per cell during SF-IMRT

Mean baseline level of γ-H2AX foci per nucleus for this group of patients was 0.186 ± 0.05 (standard deviation). An increase in radiation-induced γ-H2AX foci were clearly visualised in patient samples taken 30 minutes after each 1.8Gy fraction of SF-IMRT with green fluorescent foci seen within dark blue stained cell nuclei (fig. 2.1). The initial phase of the study demonstrated that there was an increase in γ-H2AX foci levels following daily treatment in the first week of radiotherapy for the first cohort of 4 patients (fig 2.2). However, there was no statistically significant difference in the increased foci levels following each fraction of radiotherapy during the first week of treatment (0.438 v 0.334 v 0.209 v 0.444 v 0.412, p=0.0983), (fig 2.3 and table 2.2). In view of this finding, we proceeded to omit daily blood sampling during the first week of treatment and continue with weekly blood samples as planned for the remainder of the cohort of patients.

There was a statistically significant increase in foci levels seen in post-treatment samples compared to pre-treatment levels and this appeared consistently between samples taken at the same time during each week of radiotherapy (fig. 2.4 and table 2.3). Throughout the entire course of radiotherapy, γ-H2AX focus yields were 2-3 fold higher in blood samples taken following SF-IMRT compared to pre-treatment samples. Throughout a six week course of SF-IMRT the mean γ-H2AX focus per nucleus was 0.170 ± 0.025 pre-treatment and 0.493 ± 0.042 post SF-IMRT, with a mean increase in foci numbers per cell nuclei of 0.323 ± 0.030 ($p<0.0001$), (fig.2.5).

The post radiation increase in mean γ-H2AX levels varied slightly from one week to another (fig. 2.6). However, there was no statistically significant difference in the

observed increase in γ-H2AX foci levels following SF-IMRT between samples taken during different weeks of treatment (0.317 v 0.307 v 0.323 v 0.364 v 0.311 v 0.334, p=0.718), suggesting that there is no accumulation of foci in lymphocytes. In addition, there was no statistically significant difference between baseline foci levels compared to foci levels taken at 2 weeks (0.186 v 0.252, p=0.199) and also at 6 weeks (0.186 v 0.159, p=0.424) post-radiotherapy, indicating no long-term accumulation of damage after completion of treatment.

2.4.3 Ex-vivo lymphocyte irradiation

As expected, there are low numbers of γ-H2AX foci in unirradiated cells (0.05 foci per nucleus), which increase following irradiation. The data in figure 2.7 demonstrate a clear dose response in γ-H2AX foci formation at 30 minutes following ex-vivo irradiation of lymphocytes from healthy volunteers. From this graph we can see that these data support a dose response that is linear at early time points over this dose range, and indicate an estimated 3.092 foci are induced per Gy above background levels of 0.47 foci.

2.5 Discussion

This *in-vivo* study was undertaken to evaluate the use of γ-H2AX as a marker for radiation damage in patients undergoing SF-IMRT. A cohort of patients with brain tumours was chosen, as the proportion of blood volume in the brain lying within the directly irradiated target area is relatively low (approximately 15%) [367] and this

may imply that a significant proportion of damage expressed as foci formation in lymphocytes results from radiation deposited outside the target volume, allowing for a more accurate measurement of non-target, low-dose radiation exposure from SF-IMRT.

The use of peripheral blood lymphocytes to demonstrate DNA DSBs following in vivo SF-IMRT has the advantage of acquiring material for analysis through a minimally invasive procedure and has been shown to have relatively low background levels of γ-H2AX foci [338,350,351,368]. Background levels in this in-vivo study have shown to be 0.186 ± 0.05 foci per cell and is broadly in line with other studies, allowing for inter-individual variability [325,338,340,343,345,349,356,364].

The results confirm that γ-H2AX foci can be visualised in lymphocytes of patients undergoing standard therapeutic dose radiotherapy, and in particular following SF-IMRT. It clearly demonstrates that there is a reproducible and statistically significant increase in foci numbers following a single fraction of radiotherapy, which appears to be constant between daily fractions of radiotherapy within the first week of treatment. In view of this finding, daily blood tests for change in γ-H2AX foci levels were discontinued for the remainder of the patients. This meant less invasive sampling procedures for the study patients, whilst still facilitating the measurements of γ-H2AX foci levels over the course of radiotherapy.

The results demonstrate that there is an increase in γ-H2AX foci levels between successive doses during a 6 week course of treatment and appears to be consistent

each week throughout the course of treatment. However, despite the slight difference in radiation induced foci from one week to another during treatment, this variation was not found to be statistically significant. γ-H2AX foci levels returned to baseline by two weeks following a six-week course of radiotherapy, suggesting that there was no accumulation of DNA-damage in this lymphocyte population, likely to be a reflection of the short half-life of these cells in the blood and efficient repair of damage.

Ex vivo irradiation was performed on peripheral blood lymphocytes from healthy volunteers to confirm a linear dose response with foci induction using the same γ-H2AX assay utilised for the in vivo work. The close correlation of DNA DSBs and γ-H2AX foci induction with radiation dose has been well documented in the past [279,288,289,313,325,329,337,338,340,347], even to doses as low as 0.02Gy using in vitro irradiation of peripheral blood lymphocytes [337]. The data from this ex vivo experiment demonstrate 3.092 foci per cell per Gy, whilst others, evaluating foci induction within lymphocytes, have reported slightly higher figures of 9 foci per cell per Gy (with 220kVp x-rays) [369], 12.6 foci per cell per Gy (with 137Cs source) [337] and 14.7 foci per cell per Gy (with 150kV) [327]. In addition, we have demonstrated 0.47 foci per cell with 0.1Gy, whereas others have measured 1-1.4 foci [337,338], although the background γ-H2AX foci levels in this cohort appear to be similar to other groups at approximately 0.05 foci per cell [369]. The differences seen may reflect inter-individual variability and it must be noted that samples were analysed in only 2 healthy volunteers in this experiment. However, it can also be accounted for by differences in assay technique and variability in foci counting between researchers when this is carried out manually.

Previous reports have exploited γ-H2AX focus formation as a sensitive tool for in vivo detection of DSB following radiation exposure with diagnostic computed tomography (CT) scans [327,338]. One study utilized this assay to demonstrate γ-H2AX foci levels following diagnostic CT scans of the thorax and abdomen, with levels found to increase linearly with the dose delivered and length of body exposed [338]. Similarly, it has been used to examine DNA damage following radiotherapy to different sites of the body and tumour types, demonstrating a linear relationship to the integrated total body radiation dose [340]. Comparable to our results, both studies demonstrated that background levels of foci were achieved by 24 hours following exposure to radiation. However, other groups have suggested that a proportion of radiation induced DSBs remain unrepaired after 24 hours [349] and may be a reflection of an inter-individual's variability and radiation sensitivity [347]. Furthermore, this study has demonstrated that any variation in radiation induced foci seen from one week to another during treatment is not statistically significant and, therefore, one could justify sampling blood and analysing for foci induction at just one time point during treatment, rather than on a weekly basis, to give an indication of the level of radiation damage induced.

There have been relatively few studies looking at γ-H2AX induction within peripheral blood lymphocytes following in vivo therapeutic radiation [340,347,349] and even fewer data exploring and quantifying γ-H2AX foci induction following SF-IMRT [356,366]. The data from this study demonstrates an increase of 0.323 foci per cell following SF-IMRT and is comparable to that found from a similar study by Zwicker and colleagues[356], assessing γ-H2AX foci levels in patients undergoing IMRT to the prostate . They found a mean 0.47 foci per nucleus following step and shoot IMRT (with a mean difference of 0.42 foci per nucleus after subtracting baseline

levels). Similarly, El-Saghire and colleagues have demonstrated an increase in γ-H2AX foci levels within blood samples taken 30 minutes following the first fraction of step and shoot IMRT, with induced foci level reported in the range 0.194 – 0.622 foci per cell among 8 patients (giving a mean increase of 0.47 foci per cell) [366].

The data also confirm that γ-H2AX foci levels returned to baseline by two weeks after completing a six-week course of radiotherapy. Other studies have documented detailed kinetics of γ-H2AX foci and demonstrated a persistence of over 20% of original foci numbers at 8 hours after exposure to in vitro radiation. With low doses, such as 0.02Gy, foci numbers return to near baseline levels by 48 hours post exposure, although with doses greater than 1Gy, foci numbers were still persistent and measured at 6.6% of original levels compared to levels identified 30minutes after in vitro radiation [337]. Some groups have proposed that, even following radiation doses in the region of 1.2mGy (0.0012Gy), there is a persistence of foci numbers in cell cultures for up to 14 days, indicating that some cells are unable to repair DSB efficiently [279]. A study examining γ-H2AX foci levels in patients with prostate cancer undergoing IMRT, also demonstrated some persistence of foci levels 18-24 hours following IMRT, associated with inactivation of cell cycle arrest under doses of 200mGy [366]. Suggestions have been made that this could be compatible with continuing unrepaired DNA DSBs, which may in turn be a cause of cancer induction as a result of these low radiation doses. However, the findings from the study presented in this chapter suggest that there was no accumulation of DNA damage in this lymphocyte population, likely a reflection of short half-life of these cells in the blood and efficient repair of damage within this particular sample population.

The method of foci counting can be labour and time intensive and may pose issues with quantification. This is particularly relevant in samples with numerous foci and where there is evidence of foci coalescence, often resulting in difficult quantification and subsequent underscoring of foci. Manual foci counting may also be subject to inter-observer variability; although we have attempted to address this issue by utilizing a single scorer. In order to exclude significant observer bias, a proportion of samples were independently counted by two people. It was, however, not feasible to utilize two independent scorers to manually count the whole dataset, due to the time taken to count each slide manually (which, on average, took over 60 minutes per slide).

One method that has been increasingly employed is that of automated foci counting systems, as a way of decreasing observer variation, as well as reducing time and labour to analyse foci distribution [345]. Validation is essential to enable the extension of these methods to analyse foci size and intensity [311] and there are now developments in image analysis algorithms incorporated into image acquisition software programs to enable this. Flow cytometry methods have also been used to identify γ-H2AX foci as a fast and relatively effective tool due to their high throughput, although they may be associated with loss of sensitivity in comparison to evaluating foci counts and size [311,329,370] and there have been reports that manual foci counting can identify γ-H2AX foci following up to 10 times lower doses of radiation than other methods [279].

The dose from scattered radiation as a result of radiotherapy measured within circulating lymphocytes is not easy to establish. Groups have acknowledged that there may be an effect of partial irradiation with attempts to distinguish cells that

have been directly irradiated from those that have not within the blood pool [325,347]. However, further work with mathematical modelling would be required to explore and accurately associate our findings to scatter dose.

2.6 Conclusion

This chapter confirms that ex-vivo irradiated lymphocytes demonstrate a linear dose response in γ-H2AX foci formation 30 minutes after radiation exposure. Furthermore, the in vivo experiment demonstrates that γ-H2AX foci induction is a sensitive and reproducible measure of DNA damage in lymphocytes of patients undergoing radiotherapy, in particular SF-IMRT, to the brain and may be useful as a marker of DNA damage.

IMRT is a potential source of increased radiation exposure. Higher γ-H2AX foci numbers following SF-IMRT may be used as a surrogate measure for DNA DSB, the repair of which can be a source of stochastic change, in particular at low doses of radiation, where cellular systems to eradicate DNA DSBs may not be active. This, therefore, may have implications for long-term radiation risk, including the potential risk of second malignancies. Quantification of γ-H2AX foci induction following differing radiation delivery techniques may provide useful information for the comparison of DNA damage and, therefore, the long term effects produced by these techniques.

Study Patient	Age	Gender	Tumour	PTV size (cm^3)	Dose delivered (Gy)	Dose/fraction (Gy)	Number of fields	Monitor units (MU)	Dose rate (MU/min)	Beam on time (sec)
1SF-IMRT	47	M	Meningioma parasagittal	288	50.4	1.8	6	548	400	130
2SF-IMRT	52	F	Meningioma	70.6	50.4	1.8	5	478	400	115
3SF-IMRT	53	F	meningioma parasagittal	48.8	50.4	1.8	4	393	400	98
4SF-IMRT	48	M	Meningioma Orbital apex	160.1	50.4	1.8	5	526	400	123
5SF-IMRT	63	F	Meningioma Torcula	105.5	50.4	1.8	5	589	400	136
6SF-IMRT	75	M	Meningioma left anterior clinoid process	83.7	50.4	1.8	5	518	400	124
7SF-IMRT	38	F	Meningioma Cerebellar pontine angle	88	50.4	1.8	5	486	400	122
8SF-IMRT	54	F	Meningioma Left optic nerve	108.7	50.4	1.8	5	461	400	115
9SF-IMRT	45	F	Meningioma right cavernous sinus	44	50.4	1.8	5	639	400	160
10SF-IMRT	52	M	Meningioma olfactory groove	55.5	50.4	1.8	5	491	400	122
11SF-IMRT	65	F	Meningioma left cavernous sinus/sphenoid wing	62.9	50.4	1.8	5	541	400	135
12SF-IMRT	38	M	Meningioma Clivus	254.9	50.4	1.8	7	1014	400	254
13SF-IMRT	45	F	Meningioma right optic nerve	100.9	50.4	1.8	5	650	400	162
14SF-IMRT	55	M	Pituitary adenoma	23.1	50.4	1.8	5	431	400	109
15SF-IMRT	59	F	Meningioma Right sphenoid wing	105.5	50.4	1.8	5	500	400	125

Table 2.1a: Individual patient characteristics and beam parameters for SF-IMRT

Abbreviations: SF-IMRT = Static field intensity modulated radiotherapy; M=male, F=female; PTV = planning target volume

	SF-IMRT	
	Median	**Range**
Number of patients	15	
Age	52	38-65
Dose (Gy)	50.4	
Dose/# (Gy)	1.8	
Monitor Units (MU)	518	393-1014
Dose rate	400	
Beam on time (seconds)	124	98-254
Number of fields	5	4-7
PTV (cm^3)	88	23.1-254.9

Table: 2.1b: Median patient characteristics and beam parameters

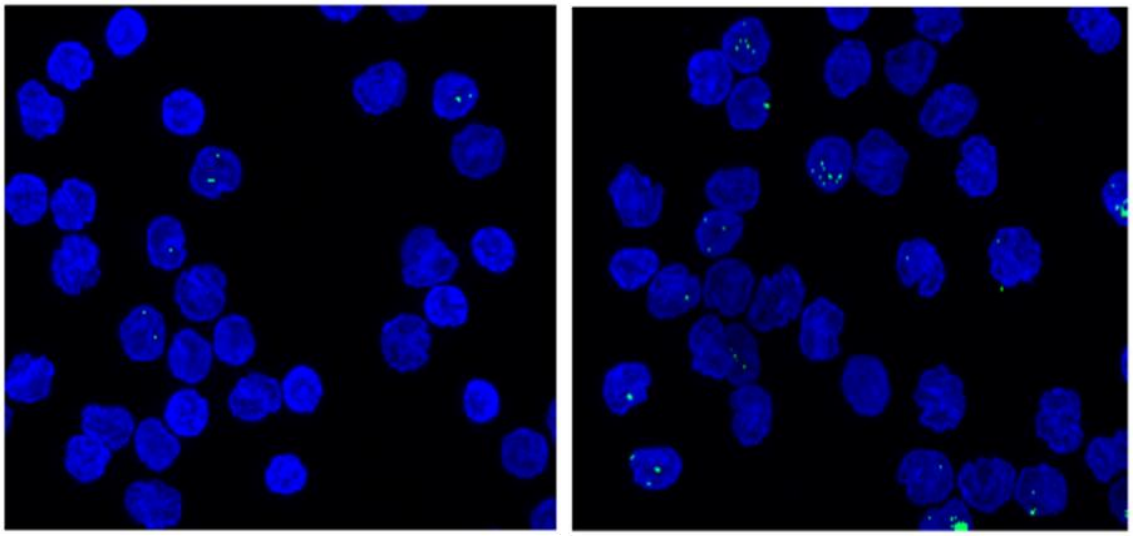

Fig.1a Fig.1b

Fig. 2.1: γ-H2AX foci prior to (fig. 1a) and 30 minutes following (fig. 1b) SF-IMRT.

There is a greater increase in γ-H2AX foci (shown as green spots) within lymphocyte nuclei (seen as blue) following exposure to SF-IMRT.

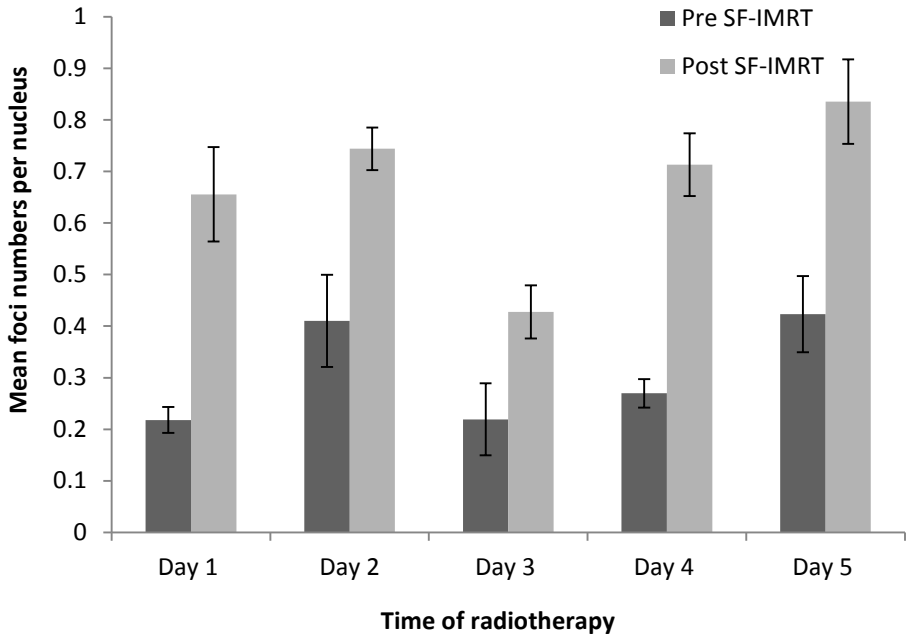

Fig. 2.2: Mean γ-H2AX foci per nucleus measurements at daily time points (after each 1.8Gy) in 4 patients during the first week of SF-IMRT

Error bars represent standard deviation.

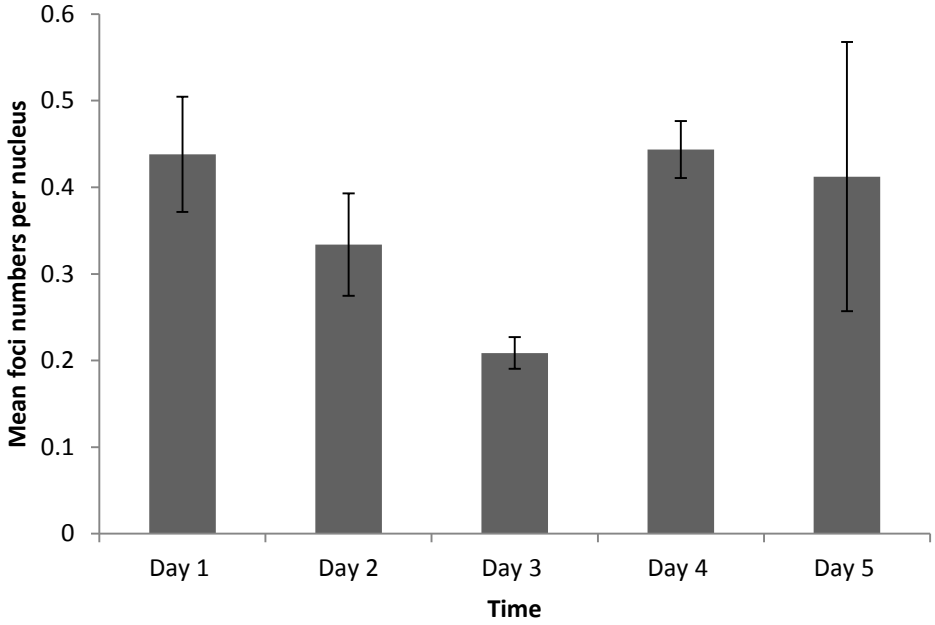

Fig 2.3: Observed difference in pre and post SF-IMRT mean γ-H2AX foci levels taken daily in 4 patients during the first week of treatment.

There is no statistically significant difference in the change in mean γ-H2AX levels from one day to another during the first week of SF-IMRT (p=0.0983).

Error bars represent standard deviation.

	Mean γ-H2AX foci per nucleus (SD)				
Day during first week	**1**	**2**	**3**	**4**	**5**
Cumulative dose at point of sampling	**1.8Gy**	**3.6Gy**	**5.4Gy**	**7.2Gy**	**9.0Gy**
Pre SF-IMRT(SD)	0.2178 (0.0252)	0.410 (0.089)	0.219 (0.0699)	0.270 (0.0278)	0.423 (0.0737)
Post SF-IMRT (SD)	0.656 (0.0916)	0.744 (0.0413)	0.428 (0.0515)	0.713 (0.061)	0.836 (0.082)
Difference (SD)	0.438 (0.066)	0.334 (0.059)	0.209 (0.018)	0.444 (0.033)	0.412 (0.155)
P values	<0.0001	0.0628	0.05	0.05	0.05

Table 2.2: Mean γ-H2AX foci per nucleus levels in 4 patients pre and post SF-IMRT for each fraction of radiotherapy during the first week of treatment.

Abbreviations: SD=standard deviation

The observed difference in γ-H2AX foci numbers between the daily fractions is not statistically significant (p= 0.0983).

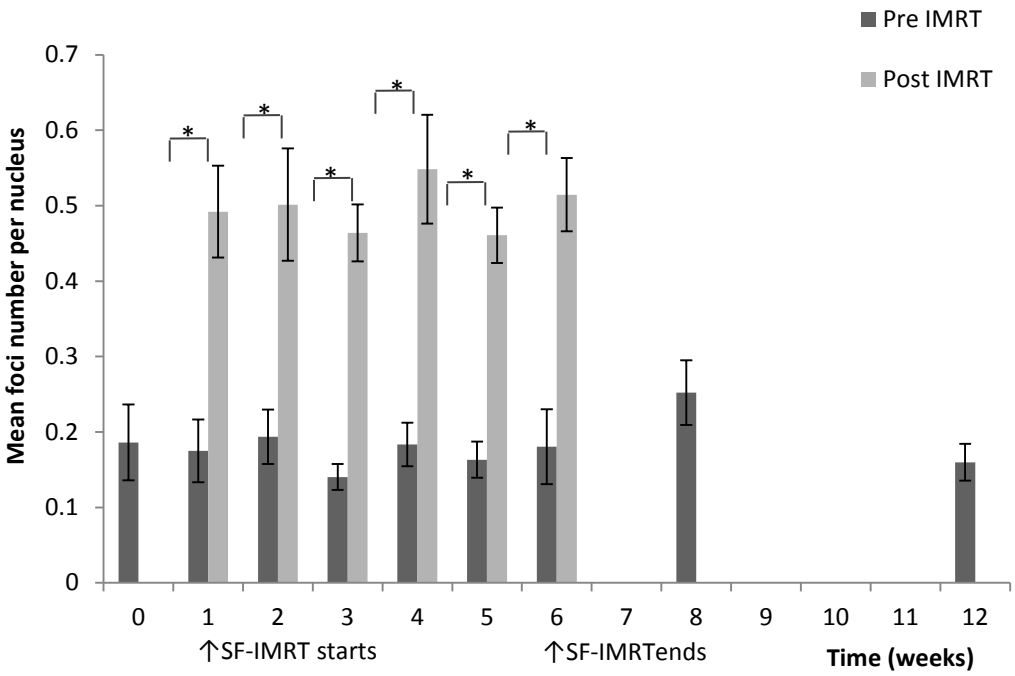

Fig.2.4: Mean γ-H2AX foci per nucleus measurements in 15 patients at weekly time points during and after a six week course of SF-IMRT.

Error bars represent standard deviation; *=p<0.05.

	Mean γ-H2AX foci per nucleus (SD)					
Week during treatment	**1**	**2**	**3**	**4**	**5**	**6**
Cumulative dose at point of sampling	**1.8Gy**	**10.8Gy**	**19.8Gy**	**28.8Gy**	**37.8Gy**	**46.8Gy**
Pre SF-IMRT (SD)	0.175 (0.161)	0.193 (0.139)	0.140 (0.067)	0.183 (0.112)	0.149 (0.089)	0.180 (0.185)
Post SF-IMRT (SD)	0.492 (0.235)	0.501 (0.287)	0.463 (0.146)	0.548 (0.279)	0.460 (0.132)	0.514 (0.182)
Difference (SD)	0.317 (0.158)	0.307 (0.199)	0.323 (0.114)	0.364 (0.223)	0.311 (0.169)	0.334 (0.077)
P values	<0.0001	<0.0001	<0.0001	<0.0001	<0.0001	<0.0001

Table 2.3: Mean γ-H2AX foci per nucleus levels pre and post SF-IMRT for each week during treatment.

There is a statistically significant difference in foci numbers in samples taken weekly pre and post-treatment and calculated at the same time during each week of treatment. The difference observed is independent of treatment week.

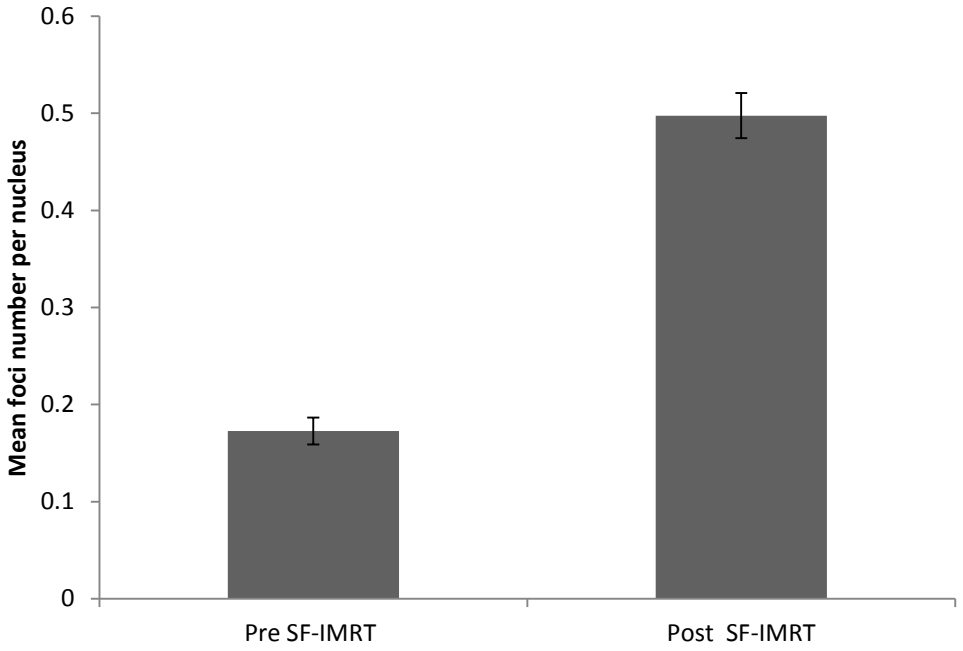

Fig. 2.5: Mean γ-H2AX foci per nucleus measurements over a six week course of SF-IMRT.

There is an increase of 0.323 ± 0.030 ($p<0.0001$) mean γ-H2AX foci seen within lymphocyte nuclei following SF-IMRT over a whole course of treatment.

Error bars represent standard deviation.

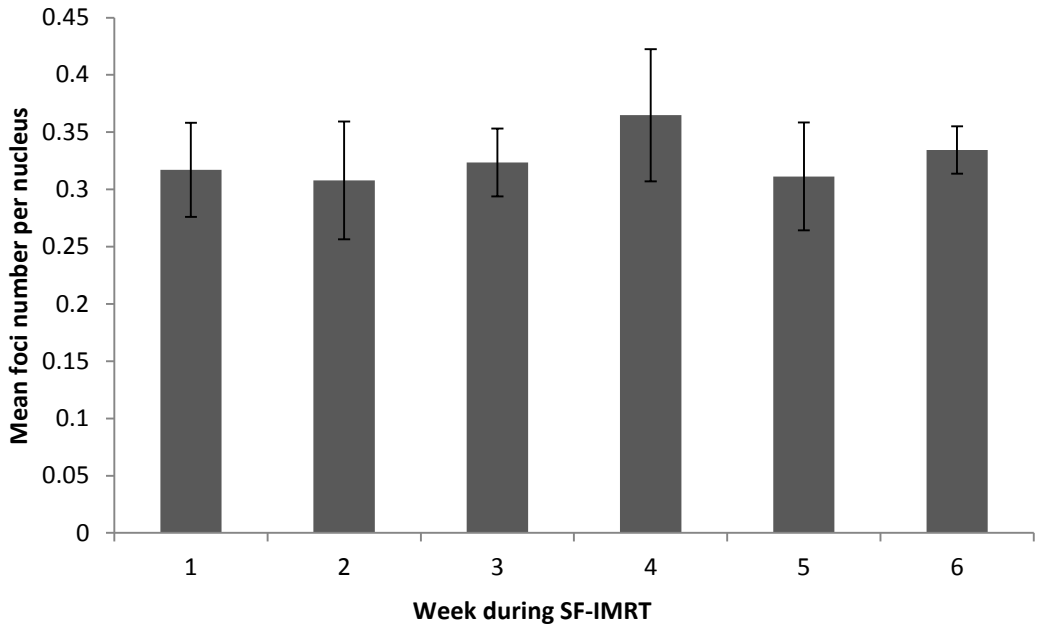

	Mean γ-H2AX foci per nucleus (SD)					
Week during treatment	**1**	**2**	**3**	**4**	**5**	**6**
Cumulative dose at point of sampling	**1.8Gy**	**10.8Gy**	**19.8Gy**	**28.8Gy**	**37.8Gy**	**46.8Gy**
Difference in mean γ-H2AX foci (SD)	0.317 (0.158)	0.307 (0.199)	0.323 (0.114)	0.364 (0.223)	0.311 (0.169)	0.334 (0.773)

Fig.2.6: Observed difference in pre and post SF-IMRT mean γ-H2AX levels taken weekly during treatment.

There is no statistically significant difference in the change in mean γ-H2AX levels from one week to another during a course of SF-IMRT.

Error bars represent standard deviation.

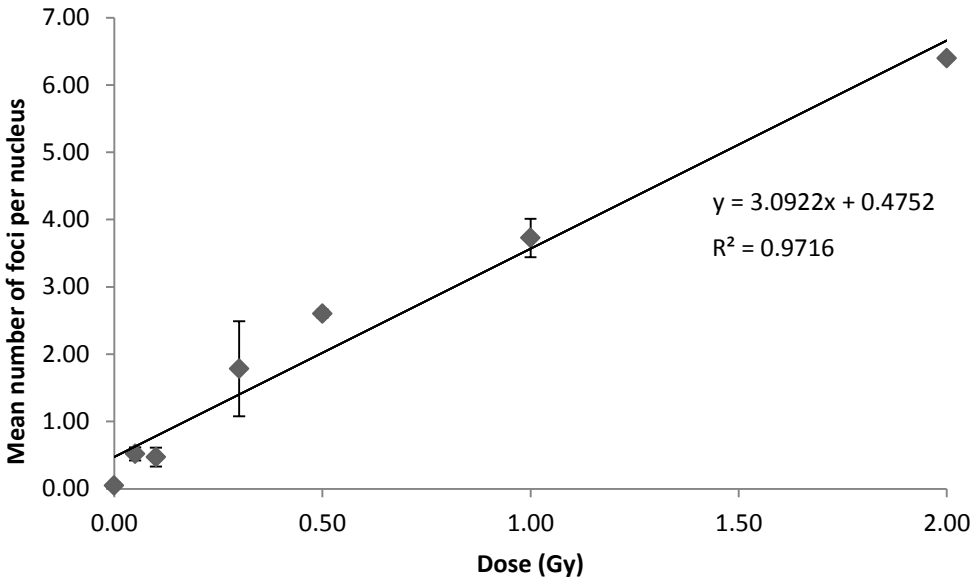

Fig. 2.7: Mean γ-H2AX foci numbers lymphocytes of healthy volunteers counted 30 minutes following ex-vivo irradiation at varying dose levels.

A linear fit to the data gives an estimated 3.092 foci induced per Gy above background levels of 0.47 foci.

Error bars represent standard deviation.

Chapter 3

γ-H2AX as a reproducible and sensitive marker for the comparison of DNA damage from static-field intensity modulated radiotherapy (SF-IMRT), volumetric modulated arc therapy (RapidArc™) and 3D-conformal radiotherapy (CRT).

3.1 Aims

- To confirm that γ-H2AX is a sensitive and reproducible measure of DNA damage in patients undergoing volumetric modulated arc therapy (RapidArc™ [RA]) and 3D-conformal radiotherapy (CRT) to the brain where direct irradiation of circulating blood is minimal.
- To quantify γ-H2AX foci induction at various time points following RA and CRT.
- To investigate whether foci induction following RA and CRT remains constant between successive doses during a 6 week course of treatment.
- To determine the feasibility of using the γ-H2AX assay for comparison of γ-H2AX foci induction for differing radiation techniques (SF-IMRT, RA, CRT).

- To explore whether the differences seen between techniques may be due to low dose whole body exposure.
- To document dose (using various radiotherapy techniques) to regions outside the target volume using a phantom and correlating this with in-vivo data from γ-H2AX foci analysis.

3.2 Introduction

There are now various ways to deliver external beam radiation and attempts have been made to provide increasing target volume conformality. Intensity modulated arc therapy (IMAT) or Volumetric modulated arc therapy (RapidArc™ [RA]), a solution to IMAT, is a novel IMRT delivery technique. It has been shown to achieve radiotherapy plans comparable to static-field IMRT (SF-IMRT), in terms of conformality, with the advantage of shorter treatment times [59,62,213,371,372]. RapidArc™ (RA), in contrast to SF-IMRT, requires a lower number of monitor units and beam-on time to deliver an equivalent tumour dose [25,60,61,373] and may therefore produce a lower whole body exposure [66,373,374]. 3D-conformal radiotherapy has been used for many years and, although also uses a lower number of monitor units and beam on time, it is often inferior to both SF-IMRT and RA in terms of tumour conformality.

The study described in chapter 2 was extended to assess γ-H2AX foci induction in peripheral blood lymphocytes as a marker for DNA damage in patients undergoing radiotherapy using various techniques and confirm its sensitivity and reproducibility as a measure of radiation exposure. Comparison of DNA damage levels is made in

patients treated with static-field IMRT [SF-IMRT], volumetric modulated arc therapy (RapidArc^{TM} [RA]) or 3D-conformal radiotherapy [CRT] techniques delivered to equivalent target volumes and doses within the central nervous system. Attempts have been made to establish whether this DNA damage, measured as γ-H2AX foci levels, is due to low dose radiation as a result of the radiation technique employed.

3.3 Methods and Materials

3.3.1 In-vivo lymphocyte irradiation

3.3.1.1 Patient selection

Following confirmation of the feasibility of using the γ-H2AX assay in patients undergoing SF-IMRT (Chapter 2), further patients at UCLH undergoing radical brain radiotherapy using RA and CRT were also recruited prospectively as part of the study entitled "Evaluation of DNA damage and radiation exposure in patients receiving intensity modulated radiotherapy". Inclusion criteria encompassed all patients with a histological diagnosis of a central nervous system tumour undergoing radiotherapy treatment and who were suitable to attend regular follow up. Exclusion criteria comprised patients undergoing neoadjuvant, adjuvant or concurrent chemotherapy and those who had a previous or concurrent illness which may have interfered with either completion of therapy or follow up. The study protocol was approved by the local ethics committee (ref: 06/Q0512/98) and written informed consent was obtained from all patients. The radiotherapy technique used

for these patients was chosen according to the indications set out by the treating clinician.

3.3.1.2 Sample Collection, Processing and γ-H2AX Foci Analysis

4ml peripheral blood samples were collected as outlined in chapter 2 (see *section 2.3.12*). Detailed beam data were collected for each patient *(see section 2.3.1.2 and appendix A)*. Blood samples were processed and analysed as in chapter 2 (see *sections 2.3.1.3 and 2.3.1.4*)

3.3.2 TLD Measurements

A Rando-phantom was used to further demonstrate dose to body regions outside the target volume with typical SF-IMRT, RA and CRT plans. Thermoluminescent dosimeter (TLD-100H (LiF)) chips (Bicon-Harshow), all 3x3x1mm^3 in size, were used for this purpose and dose recorded using a Harshaw TLD Reader Model 5500.

Initially, four TLD-100H chips were irradiated with 100MU at 5cm depth in solid water (local reference conditions ensuring 1Gy equivalent to 100MU) to provide a TLD reading to dose in Gy conversion factor.

Subsequently, 2 TLD-100H chips were placed in each of the three following positions: right and left shoulder regions (25cm from the central axis of the beam and 10cm laterally from the centre) and the mid pelvic region (60cm from the isocentre, placed approximately at the centre), at a depth of 10cm from the phantom

surface (fig. 3.9). A typical plan from each of the radiotherapy techniques being investigated and with equivalent irradiated tumour volumes was transferred to the Rando-phantom and radiation dose delivered. Dose delivered to the prescription point was 4 fractions of 1.8Gy each (a total of 7.2Gy) for all plans. This was because the dose read out for just a single fraction of 1.8Gy was felt to be too small to be recorded accurately by the TLD chips. Therefore the estimated dose read out after one 1.8Gy fraction of radiotherapy was calculated by dividing the actual dose equivalent read out obtained following 4 fractions by 4. It should be noted that these estimates are taken in regions for which no data are available from the treatment planning system since they are beyond the region that is scanned for planning purposes in individual patients.

The mean of 2 TLD measurements at each site represented the outcomes variable at that point and the mean of all TLD chips placed at various positions was calculated to give the mean dose to areas outside the target volume.

3.3.3 Statistical Analysis

Data evaluation and statistical analysis was performed using PASW 18.0 statistical package. Paired t-tests were used to test for statistical difference between pre and post-radiotherapy samples and repeated measures anova (Greenhouse-Geisser) was used to test for statistical difference between the samples taken at different weeks of treatment. One-way anova and post hoc tests (Bonferonni) were used to test for statistical difference between the radiotherapy delivery techniques and univariate analysis of regression was used to assess for confounding factors, such

as planning target volume, monitor units and beam on time. Statistical significance was set at 5%.

Mean dispersion index (MDI) was used to determine whether the distribution of foci numbers per cell deviated from the Poisson distribution. The MDI can quantify whether the observed occurrences are clustered or dispersed compared to a standard statistical model. The MDI was used to measure deviation away from the expected Poisson distribution and, in particular, to determine whether different techniques would produce different effects on foci distribution within cell nuclei. The MDI was calculated as the variance:mean ratio with MDI values above 1 implying overdispersion away from the Poisson distribution.

3.4 Results

3.4.1 Patient Characteristics

25 patients were recruited in total, with the radiotherapy technique used based on clinical indication. One patient, due to receive CRT, withdrew from the study after a baseline blood sample was taken, leaving 24 fully evaluable patients. All radiotherapy was delivered using a linear accelerator, 6MV photons at a median dose of 50.4Gy in 28 fractions. 15 patients received SF-IMRT for meningiomas (14) and pituitary adenoma (1) (the details of which have been recorded in chapter 2). 5 patients received RA for meningiomas (1), pituitary adenoma (1), craniopharyngiomas (2) or astrocytoma (1). 4 patients received CRT for pituitary adenomas (3) and meningioma (1). Patient characteristics and beam parameters

are summarized in table 3.1. The lower numbers of patients recruited to the RA and CRT groups were determined based on the variance in the initial data.

3.4.2 Beam characteristics and quantification of γ-H2AX foci per cell during RapidArc™ (RA)

Radiotherapy using RapidArc™ (RA) was delivered to a median planning target volume (PTV) of 94 cm^3 (range 16.9 to 506.9 cm^3). A median of 1 arc (range 1 to 2 arcs) was used with a median of 323 MU (range 284 to 470 MU) and at a dose rate of 600 MU/min. The median 'beam on time' was 98 seconds (range 96 to 188 seconds). One patient with a target volume of 506.9 cm^3, treated to a dose of 54.9Gy in 1.8Gy per fraction for an astrocytoma, required 2 arcs for adequate dose conformality. This necessitated 470 monitor units and a beam-on-time of 188 seconds. The patient with the smallest target volume (16.9 cm^3), treated to a dose of 50.4Gy in 1.8Gy per fraction, needed 343 monitor units and a beam on time of 98 seconds. However, the patient with the shortest beam on time (96 seconds) and lowest number of monitor units (284 MU) had a target volume of 79 cm^3.

Baseline γ-H2AX foci levels in the RA cohort of patients were 0.166 ± 0.05. An increase in radiation-induced γ-H2AX foci was clearly visualised in patient samples taken 30 minutes after each 1.8Gy fraction of RA (fig.3.1). Similarly to SF-IMRT, there is a statistically significant increase in γ-H2AX foci levels following RA treatment and this was consistent between samples taken at the same time during each week of radiotherapy (fig. 3.1 and table 3.2). Throughout the entire course of radiotherapy, there is a statistically significant increase in γ-H2AX foci following RA compared to pre-treatment samples (fig. 3.3). The mean γ-H2AX foci per nucleus

was 0.175 ± 0.067 pre-treatment and 0.360 ± 0.101 post RA, with a mean increase of 0.185 ± 0.081 ($p<0.0001$) over a 6 week course of RA radiation therapy.

Furthermore, in a similar way to SF-IMRT, the post RA increase in mean γ-H2AX levels varied slightly from one week to another. However, there was no statistically significant difference in the observed increase in γ-H2AX foci levels following RA between samples taken during different weeks of treatment (0.135 v 0.241 v 0.203 v 0.201 v 0.173 v 0.156, $p=0.333$). In addition, there was no statistically significant difference between baseline foci levels compared to foci levels taken at 2 weeks (0.166 v 0.197, $p=0.585$) and also at 6 weeks (0.166 v 0.198, $p=0.706$) post-radiotherapy, indicating no long-term accumulation of damage after completion of treatment.

3.4.3 Beam characteristics and quantification of γ-H2AX foci per cell during CRT

CRT was delivered using 3 fields to treat a median planning target volume (PTV) of 39 cm^3 (range 29.5 to 160 cm^3). This was performed using a median of 256 MU (range 240 to 339 MU), at a dose rate of 600 MU/min and with a median 'beam on time' of 57.7 seconds (range 51.5 to 72 seconds). The patient with the largest tumour volume (160 cm^3) required 261 monitor units and a beam-on-time of 72 seconds. However, the largest monitor units (339 MU) were required for a target volume of 30.4 cm^3 and radiation was delivered in 51.5 seconds. The patient with the smallest tumour volume of 29.5 cm^3 required 251 monitor units and a beam-on-time of 58 seconds.

Baseline γ-H2AX foci levels in this cohort of patients were 0.108 ± 0.60. An increase in radiation-induced γ-H2AX foci could be visualised in patient samples taken 30 minutes after each 1.8Gy fraction of CRT. Similarly to the other radiation techniques, there is a statistically significant increase in γ-H2AX foci levels following CRT treatment and this was consistent between samples taken at the same time during each week of radiotherapy (fig. 3.4 and table 3.3). Throughout the entire six week course of radiotherapy, there is a statistically significant increase in γ-H2AX foci following CRT compared to pre-treatment samples (fig. 3.5). The mean γ-H2AX foci per nucleus over a whole course of CRT was 0.104 ± 0.090 pre-treatment and 0.247 ± 0.125 post CRT, with a mean difference of 0.142 ± 0.041 ($p<0.0001$).

In a similar way to SF-IMRT and RA, the post CRT increase in mean γ-H2AX levels varied slightly from one week to another (fig. 3.6). However, there was no statistically significant difference in the observed increase in γ-H2AX foci levels following CRT between samples taken during different weeks of treatment (0.148 v 0.140 v 0.121 v 0.148 v 0.161 v 0.137, $p=0.817$). In addition, there was no statistically significant difference between baseline foci levels compared to foci levels taken at 2 weeks (0.108 v 0.053, $p=0.271$) and also at 6 weeks (0.108 v 0.045, $p=0.335$) after completion of radiotherapy, indicating no long-term accumulation of damage after completion of treatment.

3.4.4 Comparison of radiotherapy treatment groups

3.4.4.1 γ-H2AX Measurements

There is a reproducible increase in the number of γ-H2AX foci per nucleus following radiotherapy associated with all delivery techniques described (fig.3.7a-c).

However, the overall increase in mean γ-H2AX foci levels per nucleus following irradiation varies significantly between the techniques (SF-IMRT v RA v CRT: 0.322 v 0.185 v 0.142, p=0.005), (table 3.4). There is a statistically significant greater increase in mean γ-H2AX foci levels per nucleus over the whole course of treatment with SF-IMRT compared to both RA and CRT (SF-IMRT v RA: 0.322 v 0.185, p=0.044; SF-IMRT v CRT: 0.322 v 0.142, p=0.013) (fig. 3.8). However, the small increase in mean γ-H2AX foci levels following radiotherapy seen with RA compared to CRT is not statistically significant (0.185 v 0.142, p=1.00).

Any difference observed in the pre radiotherapy mean γ-H2AX foci values between the various treatment groups is not statistically significant (SF-IMRT v RA v CRT: 0.170 v 0.175 v 0.104, p=0.378). Likewise, the difference seen in baseline values is also not statistically significant; SF-IMRT v RA v CRT: 0.186 v 0.166 v 0.108, p=0.667.

3.4.4.2 Planning target volume

The univariate analysis for regression demonstrates that the planning target volume is not directly related to the differences seen in γ-H2AX foci numbers after radiotherapy, $F(1,20)=0.851$, $p=0.367$. There continues to be a statistically significant effect of radiotherapy technique on change in foci numbers following irradiation after controlling for the effect of target volume, $F(2,20)=6.991$, $p=0.005$, suggesting that any difference in planning target volumes between the groups does not have an effect on the difference in foci numbers seen between the groups.

3.4.4.3 Beam Parameters

The covariates, monitor units and beam on time, were also not directly related to the change in foci numbers after radiotherapy: $F(1,20)=0.375$, $p=0.547$, $F(1,14)=0.008$, $p=0.928$ respectively. There continued to be an effect from radiation technique on change in foci numbers when controlling for the effect of 'monitor units' and 'beam on time', $F(2:12)=7.814$, $p=0.007$.

3.4.4.4 TLD measurements

Table 3.5 demonstrates the reference reading obtained from 4 TLD chips irradiated with 100 monitor units at 5cm depth in solid water, so that 1Gy is equivalent to 100 MU and therefore provided a TLD reading : Gy factor. The mean of these reference readings provides a value of 1296.57 (with a standard deviation of 114.77 and coefficient of variation (standard deviation/mean) of 9%) read out equivalent for each Gy. For the purposes of likely low doses to areas at some distance from the target volume, we used a conversion factor of 12.97 per cGy.

The TLD measurements from chips placed in regions outside the target area similarly suggest that there is a greater mean dose to all areas measured outside the primary target volume following SF-IMRT compared to both RA and CRT. Table 3.6 details the TLD measurements and equivalent dose from each TLD chip placed at the right and left shoulders and the mid pelvis regions following four fractions of 1.8Gy per fraction (and also after one 1.8Gy fraction) using one radiotherapy plan from each of the three different radiation techniques. As expected, the greatest dose is demonstrated in TLDs located

closest to the target volume (those placed at the level of the shoulders), with the lowest dose seen within TLDs placed furthest away from the target volume (mid pelvis). Table 3.7 documents the mean and the standard deviation (SD) of scattered dose according to radiation technique. The mean dose to areas outside the target volume, taking into account all TLDs placed, is higher with SF-IMRT (SF-IMRT v RA v CRT: 0.196cGy v 0.144cGy v 0.116cGy). These measurements illustrate an increased dose to non-target areas with SF-IMRT by a factor of 1.4 and 1.7 in comparison to RA and CRT respectively.

Assuming the same dose response as seen in our ex-vivo data from lymphocytes of healthy volunteers (from section 2.4.3), we can also estimate the whole body exposure per fraction associated with the different radiotherapy techniques using this data. The ex-vivo data suggests 3.092 foci induced per Gy, above background levels of 0.47 foci. Therefore the 0.322 increase in mean γ-H2AX foci with SF-IMRT would suggest an estimated mean whole body exposure of 0.104Gy. Similarly, the estimated mean whole body exposure with RA and CRT is 0.060Gy and 0.046Gy respectively (table 3.8).

3.4.4.5 γ-H2AX Foci distribution

Since we hypothesized that SF-IMRT may specifically increase low dose whole body exposure, foci distributions were also analysed in these samples to ascertain whether there was a greater change in cells with low foci numbers (fig. 3.10), suggesting exposure to low radiation doses. Following SF-IMRT, the percentage of cells without any foci was lower than after both RA and CRT (IMRT 11% reduction in cells with no foci post treatment, RA 6.6% reduction, CRT 5.9% reduction,

p<0.0001). Conversely, there is a greater percentage increase in cells with 1-2 foci and 3-5 foci following SF-IMRT compared to RA and CRT (1-2 foci: SF-IMRT 7.1 %, RA 3.7%, CRT 4% more cells, p=0.002; 3-5 foci: SF-IMRT 2.8%, RA 1.7% and CRT 1.6% more cells, p=0.002). Interestingly there is a greater percentage increase in cells with 6-10 foci following SF-IMRT compared to CRT (SF-IMRT 1.5%, CRT 0.2%, p=0.008), but no statistically significant difference between SF-IMRT and RA (1.5% and 1.1% respectively, p=0.857) (fig 3.10). There is no statistically significant difference in the percentage increase of cells with over 10 foci following the three radiotherapy techniques.

We used the mean dispersion index (MDI) to measure deviation away from the expected Poisson distribution to further investigate whether different techniques produced different effects on foci distribution. MDI levels above 1 indicate overdispersion. There was evidence of some overdispersion in baseline samples associated with all radiotherapy techniques. Following irradiation there was a clear change, with evidence of more deviation away from Poisson distributions, associated with MDIs above 2. However, the MDI with SF-IMRT was greater than with RA and CRT (4.11 v 3.13 v 2.60 respectively; an increase in MDI of 1.61, 1.10, and 0.81 from baseline respectively) (table 3.9). This data demonstrates that the distribution of foci does not follow a simple Poisson distribution and may, in fact, represent a combination of cells that are directly irradiated as well as those cells that are indirectly irradiated.

3.5 Discussion

The results from this comparative study have attempted to quantify the DNA damage produced following different radiation techniques. Similarly to SF-IMRT, there is a statistically significant increase in γ-H2AX foci per nucleus in post-radiotherapy samples compared to pre-treatment samples for both the RA and CRT groups (0.174 pre and 0.360 post RA, $p \leq 0.0001$ and 0.104 pre and 0.247 post CRT, $p<0.0001$). In addition, any difference documented between the samples taken during the different weeks of treatment for each technique is not statistically significant ($p=0.333$ and $p=0.817$ respectively).

There was some variation in baseline foci numbers between patients and it is noteworthy that baseline levels in the group of patients treated with CRT tended to be lower than in the IMRT groups, although they are still generally similar to baseline foci levels in unirradiated cells reported in the literature [311,325,327,338,340,345,349,356]. Since these samples were collected and analysed in separate batches, this variation in baseline levels may reflect subtle changes in staining quality between experiments, but will not affect the main comparison in which foci change from baseline levels was analysed.

To date, there are very few published data investigating the use of this assay in prospective studies to compare treatment techniques. This study has confirmed that the γ-H2AX assay is sensitive enough to assess and quantify DNA-damage in patients receiving different radiotherapy delivery techniques.

There are a greater number of foci produced following irradiation with SF-IMRT compared to both RA and CRT. Reproducible but smaller increases in γ-H2AX foci can be seen following RA and CRT (SF-IMRT 0.322 v RA 0.185 v CRT 0.142 foci per cell, p=0.005). Extrapolating from the ex-vivo data from chapter 2, there is an increase in whole body exposure with SF-IMRT compared to both RA and CRT of 1.7 and 2.3 fold respectively, which is broadly in line with changes in TLD measurements taken from regions some distance away from the tumour target volume.

There are also differences observed in foci distributions following radiation using different treatment techniques, with a greater proportion of cells displaying lower foci numbers (between 1 to 5 foci per nucleus) compared to cells with greater foci numbers per cell. This was associated with a greater change in the mean dispersion index following SF-IMRT compared to both RA and CRT; similar to results from ex vivo irradiation experiments to reflect the effect of partial body irradiation [325], but may also mirror the effects of DNA damage as a result of low dose radiation. These findings are analogous to those of Zwicker et al. who, despite not managing to identify a statistically significant difference in γ-H2AX foci numbers between techniques, did demonstrate more delivery of doses below 20% of the total dose and less doses of between 30-90% with IMRT compared to conventional 3D conformal treatments in patients with prostate cancer [356].

Given these findings, it is feasible that this difference results from the increased low dose radiation to non-target regions delivered by SF-IMRT. This extra low-dose exposure is produced through various treatment delivery factors, including increased monitor units and ‘beam on time’, which are functions of the complexity of

static-field intensity-modulation, its delivery technique and collimator design [236]. Scattered radiation can originate from internal scatter within the patient and is dependent on the dose delivered. Importantly, the extra low dose is also a consequence of scatter from the linac head, multi-leaf collimators, and is generally dependent on the number of monitor units. It has been shown previously that the number of radiotherapy fields has a direct effect on the amount of radiation delivered to distant sites, thereby increasing the scattered dose [255]. Beam modifiers can dramatically increase the amount of scattered radiation within the body and dynamic multileaf collimation fields require 2 to 14 times the number of monitor units than an open static field [252]. In vitro studies have demonstrated, using the γ-H2AX assay in human fibroblasts, a relative increase in linear energy transfer (LET) and DNA-DSB per unit dose in blocked beam configurations and in the penumbra of a 6MV photon beam [375] compared to levels seen with an open beam. As a consequence, techniques, such as SF-IMRT, require a significant increase in monitor units and beam on time compared to conventional techniques [236,239]. This suggests that the high dose gradients produced by techniques, such as SF-IMRT, result in non-negligible extra dose to the surrounding normal tissues. Early work has documented that an increase in the number of monitor units required for techniques, such as tomotherapy, in comparison to conventional techniques, results in a much higher whole body dose [236,241,244,246] and some have even suggested that dynamic leaf MLC IMRT is associated with higher monitor unit requirements compared to step and shoot IMRT [250-252].

Conversely, as can be seen with data from this chapter, both RA and CRT require fewer monitor units and beam on time, although in terms of treatment planning and target definition, CRT often provides inferior target dose conformality than both SF-IMRT and RA. In fact, there have been various studies documenting the reduction

in beam on times and monitor units with RA in comparison to SF-IMRT [25,59-61,63], with a reduction in monitor units in the range of 37-66% [60,61,376] and a similar reduction in treatment times [25], which is comparable to the findings in the work presented here. This may in turn have benefits of a reduction in leakage radiation and therefore a reduction of integral radiation dose to the rest of the body [58,65,66].

Although it has been postulated that increased beam on time and monitor units (and also target volume) have an effect on the increased foci numbers and therefore whole body dose, the data from this study (and others [376]) has not been able to confirm that these confounding factors are directly implicated in the increased γ-H2AX foci levels. This may, of course be limited by the small sample size within this patient cohort and further studies may be able to determine the true role of these factors.

Nevertheless, this is the first study to demonstrate a significant difference in the level of DNA-damage in patient blood lymphocytes in a comparison between SF-IMRT and arc-based IMRT techniques. One would predict a lower level of low-dose irradiation-induced DNA damage with CRT compared to both SF-IMRT and RA and these data demonstrate that the γ-H2AX assay was sensitive enough to detect differences in whole body exposure between SF-IMRT and CRT, which previous studies have not achieved [356]. No statistically significant difference was observed between foci numbers in patients treated with CRT and RA, although RA tended to produce slightly higher levels than CRT, as would be predicted. Larger patient numbers would be necessary to estimate the size of this difference accurately.

Dose measurements using TLD and similar devices can give estimates of non-target dose and the values presented here are in line with literature reports of peripheral, whole body dose assessments, which may suggest that this dose is as a result of scatter with doses of approximately 1% or less of the total dose recorded at distances approximately 20cm or more from the target edge [249,376,377]. From this, estimated scattered dose and organ equivalent doses appear to reduce as the distance from the target edge increases and some have compared these measurements between techniques as a rudimentary measure of scatter dose [376,377].

γ-H2AX within lymphocytes (which may reflect a combination of background irradiation, direct radiation as well as scattered irradiation) is useful to estimate dose delivered to the whole body, even in the presence of partial body irradiation due to lymphocyte redistribution [340,355]. However, it should be pointed out that modelling the dose delivered from external beam radiotherapy to a circulating population of lymphocytes is not straightforward for a number of reasons. Irradiated lymphocytes may be mixed with those that are unirradiated and there is a continuous exchange of lymphocytes between blood and tissues as well as lethal damage to some lymphocytes, all of which need to be taken into consideration. A recent publication has proposed a dynamic model, which predicts a significant dose to blood during transit through target volumes in brain (which others have also highlighted [340,347]), but does not include an estimate of the effect of scattered dose to the whole blood volume beyond the brain and does not account for repair or loss of damaged cells between doses, as the results from this data imply [378]. It is clear that, due to their circulation through the high and low-dose volumes, the dose received by any one peripheral lymphocyte may not bear a linear relationship to

delivered dose at the target or at any specific point as measured by TLD within a Rando-phantom.

Nevertheless, this comparison with TLD measurements shows that the trend towards higher integral dose, estimated from foci counts, parallels an increase in measured peripheral doses, which would be expected. Since the majority of lymphocytes at any one time will be outside the high-dose target volume, the majority of the foci may result from low-dose exposure. This could explain why this assay appears to be sensitive enough to pick up differences between treatment techniques.

The effects of low-dose radiation on second malignancy risks have been widely discussed and estimated in the past. There is evidence that the incidence of cancer increases steeply as a function of low radiation doses, then plateaus, but does not fall rapidly at high doses because of cell kill [266]. The exact dose plateau is difficult to determine, with varying reports in the literature. Some have suggested a dose of 10Gy, beyond which the risk of carcinogenesis exponentially declines [379]. However, the accumulation of incomplete repair of sublethal damage, as suggested by some groups with IMRT [366], is a potential source of increased radiation exposure and, therefore, may be associated with an increased risk in secondary malignancies. Attempts have been made to estimate the risk of radiation-induced malignancies following various modalities of treatment, with results pointing to as much as a doubling of the relative incidence rate after IMRT compared to conventional techniques [147,148], although some have estimated much lower levels when using lower energies [380]. The findings in the study presented in this chapter suggest that the level of low-dose DNA-damage experienced by circulating

lymphocytes was indeed significantly higher with SF-IMRT than CRT and RA, but that RA produced levels similar to those seen with CRT. A linear no-threshold dose model predicts that even small increases in whole-body exposure, as described here would be associated with increased risk. Modelling studies have proposed a non-linear response to dose, with tissues exposed to low dose irradiation at increased risk of second cancers [267-269]. In fact, recent large scale epidemiological studies examining the relationship between low radiation doses and risk of childhood malignancy [381,382] are consistent with this linear no threshold cancer risk model.

As oncological treatments become more effective, there are a growing number of patients alive many years after treatment. Therefore, damage to normal tissues that manifests itself over the longer term becomes an important consideration in the choice of treatment plans and modalities. Dose-response relationships for tumours and therefore dosimetry for treatments has been fairly well documented. However, dosimetry for late effects is performed on a relatively ad hoc manner. Through our direct measurements of DNA damage, these results point to increased low dose irradiation-induced damage from SF-IMRT compared to RA and CRT for brain tumours, which may have implications in the choice of radiotherapy delivery techniques, especially in children and young adults with good prognosis disease. The results demonstrated here are generated on a small cohort of patients and, therefore, experiments with a larger group of participants may demonstrate further conclusive evidence of the increased DNA damage from SF-IMRT in comparison to other techniques and may also demonstrated a statistical difference between RA and 3D- CRT. Further mathematical modelling of the data may allow a more accurate assessment and correlation of the DNA damage and scatter dose.

As developments in radiotherapy techniques move forward, it is important to be wary of the potential effects not just to the tumour, but also to normal tissue and the resulting long term consequences. Techniques, such as proton therapy are now coming to the fore and one would expect a lower whole body dose, as many groups are beginning to investigate [383-388], although it is associated with secondary neutrons and therefore warrants further investigation.

3.6 Conclusion

The data presented in this chapter has demonstrated that, using the sensitive γ-H2AX assay as a marker of double stranded DNA damage, a difference can be observed following irradiation using different radiotherapy delivery techniques, with a statistically significant difference between SF-IMRT and RA or CRT. However, no statistically significant difference was seen between RA and CRT and further studies with larger sample sizes may be required to demonstrate this clearly. There are greater numbers of lymphocytes observed with low foci numbers following SF-IMRT compared to other techniques, which may reflect a greater low dose radiation to areas outside the target volume. This low dose may, in turn, have an effect on the long term carcinogenic risks associated with various radiation techniques and may ultimately influence choice of technique in certain patient populations.

There has been growing interest in the use of proton therapy; harnessing its distinct 'Bragg-peak' properties to allow dose escalation, whilst further minimizing dose to

normal structures. Extending this γ-H2AX comparison to proton therapy would be valuable to allow quantification of DNA damage (and whole body dose) to areas outside the target volume and provide assessment of the potential long term complications of this delivery technique.

Parameter	SF-IMRT		RA		CRT	
	Median	Range	Median	Range	Median	Range
Number of patients	15		5		4	
Age	52.5	38-65	54	40-68	60	29-68
Dose (Gy)	50.4		50.4	50.4-54.9	50.4	
Dose/# (Gy)	1.8		1.8	1.8-1.85	1.8	
Monitor Units (MU)	518	393-1014	323	284-470	256	240-339
Dose rate (MU/min)	400		600		600	
Beam on time (seconds)	124	98-254	98	96-188	57.75	51.5-72
Number of fields or arcs	5	4-7	1	1-2	3	
PTV (cm^3)	88	23.1-288	94	16.9-506.9	39	29.5-160

Table 3.1: Patient characteristics and beam parameters for all treatment groups.

Abbreviation: SF-IMRT=Static-field IMRT; RA=RapidArc^{TM}; CRT=3D-conformal radiotherapy; PTV = planning target volume

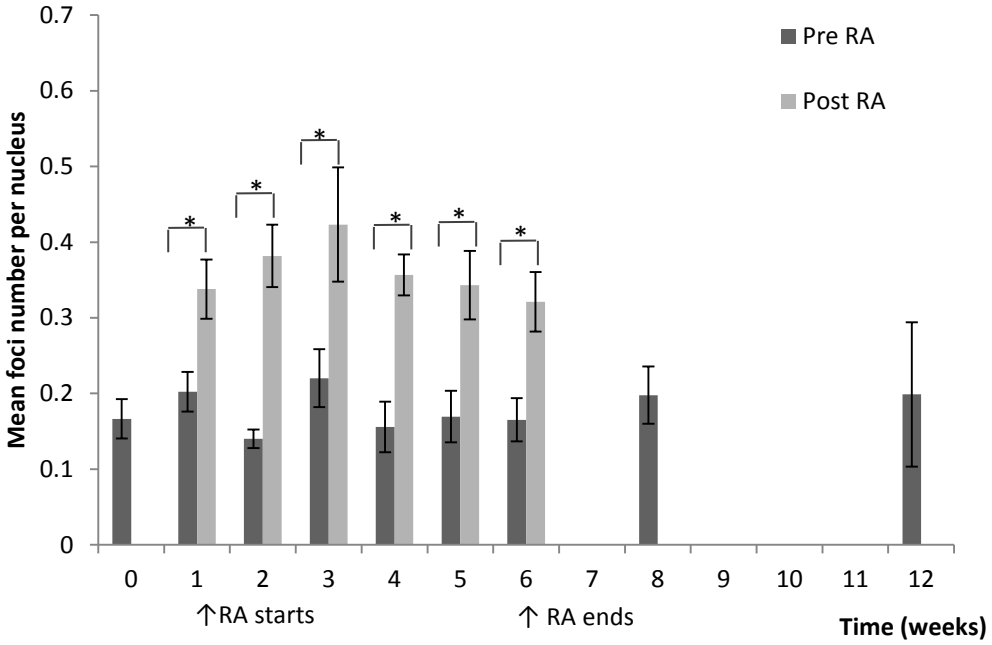

Fig. 3.1: Mean γ-H2AX foci per nucleus measurements at weekly time points during and after a six week course of RA.

Error bars represent standard deviation; *=p<0.05.

	Mean γ-H2AX foci per nucleus (SD)					
Week during treatment	**1**	**2**	**3**	**4**	**5**	**6**
Cumulative dose at point of sampling	**1.8Gy**	**10.8Gy**	**19.8Gy**	**28.8Gy**	**37.8Gy**	**46.8Gy**
Pre RA (SD)	0.202 (0.058)	0.140 (0.027)	0.220 (0.085)	0.155 (0.074)	0.169 (0.076)	0.165 (0.063)
Post RA (SD)	0.337 (0.087)	0.381 (0.092)	0.423 (0.168)	0.356 (0.060)	0.343 (0.101)	0.321 (0.088)
Difference (SD)	0.135 (0.051)	0.241 (0.102)	0.203 (0.128)	0.201 (0.075)	0.173 (0.036)	0.156 (0.052)
P values	0.004	0.006	0.024	0.004	<0.0001	<0.003

Table 3.2: Mean γ-H2AX foci per nucleus levels pre and post RA for each week during treatment.

Abbreviations: SD=standard deviation

There is a statistically significant difference in foci numbers in samples taken weekly pre and post-treatment and calculated at the same time during each week of treatment. The difference observed is independent of treatment week.

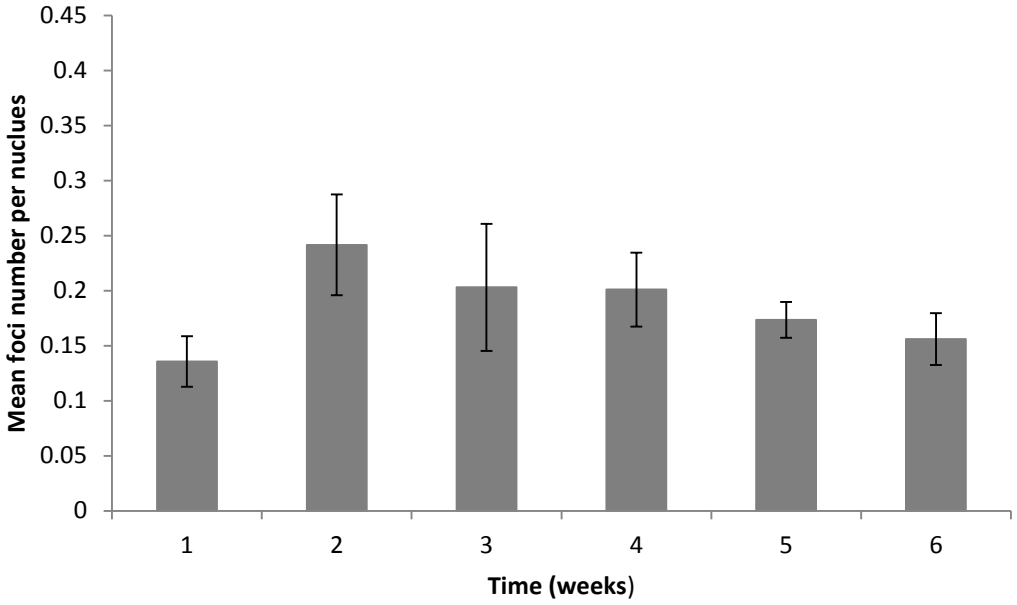

	Mean γ-H2AX foci per nucleus (SD)					
Week during treatment	**1**	**2**	**3**	**4**	**5**	**6**
Cumulative dose at point of sampling	**1.8Gy**	**10.8Gy**	**19.8Gy**	**28.8Gy**	**37.8Gy**	**46.8Gy**
Difference (SD)	0.135 (0.051)	0.241 (0.102)	0.203 (0.128)	0.201 (0.075)	0.173 (0.036)	0.156 (0.052)

Fig.3.2: Observed difference in pre and post RA mean γ-H2AX levels taken weekly during treatment.

There is no statistically significant difference in the change in mean γ-H2AX levels from one week to another during a course of RA.

Error bars represent standard deviation.

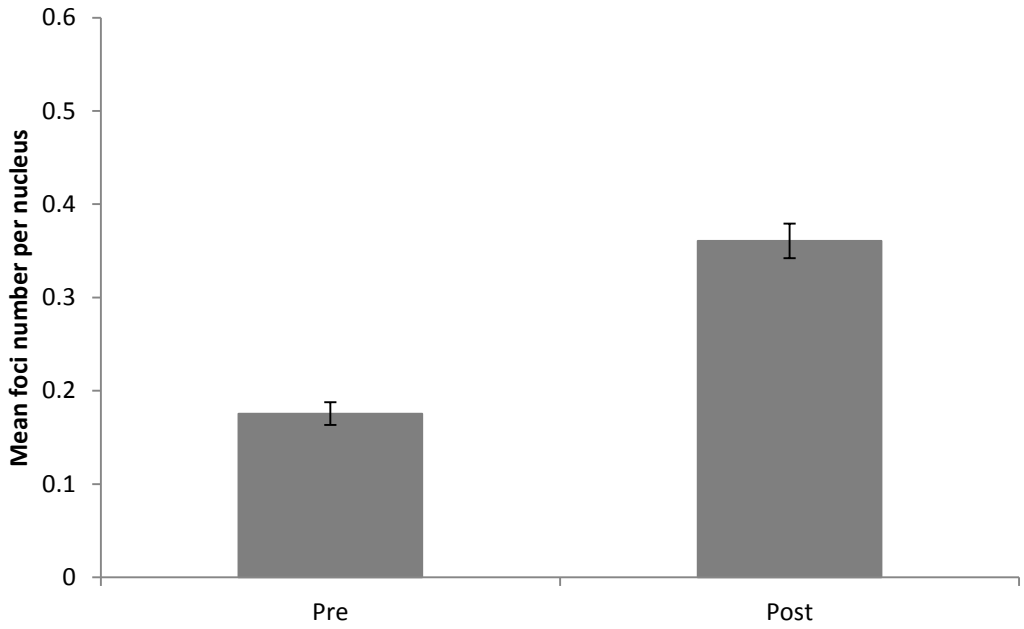

Fig. 3.3: Mean γ-H2AX foci per nucleus measurements pre and post irradiation over a six week course of RA.

There is an increase of 0.185 ± 0.081 ($p<0.0001$) mean γ-H2AX foci seen within lymphocyte nuclei following RA over a whole 6 week course of treatment.

Error bars represent standard deviation

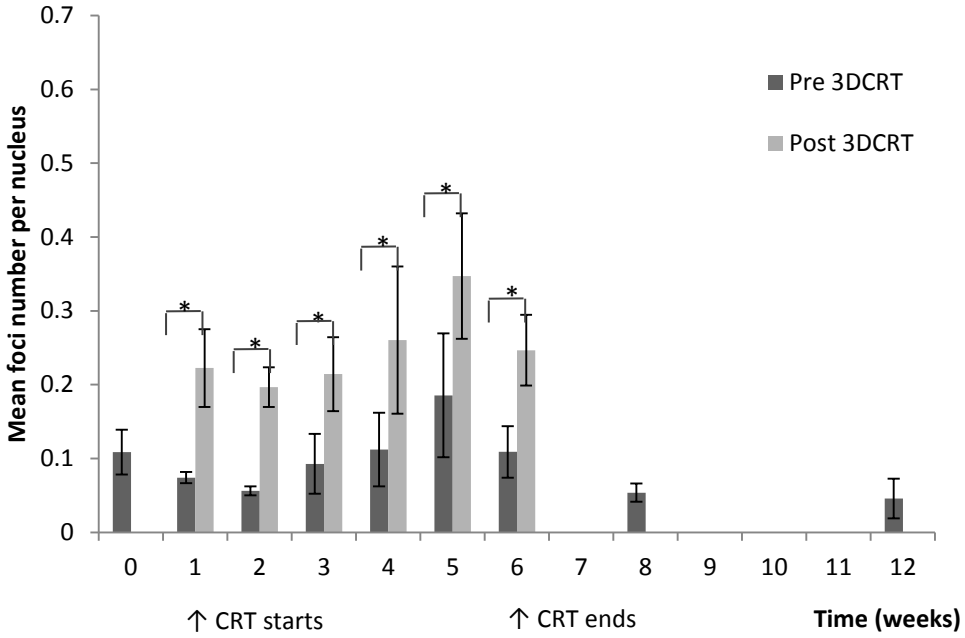

Fig. 3.4: Mean γ-H2AX foci per nucleus measurements at weekly time points during and after a six week course of CRT.

Error bars represent standard deviation; *=p<0.05

	Mean γ-H2AX foci per nucleus (SD)					
Week during treatment	**1**	**2**	**3**	**4**	**5**	**6**
Cumulative dose at point of sampling	**1.8Gy**	**10.8Gy**	**19.8Gy**	**28.8Gy**	**37.8Gy**	**46.8Gy**
Pre CRT (SD)	0.074 (0.015)	0.056 (0.011)	0.092 (0.081)	0.112 (0.099)	0.185 (0.167)	0.108 (0.069)
Post CRT (SD)	0.222 (0.105)	0.196 (0.053)	0.214 (0.100)	0.260 (0.199)	0.347 (0.169)	0.246 (0.095)
Difference (SD)	0.148 (0.098)	0.140 (0.045)	0.121 (0.037)	0.148 (0.104)	0.161 (0.059)	0.137 (0.041)
P values	0.057	0.009	0.008	0.006	0.012	0.007

Table 3.3: Mean γ-H2AX foci per nucleus levels pre and post CRT for each week during treatment.

Abbreviations: CRT=3D conformal radiotherapy; SD=standard deviation

There is a statistically significant difference in foci numbers in samples taken weekly pre and post-treatment and calculated at the same time during each week of treatment. The difference observed is independent of treatment week.

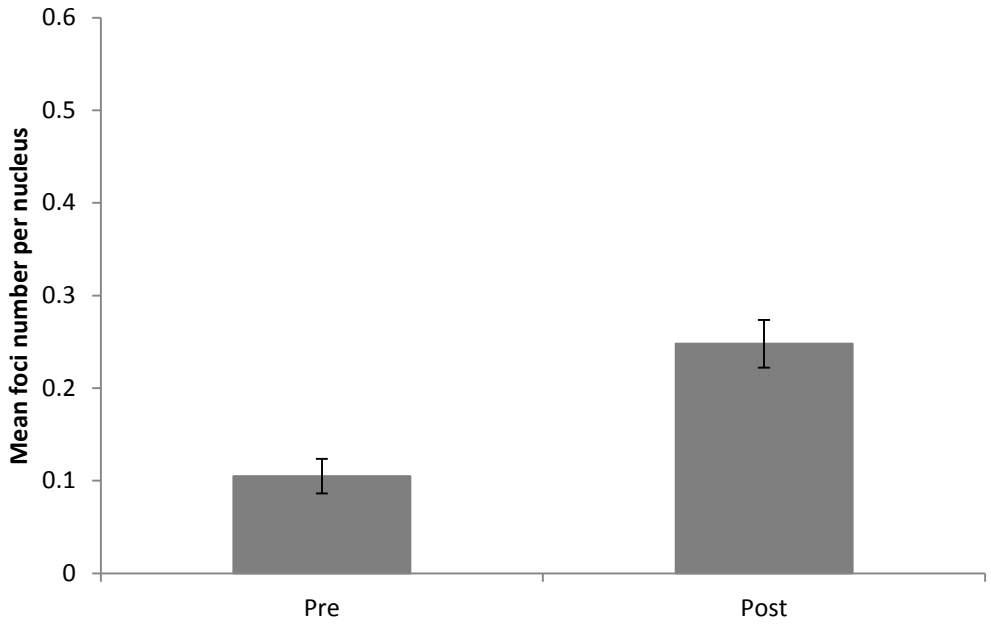

Fig.3.5: Mean γ-H2AX foci per nucleus measurements pre and post irradiation over a six week course of CRT.

There is an increase of 0.142 ± 0.041 ($p<0.0001$) mean γ-H2AX foci seen within lymphocyte nuclei following CRT over a whole 6 week course of treatment.

0.104 ± 0.090 mean γ-H2AX foci pre-treatment and 0.247 ± 0.125 post CRT with a mean difference of 0.142 ± 0.041 ($p<0.0001$).

Error bars represent standard deviation.

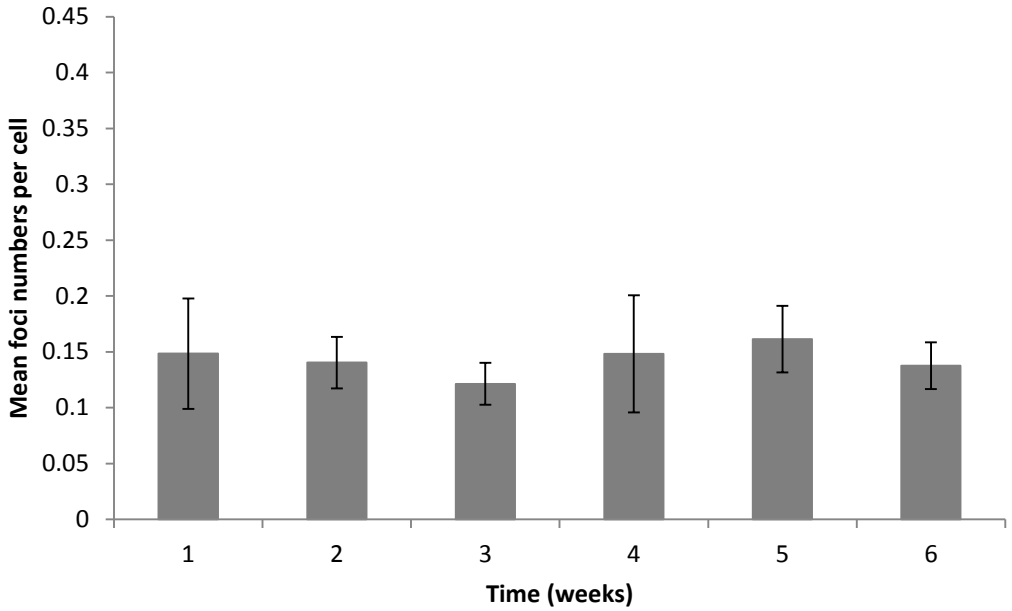

	Mean γ-H2AX foci per nucleus (SD)					
Week during treatment	**1**	**2**	**3**	**4**	**5**	**6**
Cumulative dose at point of sampling	**1.8Gy**	**10.8Gy**	**19.8Gy**	**28.8Gy**	**37.8Gy**	**46.8Gy**
Difference (SD)	0.148 (0.098)	0.140 (0.045)	0.121 (0.037)	0.148 (0.104)	0.161 (0.059)	0.137 (0.041)

Fig.3.6: Observed difference in pre and post CRT mean γ-H2AX levels taken weekly during treatment.

There is no statistically significant difference in the change in mean γ-H2AX levels from one week to another during a course of CRT.

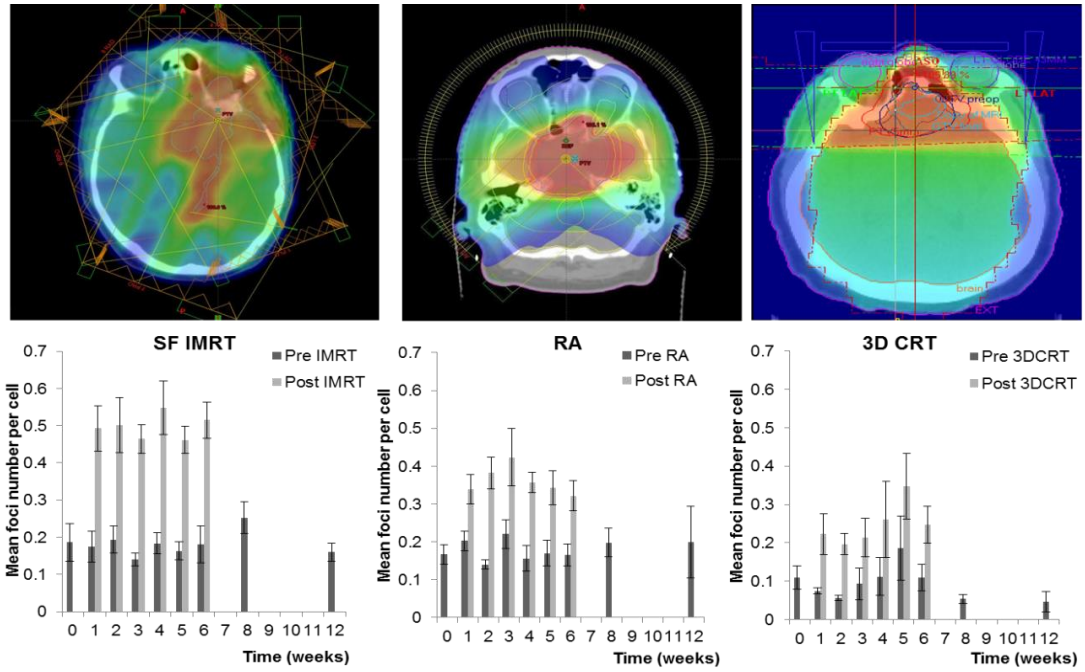

Fig.3.7: Mean γ-H2AX foci per nucleus measurements at weekly time points during and after a six week course of SF-IMRT, RA and 3D CRT respectively.

Images demonstrate typical PTV volumes and isodose colour wash levels for each radiotherapy technique.

Error bars represent standard deviation; *=p<0.05.

Radiotherapy technique	Mean γ-H2AX foci per nucleus (SD)		
	Pre RT	Post RT	Difference
SF-IMRT	0.170	0.493	0.322
RA	0.175	0.360	0.185
CRT	0.104	0.247	0.142

Table 3.4: Overall mean γ-H2AX foci per nucleus measurements before and after irradiation with mean change in γ-H2AX foci levels seen with different radiotherapy technique.

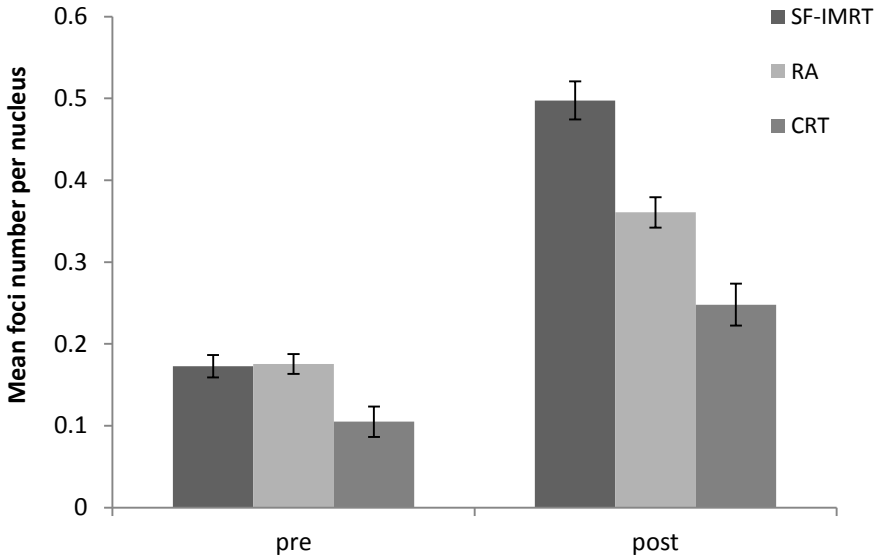

Fig. 3.8a: Pre and post radiotherapy γ-H2AX foci values for all three radiation techniques

Error bars represent standard deviation.

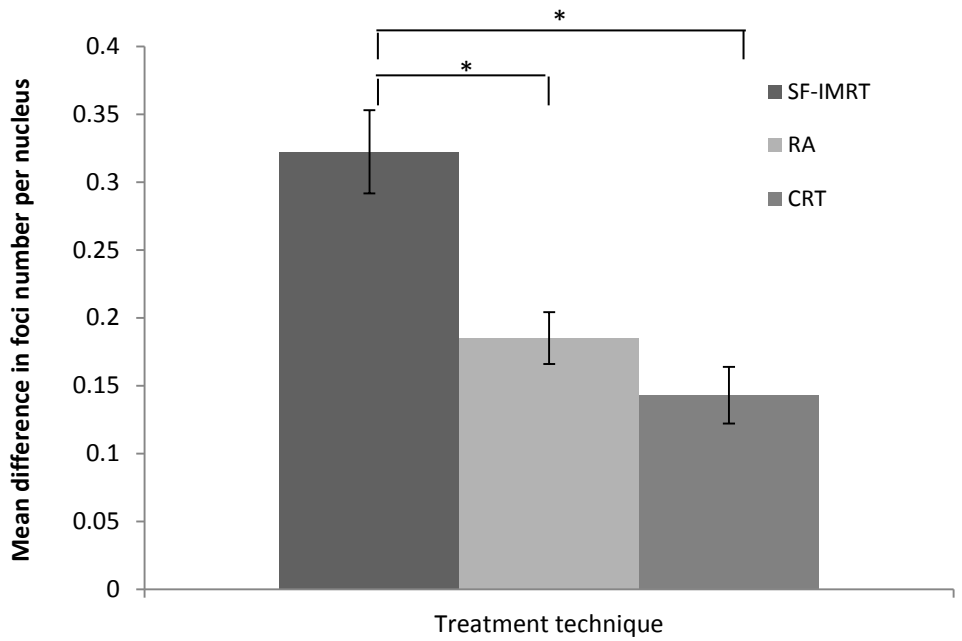

Fig. 3.8b: Overall change in mean γ-H2AX foci per nucleus following treatment with all radiotherapy techniques, calculated as the difference between pre and post-treatment samples over a course of radiotherapy.

There is a greater increased change in mean γ-H2AX foci levels with SF-IMRT compared to RA and CRT ($p=0.044$ and $p=0.013$ respectively).

Error bars represent standard deviation; *=$p<0.05$.

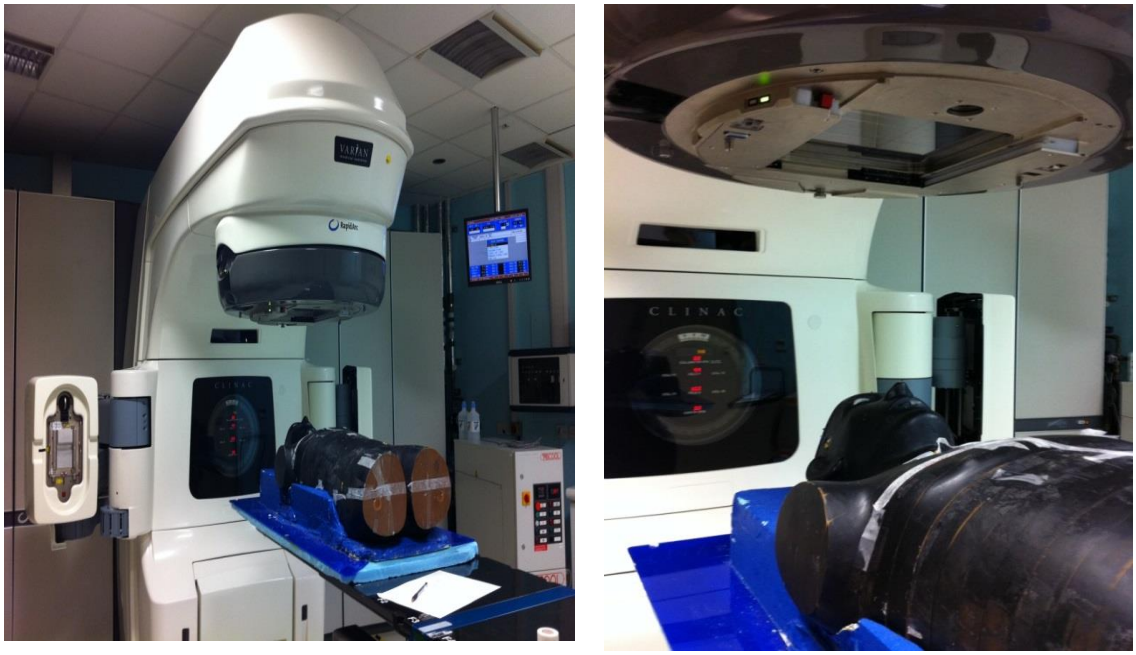

Fig. 3.9: A Rando-phantom used to demonstrate dose to areas outside target volume with typical SF-IMRT, RA and CRT plans.

TLD-100H (LiF) chips (Bicon-Harshow) were placed at a depth of 10cm from phantom surface and in specific areas: right and left shoulders (25 cm from the axis of the beam, 10 cm lateral to the centre), mid pelvis region (at midline and 60cm from the central axis of the beam). Radiation was delivered to the Rando-phantom using a typical plan for each of the study techniques and dose recorded from the TLDs.

TLD number	Reference reading
1	1216.122
2	1313.973
3	1204.079
4	1452.088
Mean	1296.566
SD (COV)	114.768 (9%)

Table 3.5: TLD readout values

Four TLD chips were irradiated with 100MU at 5cm deep in solid water to provide a TLD reading to Gy factor (conversion factor) of 12.97 TLD reading per Gy.

TLD= thermoluminescent dosimeter; SD=standard deviation; COV=coefficient of variation

		SF-IMRT				RA				CRT			
TLD Position	**TLD Number**	**TLD reading after 4 fractions**	**Dose after 4 fractions (cGy)**	**Dose after 1 fraction (cGy)**	**Mean dose (cGy)**	**TLD Reading after 4 fractions**	**Dose after 4 fractions (cGy)**	**Dose after 1 fraction (cGy)**	**Mean dose (cGy)**	**TLD reading after 4 fractions**	**Dose after 4 fractions (cGy)**	**Dose after 1 fraction (cGy)**	**Mean dose (cGy)**
Left Shoulder	1	15.309	1.181	0.295	0.280	8.978	0.692	0.173	0.172	7.115	0.549	0.137	0.139
	2	13.699	1.057	0.264		8.838	0.682	0.170		7.258	0.560	0.140	
Right Shoulder	1	12.769	0.985	0.246	0.257	11.302	0.872	0.218	0.221	8.586	0.662	0.166	0.154
	2	13.895	1.072	0.268		11.632	0.897	0.224		7.352	0.567	0.142	
Mid pelvis	1	2.737	0.211	0.053	0.051	2.035	0.157	0.039	0.039	1.806	0.139	0.035	0.056
	2	2.513	0.194	0.048		2.023	0.156	0.039		3.983	0.307	0.077	

Table 3.6: TLD readings taken at different positions in a Rando phantom following irradiation after 4 fractions of 1.8Gy per fraction using one typical radiotherapy plan from each radiation technique.

Abbreviation: SF-IMRT=Static-field IMRT; RA=RapidArc^{TM}; CRT=3Dconformal radiotherapy; TLD=thermoluminescent dosimeter.

Dose was calculated after the 4 fractions of radiotherapy using the TLD conversion factor. Dose was then calculated for each fraction of radiotherapy, providing a mean dose per fraction.

	Mean Dose in cGy (SD)		
	SF-IMRT	**RA**	**CRT**
Left Shoulder	0.280 (0.022)	0.172 (0.002)	0.139 (0.002)
Right Shoulder	0.257 (0.015)	0.221 (0.004)	0.154 (0.017)
Mid Pelvis	0.051 (0.003)	0.039 (0.0001)	0.056 (0.030)
Mean dose to area outside target volume	0.196 (0.126)	0.144 (0.094)	0.116 (0.053)

Table 3.7: Comparison of dose in Rando-phantom with different radiotherapy techniques as measured with TLDs at non-target sites.

Abbreviation: SF-IMRT=Static-field IMRT; RA=RapidArc^{TM}; CRT=3Dconformal radiotherapy; SD=standard deviation

Dose delivered to the Rando-phantom was the equivalent of one individual fraction (1.8Gy).

Radiotherapy Technique	Mean increase in γ-H2AX foci number per nucleus	Mean TLD measurements (cGy)	Estimated whole body exposure (Gy)
SF-IMRT	0.322	0.196	0.104
RA	0.185	0.144	0.060
CRT	0.142	0.116	0.046

Table 3.8: Mean increase in γ-H2AX foci numbers, TLD measurements at non-target sites and estimated whole body exposure following three radiotherapy techniques.

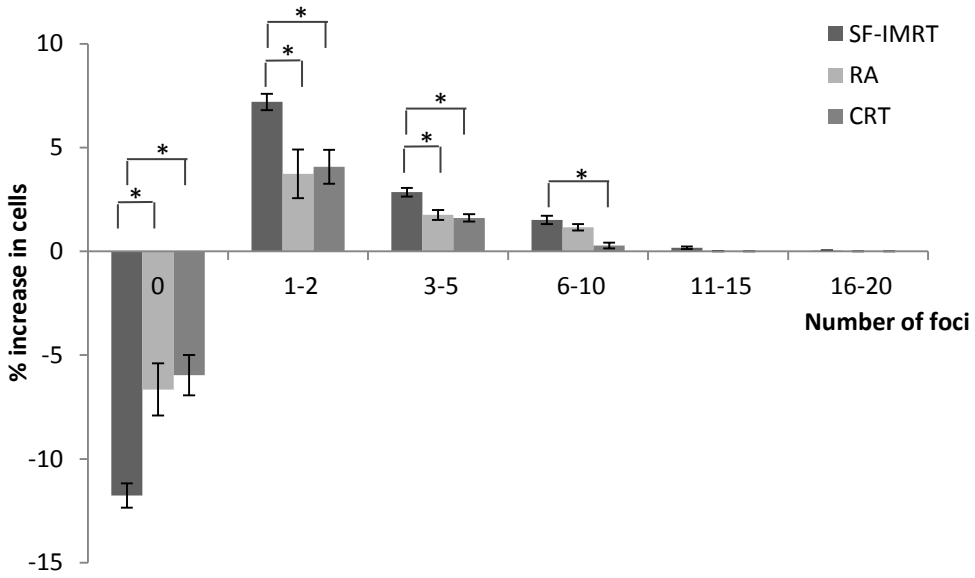

Foci groups	% increase in cells with foci groupings			P value for comparison		
	SF-IMRT	RA	CRT	SF-IMRT v RA	SF-IMRT v CRT	RA v CRT
0	-11.76	-6.65	-5.96	0.001	0.001	1.000
1-2	7.19	3.73	4.07	0.005	0.019	1.000
3-5	2.85	1.75	1.61	0.015	0.011	1.000
6-10	1.51	1.15	0.28	0.857	0.008	0.153
11-15	0.16	0.008	0	0.339	0.373	1.000
16-20	0.03	0	0	0.629	0.741	1.000

Fig. 3.10: Comparison of mean percentage increase in cells with specified numbers of γ-H2AX foci following a course of radiotherapy with SF-IMRT, RA and CRT.

There is a greater increase in the number of cells with 1-2 and 3-5 foci following SF-IMRT compared with RA and CRT and fewer cells with no foci.

Error bars represent standard deviation; *=p<0.001.

Radiotherapy Technique	Mean Dispersion Index		
	Pre RT	Post RT	Difference (Post-Pre)
SF-IMRT	2.50	4.11	1.61
RA	2.04	3.13	1.10
CRT	1.79	2.60	0.81

Table 3.9: Pre, post and change in mean dispersion indices (MDI) for all techniques.

There is a greater change in MDI with SF-IMRT compared to RA and CRT.

Chapter 4

IMRT for Meningioma

Preliminary results from a phase I/II study of intensity modulated radiotherapy in the treatment of meningioma

4.1 Aims

- To prospectively assess the feasibility and efficacy of delivering intensity modulated radiotherapy (IMRT) to patients for the treatment of meningioma.
- To evaluate the potential of IMRT to reduce dose to the neurological dose limiting structures.
- To prospectively assess and document toxicity and outcome data.
- To assess progression free survival and the incidence of repeat intervention.
- To measure quality of life as measured by the EORTC QLQ-C30 and QLQ-BN20 questionnaire.

4.2 Introduction

Intensity modulated radiotherapy (IMRT) offers a significant benefit for the treatment of brain tumours, in particular meningioma. It provides excellent dose conformality to irregularly shaped tumour volumes, and with steep dose gradients, has the ability to spare critical structures; an essential factor when treating patients with good prognosis tumours, such as meningioma, where long term survival is expected. Retrospective series suggest a role for radiotherapy in the treatment of meningiomas, [174,178,179,184,185,188,211], although 3D conformal radiotherapy techniques were found to be limited in areas close to critical structures [210].

For this reason, IMRT has been found to be valuable for tumours of the skull base, although studies examining this have been largely retrospective [201,213,215,220,226]. Few groups have demonstrated outcomes in a prospective manner [217], where valuable information can be gained regarding long term toxicity and tolerability of treatment.

A prospective phase I/II study was designed by Professor Short and Dr Guerrero Urbano to examine the use and feasibility of IMRT in biopsy proven meningioma and to assess the long term toxicity, quality of life and outcomes of patients over a period of prolonged follow-up.

4.3 Methods and Materials

4.3.1 Patient Selection

Patients at University College London Hospital (UCLH) with histologically confirmed meningioma deemed to require fractionated radiotherapy were recruited prospectively and treated with static field IMRT using a dose of 50.4Gy in 28 daily fractions.

All enrolled patients were recruited as part of the study entitled “A phase I/II study of intensity modulated radiotherapy in meningiomas”. Inclusion criteria encompassed all patients with histologically confirmed meningioma. These could comprise atypical or malignant histology (WHO grades II or III), completely or partially resected as assessed on an MRI scan 3-4 months after surgery; benign meningioma (grade I) partially resected as assessed on MRI 3-4 months after surgery and considered to require post-operative radiotherapy, those with evidence of brain and/or bone/dural invasion. All included patients were over 18 years of age, with a performance status of 0-2 and included those patients who were suitable to attend regular follow up and undergo visual assessment if appropriate. Exclusion criteria comprised patients who had received previous radiotherapy to the meninges or brain interfering with the protocol treatment plan, previous malignancy except non-melanoma skin cancer, those with a previous or concurrent illness which was felt to interfere with either completion of treatment or follow-up. The study protocol (designed and set up by Professor Short and Dr Gurerro Urbano) was approved by the local ethics committee (ref: 06/Q051/97). I was involved in the study from the time of patient recruitment. Written informed consent was obtained from all patients.

All patients were treated with radiotherapy according to the indications set out by the treating clinician. Patients were given encouragement to adhere to the protocol treatment and follow-up, although they had the right to withdraw consent for participation in any aspect of the study. Reasons for patient withdrawal were classified as:

a) Patient withdraws consent from protocol treatment and/or follow up
b) Intercurrent illness preventing further treatment
c) Any change in patient's condition which justified withdrawal from study or discontinuation from treatment in the opinion of the treating clinician.

4.3.2 Trial Interventions

4.3.2.1 General

All patients were required to undergo at least a biopsy to confirm the histological diagnosis. Surgical resection before irradiation (if appropriate) was performed following local guidelines and was as radical as was safe and at the discretion of the operating surgeon. Indications for radiotherapy were established in a consultant-led multidisciplinary meeting (MDT) and were in line with the inclusion criteria as above.

4.3.2.2 IMRT procedure

4.3.2.2.1 Planning and immobilisation

All patients were immobilised in a custom made thermoplastic shell. A planning CT scan was carried out in the treatment position (supine) and with the immobilisation shell in place. Scans were acquired at 2.5mm intervals through the whole brain,

from vertex to the bottom of the C2 vertebrae and transferred to a contouring workstation for tumour and normal structure delineation.

4.3.2.2.2 Target volume definition

Image fusion of the planning CT scan with diagnostic and/or post-operative MRI scans was performed to aid volume definition. Target volume definition was performed according to ICRU 50and 62 guidelines [106,107]. GTV was defined as the gross visible residual tumour, seen as the region of enhancement on the post-operative MRI, areas of thickened dura and involved bone and/or brain on both the MRI and planning CT scan. The GTV was delineated taking into consideration the maximum information available from both CT and MRI. If no residual tumour was seen on the post-operative MRI or planning CT scan, then a 'GTV equivalent' was created using the pre-operative MRI to define the extent of tumour (respecting anatomical boundaries so that this did not result in a larger GTV than if the tumour was not resected) and any associated dural or bone thickening.

A 1cm margin was added to the GTV or GTV equivalent in the plane of the dura to create the CTV (clinical target volume), accounting for subclinical spread of disease. This was not routinely extended into the normal brain or bony structures, unless there was evidence of brain involvement or abnormal /hyperostotic bone. A margin of 3mm was added to the CTV symmetrically to create the PTV (planning target volume), reflecting the geometric accuracy of the immobilisation system.

Organs at risk, such as optic chiasm, right and left optic nerves, right and left ocular globes, right and left lenses, right and left lacrimal glands, pituitary gland, right and

left inner ear, whole brain, right and left temporal lobes, right and left hippocampus, hypothalamic region, brain stem and spinal cord were delineated in all patients. The exact anatomical locations of these organs were drawn in accordance with radiation anatomy available and with the assistance of a neuroradiologist (in particular for the location of the hippocampi). A 3mm margin was added to the OARs to produce a planning organ at risk volume (PRV).

4.3.2.2.3 IMRT planning

A 5 - 9 field technique was used to create an IMRT plan using Eclipse^{TM} treatment planning system (TPS), with optimisations to allow adequate dose coverage of the PTV, whilst respecting dose objectives and constraints of organs at risk. Details of dose objectives for the PTV and organs at risk can be found in tables 4.1a and 4.1b. Radiotherapy planning was undertaken by me in conjunction with dosimetrists and physicists in UCLH radiotherapy physics department, allowing me to gain valuable experience of the IMRT planning process.

A total dose of 50.4.Gy in 28 daily fractions over 5.5 weeks using MV photons was prescribed to the mean target dose (the mean dose point on the dose volume histogram, such that the prescription dose is received by 50% of the PTV). Dose distributions were corrected for bone and soft tissue inhomogeneities and normalised to the mean target dose. The minimum and maximum doses to the PTV were kept within 90-107% of the prescription dose, such that the $D_{98\%}$ received no less than 90% of the dose, $D_{95\%}$ no less than 95%, $D_{50\%}$ no less than 50%, $D_{5\%}$ no more than 105% and the $D_{2\%}$ no more than 107% of the prescribed dose as specified by ICRU 83 [110].

Dose objectives for radiosensitive structures and organs at risk were set according to reports on normal tissue complication probability models [124,125] and assessed from dose volume histograms created by the TPS. Some organs at risk were set as dose constraints and prioritised accordingly against coverage of the PTV (usually optic chiasm, brain stem, optic nerves and globes). However for other organs at risk, a lower priority was given, and for others, such as hippocampi, whole brain, temporal lobes, hypothalamus, inner ear, dose was recorded without setting a specific dose constraint. Table 4.1b gives the details of organs at risk and dose objectives set.

4.3.3 Treatment planning assessment and delivery

Assessment of treatment planning was undertaken as per ICRU 83 [110], with the following parameters derived and recorded: $D_{2\%,}$ $D_{50\%}$, $D_{98\%}$, volume of 95% isodose, volume of PTV and standard deviation (SD) of mean dose to PTV.

Homogeneity index (HI) was derived using the formula: $HI = \frac{(D_{2\%} - D_{98\%})}{D_{50\%}}$. Conformity index (CI) was derived using $CI = \left(\frac{TV\ PI^2}{TV\ x\ PIV}\right)\ x\ 100\%$ [126], where TVPI = volume of target covered by the prescription isodose and PIV=volume of prescription isodose. However, CI using guidance from ICRU 62, calculated as $CI = \frac{TV_{95\%}}{PTV}$ [107] (where $TV_{95\%}$ = Treated volume covered by 95% isodose) was also used as a comparison.

Patients were treated daily (Monday to Friday) for 28 fractions. Imaging for patient set up purposes was performed using daily kV imaging for the first 3 fractions of treatment and weekly thereafter. Cone beam CT imaging was performed weekly

during treatment to ensure accuracy of set up and dose coverage of PTV and critical structures. Patients were moved on set to correct for any systematic shifts in accordance with the treatment imaging.

4.3.4 Clinical evaluation and follow up

Patients were assessed at set time points with a relevant clinical history, full examination, CTCAE version 3.0 toxicity scores [389], mini mental test examinations, pituitary function tests, visual assessments, and self-completed quality of life questionnaires (EORTC QLQ-C30 and QLQ-BN20) [390] (see appendix B and C). Assessments were carried out at baseline and at 3 months, 6 months and yearly following IMRT, with the aim of collecting data for the life span of each patient and for a minimum of a 10 year period following IMRT. Acute toxicities were assessed and recorded during IMRT: at weeks 1-2, weeks 3-4, weeks 5-6 and also soon after completing IMRT during weeks 9-10. MRI scans were performed (with added diffusion and perfusion weighted sequences) at 3 months, 1 year and yearly intervals thereafter following IMRT. Recurrence was defined as in-field, marginal or out of field. Definitions of recurrence vary in the literature and some groups have described in-field recurrence for glioblastomas as ≥95% of recurrence within the high dose volume; marginal as > 95% of recurrence outside the high dose volume and distant (or out of field recurrence) as outside the radiation field (<20% isodose line) [391]. Others have defined central or in-field recurrence as a recurrence within the region that has received ≥90% of the prescribed dose and marginal or out of field as a recurrence within the region that received <90% of the prescribed dose [392]. However, those used by Press et al. to assess meningioma recurrence following IMRT have been employed in this study: *in-field* if ≥90% of the enhancing recurrence is within the prescription isodose volume; *distant* if recurrence

is completely outside of the prescribed isodose volume; *out of field (marginal)* if recurrence volumes are not distant and > 90% of the recurrence is situated outside the prescription isodose volume, and as *both* if neither fully in field nor marginal [393]. A schematic diagram of the study is demonstrated in fig. 4.1.

Assessment of quality of life data was carried out in accordance with the EORTC QLQ-C30 scoring manual [394]. Data from the 30 questions from QLQ-C30 were divided into 3 separate scales according to the issue addressed by particular questions: global health status/QoL scale, functional scale and symptom scale. The functional scale was subdivided into a further five subscales (physical functioning, role functioning, emotional functioning, cognitive functioning and social functioning) and the symptom scale was subdivided into 9 categories. The average of the items contributing to each scale was calculated to produce a raw score:

$$RawScore = RS = (I_1 + I_2 + \ldots + I_n) \div n,$$

where I_1, I_2 etc. indicate the score from a particular question answered.

In accordance with the scoring manual [394], when data was missing but more than 50% of the subscale (subgroups) questions were answered, raw scores were calculated for only those items answered. Conversely, if more than 50% of a subscale was not answered, then the whole subscale could not be assessed and was therefore considered missing.

In order to standardise the scores, a linear transformation was carried out so that scores ranging from 0 to 100 were produced. The following equations were used for the various scale groups to create these scores:

$$Functional\ scale = \left(1 - \frac{(RS-1)}{range}\right) x\ 100$$

$$Global\ Health\ status\ QoL\ scale\ = \left(\frac{(RS-1)}{range}\right) x\ 100$$

$$Symptom\ scale\ = \left(\frac{(RS-1)}{range}\right) x\ 100 \quad ,$$

where RS is the raw score and range is the difference between the maximum and minimum possible scores in that particular category. For example the functional and symptom items are scored between 1 and 4, so the range is 3. However the global health status/QoL items are scored between 1 and 7, so the range is 6.

The 20 questions from QLQ-BN20 were assessed in a similar way, so that the answers to questions were grouped into 11 groups: 1 functional scale and 10 symptom scales. Raw scores were produced and a linear transformation score generated in the same way as QLQ-C30 [395,396].

Data analysis and statistical tests were performed using PASW version 18.0 statistical package. One way analysis of variance (ANOVA) was applied to compare QLQ-C30 and QLQ-BN20 scores between different time points (baseline and during follow up). Statistical significance was set at 5%.

4.4 Results

4.4.1 Patient and tumour characteristics

28 patients were recruited and consented to study entry, although 2 patients were deemed ineligible for study inclusion due to lack of histological diagnosis of meningioma. The remaining 26 patient cohort had a median age of 49.5 years (range 38-76 years) with a slightly higher ratio of female patients compared to male patients (1.17:1). A large proportion of patients (80.8%) were considered to have a WHO performance status of 0 at the time of radiotherapy, with a small number assessed with a performance status of 1 (19.2%) and no patients with a performance status of over 1.

All patients had biopsy proven meningioma as part of their eligibility into the study. 16 (61.5%) patients were classified with WHO grade I tumours and 9 patients (34.6%) with a WHO grade II meningioma. There were no patients classified with a WHO grade III meningioma. However, in 1 patient, the tumour biopsy sample, although consistent with meningioma, was felt too small to grade and the risk of re-biopsy too great in terms of further visual impairment. 57.7% of tumours occurred in skull base locations, of which almost half (46.7%) occurred in the sphenoid wing. Detailed patient and tumour characteristics are summarized in table 4.2.

4.4.2 Radiotherapy delivery and plan assessment

The timing of radiotherapy occurred at various points in a patient's presentation. Most instances were at recurrence (42.3%), although a smaller percentage (23.1%) took place as primary treatment (usually because of the risks of surgery) or following surgery (34.6%). All radiotherapy was delivered using a linear accelerator with 6MV photons at a dose of 50.4Gy in 28 fractions over 5 and a half weeks and using a median of 5 intensity modulated fields (range 5 to 7 fields) in order to achieve optimised treatment plans. Optimal plans provided coverage of the PTV by the 95% isodose with sparing of the adjacent critical structures. Figure 4.2 show typical plans with good conformality of complex shaped planning target volumes by the 95% isodose. Figures 4.3 and 4.4 demonstrate typical plans from 2 patients to compare the coverage by the 95% isodose with that from the 10% isodose. It also demonstrates the sharp fall in dose gradients to allow sparing of high dose to organs at risk so that dose objectives were met.

The median tumour volume (planning target volume [PTV]) irradiated for all patients was 107.1cm^3 (range 15.2 to 338.0cm^3). Table 4.3 details the significant treatment assessment parameters. The median volume of the PTV covered by the prescription isodose (TVPI) was 101.05cm^3 (range 14.8 to 310.3 cm^3); equivalent to a median of 95.6% (range 91.8 to 99.0%) of the target volume covered by the treatment isodose (TVPI). The median near minimum dose or dose received by at least 98% of the PTV ($D_{98\%}$) was 47.4Gy (range 45.7 to 48.9Gy), which equates to 94.1% (range 90.6 to 96.9%) of the prescribed dose. The median near maximum dose or dose received by at least 2% of the PTV ($D_{2\%}$) was 52.8Gy (range 51.4 to 53.7Gy), equivalent to a median of 104.7% (range 102.0 to 107.0%) of the prescribed dose. The maximum dose received by at least 50% of the PTV ($D_{50\%}$)

was 50.5Gy (range 50.3 to 50.8Gy), equating to a median of 100.17% (range 99.7 to 100.6%) of the prescribed dose.

The median homogeneity index (HI) for this cohort of patients was 0.10 (range 0.05 to 0.16) and a conformity index (CI) of 77.54% (range 64.62 to 87.66%). However, when using the CI suggested from ICRU 62 [107], the CI was slightly higher at 0.96 (range 0.92 to 0.99). The patient with the highest CI did not have the highest HI and vice versa.

The organ at risk PRV doses are detailed in table 4.4. In most cases, dose objectives and organ dose tolerances were adhered to. However, there were cases where doses above the dose objective or organ tolerance were accepted. This occurred in organs such as lenses and pituitary gland, where the balance of tumour dose coverage to treat the meningioma outweighed the potential long term toxicities of cataracts or pituitary dysfunction. PRV doses above set dose constraints were also accepted in two other cases. In one patient with a suprasellar meningioma, the mean dose to the PRV optic chiasm was 51.2Gy with a maximum dose of 51.6Gy. In another patient with a right optic nerve and sphenoid wing tumour, the median dose to the right optic nerve was 50.8Gy with a maximum dose point of 54.6Gy. However, the mean dose to the left optic nerve was below the dose constraint at 28.2Gy, with a maximum point dose of 47.6Gy. These PRV doses were accepted above the specified dose constraint as the aim of treatment was to spare vision to the contralateral eye in patients with an ipsilateral blind eye.

8 patients were treated with doses to the pituitary over the recognised dose limits (at a mean dose of 49.2Gy, [range 48.8 to 51.7Gy]), although the pituitary gland was not set as a dose constraint in many cases. Similarly 7 patients received doses above the tolerance of the lenses, although these were also not set as a dose objective during IMRT planning.

4.4.3 Toxicity

4.4.3.1 Acute toxicity

On the whole treatment with IMRT was tolerated well, although 25 (96.2%) patients suffered some form of acute toxicity. 23 of these 25 patients experienced grade 1 toxicity (of which the most common were fatigue, alopecia and radiation dermatitis), whilst only 2 patients experienced a toxicity of grade 3 or more (1 patient with grade 3 fatigue and 1 patient with grade 3 retinal detachment). No patients suffered with grade 2 acute toxicity. The observed acute toxicities during and just following IMRT (during weeks 9-10) are outlined in table 4.5.

Fatigue occurred in 23 (88.5%) patients at a median onset at 3-4 weeks (range1-2 weeks to month 3) from the start of IMRT. However, this resolved at a median of 6 months (range 9-10 weeks to 24 months) following treatment. 22 out of the 23 patient experienced grade 1 fatigue. 1 patient suffered grade 3 fatigue which peaked at week 9-10, although had resolved by month 6 following IMRT.

Expected grade 1 alopecia within the IMRT treatment fields occurred in 19 patients at a median of 3-4 weeks (range 3-4 weeks to 9-10 weeks) into IMRT with hair

regrowth by month 12 following treatment, although 1 patient had persistent alopecia until month 36 following radiation. Grade 1 skin toxicity occurred in 10 (36%) patients within the treatment area at a median onset of 3-4 weeks (range 3-4 to 5-6 weeks) and with resolution of symptoms by a median of 9-10 weeks (range 9-10 to 6 months following radiation). Grade 1 mouth dryness was reported in 5 patients, all with a spontaneous resolution and short duration of symptoms (for example onset at 5-6 weeks and resolution at 9-10 weeks, onset at 1-2weeks and resolution at month 3, onset at 6 months and resolution at 12 months).

Seizure occurred in 1 patient at week 9-10 following IMRT and resolved without any intervention. 1 patient also noted a reduction in their short term memory (grade 1) at week 9-10, although this had resolved by month 3 following treatment.

5 patients developed a self-limiting grade 1 keratitis or ocular surface irritation at a median of 5-6 weeks (range 1-2 to 9-10 weeks) from the start of treatment, which had resolved in all cases by month 3. 2 patients observed grade 1 diplopia at 3-4 weeks and 5-6 weeks respectively, which resolved by month 3. I patient developed a grade 3 right inferior retinal detachment, requiring surgical repair, one day following completion of his IMRT. However, this was not felt to be as a direct consequence of his tumour or treatment.

4.4.3.2 Late toxicity

Of the 26 patients enrolled in the study, 2 patients have been lost to follow up at local hospitals; 1 at month 24 and the other patient shortly after completing IMRT. At a median follow-up of 29 months (range 9 to 58 months), 24 (92.3%) patients

have developed a late toxicity. Most patients developed a grade 1 toxicity; however a grade 2 toxicity occurred on 7 occasions (6 different patients, 23.1%) and a grade 3 toxicity in 3 patients (11.5%). Details of late toxicity are outlined in table 4.6.

The commonest late toxicity was a change in mood or personality following treatment in 12 patients. This typically occurred at a median onset of 6months (range week 5-6 to month 24) following IMRT and most experienced grade 1 mood changes, with 1 person experiencing grade 2 changes. Symptoms, such as irritation and anger were commonly cited. Mood alterations appeared to be persistent for most, although these symptoms resolved in 3 patients.

Late onset reduction in short term memory was highlighted in 11 (42.3%) patients and occurred at a median onset of 6 months (range weeks 5-6 to month 24) following IMRT. This was consistently classed as a reduction in short term, rather than long term memory, with 2 patients experiencing grade 2 memory loss (self-reported by patients and assessed formally with mini mental state examinations). Temporal lobe, and particularly hippocampi, have a role in learning, consolidation and memory and there are studies demonstrating that radiation dose to these areas may alter memory formation and neurocognition [397,398]. The median mean dose and D_{max} to the temporal lobes for the 2 patients with grade 2 memory loss was 25.2Gy (range 23.0 to 27.1Gy) and 52.3Gy (range 51.8 to 52.8Gy), with slightly higher doses received by the left temporal lobe (median mean dose: left = 26.8Gy [range 20.9 to 32.8Gy], right = 23.5Gy [range 21.6 to 25.3Gy]; D_{max}: left = 52.5Gy [range 52.4 to 52.7Gy] and right = 52.1Gy [range 51.3 to 52.8Gy]). These particular patients were treated for tumours situated in the left sphenoid wing. The median mean dose and D_{max} to hippocampi was 25.7Gy (range 25.3 to 26.1Gy) and 40.1Gy

(range 39.6 to 40.6Gy) respectively, and as expected higher doses were seen in the left hippocampus compared to the right (mean dose: left = 27.6Gy [range 22.9 to 32.3Gy], right = 23.7Gy [range 19.9 to 27.6Gy]; D_{max}: left = 47.8Gy [range 44.45 to 51.1Gy], right = 32.4Gy [range 28.1 to 36.7Gy]). The median mean dose and D_{max} to the temporal lobes for all patients experiencing memory issues was 19.6Gy (range 0.3Gy to 27.2Gy) and 50.7Gy (range 0.6Gy to 52.2Gy) with higher doses received by the left temporal lobe (mean dose: left = 20.8Gy [range 0.3 to 23.6], right = 16.0Gy [range 0.3 to 25.3Gy]; D_{max}: left = 51.7Gy [range 0.6 to 55.3Gy], right = 49.7Gy [range 0.6 to 55.5Gy]). The median mean dose and D_{max} to hippocampi was 19.7Gy (range 0.7Gy to 37.4Gy) and 37.4Gy (range 1.3Gy to 50.7Gy) respectively and similarly higher doses were seen in the left hippocampus (mean dose: left = 20.5Gy [range 0.7 to 32.2Gy], right = 17.7Gy [range 0.7 to 27.6Gy]; D_{max}: left = 43.0Gy [range 1.2 to 51.1Gy] and right = 31.5Gy [range 1.3 to 52.0Gy]). At the time of follow up, 3 patients described an improvement in memory symptoms that had developed following radiotherapy. However, the remaining 12 patients had persistent symptoms.

Late radiation dermatitis (grade 1) occurred in 1 patient at 4 years and late radiation related pain over the site of the surgical scar was recorded by clinicians in 2 patients (one at grade 2 and the other grade 3), both at 24 months following radiation.

Grade 1 somnolence or fatigue was noted as a late toxicity in 10 patients at a median onset of 6 months following radiation (range month 3 to month 24). 5 patients reported an improvement in their symptoms. However, symptoms have persisted in the remaining patients. The exact cause of somnolence and fatigue is likely to be multifactorial, but has been linked to cranial irradiation [399]; the median

mean brain dose was 16.9Gy (range 10.5Gy to 20.1Gy) and a median D_{max} brain dose of 54.4Gy (range 53.2Gy-55.2Gy). Grade 1 headaches were reported in 7 patients, while 1 patient suffered grade 2 headache, with a median time of onset at month 3 (range month 3 to month 24). Seizures occurred in 5 patients; 3 at grade1, 1 with grade 2 and another patient with grade 3 symptoms, with a median onset at month 6 (range month 3 to month 24). Seizures included auras and some were occipital in nature. 1 patient's seizure was due to non-compliance with their medication. 1 patient developed a self-limiting anomic aphasia.

3 patients developed cataracts, 2 with grade 1 (at month 12 and month 36) and 1 patient with grade 2 (at month 6). The 2 patients with grade 1 cataracts were aged 76 and 65 years, with tumours in the left frontal brain and left sphenoid wing respectively at the time of IMRT. The mean lens doses were 1.6Gy (D_{max} 2.4Gy) and 5.2Gy (D_{max} 6.0Gy) respectively. The patient with a grade 2 cataract was 51 years of age at the time of radiation and received a mean lens dose of 3.3Gy with a D_{max} of 5.2Gy for a meningioma in the olfactory grove and extending to the floor of the anterior cranial fossa. 9 patients developed a grade 1 dry eye at a median of 6 months (range month 3 to month 48) and received a median mean lacrimal gland dose of 26.9Gy (range 8.1Gy to 33.4Gy) and a median D_{max} of 33.2Gy (range 10.9Gy to 48.8Gy). 5 of these patients had tumours located either in the cavernous sinus, sphenoid wing or orbit. 1 patient with a left sphenoid wing tumour extending through the orbit developed grade 3 dry eye at month 12 requiring further treatment after receiving a mean lacrimal gland dose of 26.9Gy (D_{max} of 33.2Gy) . Interestingly, the patient with grade 3 toxicity did not receive the largest dose to the lacrimal gland. In fact, 4 patients with mean and D_{max} lacrimal doses over 26Gy and 33Gy respectively have not developed symptoms or signs of dry eye. The same

patient developed grade 1 keratitis at month 3 (with mean globe dose of 24.8Gy and D_{max} of 41.2Gy) and was managed with lubricants and anti-inflammatory eye drops.

An increase in prolactin levels (to levels outside the normal range) were also noted in 2 patients between years 1 and 2 following IMRT. They have not experienced any associated symptoms, but have been referred to local endocrinologist for further follow up and investigations. Other pituitary parameters and MRI scans of the pituitary have been unremarkable. These patients have not required any treatment for the hyperprolactinaemia to date and in 1 patient, the levels have fallen to near normal levels.

4.4.4 Clinical outcomes

17 out of 26 (65.45%) patients had an improvement in at least one baseline tumour related symptom. Table 4.7 and figure 4.5 demonstrate the change in symptoms following IMRT. Most symptoms either remained stable or improved following treatment.

6 out of 13 patients noticed a relief in their baseline headache at a median of 12 months following IMRT (range month 3 to month 24), whilst 5 patients had stable symptoms. 2 patients described a slight deterioration in their headaches from grade 1 to grade 2 at month 6 and month 12 following IMRT respectively. In addition 3 out of 4 patients noticed an improvement in their motor function at a median of 12 months following IMRT and all patients noticed an improvement in sensory symptoms at month 3 (3 patients with complete resolution). 2 patients noted an

improvement in their speech at month 3 and month 6 following IMRT respectively. 1 patient with baseline tumour related nasal stuffiness had a complete resolution of their symptoms during weeks 5-6 of treatment and this improvement has persisted to date.

5 patients experienced an improvement in visual symptoms (mainly visual field defects), whilst those with complete or almost complete visual loss tended to demonstrate stable disease, rather than improvement. Proptosis was notably improved in 3 of the 4 patients at a median of 12 months following IMRT (range week 5-6 to month12). Improvements in cranial nerve function were also seen. 3 out of 4 patients had a resolution of their baseline ptosis at a median of 6 months following treatment and all patients developed a complete resolution of numbness over the area supplied by the ophthalmic division of the trigeminal nerve by month 6 following IMRT. Resolution of CN VII neurology was also seen early after IMRT (week 5-6 and month 3).

Clinical status, as assessed by performance score, remained stable in 18 patients and improved in 1 patient at month 24. However 3 patients reported a reduction in their performance status by I point at 12 months, 24 months and 48 months respectively.

Patient reported outcomes using the EORTC QLQ-C30 and QLQ-BN20 are summarised in table 4.8 and fig. 4.6. Higher scores indicate better functioning and quality of life for the Global health status/QoL and functioning scales. However higher scores indicate worse symptomatology for all symptom scales. Overall 20

patients had returned a completed quality of life questionnaire. However, 15 patients completed this for months 3, 6, and 12 following IMRT and 6 patients had completed a form for month 24.

There is a higher patient self-reported incidence of symptoms such as fatigue, pain and insomnia overall following IMRT. Interestingly, there is also a high level of financial difficulty experienced by this patient group. Conversely, there appears to be good functioning in all subscales (physical, role, emotional, cognitive, social and future) and a reasonable level of global health/quality of life.

Figure 4.7 demonstrates the change in all subscales over the course of follow-up and documents the level of each scale at each time point: baseline, months 3, 6, 12 and 24. It can be seen that there appears to be an increase in many of the functioning scales with time (physical, role, emotional and social), although there appears to be a trend for a reduction in cognitive functioning over time. However variations in the scale with each time point was not statistically significant for most items ($p>0.05$), with the exception of appetite loss, which appears to improve over time. The observed difference of appetite loss from baseline to any other time point (month 3,6,12 or 24) is statistically significant at all time points (baseline to month 3: change in score of 22.22; baseline to month 6: 26.67; baseline to month12: 28.89; baseline to month 24: 33.33, $F(4,65): 6.0740$, $p < 0.0003$).

Radiological assessment using MRI has demonstrated an overall local control rate of 84.6% (22/26 patients) after a median follow up of 29 months (range 9-58 months). 22 patients had stable disease based on MRI findings and there were no

tumour volume reductions as assessed by the Response Evaluation Criteria in Solid Tumours (RECIST). 4 patients showed tumour progression on MRI scanning at a median of 24 months following IMRT (range 12 to 26 months). These have been identified as in-field (1 patient), marginal (2 patients) and out of field relapses (1 patient) as defined in the 'methods and materials' section. All have developed following treatment of a grade II meningioma. Fig 4.5 summarises the findings on MRI follow up and change in baseline symptoms. This demonstrates that most patients had either an improvement or stability in their baseline clinical symptoms (with a slightly higher proportion showing stable symptoms), while follow up MRI images failed to confirm any improvement in tumour volume, but did demonstrate stable appearances.

The first patient to develop recurrence was initially treated with radiotherapy following a Simpson's grade 2 surgical resection of a grade II atypical left posterior parietal meningioma with a focally high Ki67 ratio and a mitotic count of >4/10 hpf (high power field). The patient had residual symptoms from his initial treatment, including right sided motor and sensory reduction. However, he did report some change in personality from month 6 following his IMRT and following this experienced worsening of motor symptoms within the right arm. A relapse was identified on MRI scanning within the inferior portion of the original tumour (in the posterior parietal region). Further surgery confirmed a grade II recurrence with focal mitotic activity of 10/10 hpf, but <20/10 hpf and with no anaplastic or malignant progression. At the current time, this patient is alive and now recurrence free, but has residual symptoms from his surgery including motor weakness and dysphasia.

A further patient developed relapse at 24 months following IMRT. He initially underwent surgery, achieving a Simpson's grade 1 resection of a grade II chordoid left sphenoid wing meningioma with focally increased Ki67 and mitotic activity reaching 4/10 hpf, but less than 20/10 hpf. There was also evidence of brain and bone invasion in the initial meningioma. A surveillance MRI scan demonstrated an area of recurrence just at the edge of the surgical and radiation field in the floor of the anterior cranial fossa. Surgical excision was an option, but the patient declined further treatment.

The third patient initially underwent surgery for a parafalcine meningioma, although surgical resection was noted to be incomplete with a small amount of disease left surrounding the sagittal sinus (Simpson's grade 4). Histology revealed a grade II chordoid meningioma with a high mitotic rate, recorded at 6/10 hpf with brain invasion. Increase in the size of this known residual disease was noted on imaging and he therefore received radiotherapy for this recurrent parafalcine meningioma. He subsequently suffered with intermittent recurrence of his original seizures and subsequent MRI scanning demonstrated a recurrence of his tumour just lateral to the original parafalcine meningioma. He underwent surgical resection of his tumour, the histology of which confirmed a meningothelial meningioma with high mitotic activity (10/10 hpf) and with evidence of dural and brain invasion.

The fourth patient was treated with IMRT for a grade II recurrent left anterior cranial fossa meningioma with chordoid features and moderate mitotic activity of less than 4/10 hpf and a low Ki67. This was initially surgically resected and required 2 further surgical resections due to recurrences. The patient also had a history of a grade I parasagittal meningioma, previously resected. Although, complete surgical

resection had been stated in operative notes, it has been difficult to accurately allocate a Simpson's grade for these resections, although it probably falls into the Simpson's grade 1-3 group. Nevertheless, in view of the frequent recurrences of the anterior cranial fossa meningioma, this patient went on to receive post-operative IMRT. Despite this, the patient developed new onset seizures at 3 months prior to a surveillance MRI scan at month 12 following IMRT. This identified a recurrence in the right parietal region and was amenable to surgical resection. However, the patient died before surgery due to unrelated cardiac causes. There have been no further deaths within this cohort of patients at this time of follow up.

At the current median follow up of 29 months, the progression free survival is 84.6% with the incidence of repeat surgery of 15.4% and with an overall survival of 96.2%. However, it is acknowledged that the recurrence rate is 44.4% in those patients with grade II meningioma, although progression free survival within grade I patients remains at 100%.

4.5 Discussion

This prospective study has demonstrated the use of IMRT in the treatment of meningioma. Radiotherapy to treat meningioma, either in the primary or adjuvant setting, has been well documented [172-174,193,195,400] and in this group of patients, just under half (42.3%) received radiotherapy at the time of recurrence, with smaller numbers receiving radiotherapy as an adjunct to surgery (34.6%), or as primary treatment (23.1%). Over half of the 26 patients in this cohort had tumours

within the skull base region; an area notoriously difficult to treat with conventional radiation techniques (or radiosurgery) due to dose limiting adjacent critical structures [210], where IMRT can conform to the shape of the tumour and avoid the use of high dose per fraction as seen with radiosurgical techniques. The use of IGRT (in the form of cone beam CT and portal kV imaging) within this study has allowed accurate and safe delivery of IMRT.

Acceptable coverage and conformality of the tumour volume, as demonstrated by the treatment plan parameters, has been documented with this IMRT technique. The median $D_{50\%}$ (100.2% in this group) is believed to be a good measure of absorbed dose in homogenously irradiated tumours [110]. However, the homogeneity index (HI) is a more accurate measure of homogeneity of tumour dose coverage using IMRT, and in this cohort, has been shown to produce high levels of homogeneity with a value close to 0 (median HI 0.10).

Similarly, the conformity index (CI) is a measure of how accurately the volume of dose distribution conforms to the size and shape of a target volume (with values of 1 or 100% providing excellent conformality. Using the ICRU 62 definition of CI [107], a value of 0.96 was achieved. However, it has been recognised that this formula can give false optimism as it assumes that the centre of the treatment volume is always at the centre of the target volume. However, this is not always the case and may result in a good CI value whether the prescribed isodose volume has covered the target volume completely or whether it was missed altogether. The formulae created by Paddick et al. has circumvented this by evaluating, not only the ratio of independent volumes, but the volume of target covered by the prescription isodose and incorporates any over (radiation spill outside the PTV) or under coverage of the

target volume by the prescription isodose [126]. Using this formulae the CI was slightly lower at 0.78, (77.54%) in comparison to the ICRU 62 CI value of 0.96, although it is perhaps a more realistic estimate and valuable tool in assessing conformality. In fact, others have demonstrated slightly lower levels of conformality (CI of 0.47 ± 0.12) when delivering IMRT to benign intracranial tumours, including meningioma, acoustic neuromas and pituitary adenomas [213].

In practice, there is often a trade-off between homogeneity and conformality. If the priority is conformality, then an increase in inhomogeneity may be accepted, whereas if the priority is homogeneity, a slightly reduced conformity may be accepted and this is often closely related to coverage of the tumour or target volume, while also aiming to respect the dose tolerances of adjacent normal structures.

Dose reductions to organs at risk situated beside the target volume using IMRT for meningiomas have been described in the literature [213,220,224] and this is consistent in most cases seen in this study where dose limits for critical structures have been adhered to. Of course, there have been circumstances where, due to the anatomical nature of the tumour, dose tolerances for a particular organ have been exceeded, but careful thought has gone into the benefit of treating the tumour whilst increasing the potential for late organ radiation damage, against the risks of inadequate treatment but the ability to keep within normal tissue tolerance. More often than not, the choice to treat the tumour whilst exceeding the tolerance of a particular organ was made in situations where the aim was to preserve the contralateral eye in a patient with an already blind ipsilateral eye.

The prospective collection of toxicity data demonstrates patient tolerance of this particular radiation technique, with acceptable levels of acute toxicity resolving at a median of 6 months following treatment and is largely in line with other reports [191,201,217,220,400-403]. At a relatively short median follow up of 29 months, the late toxicity in this cohort of patients was well tolerated and reports in the literature have similarly demonstrated low rates of toxicity following IMRT [217].

As more than half of the patients in this study had tumours located in the skull base, dose and toxicity becomes of paramount importance and it has been demonstrated here that significant late ocular toxicity is not common. There were no reports of any deterioration in vision at this stage in ongoing follow-up. Nevertheless, grade 1 dry eye was noted in 9 of the 26 patients and grade 3 in 1 patient. There have been suggestions that dose to the lacrimal gland is associated with an increase in dry eye, with some reports concluding that a dose of over 30-34Gy can lead to a 5% incidence of dry eye and is dependent on the total dose and dose per fraction [404,405]. The incidence appears to remain static at 6% for doses between 35 to 39Gy, although rises sharply with higher doses. Reports of a 50% incidence with 45-49Gy and 90% incidence with dose of 60-65Gy have been documented following radiotherapy to the head and neck in a cohort of 78 patients [405]. However, more recently studies have suggested that maximum dose to the lacrimal gland is a more useful predictor of acute and late toxicities compared to mean dose and, in particular, the V_{20} a useful predictor of late toxicity, with suggestions of a D_{max} and mean dose of 30Gy and 25Gy threshold for acute toxicity [406]. The small numbers in our cohort make any statistical evaluation difficult. Nevertheless, the median D_{max} and mean dose in those patients with symptoms of a dry eye were 33Gy and 26Gy respectively (in those with grade 1 and grade 3 toxicity). There were of course patients who received much lower doses to the lacrimal gland, but still

demonstrated symptoms of a dry eye and it is worth mentioning that causes of a dry eye may be multifactorial and also related to damage of other ocular structures.

Changes in short term memory were also recognised by many patients as a late toxicity in this group of patients. The temporal lobes have, for a long time, thought to be involved in the process of memory formation. Groups treating nasopharyngeal tumours with IMRT have noted more neurocognitive impairment in patients who received a mean dose over 36Gy to the temporal lobes [407]; impairment increasing with doses over 53-60Gy and with V_{60} over 10% [407,408]. This compares to D_{max} of 50.7Gy and 52.3Gy in the 2 patients who experienced grade 1 and 2 short term memory problems.

However, recent attention has focused on the hippocampi, situated within the temporal lobes, and a vital part of the limbic system, involved in the formation of new memories. They are a source of multipotent stem cells and therefore sensitive to radiation, with animal studies reporting a decline in neurogenesis and cognitive function with 10Gy and perhaps with a threshold value of 5Gy [409-411]. Consequently some clinical studies have demonstrated a hippocampal dose threshold with a $D_{40\%}$ of 7.3Gy and suggestions of an association with $D_{100\%}$ over 0.0Gy, above which prospectively assessed decline in neurocognition has been documented [177]. As a result of these findings and the potential for long term reduction in neurocognition, attempts are being made to employ hippocampal sparing when irradiating the brain [398] and some have attempted to constrain the hippocampal volumes receiving 10Gy or more to less than 50%, with maximum dose points of less than 16Gy [412], whilst others have constrained this to a mean dose of less than 30Gy to at least one hippocampus [413] and this continues to be

the subject of ongoing trials [412,414]. 11 patients in this study group who developed issues with short term memory (and 2 patients with grade 2 short term memory reduction) received a median mean dose to the temporal lobes of 19.6Gy (median D_{max} of 50Gy) and a median mean dose to the hippocampi of 19Gy (median D_{max} of 37Gy). The 2 patients who developed grade 2 memory problems had a median mean dose to the temporal lobes of 25.1Gy and median D_{max} of 52.8Gy with hippocampal doses of 25.7Gy and 40.1Gy respectively. Although small in sample size, all patients receiving IMRT to the brain for meningioma do receive significant doses to the temporal lobes (in this cohort, a median mean dose of 49.8Gy [range 0.6 to 55.0Gy] and D_{max} 18.7Gy [range 0.3 to 55.9Gy]) and, in particular, to the hippocampi (overall median mean dose 18.6 [range 0.7 to 49.4Gy] and median D_{max} 33.2Gy [range 0.7 to 52.0Gy]), which may in turn have long term consequences in respect of neurocognition. Conversely, there have been reports from some groups suggesting that radiation does not necessarily play a role in the development of late neurocognitive decline [415,416]. Nevertheless, it would be useful to examine hippocampal sparing and neurocognitive sequelae prospectively in this group of good prognosis patients.

10 patients developed a form of somnolence (including symptoms of drowsiness, lethargy or fatigue) following IMRT, 5 of which have continued at last follow up. Whilst recognised as a consequence of cranial radiation and thought to be as result of some form of transient demyelination [399], reports in the past have failed to demonstrate a radiation dose dependence for somnolence syndrome following radiotherapy [417]. Nevertheless, the cause of somnolence and fatigue can be multifactorial. A recent phase III study comparing IMRT with 3D conformal radiotherapy for head and neck tumours unexpectedly found a greater incidence of fatigue within the IMRT group and postulated a relationship to higher doses within

the posterior fossa, and brainstem [116], with further reports of associations with mean dose to the cerebellum, basal ganglia and pituitary gland [418]. It is conceivable that, through IMRT and the inadvertent dose to non-target areas [216], patients receiving IMRT may experience more symptoms related to dose in these non target areas of the brain areas. However, longer follow-up within prospective studies may be able to document these findings further.

Within this prospective study, 65% of patients with meningioma had experienced an improvement in their baseline symptoms following IMRT. Patients had meningiomas within several different regions of the skull and symptoms associated with optic nerve impairment or other cranial nerve impairment seemed as likely to respond as symptoms related to other areas of the brain. However, due to the small sample size within this cohort, detailed statistical analysis to determine whether a particular deficit was more likely to respond was not performed. Nevertheless, these findings have also been seen in the literature from other studies, largely looking at optic nerve sheath or skull base meningiomas treated with radiotherapy [201,215,217,400,419-422]. Milker-Zabel and colleagues demonstrated an improvement in pre-existing neurological deficit in 39.8% patients, including a reduction in diplopia, exophthalmos and trigeminal neuralgia. Similarly, Minniti and colleagues documented an improvement in neurological deficits in 30% of patients, including vision and cranial nerve function[400]. Whereas Pirzkall and colleagues found a significant resolution in patients' neurologic deficits 6 weeks following IMRT, and similar to the cohort presented in this chapter, they also noted particular improvements in headache, visual fields and acuity, trigeminal neuralgia and motor disturbance during longer follow-up [201]. Improvement in performance status was observed in half of the 20 study patients with stability in 8 patients. Although within the cohort of patients described in this chapter, most were assessed as displaying

stability in their performance status (18 of the 26 patients) and an improvement in just 1 patient.

It was interesting to note, (although expected), that in this study the radiological findings did not match the clinical improvement in symptoms seen, with stable disease rather than an improvement in tumour dimensions seen on the MRI. This is largely in line with other studies, although some have demonstrated radiological improvement in a larger group of patients and over a longer follow up [201,215]. However, follow-up in this study is still short and it may be that the radiological changes may be appreciated over a much longer period of time.

A concern regarding radiotherapy for largely good prognosis tumours relates to long term toxicity and impairment in quality of life. Patient reported outcomes are now being highlighted as an important measure of treatment success. Quality of life assessments, using QLQ-C30 and QLQ-BN20, have been used in this study to formally assess patient reported outcome measures (PROM). The findings from this generally match those findings seen where patients were assessed by clinicians at time points following IMRT. However, financial worries were a concern for most following IMRT, but patient functioning and overall global health and quality of life did not deteriorate after IMRT. Looking closer, there appears to be a trend for improvement in most of the functioning scales but possibly a decline in cognitive functioning, although these observations did not reach statistical significance. In fact, only improvement in appetite following IMRT was found to be statistically significant. However, the clinical significance of this is uncertain and one has to question if lack of statistical significance in this setting can be used as a surrogate for lack of clinical significance. Prospective collection of data is imperative and this

is now being recognised when studies are being set up to assess new techniques. One of the few prospective studies for IMRT in the treatment of meningioma has shown improvement or stability of quality of life following IMRT over a follow-up of 10 years and, reassuringly, only small numbers of patients developing new symptoms [217].

Although the follow-up in this group of patients is limited to date, the overall progression free survival is slightly lower in comparison to other studies with a rate of 84.6% at a median of 29 months (although this was 100% in those patients with grade I tumours) and overall survival of 96.2% (1 disease unrelated death occurred in a patient with grade II meningioma). Combs' group have demonstrated local control of 98% at 1 year, 95% at 3 years and 94% at 5 years with higher control rates associated with more benign histology [217]. Others have also demonstrated favourable outcomes with recurrence free survival in grade 1 meningiomas of 97.5% at 3 years and 96.3% at 5 years and with overall survival rates of 98% and 97% at 1 and 5 years following IMRT [215].

However, it is important to note the low progression free survival rate (55.6%) in the cohort of patients with grade II histology within this prospective study. There have been documented reports in the literature regarding low tumour control rates associated with grade II or III tumours. Milker-Zabel and colleagues have demonstrated lower recurrence free survival rates for grade 2 tumours compared to grade I tumours (89% v 97.5% and 77.8% v 96.7% at 3 and 5 years respectively) [215]. Similar to this study group, they also noted radiological progression at a median of 22.3 months and 3 non tumour related deaths [215]. Others have also found similar local control and overall survival rates, although with longer follow-up

times [201,220,225]. However, it is well recognised that there is an association with grade II/III tumours and poorer local tumour control rates and survival [186,198]. Some reports suggest that factors, such as gross total resection and maximal mitotic rate ≥ 4/10 per hpf are powerful prognostic parameters [203]. In fact, 3 of the 4 patients who developed post radiotherapy recurrence in this cohort had histological specimens displaying over 4/10 mitosis per hpf.

Reports also correlate the degree of surgical resection with overall survival rates [198], suggesting a complete resection leads to a significantly greater 5 year local control rate compared to subtotal resections (39% v 0% respectively) [200] and some authors have correlated recurrence and survival rates to Simpson's grade of resection [200,423]. Reports in the literature document much higher recurrence with high grade tumours following subtotal excision compared to compete resection (93% v 63% at 5 years [169], and 71% v 57 [200]), with significantly worse local control rates (17% v 87%) [423]. Additionally recurrence risk ratios of 2.71have been calculated following Simpson's grade 1-3 resections compared to Simpson's grade 4 or 5 resections [200]. However, only one patient in the prospective study documented in this thesis had a grade 4 or more Simpson's resection, whilst the others underwent a Simpson's grade 1-3 resection. It was also interesting, but not completely unexpected, to note that 3 out of the 4 patients did develop recurrent symptoms before progressive disease was identified on imaging.

Whilst there are undoubtedly histological features from the tumour itself and the extent of surgical resection which can have prognostic implications, there is evidence to suggest that additional radiotherapy in this particular group of patients is not yet optimal. A study examining 59 patients with grade II or III meningioma and

treated with radiotherapy reported a 66% disease progression rate, 28% 5 year overall survival rate, of which over 90% died of meningioma [193]. Interestingly, they also noted that a radiation dose of 50Gy or more was independently associated with a better 5 year cause specific survival (42% v 0%). Similar results were replicated in other centres, with 5 year survival rates of 40 to 58% [204,424]. Other studies have also commented on the dose used in these higher grade meningiomas. Coke and colleagues examined 17 patients with higher grade meningiomas, delivering a median dose of 61Gy. They noted that 3 of the 5 patients who died of recurrent disease were treated with doses of less than 54Gy [425]. Others have used mean doses over 60Gy for grade II and III meningiomas with demonstrable increases in 5yr progression free survival (0% with <60Gy and 90-100% with ≥60Gy) [192]. These studies have all been retrospective studies, and it is difficult to determine the exact dose required for higher grade tumours without robust prospective data detailing outcomes and potential associated toxicity. However, there is an ongoing EORTC 22042-26042 trial aiming to prospectively evaluate the efficacy and toxicity of higher doses of radiation for grade II and II tumours, delivering 60Gy in cases with a Simpson's grade 1 to 3 resections and 60Gy with a 10Gy boost in those with a Simpson's grade 4 and 5 resection. Additionally, there is a ROAM/EORTC 1308 trial examining whether patients with atypical meningioma should receive early or late radiotherapy following complete surgical resection (Simpson's grade 1-3).

In addition to the potential benefit of higher doses in this group of meningioma patients, some groups have promoted different planning target volumes, with an increase in the CTV margin. Adeberg has recommended a margin of 1-2cm from the GTV for grade II meningiomas and a larger margin of 2-3cm for grade III

tumours [426]. However, a consensus regarding exact margins has yet to be reached.

The poor tumour control rates seen with the grade II tumours in this study may therefore be related to the dose of radiation used, as well as tumour volume irradiated, although this was a small cohort of patients and the results of the larger prospective EORTC trial will be useful. As 2 of the recurrences occurred at the edge of the radiotherapy field, it may be tempting to look at the accuracy of target delineation in greater detail, utilising other imaging modalities, such as functional MRI or molecular PET in the planning process to improve target definition and therefore radiotherapy outcome. Some groups have altered target volumes using high specificity PET tracers [427,428], although clear correlation with clinical outcome is not yet available. However, recent studies have suggested that it is the pathological features that worsen outcome from radiotherapy, rather than just a reduction in target volume margin size with IMRT [393].

As more emphasis is placed on the long term outcomes of patients undergoing therapy, especially for patients with good prognosis tumours, it is important to prospectively document the outcome, tolerability and long term consequences of such treatments. Local control and toxicity profiles appear to be well tolerated in the group of patients with grade I meningioma undergoing IMRT. Conversely, there is poor tumour control with doses of 50.4Gy and ‘standard’ clinical target volumes for the small group of patients grade II tumours and larger radiation doses and/or alterations to tumour volumes may be warranted. However, longer follow-up is necessary to fully and accurately document these findings.

4.6 Conclusion

The data presented in this chapter demonstrates that IMRT is an effective and safe treatment modality for long term control and toxicity in patients with grade I meningiomas. IMRT offers the possibility of highly conformal irradiation, especially for complex shaped, and otherwise difficult to treat meningiomas in the skull base, with the ability to spare adjacent critical structures.

Treatment in this cohort is well-tolerated with acceptable levels of acute toxicity, is not associated with deterioration in quality of life and produces an early improvement in neurology in a significant proportion of cases. Progression-free survival appears equivalent to those documented in retrospective and prospective series.

However, IMRT with doses of 50.4Gy has led to a much lower progression free survival rate in patients with grade II tumours, although this is within a small cohort of patients. Nevertheless, it is important to consider whether patients with grade II or III meningiomas warrant higher doses and larger tumour volumes than those with grade I tumours as some studies suggest [192,425], especially as this may also increase toxicity levels and this is the subject of ongoing EORTC trials.

Highly conformal plans may come at the expense of significant dose to non-delineated extra target organs and, therefore, prospectively collected data is vital to document toxicity and patient reported outcome measures. However, longer follow-

up is essential to fully document the outcomes in this group of patients. Late toxicity from treatment, especially regarding decline in neurocognition, continues to be a concern in these patients and prospective neurocognitive testing before, during and after IMRT would provide further valuable information.

Dose to non-target areas of the brain may always be of concern from photon based conformal radiotherapy. The application of protons for this indication is an area of active research, since a reduction in integral dose with protons can be achieved due to properties of its beam. The depth of the Bragg peak is energy dependent and can lead to equally highly conformal dose distribution as photon IMRT, but with greater reduction in the entry and exit doses [429]. Protons may, therefore, be a promising approach to further sparing of critical organs and perhaps, more importantly, low dose to other areas of the brain, which may in turn reduce the long term effects from radiation.

Dose volume index	Objective dose (% of prescription dose)
$D_{98\%}$	90%
$D_{95\%}$	95%
$D_{5\%}$	105%
$D_{2\%}$	107%

Table 4.1a: Dose objectives for planning target volume (PTV)

Abbreviations: $D_{95\%}$ = dose received by 95% of the PTV, $D_{5\%}$ = dose received by 5% of PTV, $D_{98\%}$ = dose received by 98% of PTV (near minimum dose), $D_{2\%}$ = dose received by 2% of PTV (near maximum dose).

Organ at risk	Dose objectives (Gy)
Brain Stem	55
Spinal cord	48
Optic nerves	50
Optic chiasm	50
Globe	45
Lenses	6
Pituitary gland	45
Cochlea	Mean dose 44

Table 4.1b: Dose objectives for organs at risk

All dose objectives are point max values unless specified.

Dose was minimised to temporal lobes (below 40Gy), where possible. Dose was recorded for other organs at risk outlined (such as hippocampi, whole brain, and hypothalamus).

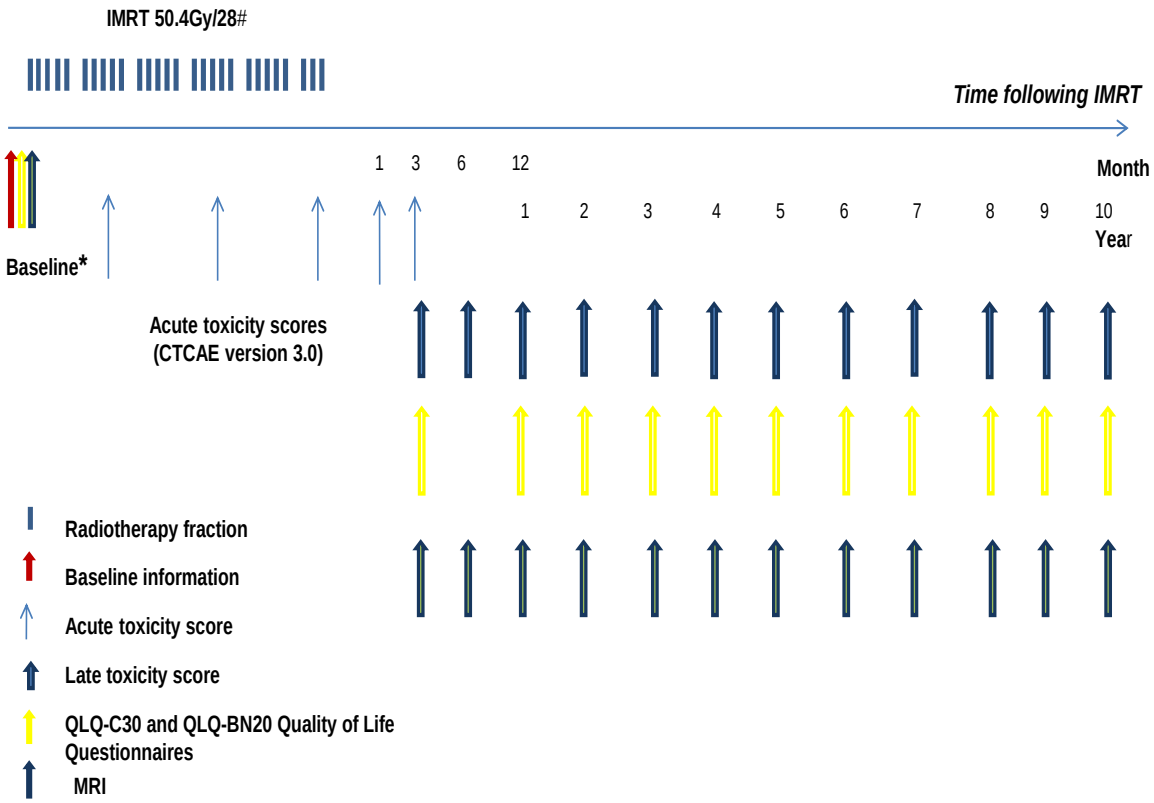

Fig.4.1: Schematic overview of IMRT study methods

Baseline information included toxicity scoring, mini neurological examination, mental test examination, visual assessment and pituitary function tests.

Acute and late toxicities were assessed using CTCAE version 3.0 toxicity scoring.

Late toxicity (including mini neurological examination, mental test examination, visual assessment and pituitary function tests) was assessed at the time points shown.

Characteristic			Number of patients (%)
Sex	Male		12 (46.2)
	Female		14 (53.8)
Age	Median		49.5
	Range		38-76
Performance Status	0		21 (80.8)
	1		5 (19.2)
	≥2		0
Tumour location	Sphenoid wing		7 (26.9)
	Cavernous sinus		1 (3.8)
	Suprasellar		3 (11.5)
	Cerebellopontine angle		1 (3.8)
	Obit sheath/orbit		1 (3.8)
	Olfactory groove		1 (3.8)
	Clivus		1 (3.8)
	Parasagittal/parafalcine		7 (23.1)
	Occipital		1 (3.8)
	Temporal		1 (3.8)
	Parietal		2 (7.7)
	Frontal		1 (3.8)
Grade	1		16 (61.5)
		Transitional	7 (26.9)
		Meningothelial	7 (26.9)
		Not recorded	2 (7.7)
	2		9 (34.6)
		Atypical	3 (11.5)
		Chordoid	4 (15.4)
		Brain invasion	1 (3.8)
		Not recorded	1 (3.8)
	3		0
	Unknown		1 (3.9)
Timing of IMRT	Primary		6 (23.1)
	Post-surgery		9 (34.6)
	At Recurrence		11 (42.3)

Table 4.2: Baseline patient and tumour characteristics

Unknown = sample too small to characterise grade

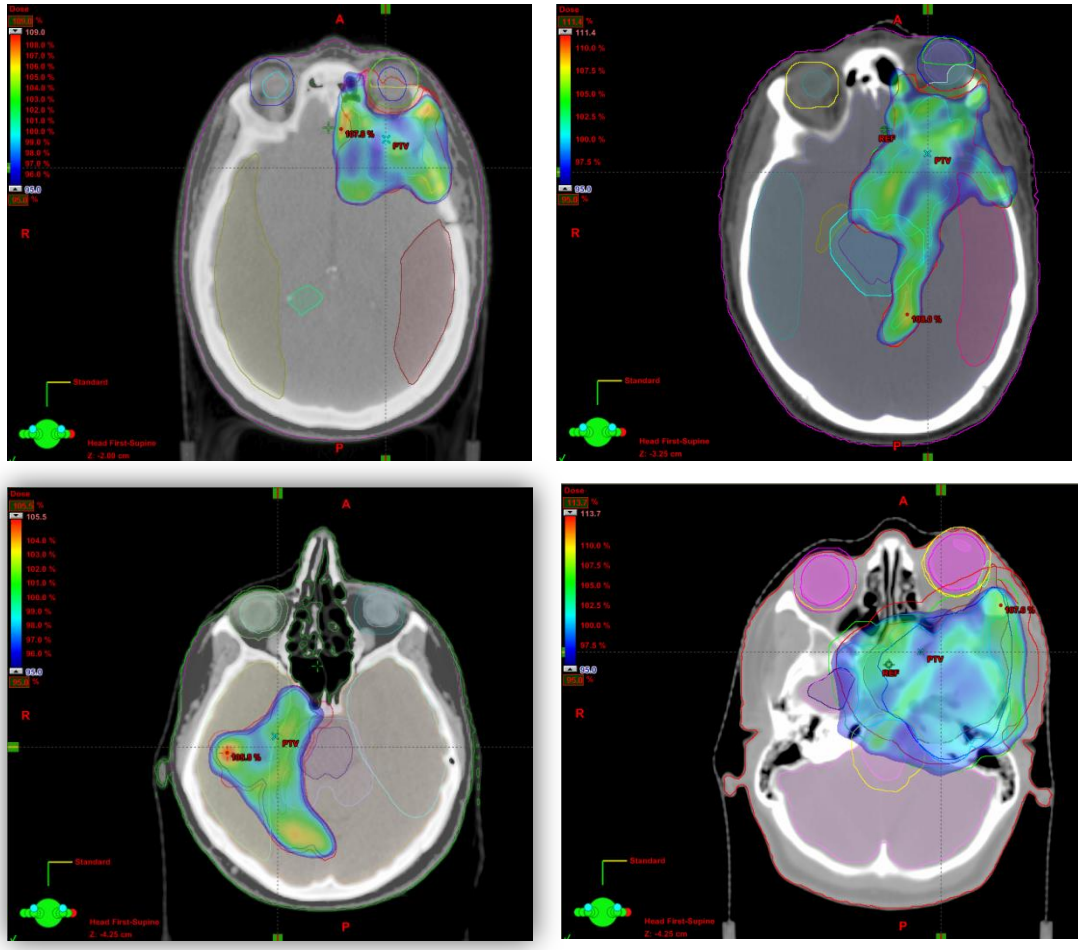

Fig 4.2: Typical IMRT plans displaying coverage of the planning target volume by the 95% isodose

Dose conformity to irregularly shaped PTVs by the 95% isodose is shown in dose colour wash, with concave dose distributions to spare organs at risk, such as optic nerve, retina and brain stem.

a)

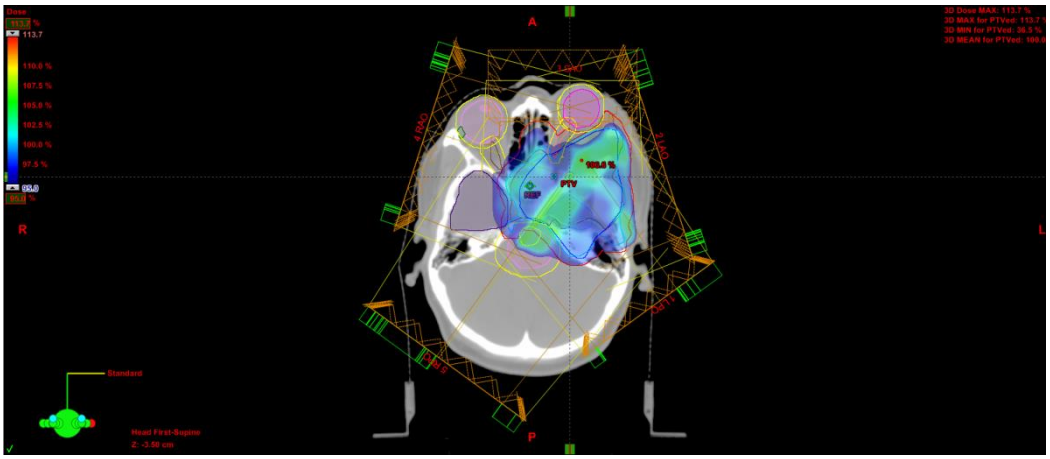

b)

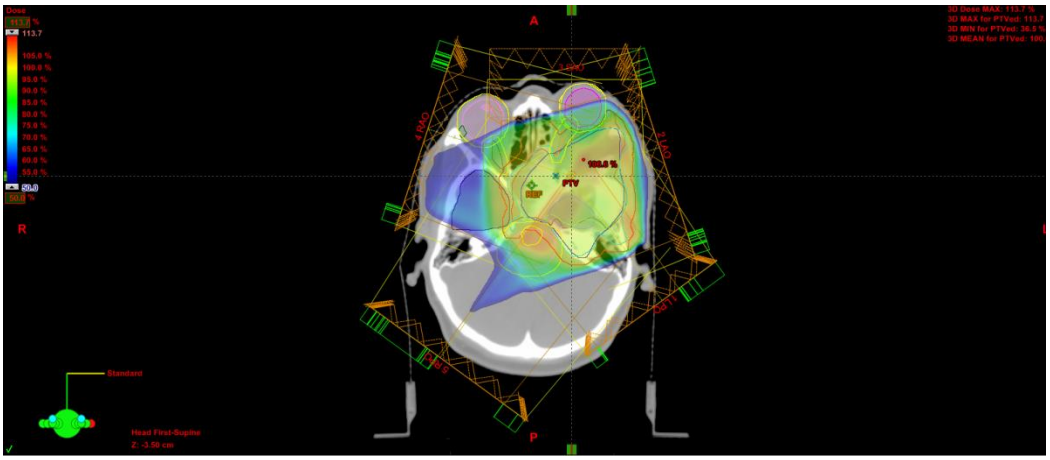

c)

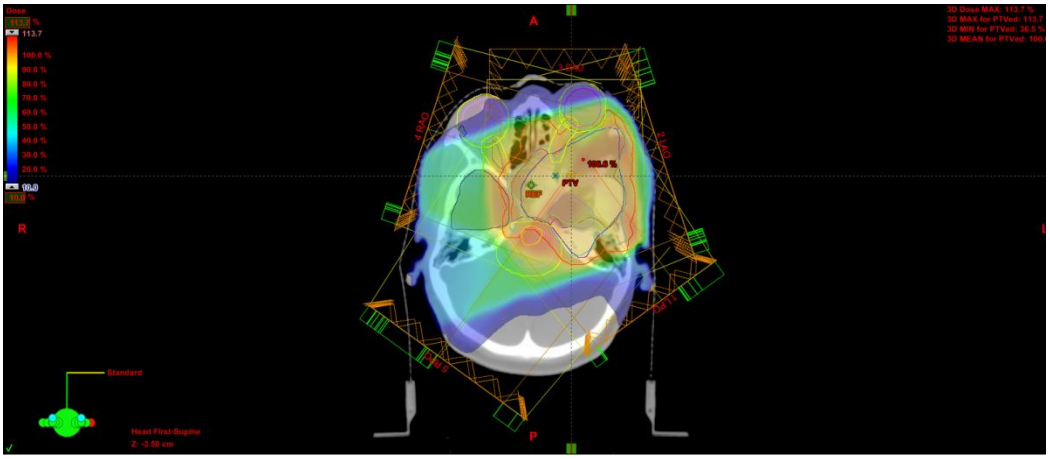

Fig 4.3: Typical plan from one patient demonstrating dose coverage (displayed as dose colour wash) by the a) 95% isodose b) 50% isodose c) 10% isodose d) 45Gy or more e) 50Gy or more

d)

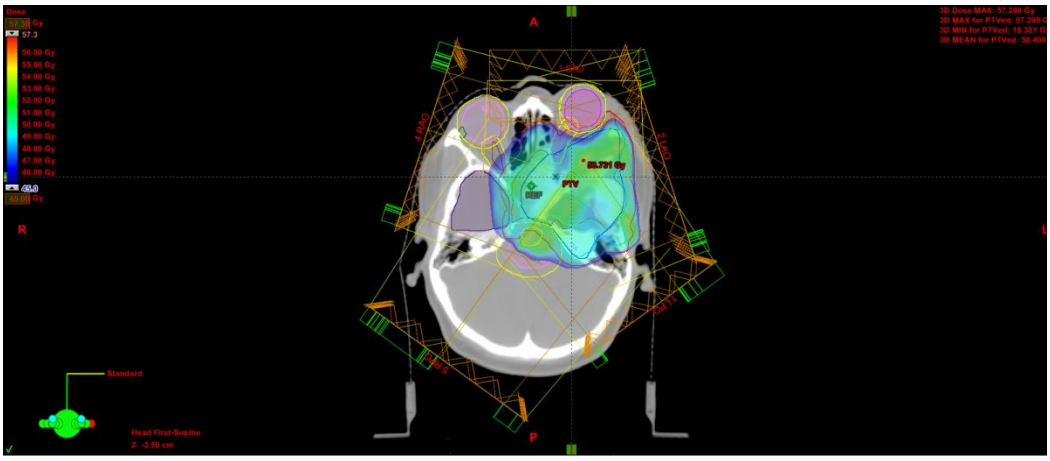

e)

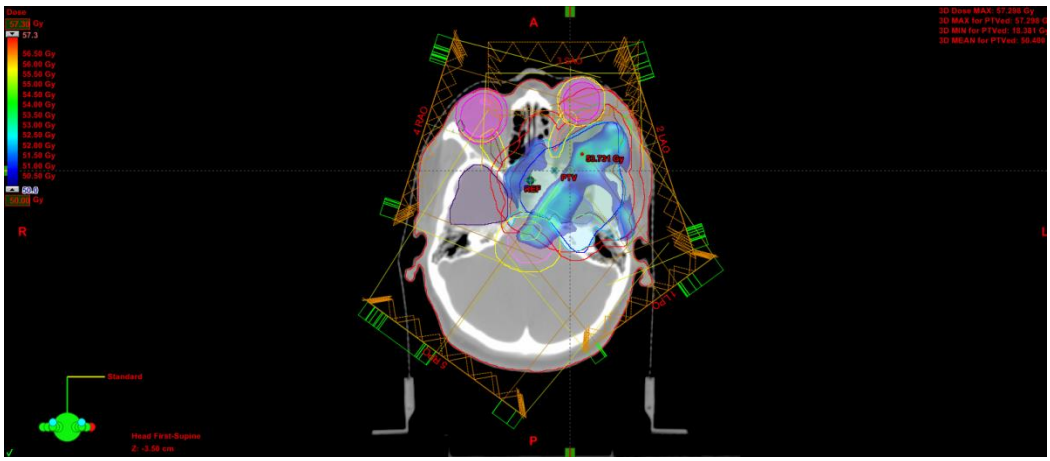

These plans are taken from the same patient and demonstrate the use of 5 modulated radiation fields to achieve tight conformality of the 95 % isodose to the planning target volume (shown as the outer red line). However figures 4.3b and 4.3c also demonstrate the dose received from the 50% isodose, in addition to the lower dose bath wash to the rest of the brain (receiving 10% or more of the dose). Almost all of the brain receives some dose of radiation from this technique, although there is less volume receiving high doses of radiation.

Figures 4.3d and 4.3e show areas of that brain that receive at least 45Gy and at least 50Gy (respectively), demonstrating the steep dose gradients close to organs at risk (and therefore respecting dose constraints of the ipsilateral and contralateral globe and optic nerves respectively).

a)

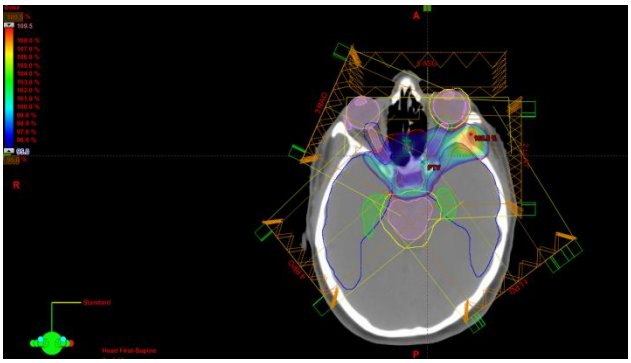

b)

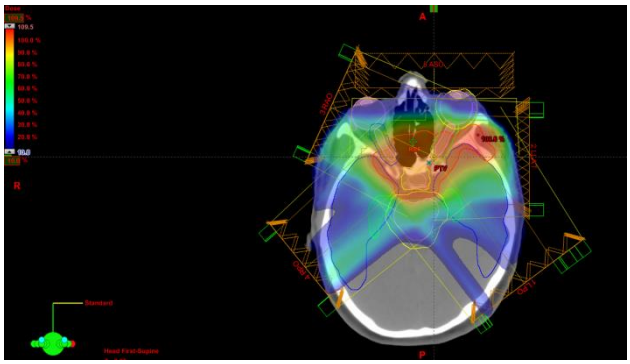

c)

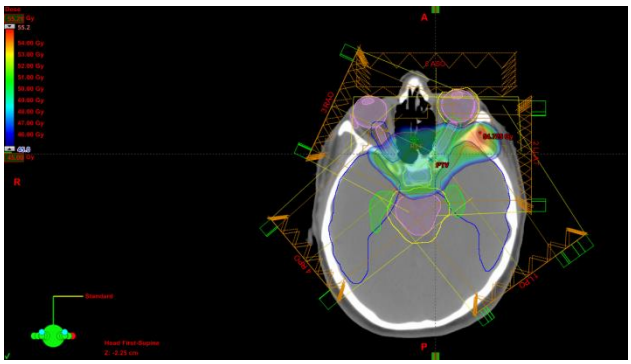

d)

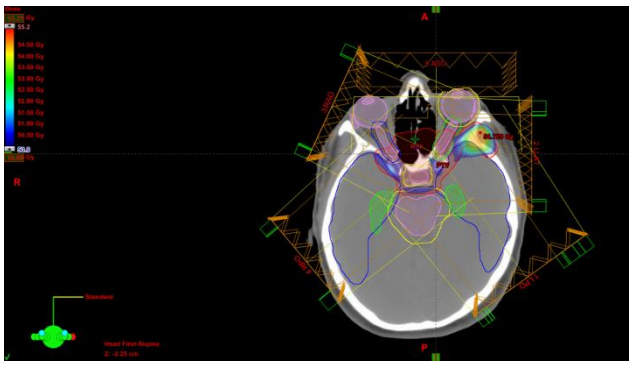

Fig 4.4 Typical plan from one patient demonstrating coverage (shown in dose colour wash) by a) 95% isodose b) 10% isodose, c) 45Gy or more d) 50Gy or more

Fig 4.4 (previous page)

These plans demonstrate tight conformality of the PTV by the 95% isodose and the lower dose bath effect by areas receiving at least 10% of the dose. Figures 4.4c and 4.4d show colour wash dose coverage to those areas receiving at least 45Gy and those receiving at least 50Gy demonstrating the steep dose gradients adjacent to organs at risk (globe and optic nerve, outlined in pink with optic nerve PRVs outlines in blue and green). Also outlined are other organs at risk: temporal lobes [blue line], hippocampi [green], brainstem [light pink], brainstem PRV (planning risk volume) [yellow], pituitary gland [pink].

Patient	PTV	D2%		D98%		D50%		TVPI	PIV	SD across target vol	HI	CI	CI ICRU 62
	(cm^3)	(%)	(Gy)	(%)	(Gy)	(%)	(Gy)	(cm^3)	(cm^3)	(%)			
1	325.8	106.1	53.5	91.4	46.0	100.4	50.6	303.3	345.4	3.5	0.15	81.75	0.93
2	158.8	104.2	52.6	93.7	47.2	100.6	50.7	145.9	169.1	2.6	0.11	79.27	0.92
3	312.1	105.3	53.1	93.4	47.1	100.1	50.5	291.8	328.9	3	0.12	82.95	0.93
4	73.3	104.7	52.8	94.7	47.7	100.0	50.4	69.6	84.7	2.5	0.10	78.02	0.95
5	167.2	105.2	53.0	93.6	47.2	100.1	50.4	160.5	185.3	2.7	0.12	83.15	0.96
6	288	103.6	52.2	94.1	47.4	100.5	50.6	277	322	2.4	0.09	82.74	0.96
7	184.7	104.0	52.4	94.0	47.4	100.5	50.7	176.5	201.9	2.4	0.10	83.53	0.96
8	15.2	104.0	52.4	95.1	47.9	100.1	50.4	14.8	22.3	2.1	0.09	64.62	0.97
9	68.1	104.5	52.7	95.0	47.9	100.2	50.5	66.6	94.4	2.4	0.09	69.00	0.98
10	48.8	102.0	51.4	96.9	48.8	100.3	50.6	48.3	63.6	1.3	0.05	75.17	0.99
11	105.5	104.6	52.7	95.4	48.1	99.9	50.4	100.1	129.3	2.3	0.09	73.45	0.95
12	160.1	105.9	53.4	93.7	47.2	100.2	50.5	148.6	177.8	2.9	0.12	77.57	0.93
13	83.7	104.2	52.5	94.7	47.8	100.2	50.5	79	95.7	2.6	0.10	77.91	0.94
14	39.9	102.5	51.7	93.9	47.3	100.6	50.7	37.2	48	2.1	0.09	72.26	0.93
15	141.2	106.1	53.5	93.5	47.1	100.0	50.4	134.9	170.8	2.8	0.13	75.46	0.96
16	338	107.1	54.0	90.6	45.7	100.0	50.4	310.3	372.6	4.2	0.16	76.45	0.92
17	61.2	107.0	53.9	95.1	47.9	99.7	50.3	59.8	75.4	2.9	0.12	77.50	0.98
18	55.5	105.1	52.9	95.4	48.1	100.1	50.5	53.8	68.9	2.1	0.10	75.69	0.97
19	254.9	105.9	53.4	92.9	46.8	100.2	50.5	241	284.9	4	0.13	79.98	0.95
20	29.5	104.7	52.8	94.6	47.7	100.0	50.4	28.7	38.3	2.3	0.10	72.90	0.97
21	100.9	105.5	53.2	93.9	47.3	100.1	50.5	96.6	108.3	2.7	0.12	85.40	0.96
22	128	103.0	51.9	95.8	48.9	100.3	50.5	126.7	165.6	1.7	0.07	75.73	0.99
23	132.1	105.4	53.1	92.5	46.6	100.2	50.5	125.4	153.6	3	0.13	77.50	0.95
24	105.5	104.0	52.4	95.5	48.1	100.1	50.4	102	112.5	2.3	0.08	87.66	0.97
25	88	103.2	52.0	96.0	48.1	100.2	50.5	87.1	117.8	1.9	0.07	73.18	0.99
26	108.7	106.5	53.7	91.5	46.1	100.4	50.6	99.8	115.2	3.4	0.15	79.54	0.92
Median	107.1	104.7	52.8	94.1	47.4	100.2	50.5	101.1	123.55	2.55	0.10	77.54	0.96

Table 4.3: IMRT plan assessment parameters

Table 4.3 (previous page)

Abbreviations:

PTV: planning target volume

$D_{2\%}$: near maximum dose; $D_{98\%}$: near minimum dose; $D_{50\%}$: median dose

TVPI (cm3) = volume of target covered by the prescription isodose; derived from eclipse treatment planning system by assessing the D100% and PTV overlap.

PIV: volume of prescription isodose;

SD across target vol (measure of homogeneity)(%) standard deviation of the mean dose across the target volume;

HI: homogeneity index; calculated as $(D_{2\%} - D_{98\%})/D_{50\%}$

CI: conformity index; derived using the formula ((volume of target covered by 95% isodose)^2/(volume of target x volume of 95% isodose))x100%

CI ICRU 62: conformity index as stipulated from ICRU62 for 3D conformal planning; derived from treated volume/PTV

	Dose objective (Gy)	Median volume of OAR (cm^3)	Median dose delivered		Median maximum dose point		Accepted dose above dose objective set		
			(Gy)	Range (Gy)	(Gy)	Range (Gy)	Number of patients	Median dose (Gy)	Dose range (Gy)
R Lens	6	0.1	3.9	0.1-7.1	5.28	0.1-14.2	3	7.06	6.33-7.16)
L Lens	6	0.1	3.6	0.1-31.3	5.4	0.1-33.8	4	15.62	9.17-31.4
R Globe	45	9.8	9.7	0.1-22.4	24.9	0.2-50.1	0	N/A	N/A
L Globe	45	9.0	11.8	0.1-37.5	27.0	0.1-49.5	0	N/A	N/A
R Optic Nerve	50	0.5	27.7	0.2-50.8	37.2	0.3-49.1	1	50.80 (D_{max}54.63)	N/A
L Optic Nerve	50	0.4	28.1	0.2-49.5	47.6	0.2-51.4	0	N/A	N/A
Optic Chiasm	50	0.4	45.1	0.3-51.2	49.1	0.4-54.1	1	51.24 (D_{max}51.62)	N/A
R Lacrimal Gland	NS	0.5	11.6	0.2-28	20.2	0.4-25.8	N/A	N/A	N/A
L Lacrimal Gland	NS	0.4	21.6	0.1-36.2	28.7	0.2-44.7	N/A	N/A	N/A
Pituitary	NS	0.45	43.1	0.4-51.7	48.3	0.4-52.9	N/A	N/A	N/A
Hypothalamus	NS	0.6	31.9	0.6-50.1	46.6	0.6-51.5	N/A	N/A	N/A
Brainstem	55	23.7	21.8	0.3-37.4	49.4	0.9-53.2	0	N/A	N/A
R Hippocampus	NS	2.3	17.9	0.6-33.3	33.4	1.3-52.0	N/A	N/A	N/A
L Hippocampus	NS	2.7	19.1	0.7-37.3	33.0	1.2-53.8	N/A	N/A	N/A
R Temporal Lobe	NS	82.5	19.0	0.2-33.3	49.7	0.5-55.9	N/A	N/A	N/A
L Temporal Lobe	NS	72.4	18.3	0.3-41.0	49.8	0.6-55.3	N/A	N/A	N/A
R Inner ear	NS	0.3	9.2	0.5-45.8	12.5	0.1-49.6	N/A	N/A	N/A
L Inner ear	NS	0.25	13.9	0.1-50.7	21.3	0.1-50.9	N/A	N/A	N/A
Whole brain	60	1351.6	13.3	6.6-20.1	53.6	52.9-55.9	0	N/A	N/A

Table 4.4 Organ at risk doses

Abbreviations: R= Right; L= Left; NS = not set; N/A = not applicable

All are PRV doses, except where dose constraints were not set for that organ.

Toxicity	Frequency	
	Number of patients	%
Fatigue	23	88.5
Alopecia	19	73.1
Skin toxicity	10	36
Mouth dryness	5	19.2
Pain (radiation related)	1	3.8
Keratitis/ocular surface irritation	5	11.5
Diplopia	2	7.7
Retinal detachment	1	3.8
Seizure	1	3.8
Short term memory impairment	1	3.8

Table 4.5: Frequency of acute toxicities

Toxicity		Frequency	
		Number of patients	%
Fatigue		10	38.5
Radiation dermatitis		1	
Radiation related pain		2	7.7
	Grade 2	*1*	
	Grade 3	*1*	
Salivary gland changes		1	3.8
Headaches		8	30.8
	Grade 2	*1*	
Seizure		5	19.2
	Grade 2	*1*	
	Grade 3	*1*	
Motor symptoms		1	3.8
Sensory symptoms			
Speech impairment		3	11.5
Memory		11	42.3
	Grade 2	*2*	
Mood/personality changes		12	46.2
	Grade 2	*1*	
Cataracts		3	11.5
	Grade 2	*1*	
Dry eye		10	38.5
	Grade 3	*1*	
Eyelid dysfunction		1	3.8
Glaucoma		1	3.8
Keratitis		1	
Optic disc oedema		1	

Table 4.6: Frequency of late toxicities

All toxicity classified as grade 1, unless stated.

Baseline Symptom/sign	Number of patients with baseline deficit	Outcome following IMRT at follow up		
		Improved	Stable	Worse
Headache	13	6	5	2
Seizure	2	1	1	0
Mood/personality	5	3	0	2
Memory	9	3	6	0
PS	22	1	18	3
Motor deficit	4	3	1	0
Sensory deficit	4	4	0	0
Expressive dysphasia	4	2	2	0
Reduced sense of smell	3	1	2	0
Nasal stuffiness	1	1	0	0
Ocular surface disease	1	1	0	0
Proptosis	4	3	1	0
Vision	14	5	7	2
CNIII	4	3	1	0
CNV	2	2	0	0
CNVII	2	2	0	0
CNVIII	2	1	1	0

Table 4.7: Outcome of baseline symptoms

Abbreviations: IMRT: Intensity modulated radiotherapy, PS =performance status

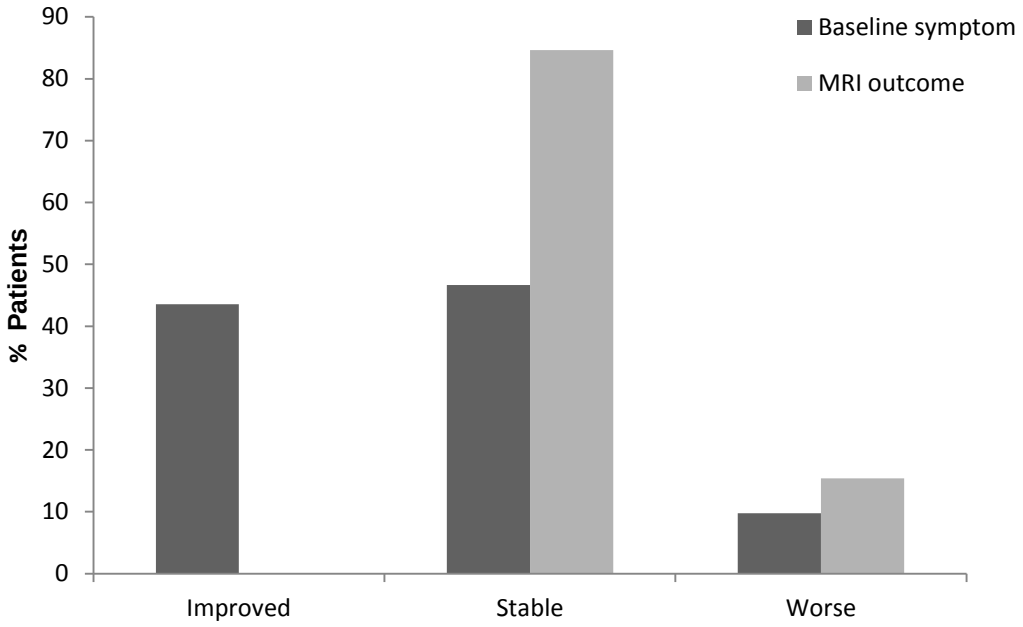

Fig. 4.5: Change in baseline symptoms and radiological assessment following IMRT

	Scale		Mean QoL score (±SD)						p value
			Overall	Baseline	Month 3	Month 6	Month12	Month24	
QLQ -C30	Global Health Status/Quality of Life	Global Health Status/QoL	58.0 (±30.8)	57.9 (±25.3)	58.9 (±30.5)	54.4 (±35.5)	66.7 (±27.6)	58.3 (±35.0)	0.8525
	Functional Scale	Physical functioning	76.2 (±26.9)	73.7 (±29.4)	73.4 (±27.1)	74.7 (±26.8)	78.2 (±25.3)	85.6 (±18.6)	0.8791
		Role functioning	65.8 (±39.3)	62.3 (±36.8)	53.3 (±42.8)	62.2 (±41.5)	70.0 (±36.3)	80.6 (±30.6)	0.5950
		Emotional functioning	72.9 (±27.8)	71.3 (±26.6)	71.7 (±25.2)	67.0 (±29.6)	72.8 (±31.1)	79.2 (±22.8)	0.9260
		Cognitive functioning	74.9 (±32.3)	75.8 (±28.9)	68.9 (±34.4)	70.0 (±35.2)	77.8 (±29.3)	69.4 (±35.6)	0.9181
		Social functioning	68.8 (±37.0)	66.7 (±35.9)	61.1 (±34.9)	65.6 (±40.1)	70.0 (±39.4)	80.6 (±26.7)	0.8564
	Symptom Scale	Fatigue	35.7 (±30.1)	41.1 (±29.7)	38.5 (±33.0)	43.7 (±31.6)	28.1 (±19.2)	20.4 (±19.1)	0.3172
		Nausea and vomiting	2.4 (±10.4)	4.2 (±15.2)	3.3 (±6.9)	3.3 (±9.3)	0.0 (±0.0)	2.8 (±6.8)	0.7970
		Pain	25.1 (±32.2)	28.3 (±30.2)	24.4 (±37.7)	28.9 (±33.0)	23.3 (±28.7)	22.2 (±25.1)	0.9773
		Dyspnoea	11.0 (±22.7)	13.3 (±29.4)	13.3 (±24.6)	9.5 (±20.4)	4.4 (±11.7)	16.7 (±18.3)	0.7138
		Insomnia	32.0 (±34.0)	40.0 (±38.4)	33.3 (±35.6)	33.3 (±33.3)	28.9 (±27.8)	11.1 (±17.2)	0.4602
		Appetite loss	13.2 (±24.4)	33.3 (±31.4)	11.1 (±16.3)	6.7 (±18.7)	4.4 (±11.7)	0.0 (±0.0)	0.0003
		Constipation	19.3 (±27.6)	23.3(±32.6)	17.8 (±24.8)	20.0 (±24.6)	15.6 (±21.3)	5.6 (±13.6)	0.6583
		Diarrhoea	8.9 (±19.2)	8.8(±18.7)	11.9 (±16.6)	15.6 (±24.8)	8.9 (±19.8)	0.0 (±0.0)	0.5371
		Financial difficulties	34.6 (±41.0)	41.7(±40.3)	42.2 (±42.7)	31.1 (±40.8)	35.6 (±44.5)	27.8 (±39.0)	0.8939
QLQ-BN20	Functional Scale	Future uncertainty	71.9 (±30.0)	74.6(±23.6)	63.3 (±32.4)	69.4 (±31.1)	68.3 (±29.4)	72.2 (±35.2)	0.8554
		Visual disorder	18.9 (±27.7)	27.2(±32.3)	24.4 (±35.4)	21.5 (±23.9)	13.3 (±22.3)	7.4 (±13.5)	0.4630
		Motor dysfunction	20.1 (±29.2)	18.3(±26.6)	26.7 (±32.2)	20.7 (±27.2)	25.9 (±33.2)	16.7 (±31.2)	0.8851
		Communication deficit	13.7 (±21.9)	10.6(±16.3)	15.1 (±19.8)	15.6 (±22.9)	21.5 (±26.7)	16.7 (±26.1)	0.6919
	Symptom Scale	Headache	19.7 (±30.6)	20.0(±27.4)	22.2 (±34.9)	22.2 (±30.0)	17.8 (±30.5)	11.1 (±17.2)	0.9400
		Seizure	1.8 (±9.3)	1.7(±7.5)	2.2 (±8.6)	0.0 (±0.0)	2.4 (±8.9)	0.0 (±0.0)	0.8559
		Drowsiness	29.1 (±31.0)	33.3(±32.4)	31.1 (±34.4)	42.2 (±36.7)	24.4 (±15.3)	16.7 (±18.3)	0.3854
		Hair loss	17.1 (±26.7)	16.7(±25.4)	28.9 (±39.6)	13.3 (±24.6)	17.8 (±21.3)	11.1 (±17.2)	0.5350
		Itchy skin	10.7 (±21.1)	15.0(±27.5)	11.1 (±20.6)	8.9 (±15.3)	8.9 (±19.8)	11.1 (±17.2)	0.9132
		Weakness of legs	16.7 (±30.7)	15.0(±33.3)	20.0 (±37.4)	24.4 (±32.0)	15.6 (±24.8)	11.1 (±17.2)	0.8681
		Bladder control	11.1 (±26.1)	11.7(±24.8)	15.6 (±30.5)	11.1 (±27.2)	13.3 (±27.6)	5.6 (±13.6)	0.9538

Table 4.8: EORTC QLQ-C30 and QLQ-BN20 Quality of Life Scores

Table 4.8 (previous page)

Abbreviations: QoL= Quality of life; SD = standard deviation

Mean scores with standard deviation shown for each scale in the QLQ-C30 and QLQ-BN20.

QLQ-C30 is subdivided into 3 scales: global health status /QoL, functional and symptom.

QLQ-BN20 is subdivided into 2 scales: functional and symptom.

p value shown for difference in each scores compared at different time points. The difference in appetite loss scores between baseline and various time points during was found to be statistically significant.

Fig 4.6: EORTC QLQ-C30 and QLQ-BN20 overall mean scores over the duration of IMRT and follow up

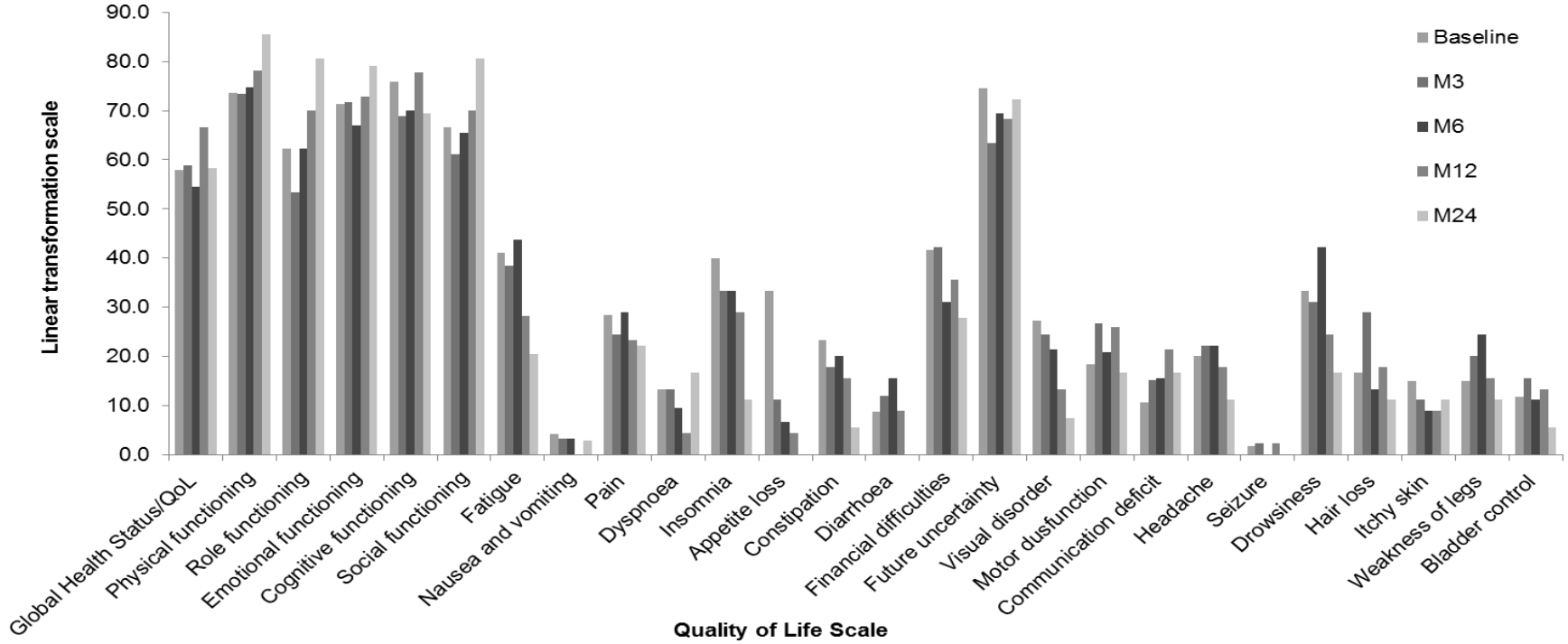

Fig 4.7: EORTC QLQ-C30 and QLQ-BN20 mean scores at baseline and at time points following IMRT

Abbreviations: M=month

Higher scores indicate better functioning/ quality of life for the Global health status/QoL and functioning scales. However higher scores indicate worse symptomatology for all symptom scales.

There is a statistical significance for change in appetite loss between baseline and all other time points following IMRT, p=0.0003.

Chapter 5

Concluding Discussion

Intensity modulated radiotherapy (IMRT) has brought an exciting dimension to radiation therapy. This sophisticated radiation technique is now being used in many clinical settings to enable improved target conformality, dose escalation and reductions in high radiation dose to organs at risks. Whilst there has been much attention paid to the advantages of this type of radiotherapy technique, there has also been recognition of the low dose radiation bath to non-target areas of the body. There have been suggestions that this potential low dose bath produced by IMRT is associated with increased whole body dose and a possible increased risk of second cancers [147,235,239,241,268,270].

The low dose bath or 'out of target dose' has been associated with increased leakage and scatter radiation from the delivery of intensity modulated techniques in comparison to 3D-conformal radiotherapy. Attempts have been made to explore this low dose bath further and whole body dose has been estimated using indirect measures [239,241,244-246,430]. However, a more direct measure, through assessment of the phosphorylation of histone H2AX (γ-H2AX), has been utilised to demonstrate DNA damage from ionising radiation, even at low doses [279] and therefore may be useful in determining low dose radiation exposure from techniques, such as IMRT.

The laboratory work in this thesis has investigated the use of γ-H2AX within peripheral blood lymphocytes of patients undergoing static field intensity modulated radiotherapy (SF-IMRT) and other radiotherapy techniques. The feasibility of using the γ-H2AX assay to identify radiation induced DNA damage within lymphocytes following in vivo irradiation has been demonstrated in chapter 2. This data has confirmed a consistent increase in γ-H2AX foci levels following irradiation; an effect that is seen after each daily fraction of SF-IMRT.

Having demonstrated the reproducibility and consistent increase in foci levels following irradiation, and the lack of any statistically significant difference in foci levels between daily doses, has allowed weekly rather than daily sampling of patients' blood. The results from chapter 2 also reveal no significant difference between the weekly γ-H2AX increase following a fraction of SF-IMRT, and this provides evidence to suggest that sampling of blood from patients for γ-H2AX before and after radiotherapy may only need to be done at one time point during a course of radiotherapy in future studies. This will have an impact, not only on reducing invasive procedures for patients, but also reducing the time for sample processing and analysis of DNA damage within peripheral blood lymphocytes.

The mean increase of 0.323 γ-H2AX foci per nucleus following a course of cranial SF-IMRT within this study (approximately 2-3 times that of baseline levels), is broadly comparable to foci levels found by other groups investigating DNA damage following IMRT to different areas of the body, such as the prostate [356,366,431]. Despite the lack of γ-H2AX foci accumulation in this particular subset of cells at 2 and 6 weeks following IMRT, others have reported a persistence of γ-H2AX foci

within other cell populations, consistent with ongoing DNA damage and lack of efficient repair [279,337,366]. The persistence of DNA damage following treatment may produce stochastic changes and could potentially have implications in long term toxicity.

The work in chapter 3 extended the findings from chapter 2 and established the feasibility and reproducibility of using γ-H2AX within lymphocytes of patients undergoing other types of radiation delivery techniques, such as volumetric modulated arc therapy (RapidArc^{TM} [RA]) and 3D-conformal radiotherapy (CRT). Similarly to SF-IMRT, these experiments have confirmed a consistent increase in DNA damage, through quantification of γ-H2AX foci levels, following treatment with other radiation techniques. However, a statistically significant greater rise in γ-H2AX foci levels was demonstrated with SF-IMRT (0.323 γ-H2AX foci per nucleus) in comparison to both RA (0.185 γ-H2AX foci per nucleus) and CRT (0.142 foci per nucleus), confirming that the γ-H2AX assay has sufficient sensitivity to identify and quantify differing levels of DNA damage in patients undergoing various radiation techniques. However, although there was a reproducible but smaller increase in γ-H2AX following RA in comparison to CRT, this difference did not reach statistical significance.

The results demonstrating different increases in γ-H2AX foci levels with the various techniques, together with the dose response data established from the ex vivo experiment in chapter 2, may point towards an increase in whole body exposure following SF-IMRT (of 1.7 and 2.3 times that after RA and CRT), although it is difficult to confirm that this is as a result of scatter radiation alone. In a similar way,

the TLD measurements (reported in chapter 3), taken at set distances outside the target volume, have documented a higher mean 'out of target dose' following treatment with SF-IMRT (0.196cGy) compared to both RA and CRT (0.144cGy and 0.116cGy respectively). As the increase in γ-H2AX foci levels (and out of target dose) is to some extent thought to be as a result of the low dose bath from SF-IMRT, foci distribution within cell nuclei was examined further in chapter 3. A greater proportion of cells displaying lower foci numbers (between 1-5 foci per nucleus), compared to cells with higher foci levels, was found following all radiation techniques examined. However, this increase in cells with lower numbers of foci was greatest in those patients undergoing SF-IMRT in comparison to those undergoing RA or CRT, which, in turn, may be compatible with a model in which there is more DNA damage, partly as a result of low dose exposure from radiation with SF-IMRT compared to the other techniques examined. However, it is acknowledged that the process of estimating low dose irradiation is not simple and there are clearly other causes of radiation induced DNA damage than from low dose scatter radiation alone.

The low dose bath effect, recognised as a result of IMRT, is caused by a complex interaction of several factors including scatter from the treatment head and collimators of the linear accelerator, as well as from internal scatter. Due to the complexity of the modulated fields and the inefficiencies of the photon beam, there is a requirement for increased beam on time and monitor units. The low dose bath is thought to be dependent on these factors as well as from dose delivered to the target volume and the beam energy used [236,239-241]. It was surprising, therefore, not to be able to demonstrate a direct correlation between increased γ-H2AX foci levels and factors such as beam on time, number of monitor units or tumour volume. Small sample size may, of course, be a reason for the lack of

correlation. The small sample size may also be a factor in the lack of statistical significance for higher γ-H2AX levels seen in patients undergoing RA compared to those treated with CRT. Nevertheless, despite the small sample size, the γ-H2AX assay was sensitive enough to detect a significant difference between SF-IMRT and other radiation techniques.

Attempting to postulate that the difference in γ-H2AX levels between the different radiation techniques is a result of scatter radiation is not easy. Distributions of γ-H2AX foci within in vitro irradiated cells show a good correlation with Poisson distributions [327], however this does not appear to be the case within in-vivo irradiated cells. The lymphocyte population within blood samples taken at any one time may represent those that have been directly irradiated, those that have received indirect radiation through scatter and those which have background levels of radiation. Trying to distinguish between these scenarios is difficult to do due to lymphocyte circulation, migrations and adhesion to vessel walls [340]. By measuring the distribution of γ-H2AX foci in lymphocytes following in vivo radiation and with knowledge of the in vitro dose response relationship of γ-H2AX formation, may provide information regarding recirculation and redistribution in the blood pool of in vivo irradiated lymphocytes. In the future, further mathematical modelling could provide a way forward to determine the fraction of lymphocytes that are directly irradiated and the fraction that receive radiation dose purely from indirect means. Models should utilise the knowledge of circulating blood volume, the total blood volume as well as the speed of blood circulation in order to estimate DNA damage to lymphocytes that circulate through the treatment field and those that endure damage through out of field radiation dose. However, it is likely that

lymphocytes can pass through a beam more than once and this will also need to be taken into account in any model.

Whilst there is still much debate regarding the significance of the increased low dose bath and whole body dose, there is no doubt that IMRT can be useful in the treatment of complex shaped tumours, where techniques such as 3D CRT have struggled to achieve an optimal therapeutic ratio. The data from chapter 4 details the feasibility, efficacy and tolerability of SF-IMRT for the treatment of meningioma, in particular within patients with a grade I meningioma. This prospective study has demonstrated that SF-IMRT can achieve good levels of homogeneity and conformality (through assessment of the homogeneity and conformality indices [HI and CI]), whilst also limiting dose to nearby critical structures; a particular problem in tumours located in the region of the skull base. While other groups have demonstrated similar findings, these have principally been through retrospective studies [201,213,215,220] and there is growing recognition of the value that prospective studies can bring.

Through collection of prospective data, this study has been able to demonstrate and detail the type, onset and duration of acute toxicities, as well as late toxicities. It has revealed a low level of high grade late toxicity and a high local control rate for patients with grade I meningioma (100%% at a median follow up of 29 months), which is comparable to other published reports in the literature [201,215,217]. However, in contrast to this, there was a low local tumour control rate in those patients treated for a grade II meningioma (55.6% at a median follow-up of 29 months) and although lower than expected, has been reported in the literature. Several factors may play a part in this poor outcome, including extent of surgical

resection and adverse histological features [186,198,200,203,423]. However, inadequate dose may be an issue here, with evidence emerging in the literature to suggest that grade II and III tumours may require higher doses in comparison to grade I tumours [192,204,424,425]. Furthermore, treatment planning volumes may need to be increased to counteract the poorer outcomes of such tumours [426]. This may be aided by utilising informative imaging during the planning process and there have been groups that have examined the use of particular high specificity PET tracers (such as 68-Gallium-Dotatoc), as well as PET/MRI, offering better soft tissue definition and therefore better tumour definition [428,432,433]. Further trials are required to formally assess the use of higher doses in higher grade tumours, as well as focusing attention to tumour definition and delineation in these higher grade meningiomas. However, due to the relative rarity of these tumours, recruitment to national or international trials is warranted in order to gain valuable and robust results.

In addition to local control and progression free survival, long term toxicity and effects on quality of life have been investigated as important measures of treatment outcome. At a relatively short median follow up of 29 months, the clinical IMRT study described in chapter 4 has prospectively documented these outcomes. There was an improvement in baseline symptoms in over 65% patients, ranging from an improvement in visual symptoms to improvements in other cranial nerve deficits. Quality of life measures generally remained stable over time, although an improvement in appetite was shown to reach statistical significance. This is broadly in line with Combs' group, who have reported on a prospective study examining IMRT and stereotactic fractionated radiotherapy in 507 patients (131 patients treated with IMRT) over a median follow up period of 107 months, demonstrating stable and even some improvements in quality of life measures [217]. However, it

is interesting to note from the results in chapter 4, that there is a trend towards a slight reduction in cognitive functioning, although this did not reach statistical significance. A prospective study with formal neurocognitive testing, perhaps through the use of EEG assessment during defined computer tasks and used as a surrogate for processing deficits associated with cognitive decline, could be invaluable to document this potential toxicity further. Radiation dose to the hippocampi has been linked to the development of neurocognitive decline [177,414] and it would also be interesting to build upon the results in chapter 4 and explore this relationship within this patient population where long term survival is expected. The clinical study described in chapter 4, does of course, require longer follow up to fully determine the outcomes of IMRT and, in particular, the potential for longer term toxicity, which may only manifest over many years.

The results from this thesis have demonstrated that IMRT enables delivery of highly conformal radiotherapy for meningioma and is associated with acceptable levels of acute and late toxicity and without a significant decline in quality of life at this stage in follow up. However, local control within the cohort of patients with grade II tumours was suboptimal; perhaps due to inadequate dose and tumour volume delineation. Nevertheless, longer follow up and prospectively collected longer term toxicity will be invaluable to fully assess the outcomes in these patients treated with IMRT. The clinical impact of the increased DNA damage and potential increased whole body dose from IMRT is still relatively unknown. Calculations have predicted an approximate doubling of radiation induced second malignancies in people living beyond 10 years [147,148], which is pertinent to the group of patients studied in this thesis.

In the future, this work could be extended by exploring the correlations of IMRT dose distributions with functional MRI assessment of irradiated normal tissues in the brain and this could also potentially be used to correlate with long term toxicity data from this population of patients. This may provide valuable information regarding dose response data for non-target areas of the brain. In a similar way, γ-H2AX may be used to prospectively correlate foci levels with long term toxicity, including second malignancies.

Highly conformal plans, using photon therapy, may always come at the expense of significant dose to some extra target organs, which could have implications regarding increased long term toxicity. The use of protons has gained increasing interest over the last few years, as there is the potential to improve the therapeutic ratio through the properties of its beam. Further work is warranted to prospectively document the feasibility and tolerance of using proton therapy in this patient population, whilst utilising γ-H2AX to establish dose response data and determine the potential reduction in whole body dose.

In summary, through the translational and clinical research described in this thesis, the biological and clinical implications of intensity modulated radiotherapy in the treatment of brain tumours have been explored. This work has encompassed translational work using γ-H2AX to document the feasibility and reproducibility of assessing DNA damage in patients undergoing different conformal external beam photon radiotherapy techniques as a means of exploring whole body dose. It has documented higher levels of γ-H2AX foci following SF-IMRT compared to other techniques studied and is the first study to document higher γ-H2AX levels following SF-IMRT in comparison to RA. The feasibility and tolerance of IMRT in a

prospective phase I/II study have been described, with documentation of the toxicities as well as both clinical and patient reported outcomes. However, data collection and analysis on longer term outcomes, both for the tumour and more importantly, normal tissue, will be ongoing. The results from this thesis add to the body of work defining the use, outcomes and associated radiation induced DNA damage from IMRT, whilst providing further information to guide future studies in this field, highlighting the role of γ-H2AX and the value of prospective clinical studies in such work.

Appendix A

Proforma for Static field IMRT (SF-IMRT) study patients

Patient Initials		
DOB		
Study ID		
Diagnosis		
Dose Regime		
Dose/#		
RT Technique Used		
Target Volume		
No. fields/ field length		
Baseline MR/CT		
Planning CT		
QA		
PC		
Baseline Sample (pre-RTP scan)		
Treatment Start		
Treatment End		
Post Samples	2 weeks	
	6 weeks	

Tpre	Time of pre-RT sample
Tbon	Time RT beam switched on
Tboff	Time RT beam switched off
Tboff-Tbon	Total treatment time
Tpost	Time of post-RT sample
Tpost-Tboff	Time between beam off and post-RT sample taken

Proforma for static field IMRT (SF-IMRT) study patients

	Date	Tpre	Tbon	Tboff	Tboff-Tbon (sec)	Tpost	Tpost-Tboff (min)	Monitor Units (MU)	Dose Rate
Week 1									
Week 2									
Week 3									
Week 4									
Week 5									
Week 6									

Proforma for RapidArc™ (RA) study patients

Patient Initials		
DOB		
Study ID		
Diagnosis		
Dose Regime		
Dose/#		
RT Technique Used		
Target Volume		
No. fields/ field length		
Baseline MR/CT		
Planning CT		
QA		
PC		
Baseline Sample (pre-RTP scan)		
Treatment Start		
Treatment End		
Post Samples	2 weeks	
	6 weeks	

Tpre	Time of pre-RT sample
Tbon	Time RT beam switched on
Tboff	Time RT beam switched off
Tboff-Tbon	Total treatment time
Tpost	Time of post-RT sample
Tpost-Tboff	Time between beam off and post-RT sample taken

Proforma for RapidArc™ (RA) study patients

	Date	Tpre	Tbon	Tboff	Tboff-Tbon (sec)	Tpost	Tpost-Tboff (min)	Monitor Units	Dose Rate
Week 1									
Week 2									
Week 3									
Week 4									
Week 5									
Week 6									

Proforma for 3D-Conformal Radiotherapy (CRT) study patients

Patient Initials		
DOB		
Study ID		
Diagnosis		
Dose Regime		
Dose/#		
RT Technique Used		
Target Volume		
No. fields/ field length		
Baseline MR/CT		
Planning CT		
QA		
PC		
Baseline Sample (pre-RTP scan)		
Treatment Start		
Treatment End		
Post Samples	2 weeks	
	6 weeks	

Tpre	Time of pre-RT sample
Tbon	Time RT beam switched on
Tboff	Time RT beam switched off
Tboff-Tbon	Total treatment time
Tpost	Time of post-RT sample
Tpost-Tboff	Time between beam off and post-RT sample taken

Proforma for 3D-Conformal Radiotherapy (CRT) study patients

	Date	Tpre	Tbon	Tboff	Tboff-Tbon (sec)	Tpost	Tpost-Tboff (min)	Monitor Units (MU)	Dose Rate
Week 1									
Week 2									
Week 3									
Week 4									
Week 5									
Week 6									

Appendix B

Acute toxicity follow-up forms

Late toxicity follow-up forms

Neurological evaluation forms

ACUTE TOXICITY FOLLOW-UP FORM

Trial number: ☐☐☐☐☐ Patient's initials: ☐☐☐

Hospital no.: _____

Please complete the corresponding grades for each visit according to the CTCAE version 3.0 acute toxicity follow up legend. Please fill in each line. If the patient has no toxicity for a particular site please fill in 0. NCI website: http://ctep.cancer.gov/reporting/ctc.htlm.

Date (dd/mm /yyyy)								
		During Radiotherapy				**Post-Radiotherapy**		
	Before RT	**Week 1-2**	**Week 3-4**	**Week 5-6**		**Week 9-10**		**Week 18**
OCULAR/VISUAL								
Cataract								
Dry eye syndrome								
Eyelid dysfunction								
Glaucoma								
Keratitis								
Night blindness								
Nystagmus								
Ocular surface disease								
Diplopia								
Optic disc oedema								
Proptosis/ enophthalmos								
Retinal detachment								
Retinopathy								
DERMATOLOGY / SKIN								
radiation dermatitis								
alopecia								
FATIGUE								
fatigue radiation related								
WHO PS								
score								
MUCOSITIS								
mucositis radiation related								

ACUTE TOXICITY FOLLOW-UP FORM

Trial number: ☐☐☐☐☐ Patient's initials: ☐☐☐

Hospital no.: _____

Please complete the corresponding grades for each visit according to the CTCAE version 3.0 acute toxicity follow up legend. Please fill in each line. If the patient has no toxicity for a particular site please fill in 0.

Date (dd/mm /yyyy)								
		During Radiotherapy				**Post-Radiotherapy**		
	Before RT	**Week 1-2**	**Week 3-4**	**Week 5-6**		**Week 9-10**		**Week 18**
PAIN								
pain due to radiation								
SALIVARY GLAND								
mouth dryness								
salivary gland changes								
NEUROLOGY								
CSF leak								
Leukoencephalopathy								
Memory impairment								
Mental status								
Mood alteration								
Cranial neuropathy:								
I (smell)								
II (vision)								
III (Pupil/ upper eyelid/ extraocular movements)								
IV (downward/ inward eye movement)								
V (motor-jaw muscles; sensory-facial)								
VI (lateral eye deviation)								
VII (motor-face; sensory-taste)								
VIII (hearing and balance)								
IX (motor-pharynx; sensory-ear, pharynx, tongue)								

ACUTE TOXICITY FOLLOW-UP FORM

Trial number: ☐☐☐☐☐ Patient's initials: ☐☐☐

Hospital no.: _____

Please complete the corresponding grades for each visit according to the CTCAE version 3.0 acute toxicity follow up legend. Please fill in each line. If the patient has no toxicity for a particular site please fill in 0.

Date (dd/mm/yyyy)								
		During Radiotherapy				**Post-Radiotherapy**		
	Before RT	**Week 1-2**	**Week 3-4**	**Week 5-6**		**Week 9-10**		**Week 18**
NEUROLOGY								
X (motor-palate, pharynx, larynx)								
XI (motor SCM/ trapezius)								
XII (motor-tongue)								
Neuropathy: motor								
Neuropathy: sensory								
Personality								
Phrenic nerve dysfunction								
Psychosis								
Pyramidal tract dysfunction								
Seizure								
Somnolence								
Speech impairment								
Syncope								
Tremor								
Neurology-Other: Specify_____ _____ _____								

LATE TOXICITY FOLLOW-UP FORM

Trial number: ☐☐☐☐☐ Patient's initials: ☐☐☐

Hospital no.: _____

Please complete the corresponding grades for each visit according to the CTCAE version 3.0 acute toxicity follow up legend. Please fill in each line. If the patient has no toxicity for a particular site please fill in 0.

DATE										
OCULAR										
Cataract										
Dry eye syndrome										
Eyelid dysfunction										
Glaucoma										
Keratitis										
Night blindness										
Nystagmus										
Ocular surface disease										
Diplopia										
Optic disc oedema										
Proptosis/ enophthalmos										
Retinal detachment										
Retinopathy										
SKIN										
radiation dermatitis										
alopecia										
FATIGUE										
fatigue radiation related										
WHO PS										
score										
MUCOSITIS										
mucositis radiation related										

LATE TOXICITY FOLLOW-UP FORM

Trial number: ☐☐☐☐☐ Patient's initials: ☐☐☐

Hospital no.: _____

Please complete the corresponding grades for each visit according to the CTCAE version 3.0 acute toxicity follow up legend. Please fill in each line. If the patient has no toxicity for a particular site please fill in 0.

DATE										
PAIN										
pain due to radiation										
SALIVARY GLAND										
mouth dryness										
salivary gland changes										
NEUROLOGY										
CSF leak										
Leukoencephalopathy										
Memory impairment										
Mental status										
Mood alteration										
Cranial neuropathy:										
I (smell)										
II (vision)										
III (Pupil/ upper eyelid/ extraocular movements)										
IV (downward/ inward eye movement)										
V (motor-jaw muscles; sensory-facial)										
VI (lateral eye deviation)										
VII (motor-face; sensory-taste)										
VIII (hearing and balance)										
IX (motor-pharynx; sensory-ear, pharynx, tongue)										
X (motor-palate, pharynx, larynx)										
XI (motor SCM/ trapezius)										

LATE TOXICITY FOLLOW-UP FORM

Trial number: ☐☐☐☐☐ Patient's initials: ☐☐☐

Hospital no.: _____

Please complete the corresponding grades for each visit according to the CTCAE version 3.0 acute toxicity follow up legend. Please fill in each line. If the patient has no toxicity for a particular site please fill in 0.

DATE										
NEUROLOGY										
XII (motor-tongue)										
Neuropathy: motor										
Neuropathy: sensory										
Personality										
Phrenic nerve dysfunction										
Psychosis										
Pyramidal tract dysfunction										
Seizure										
Somnolence										
Speech impairment										
Syncope										
Tremor										
Neurology-Other: Specify_____										

NEUROLOGIC EVALUATION FORM-1

Study number: ☐☐☐☐☐ Patient's initials: ☐☐☐

Date of assessment: ☐☐ ☐☐ ☐☐☐☐ Hospital no.: _____
dd mm yyyy

NEUROLOGIC SYMPTOMS

Headache ☐

0 = None, 1 = Minor/ intermittent, 2 = Requires non-narcotic analgesics, 3 = Requires narcotic preparation, 4 = Incapacitating, 9 = Unknown

Visual Disturbance ☐

0 = None, 1 = Acuity decreased, 2 = Field defect, 3 = Diplopia, 4 = Blind/unilaterally, 5 = Blind/bilaterally, 9 = Unknown

Speech Impairment ☐

0 = None, 1 = Minor/ intermittent, 2 = Moderate, 3 =Severe, 9 = Unknown

Sensory Symptoms ☐

0 = None, 1 = Minor/ intermittent, 2 = Moderate, 3 = Severe, 9 = Unknown

Motor Symptoms ☐

0 = None, 1 = Minor/ intermittent, 2 = Moderate, 3 = Severe, 9 = Unknown

Memory Symptoms ☐

0 = None, 1 = Recent event, 2 = Remote event, 3 = Both, 9 = Unknown

Personality changes ☐

0 = None, 1 = Minor/ intermittent, 2 = Moderate, 3 = Severe, 9 = Unknown

Seizures ☐

0 = None, 1 = Occasional (<1/week, without anticonvulsants), 2 = Occasional with anticonvulsants, 3 = Frequent (>1/week, with anticonvulsants), 4 = uncontrollable, 9 = Unknown

Other Neurological symptoms ☐

0 = None, 1 = Minimal, 2 = Moderate, 3 = Severe, 9 = Unknown

Specify: .....

NEUROLOGIC EVALUATION FORM-2

Study number: ☐☐☐☐☐ Patient's initials: ☐☐☐

Date of assessment: ☐☐ ☐☐ ☐☐☐☐ Hospital no.: _____
dd mm yyyy

NEUROLOGIC EXAM

Mental Status ☐

0 = Normal, 1 = Minor Mental confusion, 2 =Gross confusion but awake, 9 =Unknown

Somnolence ☐

0 = None, 1 = Lethargy, 2 = Rousable with difficulty, 3 = coma, 9 = Unknown

Papilloedema ☐

0 = None, 1 = Suggestive, 2 = Definite or exudate, 3 = Definite haemorrhage, atrophy, 4 = post papilledema, 9 = Unknown

Motor Deficit function ☐

0 = Normal, 1 = symptomatic weakness only, 2 = <50% decrease in function, 3 = >50% decrease in function, 5 = complete paralysis, 9 = Unknown
If paralysis, specify area: .....

Cranial Nerve Deficit ☐

0 = None, 1 =Minor/ intermittent, 2 =Moderate, 3 =Severe, 9 = Unknown
Specify: .....

Sensory Deficit ☐

0 = None, 1 = Minor/ intermittent, 2 = Moderate, 3 = Severe, 9 = Unknown

Visual test ☐

0 = Intact, 1 = Deficit sight, 2 = Deficit visual field
Specify: .....

Cerebral Deficit ☐

0 = None, 1 = Minor/ intermittent, 2 = Moderate, 3 = Severe, 9 = Unknown
Specify: .....

Reflex function ☐

0 = Normal, 1 = Abnormal

Appendix C

EORTC QLQ-C30

EORTC QLQ-BN20

Date completed by patient (D/M/Y) ⌊⌋⌊⌋⌊⌋⌊⌋⌊⌋⌊⌋
Inst ⌊⌋⌊⌋⌊⌋⌊⌋ Seq id ⌊⌋⌊⌋⌊⌋⌊⌋

EORTC QLQ-C30 (version 3)

We are interested in some things about you and your health. Please answer all of the questions yourself by circling the number that best applies to you. There are no "right" or "wrong" answers. The information that you provide will remain strictly confidential.

Please fill in your initials: ⌊⌋⌊⌋⌊⌋⌊⌋
Your birthdate (Day, Month, Year): ⌊⌋⌊⌋⌊⌋⌊⌋⌊⌋⌊⌋⌊⌋⌊⌋
Today's date (Day, Month, Year): 31 ⌊⌋⌊⌋⌊⌋⌊⌋⌊⌋⌊⌋⌊⌋⌊⌋

	Not at All	A Little	Quite a Bit	Very Much
1. Do you have any trouble doing strenuous activities, like carrying a heavy shopping bag or a suitcase?	1	2	3	4
2. Do you have any trouble taking a long walk?	1	2	3	4
3. Do you have any trouble taking a short walk outside of the house?	1	2	3	4
4. Do you need to stay in bed or a chair during the day?	1	2	3	4
5. Do you need help with eating, dressing, washing yourself or using the toilet?	1	2	3	4

During the past week:	Not at All	A Little	Quite a Bit	Very Much
6. Were you limited in doing either your work or other daily activities?	1	2	3	4
7. Were you limited in pursuing your hobbies or other leisure time activities?	1	2	3	4
8. Were you short of breath?	1	2	3	4
9. Have you had pain?	1	2	3	4
10. Did you need to rest?	1	2	3	4
11. Have you had trouble sleeping?	1	2	3	4
12. Have you felt weak?	1	2	3	4
13. Have you lacked appetite?	1	2	3	4
14. Have you felt nauseated?	1	2	3	4
15. Have you vomited?	1	2	3	4
16. Have you been constipated?	1	2	3	4

Please go on to the next page

During the past week:	Not at All	A Little	Quite a Bit	Very Much
17. Have you had diarrhea?	1	2	3	4
18. Were you tired?	1	2	3	4
19. Did pain interfere with your daily activities?	1	2	3	4
20. Have you had difficulty in concentrating on things, like reading a newspaper or watching television?	1	2	3	4
21. Did you feel tense?	1	2	3	4
22. Did you worry?	1	2	3	4
23. Did you feel irritable?	1	2	3	4
24. Did you feel depressed?	1	2	3	4
25. Have you had difficulty remembering things?	1	2	3	4
26. Has your physical condition or medical treatment interfered with your family life?	1	2	3	4
27. Has your physical condition or medical treatment interfered with your social activities?	1	2	3	4
28. Has your physical condition or medical treatment caused you financial difficulties?	1	2	3	4

For the following questions please circle the number between 1 and 7 that best applies to you

29. How would you rate your overall health during the past week?

1	2	3	4	5	6	7
Very poor						Excellent

30. How would you rate your overall quality of life during the past week?

1	2	3	4	5	6	7
Very poor						Excellent

EORTC QLQ - BN20

Patients sometimes report that they have the following symptoms. Please indicate the extent to which you have experienced these symptoms or problems during the past week.

During the past week:		Not at All	A Little	Quite a Bit	Very Much
31.	Did you feel uncertain about the future?	1	2	3	4
32.	Did you feel you had setbacks in your condition?	1	2	3	4
33.	Were you concerned about disruption of family life?	1	2	3	4
34.	Did you have headaches?	1	2	3	4
35.	Did your outlook on the future worsen?	1	2	3	4
36.	Did you have double vision?	1	2	3	4
37.	Was your vision blurred?	1	2	3	4
38.	Did you have difficulty reading because of your vision?	1	2	3	4
39.	Did you have seizures?	1	2	3	4
40.	Did you have weakness on one side of your body?	1	2	3	4
41.	Did you have trouble finding the right words to express yourself?	1	2	3	4
42.	Did you have difficulty speaking?	1	2	3	4
43.	Did you have trouble communicating your thoughts?	1	2	3	4
44.	Did you feel drowsy during the daytime?	1	2	3	4
45.	Did you have trouble with your coordination?	1	2	3	4
46.	Did hair loss bother you?	1	2	3	4
47.	Did itching of your skin bother you?	1	2	3	4
48.	Did you have weakness of both legs?	1	2	3	4
49.	Did you feel unsteady on your feet?	1	2	3	4
50.	Did you have trouble controlling your bladder?	1	2	3	4

Appendix D

List of Abstracts and Publications

Maclean J, Fersht N, Bremner F, Stacey C, Sivabalasingham S, Short, S

Meningioma causing visual impairment: Outcomes and toxicity following Intensity modulated radiotherapy

Int J Radiat Oncol Biol Phys. 2013 Mar 15; 85(4):e179-86.

S Sivabalasingham, M Worku, P Bassett, N Lalli, A Abulimiti, N Fersht, T Guerrero-Urbano, S C Short. Gamma H2AX: a sensitive biomarker for comparison of whole body dose from IMRT, RapidArc^{TM} or 3D-conformal radiotherapy.

Radiotherapy and Oncology, Vol 103, Suppl 1, May 2012, S144-S145*. ESTRO May 2012. Selected for oral presentation in Young Scientist Poster Session.*

J Maclean, S Sivabalasingham, F Bremner, D D'Souza, N Fersht, S Short

Meningioma causing visual impairment: Toxicity and outcome with IMRT.

Radiotherapy and Oncology Vol 103 suppl 1, May 2012, S406-S407) *ESTRO May 2012.*

S Sivabalasingham, M Worku, S C Short

Gamma-H2AX as a biomarker of radiation-induced DNA damage in patients receiving brain radiotherapy: a comparison of volumetric modulated arc therapy (RapidArc^{TM}) with static field intensity modulated radiotherapy (IMRT)

National Cancer Research Institute (NCRI) Cancer Conference 2011; Nov 2011; Liverpool UK. Abstract B58. *NCRI; Nov 2011.*

D Woolf, R Bakhshi, S Fawcitt, M Worku, D Ghosh, S Sivabalasingham, N Williams, S Short, K Pigott, M Keshtgar. An observational study using γ-H2AX foci to investigate cardiac doses of radiation following adjuvant radiotherapy for breast cancer: Standard external beam radiotherapy to the breast versus intraoperative radiotherapy**.** J Clin Oncol 29: 2011 (suppl; abstr TPS 129). *ASCO June 2011.*

S Sivabalasingham, M Worku, SC Short. Whole body dose, using gamma h2ax measurement, following radiotherapy: a comparison of volumetric modulated arc therapy (RapidArc^{TM}) with static field intensity modulated radiotherapy (IMRT). Radiotherapy and Oncology, Vol 99, Suppl 1, May 2011, S490*. ESTRO, May 2011.*

S Sivabalasingham, N Fersht, D D'Souza, I Rosenberg, C Stacey, P Davies, T Guerrero-Urbano, SC Short. Preliminary results from a phase I/II study of intensity modulated radiotherapy in the treatment of meningiomas**.**
Clin Oncol 2011; 23(3):S53*. UKRO, April* 2011.

S Sivabalasingham, M Worku, P Bassett, N Lalli, A Abulimiti, N Fersht, T Guerrero-Urbano, S C Short. Gamma H2AX: a sensitive biomarker for comparison of whole body dose from IMRT, RapidArc^{TM} or 3D-conformal radiotherapy. Radiotherapy and Oncology, Vol 103, Suppl 1, May 2012, S144-S145*. ESTRO May 2012. Selected for oral presentation in Young Scientist Poster Session.*

S Sivabalasingham, M Worku, G Marks, T Guerrero-Urbano, SC Short. γ-H2Ax quantification of low dose irradiation-induced DNA damage in patients receiving intensity modulated radiotherapy (IMRT). Cancéropôle Grand-Ouest **'**Biology of ionizing radiation' workshop, *France 2011. Selected for oral presentation.*

S Sivabalasingham, M Worku, G Marks, T Guerrero-Urbano, SC Short. Gamma H2AX as a biomarker of low dose irradiation-induced DNA damage in patients receiving intensity modulated radiotherapy for brain tumours. Radiotherapy & Oncology, Vol 96 Suppl. 1 (2010), Abstract number 411. *ESTRO, Barcelona, 2010. Selected for oral presentation.*

References

[1] Leibel SA, Ling CC, Kutcher GJ, Mohan R, Cordon-Cordo C Fuks Z. The biological basis for conformal three-dimensional radiation therapy. Int J Radiat Oncol Biol Phys 1991;21:805-811.

[2] Webb S. The physics of conformal radiotherapy- advances in technology. Bristol: IOP Publishing, 1997.

[3] IMRT_CWG. Intensity-modulated radiotherapy: current status and issues of interest. Int J Radiat Oncol Biol Phys 2001;51:880-914.

[4] Purdy JA, Starkschall,G. A practical Guide to 3-D Planning and Conformal Radiation Therapy. Madison WI: Advanced Medical Physics Publishing, 1999.

[5] Verhey LJ. Comparison of three-dimensional conformal radiation therapy and intensity-modulated radiation therapy systems. Semin Radiat Oncol 1999;9:78-98.

[6] Nutting C, Dearnaley DP Webb S. Intensity modulated radiation therapy: a clinical review. Br J Radiol 2000;73:459-469.

[7] Dearnaley DP. Radiotherapy of prostate cancer: established results and new developments. Semin Surg Oncol 1995;11:50-59.

[8] Morris DE, Emami B, Mauch PM, et al. Evidence-based review of three-dimensional conformal radiotherapy for localized prostate cancer: an ASTRO outcomes initiative. Int J Radiat Oncol Biol Phys 2005;62:3-19.

[9] Perez CA, Purdy JA, Harms W, et al. Three-dimensional treatment planning and conformal radiation therapy: preliminary evaluation. Radiother Oncol 1995;36:32-43.

[10] Emami B, Graham MV Purdy JA. Three-dimensional conformal radiotherapy in bronchogenic carcinoma: considerations for implementation. Lung Cancer 1994;11 Suppl 3:S117-128.

[11] Emami B, Purdy JA, Simpson JR, Harms W, Gerber R Wippold JF. 3-D conformal radiotherapy in head and neck cancer. The Washington University experience. Front Radiat Ther Oncol 1996;29:207-220.

[12] Jones RE, Takeuchi T, Eisbruch A, D'Hondt E, Hazuka M Ship JA. Ipsilateral parotid sparing study in head and neck cancer patients who receive radiation therapy: results after 1 year. Oral Surg Oral Med Oral Pathol Oral Radiol Endod 1996;81:642-648.

[13] Hazuka MB, Martel MK, Marsh L, Lichter AS Wolf GT. Preservation of parotid function after external beam irradiation in head and neck cancer patients: a feasibility study using 3-dimensional treatment planning. Int J Radiat Oncol Biol Phys 1993;27:731-737.

[14] Mackie TR. Radiation therapy treatment optimization. Introduction. Semin Radiat Oncol 1999;9:1-3.

[15] Webb S. Advances in three-dimensional conformal radiation therapy physics with intensity modulation. Lancet Oncol 2000;1:30-36.

[16] Brahme A. Design principles and clinical possibilities with a new generation of radiation therapy equipment. A review. Acta Oncol 1987;26:403-412.

[17] Webb S. The physical basis of IMRT and inverse planning. Br J Radiol 2003;76:678-689.

[18] Chao K S AS, Ozyigit G. Practical essentials of intensity modulated radiation therapy: Lippincott Willians & Wilkins, 2004.

[19] Brahme A, Roos JE Lax I. Solution of an integral equation encountered in rotation therapy. Phys Med Biol 1982;27:1221-1229.

[20] Galvin JM, Ezzell G, Eisbrauch A, et al. Implementing IMRT in clinical practice: a joint document of the American Society for Therapeutic Radiology and Oncology and the American Association of Physicists in Medicine. Int J Radiat Oncol Biol Phys 2004;58:1616-1634.

[21] Guerrero Urbano MT Nutting CM. Clinical use of intensity-modulated radiotherapy: part II. Br J Radiol 2004;77:177-182.

[22] Guerrero Urbano MT Nutting CM. Clinical use of intensity-modulated radiotherapy: part I. Br J Radiol 2004;77:88-96.

[23] Veldeman L, Madani I, Hulstaert F, De Meerleer G, Mareel M De Neve W. Evidence behind use of intensity-modulated radiotherapy: a systematic review of comparative clinical studies. Lancet Oncol 2008;9:367-375.

[24] Bhide SA, Newbold KL, Harrington KJ Nutting CM. Clinical evaluation of intensity-modulated radiotherapy for head and neck cancers. Br J Radiol 2012;85:487-494.

[25] Zheng BM, Dong XX, Wu H, Han SK Sun Y. Dosimetry Comparison between Volumetric Modulated Arc Therapy with Rapid Arcand Fixed Field Dynamic IMRT for Local-Regionally Advanced Nasopharyngeal Carcinoma. Chin J Cancer Res 2011;23:259-264.

[26] Nutting CM, Convery DJ, Cosgrove VP, et al. Reduction of small and large bowel irradiation using an optimized intensity-modulated pelvic radiotherapy technique in patients with prostate cancer. Int J Radiat Oncol Biol Phys 2000;48:649-656.

[27] Nutting CM, Morden JP, Harrington KJ, et al. Parotid-sparing intensity modulated versus conventional radiotherapy in head and neck cancer (PARSPORT): a phase 3 multicentre randomised controlled trial. Lancet Oncol 2011;12:127-136.

[28] Webb S. Advances in treatment with intensity-modulated conformal radiotherapy. Tumori 1998;84:112-126.

[29] Svensson R, Lind B Brahme A. Beam characteristics and clinical possibilities of a new compact treatment unit design combining narrow pencil beam scanning and segmental multileaf collimation. Med Phys 1998;25:2358-2369.

[30] Karlsson MG, Karlsson M Zackrisson B. Intensity modulation with electrons: calculations, measurements and clinical applications. Phys Med Biol 1998;43:1159-1169.

[31] Lief EP, Lo YC Humm JL. Electron wedges for radiation therapy. Int J Radiat Oncol Biol Phys 1998;40:233-243.

[32] Lief EP, Larsson A Humm JL. Electron dose profile shaping by modulation of a scanning elementary beam. Med Phys 1996;23:33-44.

[33] Svensson R, Larsson S, Gudowska I, Holmberg R Brahme A. Design of a fast multileaf collimator for radiobiological optimized IMRT with scanned beams of photons, electrons, and light ions. Med Phys 2007;34:877-888.

[34] Wysocka-Rabin A M HGH. Monte Carlo study on a new concept of a scanning photon beam system for IMRT. Nukleonika 2011;56:291-297.

[35] Andreassen B, Straat SJ, Holmberg R, Nafstadius P Brahme A. Fast IMRT with narrow high energy scanned photon beams. Med Phys 2011;38:4774-4784.

[36] Ling CC, Burman C, Chui CS, et al. Conformal radiation treatment of prostate cancer using inversely-planned intensity-modulated photon beams produced with dynamic multileaf collimation. Int J Radiat Oncol Biol Phys 1996;35:721-730.

[37] Spirou SV Chui CS. Generation of arbitrary intensity profiles by dynamic jaws or multileaf collimators. Med Phys 1994;21:1031-1041.

[38] Chui CS, Chan MF, Yorke E, Spirou S Ling CC. Delivery of intensity-modulated radiation therapy with a conventional multileaf collimator: comparison of dynamic and segmental methods. Med Phys 2001;28:2441-2449.

[39] Alaei P, Higgins PD, Weaver R Nguyen N. Comparison of dynamic and step-and-shoot intensity-modulated radiation therapy planning and delivery. Med Dosim 2004;29:1-6.

[40] LoSasso T, Chui CS Ling CC. Physical and dosimetric aspects of a multileaf collimation system used in the dynamic mode for implementing intensity modulated radiotherapy. Med Phys 1998;25:1919-1927.

[41] Salari E, Men C Romeijn HE. Accounting for the tongue-and-groove effect using a robust direct aperture optimization approach. Med Phys 2011;38:1266-1279.

[42] Agazaryan N Solberg TD. Segmental and dynamic intensity-modulated radiotherapy delivery techniques for micro-multileaf collimator. Med Phys 2003;30:1758-1767.

[43] van Santvoort JP Heijmen BJ. Dynamic multileaf collimation without 'tongue-and-groove' underdosage effects. Phys Med Biol 1996;41:2091-2105.

[44] Mackie TR, Holmes T, Swerdloff S, et al. Tomotherapy: a new concept for the delivery of dynamic conformal radiotherapy. Med Phys 1993;20:1709-1719.

[45] Mackie TR, Balog J, Ruchala K, et al. Tomotherapy. Semin Radiat Oncol 1999;9:108-117.

[46] Carol M, Grant WH, 3rd, Pavord D, et al. Initial clinical experience with the Peacock intensity modulation of a 3-D conformal radiation therapy system. Stereotact Funct Neurosurg 1996;66:30-34.

[47] Khoo VS, Oldham M, Adams EJ, Bedford JL, Webb S Brada M. Comparison of intensity-modulated tomotherapy with stereotactically guided conformal radiotherapy for brain tumors. Int J Radiat Oncol Biol Phys 1999;45:415-425.

[48] Chao KS, Low DA, Perez CA Purdy JA. Intensity-modulated radiation therapy in head and neck cancers: The Mallinckrodt experience. Int J Cancer 2000;90:92-103.

[49] Low DA Mutic S. Abutment region dosimetry for sequential arc IMRT delivery. Phys Med Biol 1997;42:1465-1470.

[50] Carol M, Grant WH, 3rd, Bleier AR, et al. The field-matching problem as it applies to the peacock three dimensional conformal system for intensity modulation. Int J Radiat Oncol Biol Phys 1996;34:183-187.

[51] Low DA, Mutic S, Dempsey JF, Markman J, Chao KS Purdy JA. Abutment dosimetry for serial tomotherapy. Med Dosim 2001;26:79-82.

[52] Low DA, Mutic S, Dempsey JF, Markman J, Goddu SM Purdy JA. Abutment region dosimetry for serial tomotherapy. Int J Radiat Oncol Biol Phys 1999;45:193-203.

[53] Teh BS, Woo SY Butler EB. Intensity modulated radiation therapy (IMRT): a new promising technology in radiation oncology. Oncologist 1999;4:433-442.

[54] Yu CX. Intensity-modulated arc therapy with dynamic multileaf collimation: an alternative to tomotherapy. Phys Med Biol 1995;40:1435-1449.

[55] Yu CX, Symons MJ, Du MN, Martinez AA Wong JW. A method for implementing dynamic photon beam intensity modulation using independent jaws and a multileaf collimator. Phys Med Biol 1995;40:769-787.

[56] Earl MA, Shepard DM, Naqvi S, Li XA Yu CX. Inverse planning for intensity-modulated arc therapy using direct aperture optimization. Phys Med Biol 2003;48:1075-1089.

[57] Shepard DM, Cao D, Afghan MK Earl MA. An arc-sequencing algorithm for intensity modulated arc therapy. Med Phys 2007;34:464-470.

[58] Yu CX, Li XA, Ma L, et al. Clinical implementation of intensity-modulated arc therapy. Int J Radiat Oncol Biol Phys 2002;53:453-463.

[59] Otto K. Volumetric modulated arc therapy: IMRT in a single gantry arc. Med Phys 2008;35:310-317.

[60] Yoo S, Wu QJ, Lee WR Yin FF. Radiotherapy treatment plans with RapidArc for prostate cancer involving seminal vesicles and lymph nodes. Int J Radiat Oncol Biol Phys 2010;76:935-942.

[61] Amendola BE, Amendola M, Perez N, Iglesias A Wu X. Volumetric-modulated arc therapy with RapidArc: An evaluation of treatment delivery efficiency. Rep Pract Oncol Radiother 2013;18:383-386.

[62] Amendola BE, Amendola, M., Perez N, Isglesias A, Axenfeld, E. Volumetric Modulated Arc Therapy (VMAT) Reduces Treatment Time Compared to Conventional Intensity Modulated Radiation Treatment (IMRT) of Thoracic Tumors. Journal of Thoracic Oncology 2010;7:s264.

[63] Shaffer R, Nichol AM, Vollans E, et al. A comparison of volumetric modulated arc therapy and conventional intensity-modulated radiotherapy for frontal and temporal high-grade gliomas. Int J Radiat Oncol Biol Phys 2010;76:1177-1184.

[64] Teoh M, Clark CH, Wood K, Whitaker S Nisbet A. Volumetric modulated arc therapy: a review of current literature and clinical use in practice. Br J Radiol 2011;84:967-996.

[65] Fenwick JD, Tome WA, Soisson ET, Mehta MP Rock Mackie T. Tomotherapy and other innovative IMRT delivery systems. Semin Radiat Oncol 2006;16:199-208.

[66] Palma DA, Verbakel WF, Otto K Senan S. New developments in arc radiation therapy: a review. Cancer Treat Rev 2010;36:393-399.

[67] Leksell DG. Stereotactic radiosurgery. Present status and future trends. Neurol Res 1987;9:60-68.

[68] Goodman ML. Gamma knife radiosurgery: current status and review. South Med J 1990;83:551-554.

[69] Webb S. Conformal intensity-modulated radiotherapy (IMRT) delivered by robotic linac--conformality versus efficiency of dose delivery. Phys Med Biol 2000;45:1715-1730.

[70] Webb S. Conformal intensity-modulated radiotherapy (IMRT) delivered by robotic linac--testing IMRT to the limit? Phys Med Biol 1999;44:1639-1654.

[71] Kuo JS, Yu C, Petrovich Z Apuzzo ML. The CyberKnife stereotactic radiosurgery system: description, installation, and an initial evaluation of use and functionality. Neurosurgery 2003;53:1235-1239; discussion 1239.

[72] Staffurth J. A review of the clinical evidence for intensity-modulated radiotherapy. Clin Oncol (R Coll Radiol) 2010;22:643-657.

[73] Miah AB, Bhide SA, Guerrero-Urbano MT, et al. Dose-escalated intensity-modulated radiotherapy is feasible and may improve locoregional control and laryngeal preservation in laryngo-hypopharyngeal cancers. Int J Radiat Oncol Biol Phys 2012;82:539-547.

[74] Guerrero Urbano T, Khoo V, Staffurth J, et al. Intensity-modulated radiotherapy allows escalation of the radiation dose to the pelvic lymph nodes in patients with locally advanced prostate cancer: preliminary results of a phase I dose escalation study. Clin Oncol (R Coll Radiol) 2010;22:236-244.

[75] Bourhis J, Overgaard J, Audry H, et al. Hyperfractionated or accelerated radiotherapy in head and neck cancer: a meta-analysis. Lancet 2006;368:843-854.

[76] Overgaard J, Hansen HS, Specht L, et al. Five compared with six fractions per week of conventional radiotherapy of squamous-cell carcinoma of head and neck: DAHANCA 6 and 7 randomised controlled trial. Lancet 2003;362:933-940.

[77] Overgaard J, Alsner J, Eriksen J, Horsman MR Grau C. Importance of overall treatment time for the response to radiotherapy in patients with squamous cell carcinoma of the head and neck. Rays 2000;25:313-319.

[78] Butler EB, Teh BS, Grant WH, 3rd, et al. Smart (simultaneous modulated accelerated radiation therapy) boost: a new accelerated fractionation schedule for

the treatment of head and neck cancer with intensity modulated radiotherapy. Int J Radiat Oncol Biol Phys 1999;45:21-32.

[79] Wu Q, Mohan R, Morris M, Lauve A Schmidt-Ullrich R. Simultaneous integrated boost intensity-modulated radiotherapy for locally advanced head-and-neck squamous cell carcinomas. I: dosimetric results. Int J Radiat Oncol Biol Phys 2003;56:573-585.

[80] Lauve A, Morris M, Schmidt-Ullrich R, et al. Simultaneous integrated boost intensity-modulated radiotherapy for locally advanced head-and-neck squamous cell carcinomas: II--clinical results. Int J Radiat Oncol Biol Phys 2004;60:374-387.

[81] Mohan R, Wu Q, Manning M Schmidt-Ullrich R. Radiobiological considerations in the design of fractionation strategies for intensity-modulated radiation therapy of head and neck cancers. Int J Radiat Oncol Biol Phys 2000;46:619-630.

[82] Withers HR, Taylor JM Maciejewski B. The hazard of accelerated tumor clonogen repopulation during radiotherapy. Acta Oncol 1988;27:131-146.

[83] Jones B, Tan LT Dale RG. Derivation of the optimum dose per fraction from the linear quadratic model. Br J Radiol 1995;68:894-902.

[84] Fowler JF. Is there an optimum overall time for head and neck radiotherapy? A review, with new modelling. Clin Oncol (R Coll Radiol) 2007;19:8-22.

[85] Tarnawski R, Fowler J, Skladowski K, et al. How fast is repopulation of tumor cells during the treatment gap? Int J Radiat Oncol Biol Phys 2002;54:229-236.

[86] Pickett B, Vigneault E, Kurhanewicz J, Verhey L Roach M. Static field intensity modulation to treat a dominant intra-prostatic lesion to 90 Gy compared to seven field 3-dimensional radiotherapy. Int J Radiat Oncol Biol Phys 1999;44:921-929.

[87] Cannon DM Lee NY. Recurrence in region of spared parotid gland after definitive intensity-modulated radiotherapy for head and neck cancer. Int J Radiat Oncol Biol Phys 2008;70:660-665.

[88] Verellen D, Linthout N, van den Berge D, Bel A Storme G. Initial experience with intensity-modulated conformal radiation therapy for treatment of the head and neck region. Int J Radiat Oncol Biol Phys 1997;39:99-114.

[89] Rosenberg I, Alheit H, Beardmore C, Lee KS, Warrington AP Brada M. Patient position reproducibility in fractionated stereotactic radiotherapy: an update after changing dental impression material. Radiother Oncol 1999;50:239-240.

[90] Burton KE, Thomas SJ, Whitney D, Routsis DS, Benson RJ Burnet NG. Accuracy of a relocatable stereotactic radiotherapy head frame evaluated by use of a depth helmet. Clin Oncol (R Coll Radiol) 2002;14:31-39.

[91] van Herk M, Bruce A, Kroes AP, Shouman T, Touw A Lebesque JV. Quantification of organ motion during conformal radiotherapy of the prostate by three dimensional image registration. Int J Radiat Oncol Biol Phys 1995;33:1311-1320.

[92] Padhani AR, Khoo VS, Suckling J, Husband JE, Leach MO Dearnaley DP. Evaluating the effect of rectal distension and rectal movement on prostate gland position using cine MRI. Int J Radiat Oncol Biol Phys 1999;44:525-533.

[93] Roeske JC, Forman JD, Mesina CF, et al. Evaluation of changes in the size and location of the prostate, seminal vesicles, bladder, and rectum during a course of external beam radiation therapy. Int J Radiat Oncol Biol Phys 1995;33:1321-1329.

[94] Ma Y, Chang D, Keall P, et al. Inverse planning for four-dimensional (4D) volumetric modulated arc therapy. Med Phys 2010;37:5627-5633.

[95] Kim DJ, Murray BR, Halperin R Roa WH. Held-breath self-gating technique for radiotherapy of non-small-cell lung cancer: a feasibility study. Int J Radiat Oncol Biol Phys 2001;49:43-49.

[96] Brock J, McNair HA, Panakis N, Symonds-Tayler R, Evans PM Brada M. The use of the Active Breathing Coordinator throughout radical non-small-cell lung cancer (NSCLC) radiotherapy. Int J Radiat Oncol Biol Phys 2011;81:369-375.

[97] McNair HA, Brock J, Symonds-Tayler JR, et al. Feasibility of the use of the Active Breathing Co ordinator (ABC) in patients receiving radical radiotherapy for non-small cell lung cancer (NSCLC). Radiother Oncol 2009;93:424-429.

[98] Wong VY, Tung SY, Ng AW, Li FA Leung JO. Real-time monitoring and control on deep inspiration breath-hold for lung cancer radiotherapy--combination of ABC and external marker tracking. Med Phys 2010;37:4673-4683.

[99] Suh Y, Sawant A, Venkat R Keall PJ. Four-dimensional IMRT treatment planning using a DMLC motion-tracking algorithm. Phys Med Biol 2009;54:3821-3835.

[100] Zelefsky MJ, Kollmeier M, Cox B, et al. Improved clinical outcomes with high-dose image guided radiotherapy compared with non-IGRT for the treatment of clinically localized prostate cancer. Int J Radiat Oncol Biol Phys 2012;84:125-129.

[101] Kirova YM, Castro Pena P, Hijal T, et al. Improving the definition of tumor bed boost with the use of surgical clips and image registration in breast cancer patients. Int J Radiat Oncol Biol Phys 2010;78:1352-1355.

[102] Kirby AN, Jena R, Harris EJ, et al. Tumour bed delineation for partial breast/breast boost radiotherapy: what is the optimal number of implanted markers? Radiother Oncol 2013;106:231-235.

[103] Verellen D, Depuydt T, Gevaert T, et al. Gating and tracking, 4D in thoracic tumours. Cancer Radiother 2010;14:446-454.

[104] Verellen D, De Ridder M Storme G. A (short) history of image-guided radiotherapy. Radiother Oncol 2008;86:4-13.

[105] ICRU, International Commission on Radiation Units and Measurements. Dose specification for reporting external beam therapy with photons and electrons. ICRU Report 29. International Commission on Radiation Units and Measurements, 1978.

[106] ICRU, International Commission on Radiation Units and Measurements. Prescribing, recording and reporting photon beam therapy. ICRU Report 50, 1993.

[107] ICRU, International Commission on Radiation Units and Measurements. Prescribing, recording and reporting photon beam therapy (Supplement to ICRU Report 50). ICRU Report 62. Oxford University Press, 1999.

[108] ICRU, International Commission on Radiation Units and Measurements. Prescribing, recording and reporting electron beam therapy. ICRU Report 71. J ICRU, 2004.

[109] ICRU, International Commission on Radiation Units and Measurments. Prescrbing, recording and reporting proton-beam therapy. ICRU Report 78. J ICRU, 2007.

[110] ICRU. International Commission on Radiation Units and Measurments. Prescrbing, recording and reporting photon-beam intensity-modulated radiation therapy (IMRT). ICRU Report 83. J ICRU 2010;10:1-106.

[111] Weiss E Hess CF. The impact of gross tumor volume (GTV) and clinical target volume (CTV) definition on the total accuracy in radiotherapy theoretical aspects and practical experiences. Strahlenther Onkol 2003;179:21-30.

[112] Seddon B, Bidmead M, Wilson J, Khoo V Dearnaley D. Target volume definition in conformal radiotherapy for prostate cancer: quality assurance in the MRC RT-01 trial. Radiother Oncol 2000;56:73-83.

[113] McNair HA, Adams EJ, Clark CH, Miles EA Nutting CM. Implementation of IMRT in the radiotherapy department. Br J Radiol 2003;76:850-856.

[114] Rothschild S, Studer G, Seifert B, et al. PET/CT staging followed by Intensity-Modulated Radiotherapy (IMRT) improves treatment outcome of locally advanced pharyngeal carcinoma: a matched-pair comparison. Radiat Oncol 2007;2:22.

[115] BIR, Geometric Uncertainties in Radiotherapy-Defining the Planning Target Volume. British Institute of Radiology, 2003.

[116] Gulliford SL, Miah AB, Brennan S, et al. Dosimetric explanations of fatigue in head and neck radiotherapy: an analysis from the PARSPORT Phase III trial. Radiother Oncol 2012;104:205-212.

[117] Oldham M, Neal A Webb S. A comparison of conventional 'forward planning' with inverse planning for 3D conformal radiotherapy of the prostate. Radiother Oncol 1995;35:248-262.

[118] Fraass BA, Kessler ML, McShan DL, et al. Optimization and clinical use of multisegment intensity-modulated radiation therapy for high-dose conformal therapy. Semin Radiat Oncol 1999;9:60-77.

[119] Xiao Y, Galvin J, Hossain M Valicenti R. An optimized forward-planning technique for intensity modulated radiation therapy. Med Phys 2000;27:2093-2099.

[120] Shepard DM, Earl MA, Li XA, Naqvi S Yu C. Direct aperture optimization: a turnkey solution for step-and-shoot IMRT. Med Phys 2002;29:1007-1018.

[121] Eisbruch A, Ship JA, Martel MK, et al. Parotid gland sparing in patients undergoing bilateral head and neck irradiation: techniques and early results. Int J Radiat Oncol Biol Phys 1996;36:469-480.

[122] Vicini FA, Sharpe M, Kestin L, et al. Optimizing breast cancer treatment efficacy with intensity-modulated radiotherapy. Int J Radiat Oncol Biol Phys 2002;54:1336-1344.

[123] Chao K S MR, Lee N A, Chronowski G, Low D, Wu Q, Dong L. Intensity-modulated radiation treatment techniques and clinical applications. In: E Halperi CAP, L W Brady, ed. Perez and Brady's principles and pratice of radiation oncology, ed. 5th. Philadelphia: Lippincott Willians & Wilkins, 2008; 239-263.

[124] Emami B, Lyman J, Brown A, et al. Tolerance of normal tissue to therapeutic irradiation. Int J Radiat Oncol Biol Phys 1991;21:109-122.

[125] Marks LB, Yorke ED, Jackson A, et al. Use of normal tissue complication probability models in the clinic. Int J Radiat Oncol Biol Phys 2010;76:S10-19.

[126] Paddick I. A simple scoring ratio to index the conformity of radiosurgical treatment plans. Technical note. J Neurosurg 2000;93 Suppl 3:219-222.

[127] Low DA, Harms WB, Mutic S Purdy JA. A technique for the quantitative evaluation of dose distributions. Med Phys 1998;25:656-661.

[128] Williams PC. IMRT: delivery techniques and quality assurance. Br J Radiol 2003;76:766-776.

[129] Shu HK, Lee TT, Vigneauly E, et al. Toxicity following high-dose three-dimensional conformal and intensity-modulated radiation therapy for clinically localized prostate cancer. Urology 2001;57:102-107.

[130] Cardinale RM, Benedict SH, Wu Q, Zwicker RD, Gaballa HE Mohan R. A comparison of three stereotactic radiotherapy techniques; ARCS vs. noncoplanar fixed fields vs. intensity modulation. Int J Radiat Oncol Biol Phys 1998;42:431-436.

[131] Verellen D, Linthout N Storme G. Target localization and treatment verification for intensity modulated conformal radiation therapy of the head and neck region. The AZ-VUB experience. Akademisch Ziekenhuis-Vrije Universiteit Brussel. Strahlenther Onkol 1998;174 Suppl 2:19-27.

[132] Low DA, Chao KS, Mutic S, Gerber RL, Perez CA Purdy JA. Quality assurance of serial tomotherapy for head and neck patient treatments. Int J Radiat Oncol Biol Phys 1998;42:681-692.

[133] Burman C, Chui CS, Kutcher G, et al. Planning, delivery, and quality assurance of intensity-modulated radiotherapy using dynamic multileaf collimator: a strategy for large-scale implementation for the treatment of carcinoma of the prostate. Int J Radiat Oncol Biol Phys 1997;39:863-873.

[134] Alicikus ZA, Yamada Y, Zhang Z, et al. Ten-year outcomes of high-dose, intensity-modulated radiotherapy for localized prostate cancer. Cancer 2011;117:1429-1437.

[135] Spratt DE, Pei X, Yamada J, Kollmeier MA, Cox B Zelefsky MJ. Long-term survival and toxicity in patients treated with high-dose intensity modulated radiation therapy for localized prostate cancer. Int J Radiat Oncol Biol Phys 2013;85:686-692.

[136] Zelefsky MJ, Chan H, Hunt M, Yamada Y, Shippy AM Amols H. Long-term outcome of high dose intensity modulated radiation therapy for patients with clinically localized prostate cancer. J Urol 2006;176:1415-1419.

[137] Zelefsky MJ, Levin EJ, Hunt M, et al. Incidence of late rectal and urinary toxicities after three-dimensional conformal radiotherapy and intensity-modulated radiotherapy for localized prostate cancer. Int J Radiat Oncol Biol Phys 2008;70:1124-1129.

[138] Zelefsky MJ, Yamada Y, Fuks Z, et al. Long-term results of conformal radiotherapy for prostate cancer: impact of dose escalation on biochemical tumor control and

distant metastases-free survival outcomes. Int J Radiat Oncol Biol Phys 2008;71:1028-1033.

[139] Kupelian PA, Reddy CA, Carlson TP, Altsman KA Willoughby TR. Preliminary observations on biochemical relapse-free survival rates after short-course intensity-modulated radiotherapy (70 Gy at 2.5 Gy/fraction) for localized prostate cancer. Int J Radiat Oncol Biol Phys 2002;53:904-912.

[140] Lambrecht M, Nevens D Nuyts S. Intensity-modulated radiotherapy vs. parotid-sparing 3D conformal radiotherapy. Effect on outcome and toxicity in locally advanced head and neck cancer. Strahlenther Onkol 2013;189:223-229.

[141] Lee NY, de Arruda FF, Puri DR, et al. A comparison of intensity-modulated radiation therapy and concomitant boost radiotherapy in the setting of concurrent chemotherapy for locally advanced oropharyngeal carcinoma. Int J Radiat Oncol Biol Phys 2006;66:966-974.

[142] Fuller CD, Choi M, Forthuber B, et al. Standard fractionation intensity modulated radiation therapy (IMRT) of primary and recurrent glioblastoma multiforme. Radiat Oncol 2007;2:26.

[143] Iuchi T, Hatano K, Narita Y, Kodama T, Yamaki T Osato K. Hypofractionated high-dose irradiation for the treatment of malignant astrocytomas using simultaneous integrated boost technique by IMRT. Int J Radiat Oncol Biol Phys 2006;64:1317-1324.

[144] Milker-Zabel S, Zabel A, Thilmann C, Schlegel W, Wannenmacher M Debus J. Clinical results of retreatment of vertebral bone metastases by stereotactic conformal radiotherapy and intensity-modulated radiotherapy. Int J Radiat Oncol Biol Phys 2003;55:162-167.

[145] Kuo JV, Cabebe E, Al-Ghazi M, Yakoob I, Ramsinghani NS Sanford R. Intensity-modulated radiation therapy for the spine at the University of California, Irvine. Med Dosim 2002;27:137-145.

[146] Thilmann C, Schulz-Ertner D, Zabel A, Herfarth KK, Wannenmacher M Debus J. Intensity-modulated radiotherapy of sacral chordoma--a case report and a comparison with stereotactic conformal radiotherapy. Acta Oncol 2002;41:395-399.

[147] Hall EJ Wuu CS. Radiation-induced second cancers: the impact of 3D-CRT and IMRT. Int J Radiat Oncol Biol Phys 2003;56:83-88.

[148] Kry SF, Salehpour M, Followill DS, et al. The calculated risk of fatal secondary malignancies from intensity-modulated radiation therapy. Int J Radiat Oncol Biol Phys 2005;62:1195-1203.

[149] Huang E, Teh BS, Strother DR, et al. Intensity-modulated radiation therapy for pediatric medulloblastoma: early report on the reduction of ototoxicity. Int J Radiat Oncol Biol Phys 2002;52:599-605.

[150] Claus EB, Bondy ML, Schildkraut JM, Wiemels JL, Wrensch M Black PM. Epidemiology of intracranial meningioma. Neurosurgery 2005;57:1088-1095; discussion 1088-1095.

[151] Whittle IR, Smith C, Navoo P Collie D. Meningiomas. Lancet 2004;363:1535-1543.

[152] Walcott BP, Nahed BV, Brastianos PK Loeffler JS. Radiation Treatment for WHO Grade II and III Meningiomas. Front Oncol 2013;3:227.

[153] Campbell BA, Jhamb A, Maguire JA, Toyota B Ma R. Meningiomas in 2009: controversies and future challenges. Am J Clin Oncol 2009;32:73-85.

[154] Wiemels J, Wrensch M Claus EB. Epidemiology and etiology of meningioma. J Neurooncol 2010;99:307-314.

[155] Mawrin C Perry A. Pathological classification and molecular genetics of meningiomas. J Neurooncol 2010;99:379-391.

[156] Louis DN, Ohgaki H, Wiestler OD, et al. The 2007 WHO classification of tumours of the central nervous system. Acta Neuropathol 2007;114:97-109.

[157] Perry A, Gutmann DH Reifenberger G. Molecular pathogenesis of meningiomas. J Neurooncol 2004;70:183-202.

[158] Pasquier D, Bijmolt S, Veninga T, et al. Atypical and malignant meningioma: outcome and prognostic factors in 119 irradiated patients. A multicenter, retrospective study of the Rare Cancer Network. Int J Radiat Oncol Biol Phys 2008;71:1388-1393.

[159] Yang SY, Park CK, Park SH, Kim DG, Chung YS Jung HW. Atypical and anaplastic meningiomas: prognostic implications of clinicopathological features. J Neurol Neurosurg Psychiatry 2008;79:574-580.

[160] Perry A, Scheithauer BW, Stafford SL, Lohse CM Wollan PC. "Malignancy" in meningiomas: a clinicopathologic study of 116 patients, with grading implications. Cancer 1999;85:2046-2056.

[161] Riemenschneider MJ, Perry A Reifenberger G. Histological classification and molecular genetics of meningiomas. Lancet Neurol 2006;5:1045-1054.

[162] Rogers L, Gilbert M Vogelbaum MA. Intracranial meningiomas of atypical (WHO grade II) histology. J Neurooncol 2010;99:393-405.

[163] Gabeau-Lacet D, Aghi M, Betensky RA, Barker FG, Loeffler JS Louis DN. Bone involvement predicts poor outcome in atypical meningioma. J Neurosurg 2009;111:464-471.

[164] Lee Y, Liu J, Patel S, et al. Genomic landscape of meningiomas. Brain Pathol 2010;20:751-762.

[165] Oya S, Kawai K, Nakatomi H Saito N. Significance of Simpson grading system in modern meningioma surgery: integration of the grade with MIB-1 labeling index as a key to predict the recurrence of WHO Grade I meningiomas. J Neurosurg 2012;117:121-128.

[166] Rubin G, Herscovici Z, Laviv Y, Jackson S Rappaport ZH. Outcome of untreated meningiomas. Isr Med Assoc J 2011;13:157-160.

[167] Herscovici Z, Rappaport Z, Sulkes J, Danaila L Rubin G. Natural history of conservatively treated meningiomas. Neurology 2004;63:1133-1134.

[168] Simpson D. The recurrence of intracranial meningiomas after surgical treatment. J Neurol Neurosurg Psychiatry 1957;20:22-39.

[169] Mirimanoff RO, Dosoretz DE, Linggood RM, Ojemann RG Martuza RL. Meningioma: analysis of recurrence and progression following neurosurgical resection. J Neurosurg 1985;62:18-24.

[170] Cusimano MD, Sekhar LN, Sen CN, et al. The results of surgery for benign tumors of the cavernous sinus. Neurosurgery 1995;37:1-9; discussion 9-10.

[171] Goldsmith B McDermott MW. Meningioma. Neurosurg Clin N Am 2006;17:111-120, vi.

[172] Minniti G, Amichetti M Enrici RM. Radiotherapy and radiosurgery for benign skull base meningiomas. Radiat Oncol 2009;4:42.

[173] Glaholm J, Bloom HJ Crow JH. The role of radiotherapy in the management of intracranial meningiomas: the Royal Marsden Hospital experience with 186 patients. Int J Radiat Oncol Biol Phys 1990;18:755-761.

[174] Mendenhall WM, Morris CG, Amdur RJ, Foote KD Friedman WA. Radiotherapy alone or after subtotal resection for benign skull base meningiomas. Cancer 2003;98:1473-1482.

[175] Marta GN, Correa SF Teixeira MJ. Meningioma: review of the literature with emphasis on the approach to radiotherapy. Expert Rev Anticancer Ther 2011;11:1749-1758.

[176] Rogers L Mehta M. Role of radiation therapy in treating intracranial meningiomas. Neurosurg Focus 2007;23:E4.

[177] Gondi V, Tome WA Mehta MP. Fractionated radiotherapy for intracranial meningiomas. J Neurooncol 2010;99:349-356.

[178] Pollock BE, Stafford SL, Utter A, Giannini C Schreiner SA. Stereotactic radiosurgery provides equivalent tumor control to Simpson Grade 1 resection for patients with small- to medium-size meningiomas. Int J Radiat Oncol Biol Phys 2003;55:1000-1005.

[179] Santacroce A, Walier M, Regis J, et al. Long-term tumor control of benign intracranial meningiomas after radiosurgery in a series of 4565 patients. Neurosurgery 2012;70:32-39; discussion 39.

[180] Bloch O, Kaur G, Jian BJ, Parsa AT Barani IJ. Stereotactic radiosurgery for benign meningiomas. J Neurooncol 2012;107:13-20.

[181] Lee JY, Niranjan A, McInerney J, Kondziolka D, Flickinger JC Lunsford LD. Stereotactic radiosurgery providing long-term tumor control of cavernous sinus meningiomas. J Neurosurg 2002;97:65-72.

[182] Kondziolka D, Mathieu D, Lunsford LD, et al. Radiosurgery as definitive management of intracranial meningiomas. Neurosurgery 2008;62:53-58; discussion 58-60.

[183] Sheehan JP, Williams BJ Yen CP. Stereotactic radiosurgery for WHO grade I meningiomas. J Neurooncol 2010;99:407-416.

[184] Debus J, Wuendrich M, Pirzkall A, et al. High efficacy of fractionated stereotactic radiotherapy of large base-of-skull meningiomas: long-term results. J Clin Oncol 2001;19:3547-3553.

[185] Milker-Zabel S, Zabel-du Bois A, Huber P, Schlegel W Debus J. Fractionated stereotactic radiation therapy in the management of benign cavernous sinus meningiomas : long-term experience and review of the literature. Strahlenther Onkol 2006;182:635-640.

[186] Milker-Zabel S, Zabel A, Schulz-Ertner D, Schlegel W, Wannenmacher M Debus J. Fractionated stereotactic radiotherapy in patients with benign or atypical

intracranial meningioma: long-term experience and prognostic factors. Int J Radiat Oncol Biol Phys 2005;61:809-816.

[187] Milker-Zabel S, Huber P, Schlegel W, Debus J Zabel-du Bois A. Fractionated stereotactic radiation therapy in the management of primary optic nerve sheath meningiomas. J Neurooncol 2009;94:419-424.

[188] Turbin RE, Thompson CR, Kennerdell JS, Cockerham KP Kupersmith MJ. A long-term visual outcome comparison in patients with optic nerve sheath meningioma managed with observation, surgery, radiotherapy, or surgery and radiotherapy. Ophthalmology 2002;109:890-899; discussion 899-900.

[189] Henzel M, Gross MW, Hamm K, et al. Stereotactic radiotherapy of meningiomas: symptomatology, acute and late toxicity. Strahlenther Onkol 2006;182:382-388.

[190] Landert M, Baumert BG, Bosch MM, Lutolf UM Landau K. The visual impact of fractionated stereotactic conformal radiotherapy on seven eyes with optic nerve sheath meningiomas. J Neuroophthalmol 2005;25:86-91.

[191] Baumert BG, Villa S, Studer G, et al. Early improvements in vision after fractionated stereotactic radiotherapy for primary optic nerve sheath meningioma. Radiother Oncol 2004;72:169-174.

[192] Hug EB, Devries A, Thornton AF, et al. Management of atypical and malignant meningiomas: role of high-dose, 3D-conformal radiation therapy. J Neurooncol 2000;48:151-160.

[193] Milosevic MF, Frost PJ, Laperriere NJ, Wong CS Simpson WJ. Radiotherapy for atypical or malignant intracranial meningioma. Int J Radiat Oncol Biol Phys 1996;34:817-822.

[194] Hanft S, Canoll P Bruce JN. A review of malignant meningiomas: diagnosis, characteristics, and treatment. J Neurooncol 2010;99:433-443.

[195] Aghi MK, Carter BS, Cosgrove GR, et al. Long-term recurrence rates of atypical meningiomas after gross total resection with or without postoperative adjuvant radiation. Neurosurgery 2009;64:56-60; discussion 60.

[196] Rosenberg LA, Prayson RA, Lee J, et al. Long-term experience with World Health Organization grade III (malignant) meningiomas at a single institution. Int J Radiat Oncol Biol Phys 2009;74:427-432.

[197] Palma L, Celli P, Franco C, Cervoni L Cantore G. Long-term prognosis for atypical and malignant meningiomas: a study of 71 surgical cases. Neurosurg Focus 1997;2:e3.

[198] Palma L, Celli P, Franco C, Cervoni L Cantore G. Long-term prognosis for atypical and malignant meningiomas: a study of 71 surgical cases. J Neurosurg 1997;86:793-800.

[199] Sughrue ME, Sanai N, Shangari G, Parsa AT, Berger MS McDermott MW. Outcome and survival following primary and repeat surgery for World Health Organization Grade III meningiomas. J Neurosurg 2010;113:202-209.

[200] Dziuk TW, Woo S, Butler EB, et al. Malignant meningioma: an indication for initial aggressive surgery and adjuvant radiotherapy. J Neurooncol 1998;37:177-188.

[201] Pirzkall A, Debus J, Haering P, et al. Intensity modulated radiotherapy (IMRT) for recurrent, residual, or untreated skull-base meningiomas: preliminary clinical experience. Int J Radiat Oncol Biol Phys 2003;55:362-372.

[202] Simon M, Bostrom J, Koch P Schramm J. Interinstitutional variance of postoperative radiotherapy and follow up for meningiomas in Germany: impact of changes of the WHO classification. J Neurol Neurosurg Psychiatry 2006;77:767-773.

[203] Stafford SL, Perry A, Suman VJ, et al. Primarily resected meningiomas: outcome and prognostic factors in 581 Mayo Clinic patients, 1978 through 1988. Mayo Clin Proc 1998;73:936-942.

[204] Goldsmith BJ, Wara WM, Wilson CB Larson DA. Postoperative irradiation for subtotally resected meningiomas. A retrospective analysis of 140 patients treated from 1967 to 1990. J Neurosurg 1994;80:195-201.

[205] Soyuer S, Chang EL, Selek U, Shi W, Maor MH DeMonte F. Radiotherapy after surgery for benign cerebral meningioma. Radiother Oncol 2004;71:85-90.

[206] Miralbell R, Linggood RM, de la Monte S, Convery K, Munzenrider JE Mirimanoff RO. The role of radiotherapy in the treatment of subtotally resected benign meningiomas. J Neurooncol 1992;13:157-164.

[207] Condra KS, Buatti JM, Mendenhall WM, Friedman WA, Marcus RB, Jr. Rhoton AL. Benign meningiomas: primary treatment selection affects survival. Int J Radiat Oncol Biol Phys 1997;39:427-436.

[208] Narayan S, Cornblath WT, Sandler HM, Elner V Hayman JA. Preliminary visual outcomes after three-dimensional conformal radiation therapy for optic nerve sheath meningioma. Int J Radiat Oncol Biol Phys 2003;56:537-543.

[209] Bloch O, Sun M, Kaur G, Barani IJ Parsa AT. Fractionated radiotherapy for optic nerve sheath meningiomas. J Clin Neurosci 2012;19:1210-1215.

[210] Nutting C, Brada M, Brazil L, et al. Radiotherapy in the treatment of benign meningioma of the skull base. J Neurosurg 1999;90:823-827.

[211] Pourel N, Auque J, Bracard S, et al. Efficacy of external fractionated radiation therapy in the treatment of meningiomas: a 20-year experience. Radiother Oncol 2001;61:65-70.

[212] Dufour H, Muracciole X, Metellus P, Regis J, Chinot O Grisoli F. Long-term tumor control and functional outcome in patients with cavernous sinus meningiomas treated by radiotherapy with or without previous surgery: is there an alternative to aggressive tumor removal? Neurosurgery 2001;48:285-294; discussion 294-286.

[213] Fogliata A, Clivio A, Nicolini G, Vanetti E Cozzi L. Intensity modulation with photons for benign intracranial tumours: a planning comparison of volumetric single arc, helical arc and fixed gantry techniques. Radiother Oncol 2008;89:254-262.

[214] Pirzkall A, Lohr F, Rhein B, et al. Conformal radiotherapy of challenging paraspinal tumors using a multiple arc segment technique. Int J Radiat Oncol Biol Phys 2000;48:1197-1204.

[215] Milker-Zabel S, Zabel-du Bois A, Huber P, Schlegel W Debus J. Intensity-modulated radiotherapy for complex-shaped meningioma of the skull base: long-term experience of a single institution. Int J Radiat Oncol Biol Phys 2007;68:858-863.

[216] Baumert BG, Norton IA Davis JB. Intensity-modulated stereotactic radiotherapy vs. stereotactic conformal radiotherapy for the treatment of meningioma located predominantly in the skull base. Int J Radiat Oncol Biol Phys 2003;57:580-592.

[217] Combs SE, Adeberg S, Dittmar JO, et al. Skull base meningiomas: Long-term results and patient self-reported outcome in 507 patients treated with fractionated stereotactic radiotherapy (FSRT) or intensity modulated radiotherapy (IMRT). Radiother Oncol 2013;106:186-191.

[218] Kosaki K, Ecker S, Habermehl D, et al. Comparison of intensity modulated radiotherapy (IMRT) with intensity modulated particle therapy (IMPT) using fixed beams or an ion gantry for the treatment of patients with skull base meningiomas. Radiat Oncol 2012;7:44.

[219] Grant W, 3rd Cain RB. Intensity modulated conformal therapy for intracranial lesions. Med Dosim 1998;23:237-241.

[220] Uy NW, Woo SY, Teh BS, et al. Intensity-modulated radiation therapy (IMRT) for meningioma. Int J Radiat Oncol Biol Phys 2002;53:1265-1270.

[221] Cozzi L, Clivio A, Bauman G, et al. Comparison of advanced irradiation techniques with photons for benign intracranial tumours. Radiother Oncol 2006;80:268-273.

[222] Meeks SL, Buatti JM, Bova FJ, Friedman WA, Mendenhall WM Zlotecki RA. Potential clinical efficacy of intensity-modulated conformal therapy. Int J Radiat Oncol Biol Phys 1998;40:483-495.

[223] Sankaranarayanan V, Ganesan S, Oommen S, Padmanaban TK, Stumpf J Ayyangar KM. Study on dosimetric parameters for stereotactic radiosurgery and intensity-modulated radiotherapy. Med Dosim 2003;28:85-90.

[224] Pirzkall A, Carol M, Lohr F, Hoss A, Wannenmacher M Debus J. Comparison of intensity-modulated radiotherapy with conventional conformal radiotherapy for complex-shaped tumors. Int J Radiat Oncol Biol Phys 2000;48:1371-1380.

[225] Sajja R, Barnett GH, Lee SY, et al. Intensity-modulated radiation therapy (IMRT) for newly diagnosed and recurrent intracranial meningiomas: preliminary results. Technol Cancer Res Treat 2005;4:675-682.

[226] Estall V, Fairfoul J, Jena R, Jefferies SJ, Burton KE Burnet NG. Skull base meningioma - comparison of intensity-modulated radiotherapy planning techniques using the moduleaf micro-multileaf collimator and helical tomotherapy. Clin Oncol (R Coll Radiol) 2010;22:179-184.

[227] Wiggenraad RG, Petoukhova AL, Versluis L van Santvoort JP. Stereotactic radiotherapy of intracranial tumors: a comparison of intensity-modulated radiotherapy and dynamic conformal arc. Int J Radiat Oncol Biol Phys 2009;74:1018-1026.

[228] Combs SE, Hartmann C, Nikoghosyan A, et al. Carbon ion radiation therapy for high-risk meningiomas. Radiother Oncol 2010;95:54-59.

[229] Cozzi L, Clivio A, Vanetti E, Nicolini G Fogliata A. Comparative planning study for proton radiotherapy of benign brain tumors. Strahlenther Onkol 2006;182:376-381.

[230] Slater JD, Loredo LN, Chung A, et al. Fractionated proton radiotherapy for benign cavernous sinus meningiomas. Int J Radiat Oncol Biol Phys 2012;83:e633-637.

[231] Boskos C, Feuvret L, Noel G, et al. Combined proton and photon conformal radiotherapy for intracranial atypical and malignant meningioma. Int J Radiat Oncol Biol Phys 2009;75:399-406.

[232] Bentzen S. Design of clinical trials in radiation oncology: saving lives not grays. In: Dale RG J, B, ed. Radiobiological modelling in radiation oncology. London: British institute radiology, 2007; 196-211.

[233] Mohan R, Arnfield M, Tong S, Wu Q Siebers J. The impact of fluctuations in intensity patterns on the number of monitor units and the quality and accuracy of intensity modulated radiotherapy. Med Phys 2000;27:1226-1237.

[234] Miles EA, Clark CH, Urbano MT, et al. The impact of introducing intensity modulated radiotherapy into routine clinical practice. Radiother Oncol 2005;77:241-246.

[235] Goitein M. How best to dispose of extra-tumoral dose: a cautionary note for intensity-modulated radiation therapy. Int J Radiat Oncol Biol Phys 2009;75:1-3.

[236] Williams PO Hounsell AR. X-ray leakage considerations for IMRT. Br J Radiol 2001;74:98-100.

[237] Purdy JA. Dose to normal tissues outside the radiation therapy patient's treated volume: a review of different radiation therapy techniques. Health Phys 2008;95:666-676.

[238] Howell RM, Hertel NE, Wang Z, Hutchinson J Fullerton GD. Calculation of effective dose from measurements of secondary neutron spectra and scattered photon dose from dynamic MLC IMRT for 6 MV, 15 MV, and 18 MV beam energies. Med Phys 2006;33:360-368.

[239] Verellen D Vanhavere F. Risk assessment of radiation-induced malignancies based on whole-body equivalent dose estimates for IMRT treatment in the head and neck region. Radiother Oncol 1999;53:199-203.

[240] Bortfeld TR, Kahler DL, Waldron TJ Boyer AL. X-ray field compensation with multileaf collimators. Int J Radiat Oncol Biol Phys 1994;28:723-730.

[241] Followill D, Geis P Boyer A. Estimates of whole-body dose equivalent produced by beam intensity modulated conformal therapy. Int J Radiat Oncol Biol Phys 1997;38:667-672.

[242] Gershkevitsh E, Clark CH, Staffurth J, Dearnaley DP Trott KR. Dose to bone marrow using IMRT techniques in prostate cancer patients. Strahlenther Onkol 2005;181:172-178.

[243] Followill D, Geis, P., Boyer, A. Errata. Int J Radiat Oncol Biol Phys 1997;39:783.

[244] Mutic S Low DA. Whole-body dose from tomotherapy delivery. Int J Radiat Oncol Biol Phys 1998;42:229-232.

[245] Grant W III BA, Campbell C, . Leakage considerations with a multi-leafcollimator designed intensity-modulated conformal radiotherapy (abstract). Med Phys 1994;21:921.

[246] Meeks SL, Paulino AC, Pennington EC, Simon JH, Skwarchuk MW Buatti JM. In vivo determination of extra-target doses received from serial tomotherapy. Radiother Oncol 2002;63:217-222.

[247] Ramsey C, Seibert R, Mahan SL, Desai D Chase D. Out-of-field dosimetry measurements for a helical tomotherapy system. J Appl Clin Med Phys 2006;7:1-11.

[248] Bennett BR, Lamba MA Elson HR. Analysis of peripheral doses for base of tongue treatment by linear accelerator and helical TomoTherapy IMRT. J Appl Clin Med Phys 2010;11:3136.

[249] Lissner S, Schubert K, Wiezorek T, et al. Investigations of peripheral dose for helical tomotherapy. Z Med Phys 2013;23:324-331.

[250] Adams EJ, Convery DJ, Cosgrove VP, et al. Clinical implementation of dynamic and step-and-shoot IMRT to treat prostate cancer with high risk of pelvic lymph node involvement. Radiother Oncol 2004;70:1-10.

[251] Longobardi B, De Martin E, Fiorino C, et al. Comparing 3DCRT and inversely optimized IMRT planning for head and neck cancer: equivalence between step-and-shoot and sliding window techniques. Radiother Oncol 2005;77:148-156.

[252] Sharma DS, Animesh, Deshpande SS, et al. Peripheral dose from uniform dynamic multileaf collimation fields: implications for sliding window intensity-modulated radiotherapy. Br J Radiol 2006;79:331-335.

[253] Lillicrap SC, Morgan HM Shakeshaft JT. X-ray leakage during radiotherapy. Br J Radiol 2000;73:793-794.

[254] Klein EE, Maserang B, Wood R Mansur D. Peripheral doses from pediatric IMRT. Med Phys 2006;33:2525-2531.

[255] Woo TC, Pignol JP, Rakovitch E, et al. Body radiation exposure in breast cancer radiotherapy: impact of breast IMRT and virtual wedge compensation techniques. Int J Radiat Oncol Biol Phys 2006;65:52-58.

[256] Kry SF, Salehpour M, Followill DS, et al. Out-of-field photon and neutron dose equivalents from step-and-shoot intensity-modulated radiation therapy. Int J Radiat Oncol Biol Phys 2005;62:1204-1216.

[257] Kan MW, Leung LH, Kwong DL, Wong W Lam N. Peripheral doses from noncoplanar IMRT for pediatric radiation therapy. Med Dosim 2010;35:255-263.

[258] Xu XG, Bednarz B Paganetti H. A review of dosimetry studies on external-beam radiation treatment with respect to second cancer induction. Phys Med Biol 2008;53:R193-241.

[259] Boice JD, Jr., Day NE, Andersen A, et al. Second cancers following radiation treatment for cervical cancer. An international collaboration among cancer registries. J Natl Cancer Inst 1985;74:955-975.

[260] Brenner DJ, Curtis RE, Hall EJ Ron E. Second malignancies in prostate carcinoma patients after radiotherapy compared with surgery. Cancer 2000;88:398-406.

[261] Chaturvedi AK, Engels EA, Gilbert ES, et al. Second cancers among 104,760 survivors of cervical cancer: evaluation of long-term risk. J Natl Cancer Inst 2007;99:1634-1643.

[262] Pierce DA Preston DL. Radiation-related cancer risks at low doses among atomic bomb survivors. Radiat Res 2000;154:178-186.

[263] Preston DL, Pierce DA, Shimizu Y, Ron E Mabuchi K. Dose response and temporal patterns of radiation-associated solid cancer risks. Health Phys 2003;85:43-46.

[264] Ruben JD, Lancaster CM, Jones P Smith RL. A comparison of out-of-field dose and its constituent components for intensity-modulated radiation therapy versus conformal radiation therapy: implications for carcinogenesis. Int J Radiat Oncol Biol Phys 2011;81:1458-1464.

[265] Huang J, Kestin LL, Ye H, Wallace M, Martinez AA Vicini FA. Analysis of second malignancies after modern radiotherapy versus prostatectomy for localized prostate cancer. Radiother Oncol 2011;98:81-86.

[266] Hall EJ. Intensity-modulated radiation therapy, protons, and the risk of second cancers. Int J Radiat Oncol Biol Phys 2006;65:1-7.

[267] Takam R, Bezak E Yeoh EE. Risk of second primary cancer following prostate cancer radiotherapy: DVH analysis using the competitive risk model. Phys Med Biol 2009;54:611-625.

[268] Ruben JD, Davis S, Evans C, et al. The effect of intensity-modulated radiotherapy on radiation-induced second malignancies. Int J Radiat Oncol Biol Phys 2008;70:1530-1536.

[269] Dorr W Herrmann T. Cancer induction by radiotherapy: dose dependence and spatial relationship to irradiated volume. J Radiol Prot 2002;22:A117-121.

[270] Diallo I, Haddy N, Adjadj E, et al. Frequency distribution of second solid cancer locations in relation to the irradiated volume among 115 patients treated for childhood cancer. Int J Radiat Oncol Biol Phys 2009;74:876-883.

[271] Hall EJ Hei TK. Genomic instability and bystander effects induced by high-LET radiation. Oncogene 2003;22:7034-7042.

[272] Hall EJ. The bystander effect. Health Phys 2003;85:31-35.

[273] Hall EJ. Henry S. Kaplan Distinguished Scientist Award 2003. The crooked shall be made straight; dose-response relationships for carcinogenesis. Int J Radiat Biol 2004;80:327-337.

[274] Brenner DJ, Doll R, Goodhead DT, et al. Cancer risks attributable to low doses of ionizing radiation: assessing what we really know. Proc Natl Acad Sci U S A 2003;100:13761-13766.

[275] Brenner DJ Elliston CD. Estimated radiation risks potentially associated with full-body CT screening. Radiology 2004;232:735-738.

[276] Brenner DJ. Radiation risks potentially associated with low-dose CT screening of adult smokers for lung cancer. Radiology 2004;231:440-445.

[277] Land CE. Estimating cancer risks from low doses of ionizing radiation. Science 1980;209:1197-1203.

[278] Wiezorek T, Georg D, Schwedas M, Salz H Wendt TG. Experimental determination of peripheral photon dose components for different IMRT techniques and linear accelerators. Z Med Phys 2009;19:120-128.

[279] Rothkamm K Lobrich M. Evidence for a lack of DNA double-strand break repair in human cells exposed to very low x-ray doses. Proc Natl Acad Sci U S A 2003;100:5057-5062.

[280] Olive PL. The role of DNA single- and double-strand breaks in cell killing by ionizing radiation. Radiat Res 1998;150:S42-51.

[281] Lett JT. Damage to cellular DNA from particulate radiations, the efficacy of its processing and the radiosensitivity of mammalian cells. Emphasis on DNA double strand breaks and chromatin breaks. Radiat Environ Biophys 1992;31:257-277.

[282] Jackson SP. Sensing and repairing DNA double-strand breaks. Carcinogenesis 2002;23:687-696.

[283] Rothkamm K, Kruger I, Thompson LH Lobrich M. Pathways of DNA double-strand break repair during the mammalian cell cycle. Mol Cell Biol 2003;23:5706-5715.

[284] Lassmann M, Hanscheid H, Gassen D, et al. In vivo formation of gamma-H2AX and 53BP1 DNA repair foci in blood cells after radioiodine therapy of differentiated thyroid cancer. J Nucl Med 2010;51:1318-1325.

[285] Takahashi A Ohnishi T. Does gammaH2AX foci formation depend on the presence of DNA double strand breaks? Cancer Lett 2005;229:171-179.

[286] Panier S Durocher D. Regulatory ubiquitylation in response to DNA double-strand breaks. DNA Repair (Amst) 2009;8:436-443.

[287] Vignard J, Mirey G Salles B. Ionizing-radiation induced DNA double-strand breaks: a direct and indirect lighting up. Radiother Oncol 2013;108:362-369.

[288] Rogakou EP, Boon C, Redon C Bonner WM. Megabase chromatin domains involved in DNA double-strand breaks in vivo. J Cell Biol 1999;146:905-916.

[289] Rogakou EP, Pilch DR, Orr AH, Ivanova VS Bonner WM. DNA double-stranded breaks induce histone H2AX phosphorylation on serine 139. J Biol Chem 1998;273:5858-5868.

[290] Stiff T, O'Driscoll M, Rief N, Iwabuchi K, Lobrich M Jeggo PA. ATM and DNA-PK function redundantly to phosphorylate H2AX after exposure to ionizing radiation. Cancer Res 2004;64:2390-2396.

[291] Bassing CH Alt FW. H2AX may function as an anchor to hold broken chromosomal DNA ends in close proximity. Cell Cycle 2004;3:149-153.

[292] Paull TT, Rogakou EP, Yamazaki V, Kirchgessner CU, Gellert M Bonner WM. A critical role for histone H2AX in recruitment of repair factors to nuclear foci after DNA damage. Curr Biol 2000;10:886-895.

[293] Sedelnikova OA, Rogakou EP, Panyutin IG Bonner WM. Quantitative detection of (125)IdU-induced DNA double-strand breaks with gamma-H2AX antibody. Radiat Res 2002;158:486-492.

[294] Kuo LJ Yang LX. Gamma-H2AX - a novel biomarker for DNA double-strand breaks. In Vivo 2008;22:305-309.

[295] Thompson LH. Recognition, signaling, and repair of DNA double-strand breaks produced by ionizing radiation in mammalian cells: the molecular choreography. Mutat Res 2012;751:158-246.

[296] Fernandez-Capetillo O, Lee A, Nussenzweig M Nussenzweig A. H2AX: the histone guardian of the genome. DNA Repair (Amst) 2004;3:959-967.

[297] Pilch DR, Sedelnikova OA, Redon C, Celeste A, Nussenzweig A Bonner WM. Characteristics of gamma-H2AX foci at DNA double-strand breaks sites. Biochem Cell Biol 2003;81:123-129.

[298] Koike M, Sugasawa J, Koike A Kohno Y. p53 phosphorylation in mouse skin and in vitro human skin model by high-dose-radiation exposure. J Radiat Res 2005;46:461-468.

[299] Paques F Haber JE. Multiple pathways of recombination induced by double-strand breaks in Saccharomyces cerevisiae. Microbiol Mol Biol Rev 1999;63:349-404.

[300] Shrivastav M, De Haro LP Nickoloff JA. Regulation of DNA double-strand break repair pathway choice. Cell Res 2008;18:134-147.

[301] Ueno S, Kashimoto T, Susa N, et al. Assessment of DNA damage in multiple organs of mice after whole body X-irradiation using the comet assay. Mutat Res 2007;634:135-145.

[302] Belli M, Cherubini R, Dalla Vecchia M, et al. DNA DSB induction and rejoining in V79 cells irradiated with light ions: a constant field gel electrophoresis study. Int J Radiat Biol 2000;76:1095-1104.

[303] Ager DD, Dewey WC, Gardiner K, Harvey W, Johnson RT Waldren CA. Measurement of radiation-induced DNA double-strand breaks by pulsed-field gel electrophoresis. Radiat Res 1990;122:181-187.

[304] Iliakis GE, Cicilioni O Metzger L. Measurement of DNA double-strand breaks in CHO cells at various stages of the cell cycle using pulsed field gel electrophoresis: calibration by means of 125I decay. Int J Radiat Biol 1991;59:343-357.

[305] Lobrich M, Shibata A, Beucher A, et al. gammaH2AX foci analysis for monitoring DNA double-strand break repair: strengths, limitations and optimization. Cell Cycle 2010;9:662-669.

[306] Ostling O, Johanson KJ, Blomquist E Hagelqvist E. DNA damage in clinical radiation therapy studied by microelectrophoresis in single tumour cells. A preliminary report. Acta Oncol 1987;26:45-48.

[307] Ostling O Johanson KJ. Microelectrophoretic study of radiation-induced DNA damages in individual mammalian cells. Biochem Biophys Res Commun 1984;123:291-298.

[308] Singh NP, McCoy MT, Tice RR Schneider EL. A simple technique for quantitation of low levels of DNA damage in individual cells. Exp Cell Res 1988;175:184-191.

[309] Nelson G, Buhmann M von Zglinicki T. DNA damage foci in mitosis are devoid of 53BP1. Cell Cycle 2009;8:3379-3383.

[310] Nakamura AJ, Rao VA, Pommier Y Bonner WM. The complexity of phosphorylated H2AX foci formation and DNA repair assembly at DNA double-strand breaks. Cell Cycle 2010;9:389-397.

[311] Ivashkevich A, Redon CE, Nakamura AJ, Martin RF Martin OA. Use of the gamma-H2AX assay to monitor DNA damage and repair in translational cancer research. Cancer Lett 2012;327:123-133.

[312] Rothkamm K Horn S. gamma-H2AX as protein biomarker for radiation exposure. Ann Ist Super Sanita 2009;45:265-271.

[313] Qvarnstrom OF, Simonsson M, Johansson KA, Nyman J Turesson I. DNA double strand break quantification in skin biopsies. Radiother Oncol 2004;72:311-317.

[314] Koike M, Mashino M, Sugasawa J Koike A. Dynamic change of histone H2AX phosphorylation independent of ATM and DNA-PK in mouse skin in situ. Biochem Biophys Res Commun 2007;363:1009-1012.

[315] Simonsson M, Qvarnstrom F, Nyman J, Johansson KA, Garmo H Turesson I. Low-dose hypersensitive gammaH2AX response and infrequent apoptosis in epidermis from radiotherapy patients. Radiother Oncol 2008;88:388-397.

[316] Nowak E, Etienne O, Millet P, et al. Radiation-induced H2AX phosphorylation and neural precursor apoptosis in the developing brain of mice. Radiat Res 2006;165:155-164.

[317] Gavrilov B, Vezhenkova I, Firsanov D, et al. Slow elimination of phosphorylated histone gamma-H2AX from DNA of terminally differentiated mouse heart cells in situ. Biochem Biophys Res Commun 2006;347:1048-1052.

[318] Rube CE, Dong X, Kuhne M, et al. DNA double-strand break rejoining in complex normal tissues. Int J Radiat Oncol Biol Phys 2008;72:1180-1187.

[319] Koike M, Mashino M, Sugasawa J Koike A. Histone H2AX phosphorylation independent of ATM after X-irradiation in mouse liver and kidney in situ. J Radiat Res 2008;49:445-449.

[320] Yoon AJ, Shen J, Wu HC, et al. Expression of activated checkpoint kinase 2 and histone 2AX in exfoliative oral cells after exposure to ionizing radiation. Radiat Res 2009;171:771-775.

[321] Szeto YT, Benzie IF, Collins AR, et al. A buccal cell model comet assay: development and evaluation for human biomonitoring and nutritional studies. Mutat Res 2005;578:371-381.

[322] Colin C, Devic C, Noel A, et al. DNA double-strand breaks induced by mammographic screening procedures in human mammary epithelial cells. Int J Radiat Biol 2011;87:1103-1112.

[323] Redon CE, Nakamura AJ, Gouliaeva K, Rahman A, Blakely WF Bonner WM. The use of gamma-H2AX as a biodosimeter for total-body radiation exposure in non-human primates. PLoS One 2010;5:e15544.

[324] Chua ML, Somaiah N, A'Hern R, et al. Residual DNA and chromosomal damage in ex vivo irradiated blood lymphocytes correlated with late normal tissue response to breast radiotherapy. Radiother Oncol 2011;99:362-366.

[325] Horn S, Barnard S Rothkamm K. Gamma-H2AX-based dose estimation for whole and partial body radiation exposure. PLoS One 2011;6:e25113.

[326] Kuhne M, Riballo E, Rief N, Rothkamm K, Jeggo PA Lobrich M. A double-strand break repair defect in ATM-deficient cells contributes to radiosensitivity. Cancer Res 2004;64:500-508.

[327] Rothkamm K, Balroop S, Shekhdar J, Fernie P Goh V. Leukocyte DNA damage after multi-detector row CT: a quantitative biomarker of low-level radiation exposure. Radiology 2007;242:244-251.

[328] Camphausen K, Burgan W, Cerra M, et al. Enhanced radiation-induced cell killing and prolongation of gammaH2AX foci expression by the histone deacetylase inhibitor MS-275. Cancer Res 2004;64:316-321.

[329] Andrievski A Wilkins RC. The response of gamma-H2AX in human lymphocytes and lymphocytes subsets measured in whole blood cultures. Int J Radiat Biol 2009;85:369-376.

[330] Bonner WM, Redon CE, Dickey JS, et al. GammaH2AX and cancer. Nat Rev Cancer 2008;8:957-967.

[331] Bhogal N, Jalali F Bristow RG. Microscopic imaging of DNA repair foci in irradiated normal tissues. Int J Radiat Biol 2009;85:732-746.

[332] Muslimovic A, Ismail IH, Gao Y Hammarsten O. An optimized method for measurement of gamma-H2AX in blood mononuclear and cultured cells. Nat Protoc 2008;3:1187-1193.

[333] MacPhail SH, Banath JP, Yu TY, Chu EH, Lambur H Olive PL. Expression of phosphorylated histone H2AX in cultured cell lines following exposure to X-rays. Int J Radiat Biol 2003;79:351-358.

[334] Olive PL Banath JP. Phosphorylation of histone H2AX as a measure of radiosensitivity. Int J Radiat Oncol Biol Phys 2004;58:331-335.

[335] Ismail IH, Wadhra TI Hammarsten O. An optimized method for detecting gamma-H2AX in blood cells reveals a significant interindividual variation in the gamma-H2AX response among humans. Nucleic Acids Res 2007;35:e36.

[336] Avondoglio D, Scott T, Kil WJ, Sproull M, Tofilon PJ Camphausen K. High throughput evaluation of gamma-H2AX. Radiat Oncol 2009;4:31.

[337] Redon CE, Dickey JS, Bonner WM Sedelnikova OA. gamma-H2AX as a biomarker of DNA damage induced by ionizing radiation in human peripheral blood lymphocytes and artificial skin. Adv Space Res 2009;43:1171-1178.

[338] Lobrich M, Rief N, Kuhne M, et al. In vivo formation and repair of DNA double-strand breaks after computed tomography examinations. Proc Natl Acad Sci U S A 2005;102:8984-8989.

[339] Sedelnikova OA, Pilch DR, Redon C Bonner WM. Histone H2AX in DNA damage and repair. Cancer Biol Ther 2003;2:233-235.

[340] Sak A, Grehl S, Erichsen P, et al. gamma-H2AX foci formation in peripheral blood lymphocytes of tumor patients after local radiotherapy to different sites of the body: dependence on the dose-distribution, irradiated site and time from start of treatment. Int J Radiat Biol 2007;83:639-652.

[341] Marchetti F, Coleman MA, Jones IM Wyrobek AJ. Candidate protein biodosimeters of human exposure to ionizing radiation. Int J Radiat Biol 2006;82:605-639.

[342] Celeste A, Fernandez-Capetillo O, Kruhlak MJ, et al. Histone H2AX phosphorylation is dispensable for the initial recognition of DNA breaks. Nat Cell Biol 2003;5:675-679.

[343] Doai M, Watanabe N, Takahashi T, et al. Sensitive immunodetection of radiotoxicity after iodine-131 therapy for thyroid cancer using gamma-H2AX foci of DNA damage in lymphocytes. Ann Nucl Med 2013;27:233-238.

[344] May MS, Brand M, Wuest W, et al. Induction and repair of DNA double-strand breaks in blood lymphocytes of patients undergoing (1)(8)F-FDG PET/CT examinations. Eur J Nucl Med Mol Imaging 2012;39:1712-1719.

[345] Roch-Lefevre S, Mandina T, Voisin P, et al. Quantification of gamma-H2AX foci in human lymphocytes: a method for biological dosimetry after ionizing radiation exposure. Radiat Res 2010;174:185-194.

[346] Golfier S, Jost G, Pietsch H, et al. Dicentric chromosomes and gamma-H2AX foci formation in lymphocytes of human blood samples exposed to a CT scanner: a

direct comparison of dose response relationships. Radiat Prot Dosimetry 2009;134:55-61.

[347] Li P, Du CR, Xu WC, et al. Correlation of dynamic changes in gamma-H2AX expression in peripheral blood lymphocytes from head and neck cancer patients with radiation-induced oral mucositis. Radiat Oncol 2013;8:155.

[348] Banath JP, Macphail SH Olive PL. Radiation sensitivity, H2AX phosphorylation, and kinetics of repair of DNA strand breaks in irradiated cervical cancer cell lines. Cancer Res 2004;64:7144-7149.

[349] Fleckenstein J, Kuhne M, Seegmuller K, et al. The impact of individual in vivo repair of DNA double-strand breaks on oral mucositis in adjuvant radiotherapy of head-and-neck cancer. Int J Radiat Oncol Biol Phys 2011;81:1465-1472.

[350] Geisel D, Heverhagen JT, Kalinowski M Wagner HJ. DNA double-strand breaks after percutaneous transluminal angioplasty. Radiology 2008;248:852-859.

[351] Porcedda P, Turinetto V, Lantelme E, et al. Impaired elimination of DNA double-strand break-containing lymphocytes in ataxia telangiectasia and Nijmegen breakage syndrome. DNA Repair (Amst) 2006;5:904-913.

[352] Kuefner MA, Grudzenski S, Hamann J, et al. Effect of CT scan protocols on x-ray-induced DNA double-strand breaks in blood lymphocytes of patients undergoing coronary CT angiography. Eur Radiol 2010;20:2917-2924.

[353] Kuefner MA, Grudzenski S, Schwab SA, et al. DNA double-strand breaks and their repair in blood lymphocytes of patients undergoing angiographic procedures. Invest Radiol 2009;44:440-446.

[354] Geisel D, Zimmermann E, Rief M, et al. DNA double-strand breaks as potential indicators for the biological effects of ionising radiation exposure from cardiac CT and conventional coronary angiography: a randomised, controlled study. Eur Radiol 2012;22:1641-1650.

[355] Redon CE, Nakamura AJ, Gouliaeva K, Rahman A, Blakely WF Bonner WM. Q(gamma-H2AX), an analysis method for partial-body radiation exposure using gamma-H2AX in nonhuman primate lymphocytes. Radiat Meas 2011;46:877-881.

[356] Zwicker F, Swartman B, Sterzing F, et al. Biological in-vivo measurement of dose distribution in patients' lymphocytes by gamma-H2AX immunofluorescence staining: 3D conformal- vs. Step-and-shoot IMRT of the prostate gland. Radiat Oncol 2011;6:62.

[357] Rube CE, Grudzenski S, Kuhne M, et al. DNA double-strand break repair of blood lymphocytes and normal tissues analysed in a preclinical mouse model: implications for radiosensitivity testing. Clin Cancer Res 2008;14:6546-6555.

[358] Koch U, Hohne K, von Neubeck C, et al. Residual gammaH2AX foci predict local tumour control after radiotherapy. Radiother Oncol 2013;108:434-439.

[359] Rube CE, Fricke A, Schneider R, et al. DNA repair alterations in children with pediatric malignancies: novel opportunities to identify patients at risk for high-grade toxicities. Int J Radiat Oncol Biol Phys 2010;78:359-369.

[360] Bourton EC, Plowman PN, Smith D, Arlett CF Parris CN. Prolonged expression of the gamma-H2AX DNA repair biomarker correlates with excess acute and chronic toxicity from radiotherapy treatment. Int J Cancer 2011.

[361] Goutham HV, Mumbrekar KD, Vadhiraja BM, et al. DNA double-strand break analysis by gamma-H2AX foci: a useful method for determining the overreactors to radiation-induced acute reactions among head-and-neck cancer patients. Int J Radiat Oncol Biol Phys 2012;84:e607-612.

[362] Rube CE, Fricke A, Wendorf J, et al. Accumulation of DNA double-strand breaks in normal tissues after fractionated irradiation. Int J Radiat Oncol Biol Phys 2010;76:1206-1213.

[363] Werbrouck J, De Ruyck K, Beels L, et al. Prediction of late normal tissue complications in RT treated gynaecological cancer patients: potential of the gamma-H2AX foci assay and association with chromosomal radiosensitivity. Oncol Rep 2010;23:571-578.

[364] Werbrouck J, Duprez F, De Neve W Thierens H. Lack of a correlation between gammaH2AX foci kinetics in lymphocytes and the severity of acute normal tissue reactions during IMRT treatment for head and neck cancer. Int J Radiat Biol 2011;87:46-56.

[365] Vasireddy RS, Sprung CN, Cempaka NL, Chao M McKay MJ. H2AX phosphorylation screen of cells from radiosensitive cancer patients reveals a novel DNA double-strand break repair cellular phenotype. Br J Cancer 2010;102:1511-1518.

[366] El-Saghire H, Vandevoorde C, Ost P, et al. Intensity modulated radiotherapy induces pro-inflammatory and pro-survival responses in prostate cancer patients. Int J Oncol 2014;44:1073-1083.

[367] Lassen NA. Cerebral blood flow and oxygen consumption in man. Physiol Rev 1959;39:183-238.

[368] Pouliliou S Koukourakis MI. Gamma histone 2AX (gamma-H2AX)as a predictive tool in radiation oncology. Biomarkers 2014;19:167-180.

[369] Scherthan H, Hieber L, Braselmann H, Meineke V Zitzelsberger H. Accumulation of DSBs in gamma-H2AX domains fuel chromosomal aberrations. Biochem Biophys Res Commun 2008;371:694-697.

[370] Beaton LA, Marro L, Malone S, et al. Investigating gamma H2AX as a Biomarker of Radiosensitivity Using Flow Cytometry Methods. ISRN Radiol 2013;2013:704659.

[371] Dobler B, Groeger C, Treutwein M, et al. Commissioning of volumetric modulated arc therapy (VMAT) in a dual-vendor environment. Radiother Oncol 2011;99:86-89.

[372] Maclean J, Stacey, D'Souza,D, Fersht, N and Short,SC. RapidArc radiotherapy for brain tumours - acute toxicity and dosimetric data. . Eur J Clin and Med Oncol. 2011.

[373] Cozzi L, Dinshaw KA, Shrivastava SK, et al. A treatment planning study comparing volumetric arc modulation with RapidArc and fixed field IMRT for cervix uteri radiotherapy. Radiother Oncol 2008;89:180-191.

[374] Vivekanandan N, Sriram P, Kumar SA, Bhuvaneswari N Saranya K. Volumetric modulated arc radiotherapy for esophageal cancer. Med Dosim 2012;37:108-113.

[375] Syme A, Kirkby C, Mirzayans R, MacKenzie M, Field C Fallone BG. Relative biological damage and electron fluence in and out of a 6 MV photon field. Phys Med Biol 2009;54:6623-6633.

[376] Kim DW, Chung WK, Shin D, et al. Risk of second cancer from scattered radiation of intensity-modulated radiotherapies with lung cancer. Radiat Oncol 2013;8:47.

[377] Kim S, Min BJ, Yoon M, et al. Secondary radiation doses of intensity-modulated radiotherapy and proton beam therapy in patients with lung and liver cancer. Radiother Oncol 2011;98:335-339.

[378] Yovino S, Kleinberg L, Grossman SA, Narayanan M Ford E. The etiology of treatment-related lymphopenia in patients with malignant gliomas: modeling radiation dose to circulating lymphocytes explains clinical observations and suggests methods of modifying the impact of radiation on immune cells. Cancer Invest 2013;31:140-144.

[379] Schneider U Kaser-Hotz B. A simple dose-response relationship for modeling secondary cancer incidence after radiotherapy. Z Med Phys 2005;15:31-37.

[380] Schneider U, Lomax A, Pemler P, et al. The impact of IMRT and proton radiotherapy on secondary cancer incidence. Strahlenther Onkol 2006;182:647-652.

[381] Pearce MS, Salotti JA, Little MP, et al. Radiation exposure from CT scans in childhood and subsequent risk of leukaemia and brain tumours: a retrospective cohort study. Lancet 2012;380:499-505.

[382] Kendall GM, Little MP, Wakeford R, et al. A record-based case-control study of natural background radiation and the incidence of childhood leukaemia and other cancers in Great Britain during 1980-2006. Leukemia 2013;27:3-9.

[383] Yoon M, Ahn SH, Kim J, et al. Radiation-induced cancers from modern radiotherapy techniques: intensity-modulated radiotherapy versus proton therapy. Int J Radiat Oncol Biol Phys 2010;77:1477-1485.

[384] Tessa CL, Berger T, Kaderka R, et al. Characterization of the secondary neutron field produced during treatment of an anthropomorphic phantom with x-rays, protons and carbon ions. Phys Med Biol 2014;59:2111-2125.

[385] Paganetti H, Athar BS, Moteabbed M, J AA, Schneider U Yock TI. Assessment of radiation-induced second cancer risks in proton therapy and IMRT for organs inside the primary radiation field. Phys Med Biol 2012;57:6047-6061.

[386] Beltran C, Roca M Merchant TE. On the benefits and risks of proton therapy in pediatric craniopharyngioma. Int J Radiat Oncol Biol Phys 2012;82:e281-287.

[387] Athar BS Paganetti H. Comparison of second cancer risk due to out-of-field doses from 6-MV IMRT and proton therapy based on 6 pediatric patient treatment plans. Radiother Oncol 2011;98:87-92.

[388] Athar BS, Bednarz B, Seco J, Hancox C Paganetti H. Comparison of out-of-field photon doses in 6 MV IMRT and neutron doses in proton therapy for adult and pediatric patients. Phys Med Biol 2010;55:2879-2891.

[389] Trotti A, Colevas AD, Setser A, et al. CTCAE v3.0: development of a comprehensive grading system for the adverse effects of cancer treatment. Semin Radiat Oncol 2003;13:176-181.

[390] Aaronson NK, Ahmedzai S, Bergman B, et al. The European Organization for Research and Treatment of Cancer QLQ-C30: a quality-of-life instrument for use in international clinical trials in oncology. J Natl Cancer Inst 1993;85:365-376.

[391] Minniti G, Amelio D, Amichetti M, et al. Patterns of failure and comparison of different target volume delineations in patients with glioblastoma treated with conformal radiotherapy plus concomitant and adjuvant temozolomide. Radiother Oncol 2010;97:377-381.

[392] Askoxylakis V, Zabel-du Bois A, Schlegel W, Debus J, Huber P Milker-Zabel S. Patterns of failure after stereotactic radiotherapy of intracranial meningioma. J Neurooncol 2010;98:367-372.

[393] Press RH, Prabhu RS, Appin CL, et al. Outcomes and patterns of failure for grade 2 meningioma treated with reduced-margin intensity modulated radiation therapy. Int J Radiat Oncol Biol Phys 2014;88:1004-1010.

[394] Fayers PM, Aaronson NK, Bjordal K, et al. The EORTC QLQ-C30 Scoring Manual. Brussels: European Organisation for Research and Treatment of Cancer, 2001.

[395] Taphoorn MJ, Claassens L, Aaronson NK, et al. An international validation study of the EORTC brain cancer module (EORTC QLQ-BN20) for assessing health-related quality of life and symptoms in brain cancer patients. Eur J Cancer 2010;46:1033-1040.

[396] Khoshnevisan A, Yekaninejad MS, Ardakani SK, Pakpour AH, Mardani A Aaronson NK. Translation and validation of the EORTC brain cancer module (EORTC QLQ-BN20) for use in Iran. Health Qual Life Outcomes 2012;10:54.

[397] Tofilon PJ Fike JR. The radioresponse of the central nervous system: a dynamic process. Radiat Res 2000;153:357-370.

[398] Kazda T, Jancalek R, Pospisil P, et al. Why and how to spare the hippocampus during brain radiotherapy: the developing role of hippocampal avoidance in cranial radiotherapy. Radiat Oncol 2014;9:139.

[399] Faithfull S Brada M. Somnolence syndrome in adults following cranial irradiation for primary brain tumours. Clin Oncol (R Coll Radiol) 1998;10:250-254.

[400] Minniti G, Clarke E, Cavallo L, et al. Fractionated stereotactic conformal radiotherapy for large benign skull base meningiomas. Radiat Oncol 2011;6:36.

[401] Becker G, Jeremic B, Pitz S, et al. Stereotactic fractionated radiotherapy in patients with optic nerve sheath meningioma. Int J Radiat Oncol Biol Phys 2002;54:1422-1429.

[402] Andrews DW, Faroozan R, Yang BP, et al. Fractionated stereotactic radiotherapy for the treatment of optic nerve sheath meningiomas: preliminary observations of 33 optic nerves in 30 patients with historical comparison to observation with or without prior surgery. Neurosurgery 2002;51:890-902; discussion 903-894.

[403] Berman D Miller NR. New concepts in the management of optic nerve sheath meningiomas. Ann Acad Med Singapore 2006;35:168-174.

[404] Parsons JT, Bova FJ, Fitzgerald CR, Mendenhall WM Million RR. Severe dry-eye syndrome following external beam irradiation. Int J Radiat Oncol Biol Phys 1994;30:775-780.

[405] Bhandare N, Moiseenko V, Song WY, Morris CG, Bhatti MT Mendenhall WM. Severe dry eye syndrome after radiotherapy for head-and-neck tumors. Int J Radiat Oncol Biol Phys 2012;82:1501-1508.

[406] Batth SS, Sreeraman R, Dienes E, et al. Clinical-dosimetric relationship between lacrimal gland dose and ocular toxicity after intensity-modulated radiotherapy for sinonasal tumours. Br J Radiol 2013;86:20130459.

[407] Hsiao KY, Yeh SA, Chang CC, Tsai PC, Wu JM Gau JS. Cognitive function before and after intensity-modulated radiation therapy in patients with nasopharyngeal carcinoma: a prospective study. Int J Radiat Oncol Biol Phys 2010;77:722-726.

[408] Lee PW, Hung BK, Woo EK, Tai PT Choi DT. Effects of radiation therapy on neuropsychological functioning in patients with nasopharyngeal carcinoma. J Neurol Neurosurg Psychiatry 1989;52:488-492.

[409] Raber J, Rola R, LeFevour A, et al. Radiation-induced cognitive impairments are associated with changes in indicators of hippocampal neurogenesis. Radiat Res 2004;162:39-47.

[410] Nagai R, Tsunoda S, Hori Y Asada H. Selective vulnerability to radiation in the hippocampal dentate granule cells. Surg Neurol 2000;53:503-506; discussion 506-507.

[411] Tada E, Parent JM, Lowenstein DH Fike JR. X-irradiation causes a prolonged reduction in cell proliferation in the dentate gyrus of adult rats. Neuroscience 2000;99:33-41.

[412] Gondi V, Tolakanahalli R, Mehta MP, et al. Hippocampal-sparing whole-brain radiotherapy: a "how-to" technique using helical tomotherapy and linear accelerator-based intensity-modulated radiotherapy. Int J Radiat Oncol Biol Phys 2010;78:1244-1252.

[413] Pinkham MB, Bertrand KC, Olson S, et al. Hippocampal-sparing radiotherapy: the new standard of care for World Health Organization grade II and III gliomas? J Clin Neurosci 2014;21:86-90.

[414] Gondi V, Pugh SL, Tome WA, et al. Preservation of memory with conformal avoidance of the hippocampal neural stem-cell compartment during whole-brain

radiotherapy for brain metastases (RTOG 0933): a phase II multi-institutional trial. J Clin Oncol 2014;32:3810-3816.

[415] van Nieuwenhuizen D, Klein M, Stalpers LJ, Leenstra S, Heimans JJ Reijneveld JC. Differential effect of surgery and radiotherapy on neurocognitive functioning and health-related quality of life in WHO grade I meningioma patients. J Neurooncol 2007;84:271-278.

[416] Dijkstra M, van Nieuwenhuizen D, Stalpers LJ, et al. Late neurocognitive sequelae in patients with WHO grade I meningioma. J Neurol Neurosurg Psychiatry 2009;80:910-915.

[417] Littman P, Rosenstock J, Gale G, et al. The somnolence syndrome in leukemic children following reduced daily dose fractions of cranial radiation. Int J Radiat Oncol Biol Phys 1984;10:1851-1853.

[418] Powell C, Schick U, Morden JP, et al. Fatigue during chemoradiotherapy for nasopharyngeal cancer and its relationship to radiation dose distribution in the brain. Radiother Oncol 2014;110:416-421.

[419] Adeberg S, Welzel T, Rieken S, Debus J Combs SE. Prior surgical intervention and tumor size impact clinical outcome after precision radiotherapy for the treatment of optic nerve sheath meningiomas (ONSM). Radiat Oncol 2011;6:117.

[420] Lesser RL, Knisely JP, Wang SL, Yu JB Kupersmith MJ. Long-term response to fractionated radiotherapy of presumed optic nerve sheath meningioma. Br J Ophthalmol 2010;94:559-563.

[421] Abouaf L, Girard N, Lefort T, et al. Standard-fractionated radiotherapy for optic nerve sheath meningioma: visual outcome is predicted by mean eye dose. Int J Radiat Oncol Biol Phys 2012;82:1268-1277.

[422] Smee RI, Schneider M Williams JR. Optic nerve sheath meningiomas--non-surgical treatment. Clin Oncol (R Coll Radiol) 2009;21:8-13.

[423] Goyal LK, Suh JH, Mohan DS, Prayson RA, Lee J Barnett GH. Local control and overall survival in atypical meningioma: a retrospective study. Int J Radiat Oncol Biol Phys 2000;46:57-61.

[424] Younis GA, Sawaya R, DeMonte F, Hess KR, Albrecht S Bruner JM. Aggressive meningeal tumors: review of a series. J Neurosurg 1995;82:17-27.

[425] Coke CC, Corn BW, Werner-Wasik M, Xie Y Curran WJ, Jr. Atypical and malignant meningiomas: an outcome report of seventeen cases. J Neurooncol 1998;39:65-70.

[426] Adeberg S, Hartmann C, Welzel T, et al. Long-term outcome after radiotherapy in patients with atypical and malignant meningiomas--clinical results in 85 patients treated in a single institution leading to optimized guidelines for early radiation therapy. Int J Radiat Oncol Biol Phys 2012;83:859-864.

[427] Milker-Zabel S, Zabel-du Bois A, Henze M, et al. Improved target volume definition for fractionated stereotactic radiotherapy in patients with intracranial meningiomas by correlation of CT, MRI, and [68Ga]-DOTATOC-PET. Int J Radiat Oncol Biol Phys 2006;65:222-227.

[428] Gehler B, Paulsen F, Oksuz MO, et al. [68Ga]-DOTATOC-PET/CT for meningioma IMRT treatment planning. Radiat Oncol 2009;4:56.

[429] Combs SE, Ganswindt U, Foote RL, Kondziolka D Tonn JC. State-of-the-art treatment alternatives for base of skull meningiomas: complementing and controversial indications for neurosurgery, stereotactic and robotic based radiosurgery or modern fractionated radiation techniques. Radiat Oncol 2012;7:226.

[430] Sharma SD, Upreti RR Deshpande DD. Use of peripheral dose data from uniform dynamic multileaf collimation fields to estimate out-of-field organ dose in patients treated employing sliding window intensity-modulated radiotherapy. Phys Med Biol 2006;51:2987-2995.

[431] Zwicker F, Swartman B, Roeder F, et al. In vivo measurement of dose distribution in patients' lymphocytes: helical tomotherapy versus step-and-shoot IMRT in prostate cancer. J Radiat Res 2014.

[432] Thorwarth D, Henke G, Muller AC, et al. Simultaneous 68Ga-DOTATOC-PET/MRI for IMRT treatment planning for meningioma: first experience. Int J Radiat Oncol Biol Phys 2011;81:277-283.

[433] Thorwarth D, Muller AC, Pfannenberg C Beyer T. Combined PET/MR imaging using (68)Ga-DOTATOC for radiotherapy treatment planning in meningioma patients. Recent Results Cancer Res 2013;194:425-439.